Coastal Monitoring Program

NC 12 Transportation Management Plan

TIP Project B-2500

2021 UPDATE REPORT

FINAL REPORT

Elizabeth J. Sciaudone, Ph.D.

**NCSU Department of Civil, Construction,
and Environmental Engineering
Box 7908
Raleigh, NC 27695
11/16/2022**

Executive Summary: 2021 Update Report

Implemented by the N.C. Department of Transportation (NCDOT) in 2011, the primary purpose of the Coastal Monitoring Program is to assess highway vulnerability between Oregon Inlet and Rodanthe and is a condition of the 2010 Record of Decision (ROD) for the NC 12- Replacement of the Herbert C. Bonner Bridge. The program is conducted in conjunction with the U.S. Fish and Wildlife Service, providing data to aid in habitat management decisions within the Pea Island National Wildlife Refuge. This report presents detailed monitoring data for the 2021 study year. Conditions throughout the year are compared to conditions in the prior year (2020) and baseline conditions (2010).

This executive summary provides a brief overview of the report results.

Highway Vulnerability

The primary indicators of highway vulnerability considered are: 1) distance from ocean to estuarine shoreline (island width), 2) dune crest elevation less than 10 feet above the NC 12 centerline, and 3) ocean shoreline within 230 feet of the edge of pavement. Though single indicators were found at multiple study transects, four primary locations of concern based on multiple indicators were identified:

- the Canal Zone just north of the freshwater ponds (primarily dunes and 230-foot buffer, some transects with island width as well);
- near the Pea Island Visitors Center between the northernmost and middle ponds (dunes, 230-foot buffer);
- the area just south of the Pea Island Breach (island width, dunes); and
- the S-Curves in northern Rodanthe (island width, dunes, 230-foot buffer).

These four areas have previously been identified as areas of concern, with the Pea Island Breach and S-Curves locations showing consistent vulnerability throughout the study timeframe. The Pea Island Visitors Center, which has suffered from erosion of the beach and dunes, was first identified in 2017. Since that time, the USFWS elevated the Visitors Center building approximately 5 ft above its original elevation (in 2020); the building re-opened in December 2021. The S-Curves area is bypassed by the Rodanthe Bridge, which was under construction in 2021.

Morphological Indicators

The status of other morphological indicators included in the monitoring program as of 2021 are as follows:

- **Dune crest (maximum elevation at each study transect):** Elevations were highly variable during 2021 with especially large changes in the Canal Zone. Changes in elevation can be attributed to wind and water transport (decreases) and human intervention/earth moving operations (increases).
- **Dune toe position and elevation:** On average, the September 30, 2021 dune toe position was similar to that determined in 2020. The average dune toe elevation was 8.9 ft NAVD, slightly lower than the average in 2020 of 9.5 ft NAVD.
- **Beach width:** The beach width as of September 30, 2021 was slightly wider on average across the study area than that observed in October 2020 (150 ft vs. 142 ft). Beach widths in most of

the area within the Rodanthe beach nourishment project have receded to pre-project conditions.

- **Erosion resistance volume (volume of beach above mean high water from edge of pavement to ocean shoreline):** There was a slight increase in the average volume during 2021 (average of 166.5 cy/ft in 2021 versus average of 166.2 cy/ft in 2020) (for reference, a dump truck can hold 10 cy). In 2021, profile volumes increased in the northern part of the beach nourishment area, remained relatively stable near mile 10.8, and decreased slightly towards Rodanthe. As of September 30, 2021, an average of 11 cy/ft more than the April 2014 pre-project conditions remained in the study area, primarily in the northern portion. Overall, since the baseline report (2010), the erosion resistance volume shows a net decrease over the entire study area of 1.3 M cy as of September 2021, despite the addition of 580,000 cy of dredged material disposal in 2013 and 1.3 M cy of sand during the beach nourishment project in 2014.

Vegetation and Land Cover/Habitat

- **Habitat Mapping:** Color Infrared (CIR) images were used to create habitat maps for Pea Island in 2021. Habitat classification maps indicate that dominant habitat classes on Pea Island are marshes, managed wetlands, shrub, bare sand dune, and beach. The largest changes observed in 2020 were from marsh to shrub, shrub to marsh, and from water to beach. The marsh to shrub changes are attributed to succession and the shrub to marsh changes are at least partially attributable to controlled burns undertaken by the USFWS (see Appendix B).

Erosion Rate and Shoreline Predictions

A summary of the erosion rate and shoreline prediction analyses is provided. It is noted that for the erosion rate analyses, the February 1, 2022 shoreline was included, because there was no flight in December 2021.

- **Erosion rate:** Long-term erosion rate trends remain similar to those reported in previous years:
  - Accretion is observed in the first 0.8 miles (Transects 170-200 approximately), with relatively low (<+/- 2 feet/year) rates of erosion and accretion south to mile 3.
  - Erosion with rates ranging between 5 and 10 feet/year is observed from miles 3 to 7.
  - A stable to slightly accreting area exists along miles 8 and 9, where the highly vegetated dune field is in place.
  - Higher rates of erosion up to 5-12 feet/year are observed from miles 10 south into Rodanthe.
  - Slightly lower rates of erosion exist near the Rodanthe pier.
- **Current/5-Year Vulnerability:** Currently, a section in the Canal Zone, a section adjacent to the north pond and Pea Island Visitors Center area, a narrow region just south of the wide dune field area, and the Rodanthe/S-Curves section had shorelines observed within the 230-foot buffer. Two sections spanning the currently vulnerable area in the narrow section north of Rodanthe as well as sections north and south of the currently vulnerable S-Curves section were predicted to be vulnerable within 5 years. These sections are illustrated in Figures 29 to 34.
- **2030 Predicted Shoreline:** By 2030, the prediction interval band of shoreline position reaches the 230-foot critical buffer in multiple locations, including the Canal Zone, near the Visitors Center along the center of the freshwater ponds, adjacent to the southernmost pond and

immediately north and south of the Interim Bridge at the Pea Island Breach, as well as in northern Rodanthe. These sections are illustrated in Figures 35 through 40.

- **2060 Predicted Shoreline:** The 2060 prediction interval band of shoreline position reaches the critical buffer along a stretch of NC 12 in the Canal Zone south of Oregon Inlet, along the north pond and the Visitors Center and adjacent to the Pea Island Breach. The band lies within or landward of the critical buffer and roadway throughout the area of the Rodanthe Bridge. The 2060 shorelines are illustrated in Figures 42 through 47.

Breaches

The locations of the Pea Island and Rodanthe breaches (formed in 2011) continue to be monitored, with results as indicated:

- **Pea Island Breach:** The Pea Island Breach was closed for all of 2021, with the most seaward shoreline position measured in August 2021.
- **Rodanthe Breach:** The most seaward positions in this area were also observed in August 2021.

Storms

- No tropical systems directly impacted the study area in 2021. Storms with a maximum wave height of 6.6 ft or greater for a duration of 8 or more hours were recorded at the USACE Field Research Facility in January, February, March, October, and November.
- The most severe event in 2021 was a coastal storm in November 2021.The NCDOT Traveler Information Management System recorded closures during this event from November 7 to November 9, 2021.

USACE Dredging

- USACE dredging operations data indicated that in FY 2020, a total of 144,323 cubic yards were dredged in Oregon Inlet, all with USACE dredges (sidecaster or shallow draft hopper) with a total cost of $2.73M.
- In FY 2021, a total of 142,947 cubic yards were dredged by the USACE, using USACE dredges (sidecaster or shallow draft hopper), with a total cost of $2.69M.
- No material was placed directly on any of the study area beaches as the sidecaster operations do not remove material from the inlet system and the shallow draft hopper dredges generally place the material as close as possible to the surf zone at the north end of Pea Island.

Maintenance Expenses

- Maintenance expenses in 2021 totaled approximately $771,000 with most of the expenses related to general sand removal and expenses associated with the November 2021 coastal storm.

Terminal Groin Monitoring

The long-term terminal groin monitoring methodology was changed in 2017 to include a new protocol for determining the historical and project erosion rates. The historical rate is now determined as a linear regression of shoreline positions between October 1968 and October 1988. The project rate is determined as a linear regression of shoreline positions between August 1992 and December 2018. These new rates are used with the same methodology as previous reports to determine the one mile and three mile volume changes.

- **Terminal Groin Monitoring:** As of February 1, 2022, the project erosion rates are much less than the historical rates in the first three miles of the study area, and the project erosion rate does not exceed the historical rate at any point in the first six miles south of the Oregon Inlet terminal groin. The one and three mile volume calculations are well below that which would be expected using the historical rate. In summary, the construction of the groin does not appear to have caused an adverse impact to the shoreline over the six-mile study area.

Physical and Biological Monitoring

NCDOT provided physical and biological survey results which are summarized as follows:

- **Physical and Biological Condition of the Beach Sand:** Sand sampling was conducted quarterly (generally in January, April, July, and October) along 64 transects beginning 0.1 miles south of the terminal groin and continuing south every 0.2 miles to the southern terminus of the PINWR. Benthic organisms, grain size, slope and compaction, and heavy mineral content were analyzed.
    - Beginning in 2019 data were analyzed with a cubic function rather than a linear function. This function indicates an inverse relationship between grain size and species abundance.
    - Generally, grain size distributions across the study area were as expected with seasonal and long-term variations. The data also indicate that major storms have an influence over benthic numbers, but these numbers recover over time. In 2021, storms had little to no effects on the survey results.
    - Beginning in 2018, the Canal Zone, New Inlet/Pea Island Breach, and Rodanthe S-Curves areas were analyzed separately. The data indicated seasonal and long-term variation similar to that of the overall analysis. After analyzing the data from the "trouble spots" for 2019-2021, there is a constant strong inverse relationship (5-year cycle) between average grain size and average species abundance in the Pea Island Inlet area. There is a weak inverse relationship between average grain size and average species abundance in the Canal Zone and S-Curves. In the Canal Zone, the average number of species is increasing, while in the S-Curves the average number of species is decreasing. A decreasing trend in grain size at the Pea Island Inlet zone produced the second highest average species abundance since July 2013.
    - The 2021 survey year was the first time since 2014 that the average grain size for all three "trouble spots" did not exceed 1.0 mm, resulting in an abundance of benthic organisms.
    - New monitoring protocols were established for 2023 and are detailed in Appendix D.

TABLE OF CONTENTS

LIST OF FIGURES

LIST OF TABLES

1. INTRODUCTION

In December 2010, the Federal Highway Administration (FHWA) issued a Record of Decision (ROD) for TIP Project B-2500, which includes the replacement of the Bonner Bridge and a long-term solution for NC 12 between Oregon Inlet and Rodanthe. The Selected Alternative for Project B-2500 is the Parallel Bridge Corridor with NC 12 Transportation Management Plan (NC 12 TMP). As explained in the ROD, a component of the NC 12 TMP is a detailed coastal monitoring program that is designed to assist the agencies in deciding when the planning efforts for future phases of the Project B-2500 should begin. The coastal monitoring program includes detailed annual monitoring reports that summarize data collected by the N.C. Department of Transportation (NCDOT) and other agencies.

The study area for the coastal monitoring program includes both the study area of the existing terminal groin monitoring program (developed in conjunction with the U.S. Fish and Wildlife Service [USFWS], per the permit issued in June 1989) and the TIP Project B-2500 study area. The coastal monitoring program study area begins just over five miles north of the Oregon Inlet Marina and extends approximately 13 miles south of Oregon Inlet to the community of Rodanthe. The highway vulnerability analyses focus on the section of NC 12 between Transect 170 (Old Coast Guard Station, mile 0) and Transect 632 in the northern part of Rodanthe (mile 13.1). The study area includes the entire width of Hatteras Island between the ocean and estuarine (soundside) shorelines.

In August 2012, a new easement (permit) for the terminal groin monitoring was signed. The results of the terminal groin monitoring required as a condition of the 2012 easement are included in the annual coastal monitoring report. Any updates or changes in the terminal groin analysis methodology have been developed in consultation with the U.S. Fish and Wildlife Service (USFWS) and are described in this report.

The present report describes the data collection and analysis completed to update the conditions during the calendar year 2021. Conditions throughout the year are compared to the conditions reported in the 2020 Update Report, herein referred to as the 2020 report. General comparison of current erosion rates and composite vulnerability to baseline conditions (established in the Baseline Report, conditions as of January 14, 2011) are also presented. The erosion rates for the area have been updated with new shoreline position data through February 1, 2022. In addition, all assessments performed under the new terminal groin easement have been updated through February 1, 2022. This date in 2022 was used because there was no flight in December 2021, with the last flight in 2021 taking place on September 30, 2021.

The reports generated in conjunction with the NC 12 TMP coastal monitoring program are intended to meet the requirements for both TIP Project B-2500 and the easement issued in 2012 for the retention of the Oregon Inlet terminal groin.

2. DATA COLLECTION AND METHODOLOGY

The key parameters used for monitoring of the extended Oregon Inlet study area are:
- Ocean shoreline location;
- Estuarine shoreline location;

- Distance from ocean to estuarine shoreline;
- Island elevation;
- Dune crest location and elevation;
- Beach volume above mean high water, between eastern edge of pavement and ocean shoreline;
- Dune vegetation coverage;
- Land cover/habitat mapping (first presented in the 2017 update); and
- Erosion rate and road vulnerability.

The data used for this update is detailed in Table 1. Figure 1 shows the extent of the coastal monitoring program transects, and Table 2 lists the location of the transects corresponding to various landmarks along the study area. Transects 0 to 381 were the original transects established for purposes of monitoring the Oregon Inlet terminal groin. Transects are spaced 150 ft apart.

In August 2011, NCDOT implemented a new orthophotography flight schedule (in agreement with the USFWS), replacing the former terminal groin flight schedule (six times annually) with a new schedule that includes flights of the entire B-2500 study area four times annually (February, April, August, and October). The new photography is obtained at a flight altitude of 4500 ft Above Mean Ground Level (AMGL) and ground controlled in order to achieve +/- 0.5 ft accuracy (pers. comm. Rob Allen, NCDOT July 15, 2013). NCDOT generates topographic data from these lower elevation orthophotos. In June and December, NCDOT continues to fly the entirety of Hatteras and Ocracoke Islands, including the B-2500 study area, at 7500 ft AMGL but does not generate topographic data from these photos. Orthophotos from all six flight dates are used for shoreline delineation (oceanfront and soundside) and are used in the analysis of shoreline change. Parameters requiring elevation data (dune crest elevation, for example) are evaluated only at the February, April, August and October dates. Since 2013, color infrared (CIR) photography has been provided once per year (generally in April) to assist with identification of vegetation density and habitat classification.

Table 1. Orthophotos and topographic data used for 2021 monitoring update.

Date of Orthophotography	Topographic Data Available	Data Source	Notes
2/6/2021	Yes	NCDOT	
4/16/2021	Yes	NCDOT	CIR photographic data also provided
6/18/2021	No	NCDOT	
8/12/2021	Yes	NCDOT	
9/30/2021	Yes	NCDOT	
2/1/2022	Yes	NCDOT	This date used for the 2021 report because there was no flight in December 2021
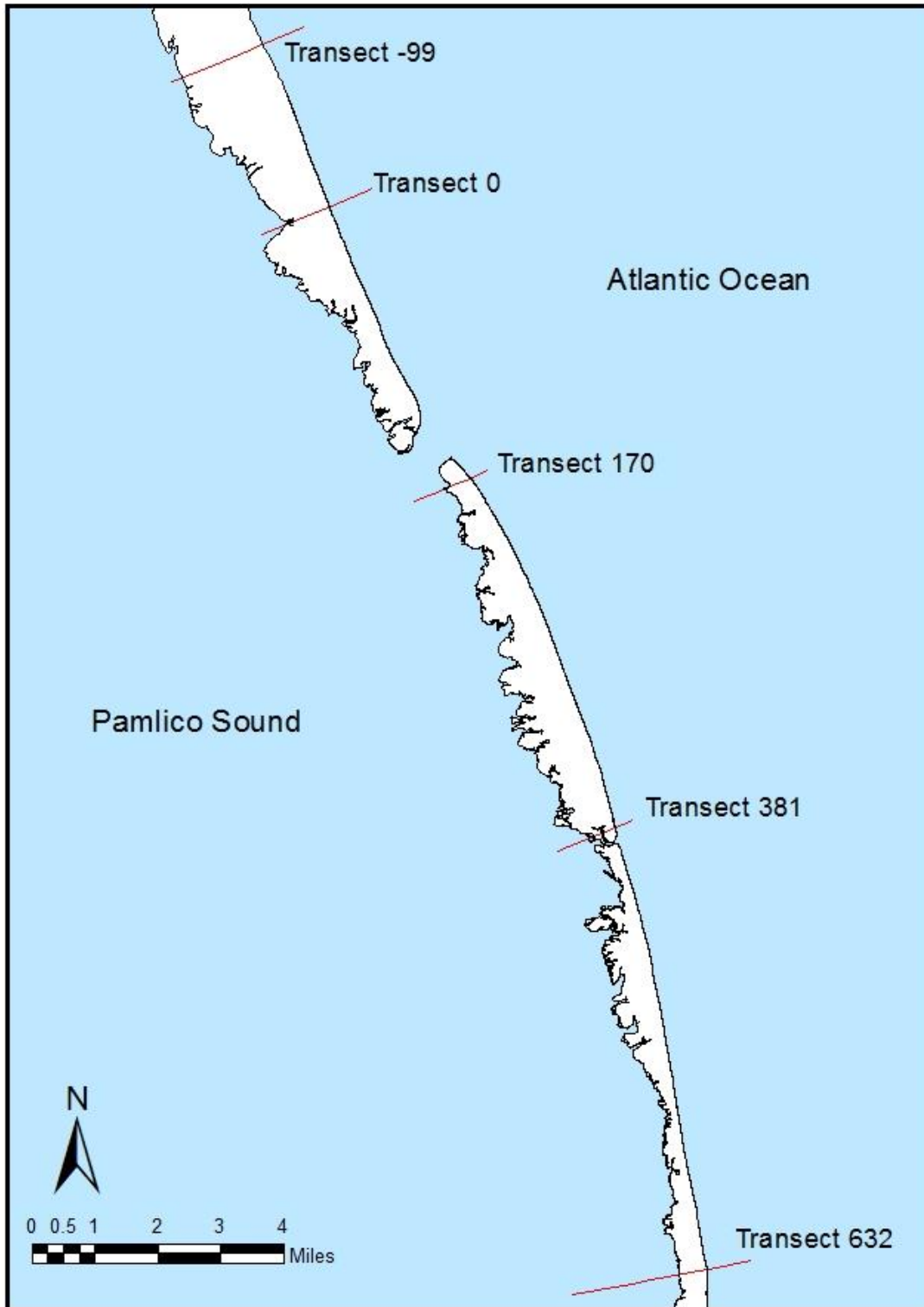
Figure 1. Coastal monitoring program with study area transect extents.

Table 2. Study area landmarks and corresponding transect numbers.

Transect Number	Miles from Transect 170	Location Description
-67	-6.7	Northernmost transect of study area (Bodie Island)
-35	-5.8	South Old Oregon Inlet Road
89	-2.3	Oregon Inlet Marina
150	-0.5	Bonner Bridge Navigation Zone - Midpoint
156	-0.4	Tip of Terminal Groin
170	0	Old Coast Guard Station
254	2.4	Northernmost Dike of Ponds
307	3.9	Pea Island National Wildlife Refuge Visitor Center
378	5.9	Southernmost Dike of Ponds
399	6.5	Oceanside Refuge parking lot
410	6.8	Soundside Refuge parking lot
578	11.6	Southernmost boundary of Refuge
604	12.3	Rodanthe Ferry Terminal
632	13.1	Southernmost transect of study area (Rodanthe Pier)

As detailed in the following sections, additional data on NCDOT roadway maintenance activities, other projects in the study area, and data from other federal and state agencies were also used in this analysis. Physical and biological monitoring has been conducted by NCDOT. Appendix A includes this monitoring of the conditions of the beach sand. Appendix B shows the regions of controlled burns undertaken in 2021 within the PINWR and was provided by USFWS.. Appendix C includes published papers that were completed as part of this research effort. Appendix D presents revisions to the physical and biological monitoring protocols that will be implemented in 2023.

The methodology used to analyze the data collected is described in the following sections. Detailed monitoring of the barrier island morphology is being undertaken along with examination and exploration of indicators of current and future vulnerability of the road.

Ocean and Estuarine Shorelines

The ocean shoreline was digitized for each of the six full study area orthophoto dates (Table 1). The shoreline is represented as the visible wet-dry line for sandy beaches (primarily on the ocean side), and the limit of the marsh vegetation is used to represent the estuarine shoreline (where the estuarine shoreline is sandy, the wet-dry line is used). Estuarine shorelines were updated for each date using the previous estuarine shorelines as a starting point. The estuarine shoreline has not been observed to change significantly over the two-month intervals between photo dates, with the exception of the areas closest to the Pea Island Breach and just south of the new Basnight (Oregon Inlet) Bridge. Because of the limited extent of changes in the estuarine shoreline, it is determined for each date using the following methodology:

- The previous shoreline (2 months prior) is displayed on the current orthophoto. (For example, the December estuarine shoreline is generally displayed on the February orthophoto.)

- Visual inspection of the digitized shoreline relative to the photo identifiable shoreline is made at a scale of 1:1200, and the digitized shoreline is corrected to the most recent orthophoto as required.

The methodology for determining the ocean shoreline is as follows:

- The ocean shoreline is digitized directly from the orthophoto for each date (without comparison with previous shorelines). It is identified as the visible wet-dry line (location where a noticeable darker line of saturated sand is observed). The wet-dry line (also known as the high water line) is used because it has a smaller horizontal displacement than the swash terminus, thus it is more suitable for long-term shoreline change analysis (Dolan et al. 1980).
- Visual inspection of the image at a scale of 1:1200 is made and the wet-dry line is manually digitized and reviewed.

The distance from the ocean shoreline to the estuarine shoreline was evaluated at each transect for the February 6, April 16, June 18, August 12, and September 30, 2021 orthophotography as well as the February 1, 2022 orthophotos. Exclusively interior channels and ponds were not considered to be a part of the estuarine shoreline for this analysis. In some cases, the island extended past the first intersection with the estuarine shoreline. In these cases, the distance to the first intersection was used.

As described in the 2011 report, the original study methodology included identifying the smallest 10% of the distances from ocean to estuarine shoreline (in the baseline report); this methodology has changed to an assessment of the locations where that distance was smaller than 1000 ft (in all subsequent reports). Island width is considered to be a vulnerability indicator for island breaching, and 1000 ft was selected based on the island widths at the locations of breaches caused by Hurricane Irene in August 2011. In the present report a width of 1000 ft is used to assess breaching vulnerability.

Island Elevation and Dune Morphology

Photogrammetrically derived digital terrain models from the February 6, April 16, August 12 and September 30, 2021 flights were used to evaluate island elevation and dune morphology. The digital terrain models include spot elevations, breaklines, and contours provided by NCDOT. These are imported into ArcGIS for further analysis. Island elevation values were extracted across each transect for each date at each transect using GIS tools.

Dune Crest/Maximum Elevation between NC 12 and Ocean Shoreline

A profile-based assessment of the maximum elevation between the eastern edge of pavement of NC 12 and the ocean shoreline was performed. The maximum elevation is then used to evaluate the potential vulnerability to wave action and overwash. The maximum elevation between the edge of pavement and shoreline is compared with the road elevation at each transect. Where the maximum elevation is less than 10 ft above the road, there is considered to be an increase in vulnerability.

Dune Toe Position and Elevation

In addition to the evaluation of maximum elevation between the road and the shoreline, identification of the dune toe position and elevation was conducted and reported for the last topographic data set available for the 2021 study year, associated with the September 30, 2021 photography.

To identify the dune toe, a partially automated algorithm was used. For initial dune toe identification, a straight line between the maximum profile elevation and the shoreline was drawn, and the maximum difference between this line and the profile elevation was identified as the toe (see Figure 2). However, in some cases the automatically extracted toe was either not suitable, or no significant dune was present on the profile. This led to the development of an inspection method where the user views the profile at each transect, and can either accept or replace the estimated dune toe, or identify a profile as having no visible dune feature. For profiles identified as "no dune," the dune toe elevation and position were not reported.
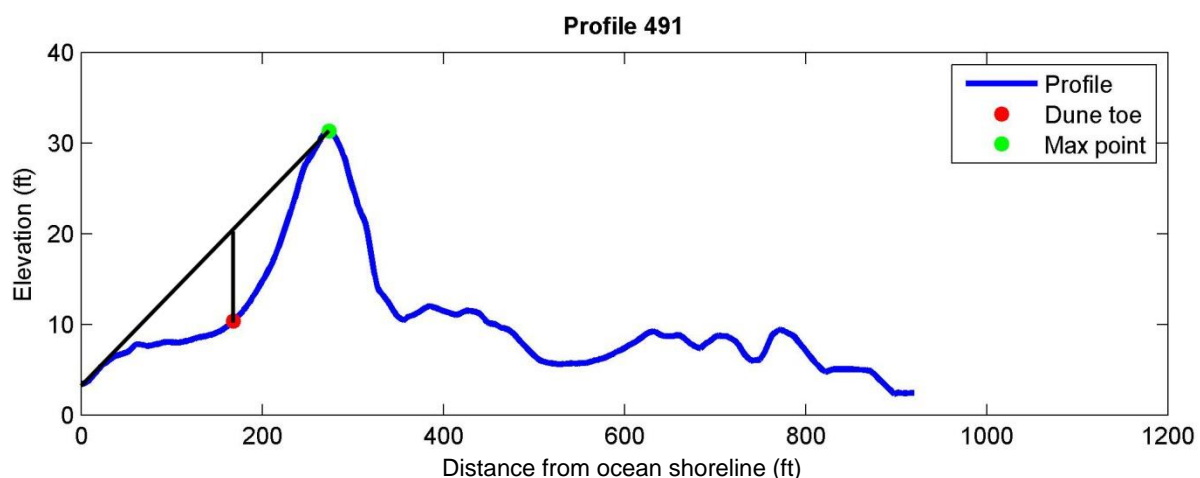
Figure 2. Schematic of dune toe identification methodology. Ocean shoreline is at horizontal position zero.

Beach Width

Dune toe identification also allows for assessment of the beach width. For this study, beach width is defined as the distance from the dune toe to the ocean shoreline. Beach width is important because for wide beaches under typical daily conditions, the dune system is unaffected by wave action and can build due to accumulation of wind-blown sand. Under continual erosion, the beach narrows and steepens, allowing more frequent impact of waves on the dune face and transitioning to an eroding dune system.

In this study, beach widths less than 100 ft are considered to contribute to vulnerability of adjacent dune fields and therefore to the highway vulnerability. Where beaches are less than 100 ft wide, elevated water levels and high waves during typical nor'easter storms can impact the dunes, reducing dune volume and height. If these conditions exist in areas where the total distance from edge of pavement to shoreline is greater than 230 ft, the narrow beach width and loss of the dune make the road increasingly vulnerable to direct wave impact and/or flooding during storm events.

Beach Volume above MHW from Edge of Pavement to Shoreline

The digital terrain models from the February 6, April 16, August 12 and September 30, 2021 flights were also employed to compute the volume of beach material between the NC 12 edge of pavement (EOP) and the ocean shoreline located at the mean high water (MHW) elevation at each transect. Mean high water was determined at the center of the study area using the VDATUM tool developed by NOAA (NOAA 2012). The MHW elevation was estimated at 1.14 ft NAVD 88. The elevations along each transect were extracted from the edge of pavement seaward using GIS tools. Volume above the 1.14 ft contour was computed using a Matlab script that functions similarly to the BMAP methodology described in previous reports, and is reported as cubic yards per ft alongshore (schematic shown in Figure 3). Computed volumes were compared with previously reported values. It is noted that the Edge of Pavement (EOP) reference line for the beach volume was adjusted to account for roadway location changes as detailed in Appendix B of the 2019 report. These changes affected reported beach volumes at Transect 376-404 adjacent to the interim bridge at the Pea Island Breach and Transects 513 to 526 adjacent to the northern end of the under-construction Rodanthe bridge.
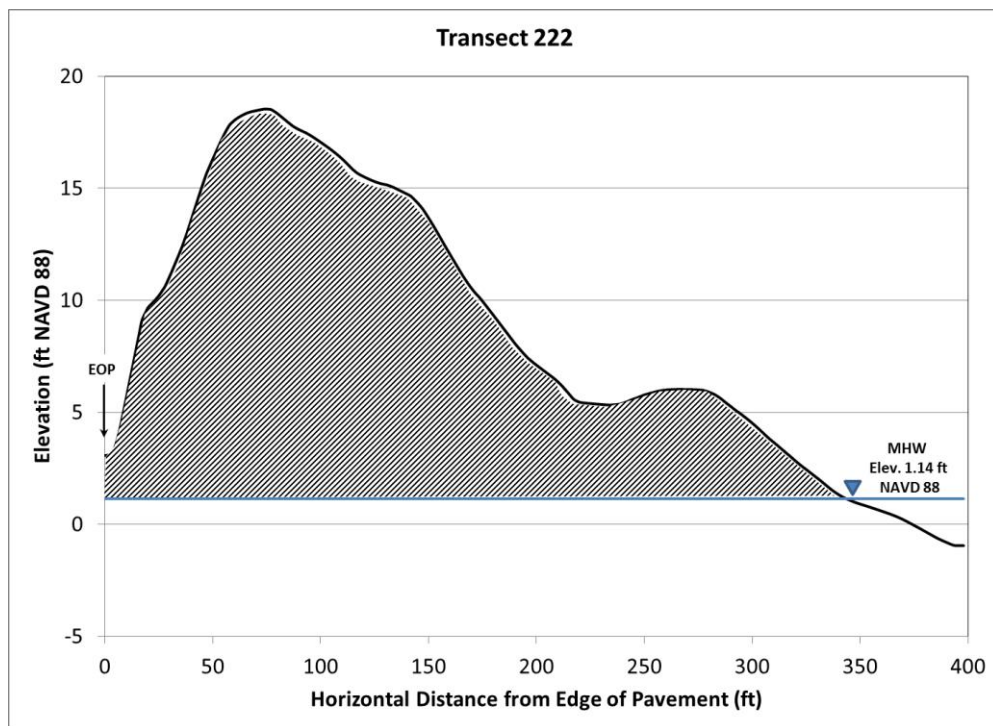
Figure 3. Schematic of unit volume computation. The cross sectional area between the horizontal position of the mean high water (MHW) contour and the edge of pavement (EOP) is calculated as shown, and then converted to unit volume in cubic yards per ft assuming a 1 ft wide profile.

Land Cover/Habitat Mapping

As part of the requirements of the 2012 easement, work has been ongoing to map and model habitat changes within the Pea Island National Wildlife Refuge (PINWR). Initial efforts were undertaken in collaboration with representatives of the PINWR to create land cover maps for the years 1998 and 2015, based on available color infrared (CIR) photography and were described in the 2017 report. In 2018, this effort was expanded and maps were created for each of the years, 2012 to 2018, as described in Appendix B of the 2018 report. *The land cover/habitat mapping replaces the vegetation analysis described in reports prior to 2018, as agreed by representatives of USFWS and NCDOT.* The present report continues the methods initially described in Appendix B of the 2018 report to map the land cover/habitat for the April 16, 2021 color infrared imagery. These methods are described below.

The CIR image was resampled to a 2 ft (0.6 m) resolution. This value was chosen to speed up computational times in ArcGIS, while maintaining enough resolution to differentiate all habitat classes. The resampled image was clipped using the polygon formed by the south end of the PINWR and the estuarine and oceanfront shorelines.

Thirteen habitat classes were identified as the main habitats that could be classified from the CIR imagery. These classes were selected in collaboration with personnel from the U.S. Fish and Wildlife Service (USFWS) and are based on the habitat types listed on the PINWR website <http://www.fws.gov/refuge/pea_island/wildlife_and_habitat/habitat_types.html>. The 13 classes are listed with their descriptions in Table 3.

Habitat classification was completed in ArcGIS using interactive supervised classification based on training polygons digitized over spatially varying locations that represent each habitat class. This method allows for a fast cell-by-cell raster classification based on classes defined by the user. Habitat classes such as *Bare Sand, Estuarine Pond, Salt Flat, Shrub*, *Marsh,* and *Water* are automatically classified using this method.

Seaward of the NC 12 Highway, classification is partially based on the supervised classification and morphological features digitized as polygons. The *Beach* is the region within the oceanfront shoreline and the dune toe. For habitat classification purposes, the horizontal extent of the dunes is defined based on elevation data and transects separated every 150 ft. The dune field is the polygon defined by the dune toe line, the dune heel line and the southern end of the refuge. The location of the dune heel is the defined by the 5 ft contour or the eastern edge of pavement, whichever is seaward (Figure 4). The 5 ft contour was chosen as the landward edge of the dune because it partially matches the edge of NC 12 highway in the northern portion of the island, and because it provides an objective metric for comparison between different dates. The location of the dune toe depends on the dune crest and the shoreline position at each transect. The dune toe is extracted based on the maximum vertical distance between the beach profile and the line traced between the dune crest and the shoreline (Figure 4).

Table 3. Definition of Habitat Classes

Value	Class	Description
1	Bare Sand (BS)	Bare sand excluding the foredune and beach areas. Bare sand includes overwash fans and unvegetated portions of the island covered with dry sand.
2	Estuarine Pond (EP)	Enclosed bodies of water within the island with minimum or no connection with estuarine water. This class does not include the three large manmade managed water ponds of the refuge.
3	Salt Flat (SF)	Estuarine areas subjected to irregular flooding by salt water. This class occurs in shallow depressions where evaporation of the high salinity ocean water concentrates salt. Sparse cover and low diversity characterize its plant density and species composition.
4	Shrub (S)	Shrubs occur in a wide range of conditions from excessively to poorly drained soils in areas protected from salt spray and flooding by salt water. These conditions may occur on stabilized sand ridges, in dune swales, and on sand flats.
5	Marsh (M)	Includes salt and emerging marshes. Salt Marsh occurs on the margins of estuarine channels and on the landward side of barrier island systems in areas under tidal influence. The brackish marsh occurs along the margins of sounds and estuaries in areas not subjected to regular flooding by salt water. Brackish marsh is subjected to irregular flooding mostly from wind tides.
6	Vegetated Dune (VD)	Vegetated dune occurs in the landward side of the dune. This habitat is exposed to salt spray and abrasive wind-blown sand.
7	Bare Sand Dune (BSD)	Un-vegetated portion of dunes limited on the ocean front by the dune toe and landward by the 5 ft (1.524 m) NAVD88 elevation contour or the eastern edge of pavement, whichever is seaward.
8	Water (W)	Estuarine and ocean water.
9	Groin (G)	Terminal groin as visible from aerial imagery.
10	Infrastructure (I)	Paved roads, parking lots, construction sites, and buildings.
11	Maritime Brush (MB)	Growing vegetation in overwash terraces behind dunes and below the 5 ft (1.524 m) NAVD88 elevation contour in areas subject to inundation by the ocean or partial burial due to wind-blown sand.
12	Managed Wetlands (MW)	Manmade impoundments with borrow canals around the perimeter that may include open water, moist soil, exposed sand/mud flats, and emergent vegetation with varying amounts and management regimes. Pea Island National Wildlife Refuge has three impoundments: 390-acre North Pond, 192-acre New Field Pond, and 208-acre South Pond.
13	Beach (B)	Bare sand between the dune toe and the wet-dry shoreline.
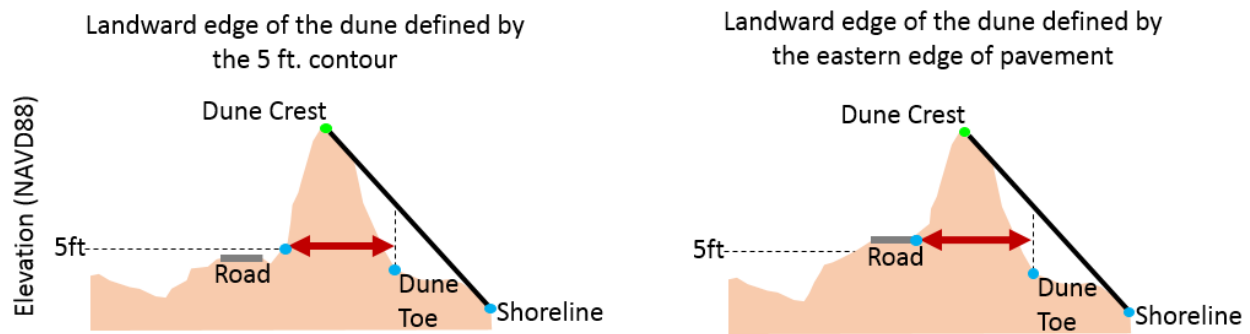
Figure 4. Definition of the horizontal extent of a dune (red arrow) on a cross-shore transect and visualization of the dune toe extraction method.

The dune is classified as *Bare Sand Dune* and *Vegetated Dune* depending on whether it is vegetated or not. Vegetated areas between the landward edge of the dune and NC 12 Highway are classified as *Maritime Brush*, excluding Shrubs. Other areas classified as Maritime Brush were digitized over the portion of overwash fans that have growing vegetation. Other classes that were digitized include the *Infrastructure*, *Groin,* and *Managed Wetlands*.

Once the automated and digitized classifications are completed, visual inspection of the resulting habitat maps is performed at 1:3,000 scale that allows correction of noise and any mis-classifications that may have resulted from the automated process. Feedback is also obtained from USFWS regarding the classifications, with edits made based on this feedback.

Erosion Rate Update

The project included an update of study area erosion rates following the methodology of Overton and Fisher (2005). To update the erosion rates, additional ocean shoreline position data were established using the aerial orthophotography for the 2021 dates (and February 2022), and added to the database of shoreline positions established in the 2010 Baseline Report (Overton 2012) and updated in subsequent reports. The erosion or accretion rates were then calculated by performing a linear regression on the shoreline position data. It is noted that for the transects surrounding the Pea Island Breach (Transects 386, 387, 388, 389, and 390), shoreline positions while the breach was active have been removed from the database, as described in the 2015 Report. Since the 2016 update, post-closure shorelines for those transects have been included in the database, and computation of erosion rates for these transects has resumed.

Critical Buffer and Vulnerability: Present and Future

The vulnerability of the NC 12 roadway at the conclusion of 2021 was assessed using the February 1, 2022 orthophotography because there was no imagery available for December 2021. Vulnerable locations were identified using the 230-foot critical buffer established in previous studies[1]. Where the

---

[1] This criterion originated with the first highway vulnerability study completed in 1991 (Stone, Overton and Fisher 1991). That work proposed a critical buffer distance of 230 ft from the edge of pavement to the active shoreline, interpreted as mean high water (MHW), to be used to indicate when a coastal highway became vulnerable to

distance from the edge of pavement to the ocean shoreline was less than or equal to 230 ft, the area was considered to be vulnerable. In previous reports, the four transects within the original Pea Island Breach (and the associated temporary bridge) were excluded from the vulnerability analysis. NCDOT completed construction of a 0.5-mile interim structure spanning the breach area in late 2017. Because the new structure is not intended as a long-term solution for the maintenance of NC 12, this analysis will continue to assess the distance between the edge of pavement (bridge) and the ocean shoreline within the interim bridge area.

Areas where the shoreline would be expected to recede to the buffer zone within 5 years (based on the updated shoreline position data) were also highlighted. This was done by predicting the expected position of the shoreline in 5 years and highlighting areas where it encroached on the 230-foot critical buffer. The newly computed erosion rate (the linear regression of the cumulative set of shoreline positions) was used to project the shoreline position 5 years into the future and in 10-year intervals from 2030 to 2060. By computing the predicted position in this way, bias toward under-predicting or over-predicting erosion based on the current position is avoided, and all historic positions in the database are incorporated.

To provide an estimate of the range of potential shoreline positions, the concept of prediction interval was used to determine the uncertainty surrounding the expected shoreline positions for the 2030, 2040, 2050, and 2060 predictions. A prediction interval is an estimate of a range in which future observations will fall, with a certain probability, given what has already been observed. The landward-most shoreline position in the 95% confidence interval range is considered a proxy for the potential "high-erosion" shoreline position, while the seaward-most position provides an estimate of the "low-erosion" case. This band of expected positions was compared with the 230-foot critical buffer to assess the potential future vulnerability of NC 12.

Storm Events

The USACE Field Research Facility (FRF), located in Duck, NC (approximately 35 miles north of the study area) maintains a variety of wave and water level measurements. The FRF defines a storm as a maximum wave height of greater than 2 m (6.6 ft) for a sustained duration greater than 8 hours. (Note: The wave height measured at the FRF, Hmo, is an energy-based statistic equal to four times the standard deviation of the sea surface elevations.) Storm events for 2021 were extracted using this criterion for the 17m waverider buoy at the FRF. In addition, the peak water level during each storm and the maximum difference between the NOAA predicted and observed water levels during the storm were compiled for the water level gage at the FRF.

Recently the data from the Traveler Information Management System (TIMS) for Dare County were made available to the CMP researchers. These data were also compiled to provide information on storm-related closures or hazardous events along NC 12 during 2021.

---

repetitive overwash and sand deposits resulting in excessive maintenance costs. This conclusion was based on the review of NCDOT maintenance records for NC 12.

NCDOT Maintenance

Information on the road maintenance conducted within the study area was provided by NCDOT, including location, type of maintenance, and cost.

Barrier Island Breaches

Hurricane Irene impacted the study area on August 27, 2011. High winds, waves, and elevated water levels on the sound side combined to cause substantial changes to the morphology of the area. In two locations, the barrier island was breached: just south of the freshwater ponds and at the north end of the community of Rodanthe. These breaches are referred to as the Pea Island Breach and the Rodanthe Breach, respectively. The Rodanthe Breach closed shortly after Hurricane Irene in 2011; however, that area was also breached during Hurricane Sandy in 2012 as described in the 2012 report. The Pea Island Breach had essentially closed by May 2013, nonetheless, later orthophotos have revealed occasional flooding at the area. The evolution of these regions was again monitored in 2021.

3. RESULTS

Distance from Ocean to Estuarine Shoreline

Table 4 shows the location of the transects where the distance from the ocean to estuarine shoreline was 1000 ft or less in at least one photography set in 2021. Overall, the locations where island widths are less than 1000 ft correspond to areas that have been identified in previous reports.

Transects 238 to 246 are located just south of the Canal Zone hot spot, adjacent to an interior channel north of the freshwater ponds which has a direct outlet to the sound. As noted in previous reports, this area can fluctuate in width but remains near the 1000 ft that is considered to be increasingly vulnerable to soundside storm surge.

Transects 408 to 423 are located at an area south of the Pea Island Breach that has remained narrow throughout the monitoring period.

Transects 535 to 576 are located just north of Rodanthe in a location that is persistently narrow, and where a beach nourishment project was completed from late July to early September 2014 (a project overview is provided in the 2014 report). The beach nourishment project increased island widths in the area temporarily, but have returned to pre-project conditions and were less than 1000 ft wide during most of 2021. This area will be bypassed by the Rodanthe Bridge, which was recently opened to traffic on July 28, 2022.

To illustrate the conditions of the full study area shoreline at the conclusion of the 2021 study year, the island width as of February 1, 2022 is shown in Figure 5. This figure illustrates the distance from the ocean to estuarine shoreline at each individual transect for this date; transects with island widths less than 1000 ft are highlighted in red. Figure 6 through Figure 11 present the locations of the island width transects on the aerial photography.

Table 4. Transects with distance from ocean to estuarine shoreline less than 1000 ft at least once in 2021. Distances less than 1000 ft are highlighted in bold.

Transect	Location	2/6/2021	4/16/2021	6/18/2021	8/12/2021	9/30/2021	2/1/2022
238	Between Old Coast Guard Station and Freshwater Ponds	1018	**954**	**971**	1022	1005	**920**
239		1024	1000	**989**	1044	1010	**935**
244		1021	**982**	1014	1055	**987**	1008
245		1007	**938**	**967**	1004	**990**	**997**
246		**993**	**917**	**927**	**947**	**982**	**976**
408	Between Refuge Parking Lots	**734**	**709**	**720**	**790**	**757**	**743**
409		**703**	**669**	**677**	**732**	**718**	**701**
410		**679**	**640**	**629**	**687**	**664**	**649**
411		**797**	**735**	**733**	**788**	**753**	**721**
412		**770**	**735**	**738**	**780**	**742**	**712**
413		**722**	**668**	**666**	**707**	**674**	**637**
414		**741**	**674**	**672**	**692**	**672**	**631**
415		**912**	**825**	**838**	**859**	**850**	**783**
416		1040	**948**	**968**	**972**	**953**	**907**
421		1054	1029	1017	1049	**999**	**980**
422		**936**	**930**	**934**	**962**	**905**	**887**
423		**941**	**963**	**951**	**973**	**929**	**909**
535	Southern PINWR/ Rodanthe S-Curves	**969**	**940**	**966**	**998**	**964**	**965**
537		**885**	**870**	**875**	**905**	**909**	**854**
540		**695**	**652**	**683**	**705**	**670**	**662**
541		**991**	**905**	**962**	**984**	**928**	**932**
542		**929**	**867**	**891**	**938**	**888**	**866**
543		**673**	**601**	**592**	**661**	**631**	**601**
544		1007	1025	**938**	1009	**979**	**933**
546		**675**	**673**	**682**	**711**	**675**	**653**
547		1016	**980**	1041	1061	1033	**997**
548		**780**	**727**	**807**	**826**	**798**	**761**
549		**919**	**843**	**906**	**936**	**940**	**898**
575		**859**	**832**	**847**	**902**	**840**	**855**
576		**808**	**770**	**783**	**834**	**780**	**781**
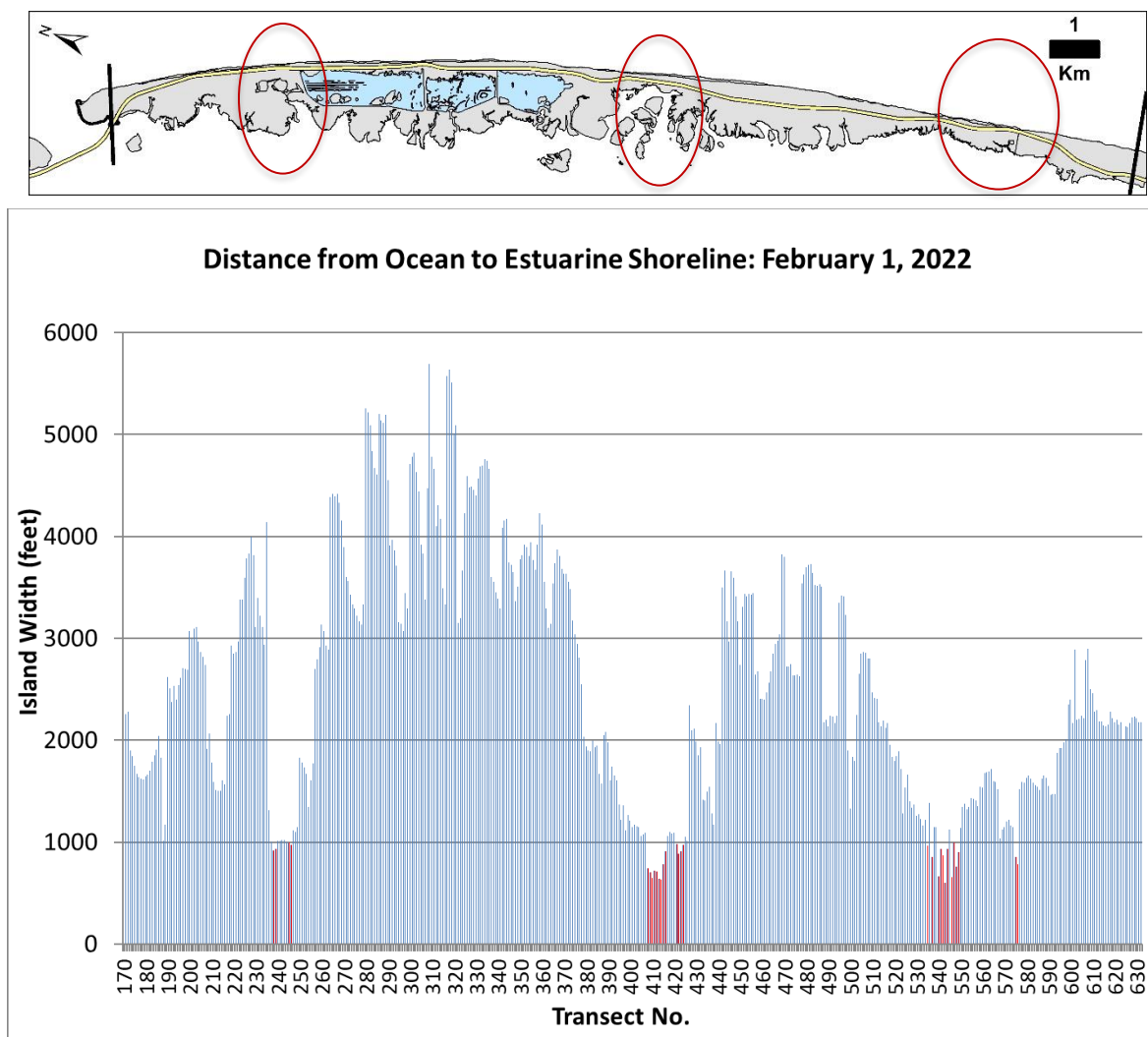
Figure 5. Summary of distance from ocean to estuarine shoreline measurements along the study area as of February 1, 2022. Red indicates distances less than 1000 ft. Transect 170 is located approximately 0.4 miles south of the tip of the terminal groin.

Legend:
- NC 12 Edge of Pavement
- February, 01, 2022 Shoreline
- February, 01, 2022 Estuarine Shoreline
- Distance less than 1000 ft to Estuarine Shoreline
- February, 01, 2022 Distance to Estuarine Shoreline

Transect numbers shown in red and aligned below transect

Scale: 0 — 500 — 1,000 — 2,000 — 3,000 — 4,000 Feet
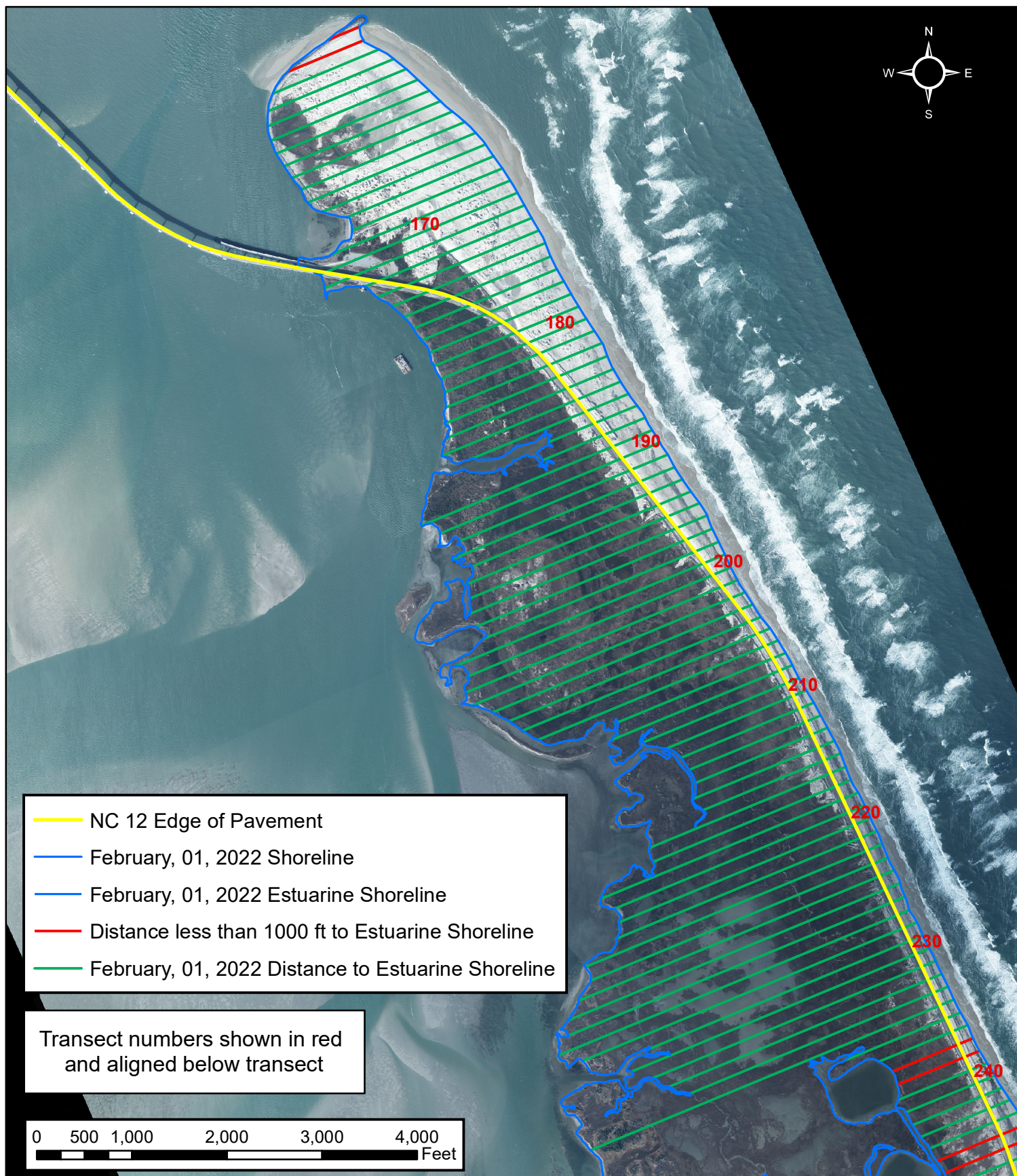
Figure 6

(View 1 of 6)

Pea Island - Distance from Ocean to Estuarine Shoreline

Prepared for the North Carolina Department of Transportation
Horizontal Datum: North Carolina State Plane Feet 1983 FIPS 3200
Orthophoto Date: February 01, 2022; Map Created: March 31, 2022

Legend

— NC 12 Edge of Pavement
— February, 01, 2022 Shoreline
— February, 01, 2022 Estuarine Shoreline
— Distance less than 1000 ft to Estuarine Shoreline
— February, 01, 2022 Distance to Estuarine Shoreline

Transect numbers shown in red and aligned below transect

0   500 1,000   2,000   3,000   4,000
Feet
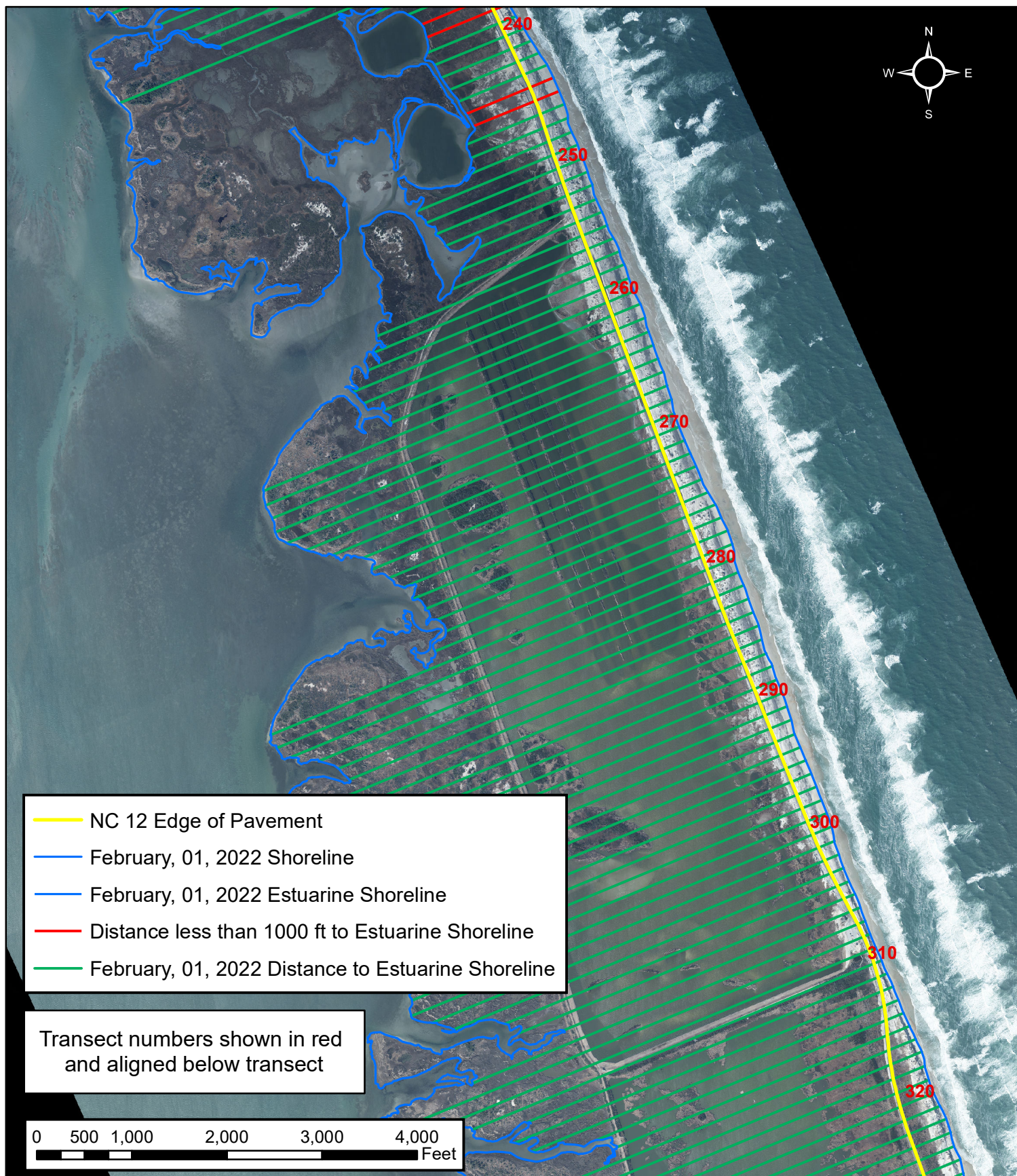
Figure 7

(View 2 of 6)

Pea Island - Distance from Ocean to Estuarine Shoreline

Prepared for the North Carolina Department of Transportation
Horizontal Datum: North Carolina State Plane Feet 1983 FIPS 3200
Orthophoto Date: February 01, 2022; Map Created: March 31, 2022

Legend:
- NC 12 Edge of Pavement
- February, 01, 2022 Shoreline
- February, 01, 2022 Estuarine Shoreline
- Distance less than 1000 ft to Estuarine Shoreline
- February, 01, 2022 Distance to Estuarine Shoreline

Transect numbers shown in red and aligned below transect

0 500 1,000 2,000 3,000 4,000 Feet
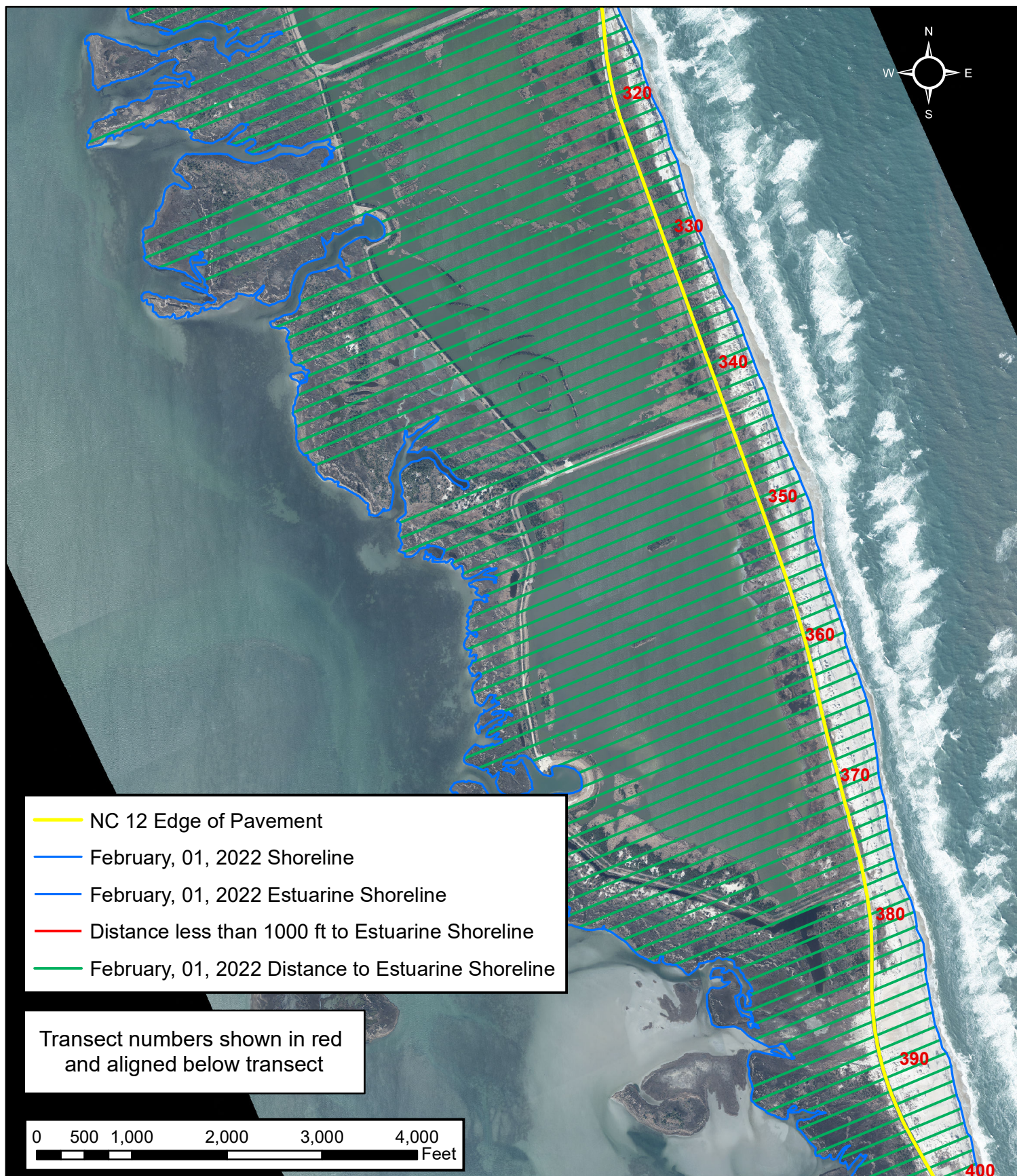
Figure 8

(View 3 of 6)

Pea Island - Distance from Ocean to Estuarine Shoreline

Prepared for the North Carolina Department of Transportation
Horizontal Datum: North Carolina State Plane Feet 1983 FIPS 3200
Orthophoto Date: February 01, 2022; Map Created: March 31, 2022

Legend:
- NC 12 Edge of Pavement
- February, 01, 2022 Shoreline
- February, 01, 2022 Estuarine Shoreline
- Distance less than 1000 ft to Estuarine Shoreline
- February, 01, 2022 Distance to Estuarine Shoreline

Transect numbers shown in red and aligned below transect

Scale: 0 500 1,000 2,000 3,000 4,000 Feet
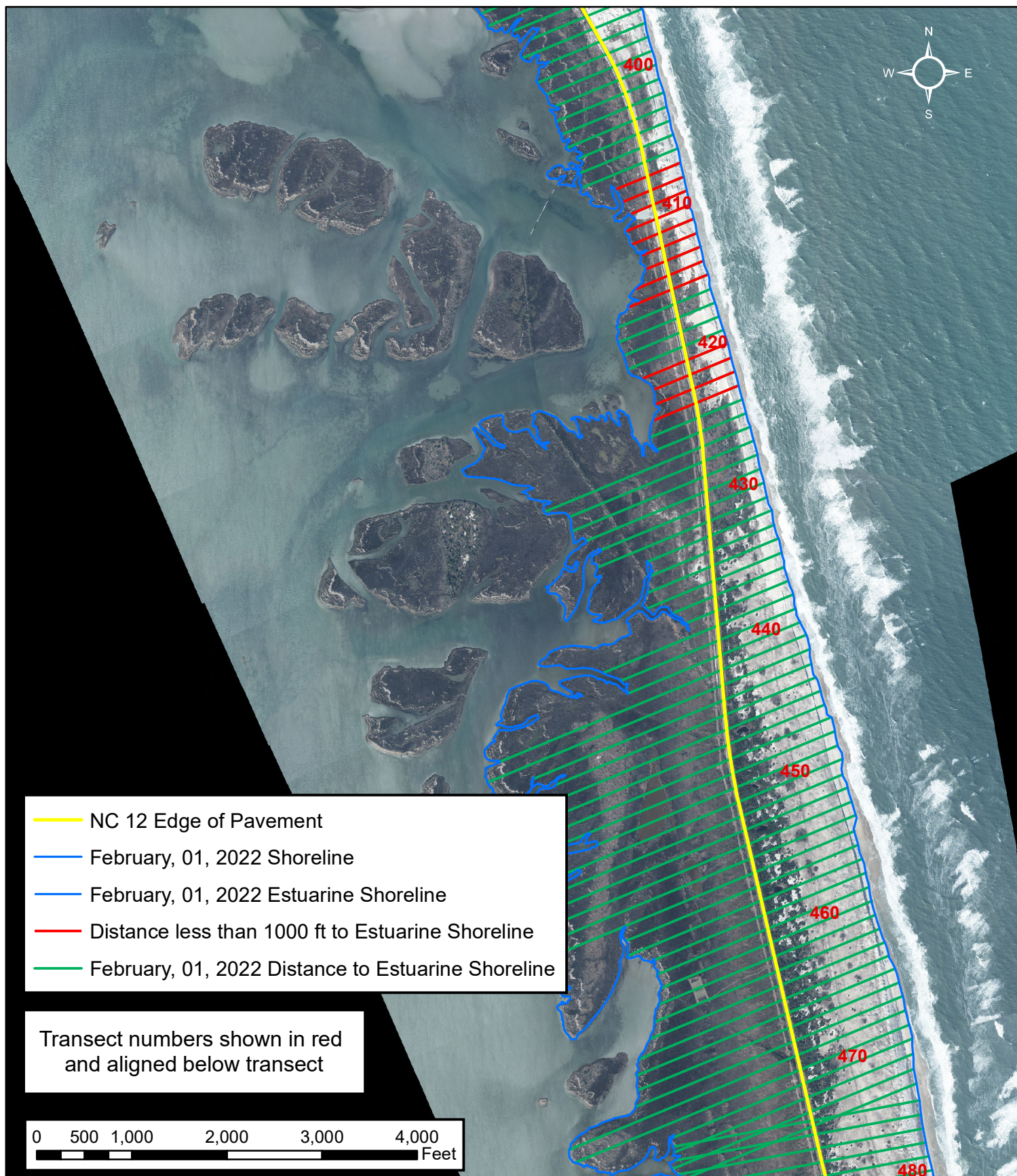
Figure 9

(View 4 of 6)

Pea Island - Distance from Ocean to Estuarine Shoreline

Prepared for the North Carolina Department of Transportation
Horizontal Datum: North Carolina State Plane Feet 1983 FIPS 3200
Orthophoto Date: February 01, 2022; Map Created: March 31, 2022
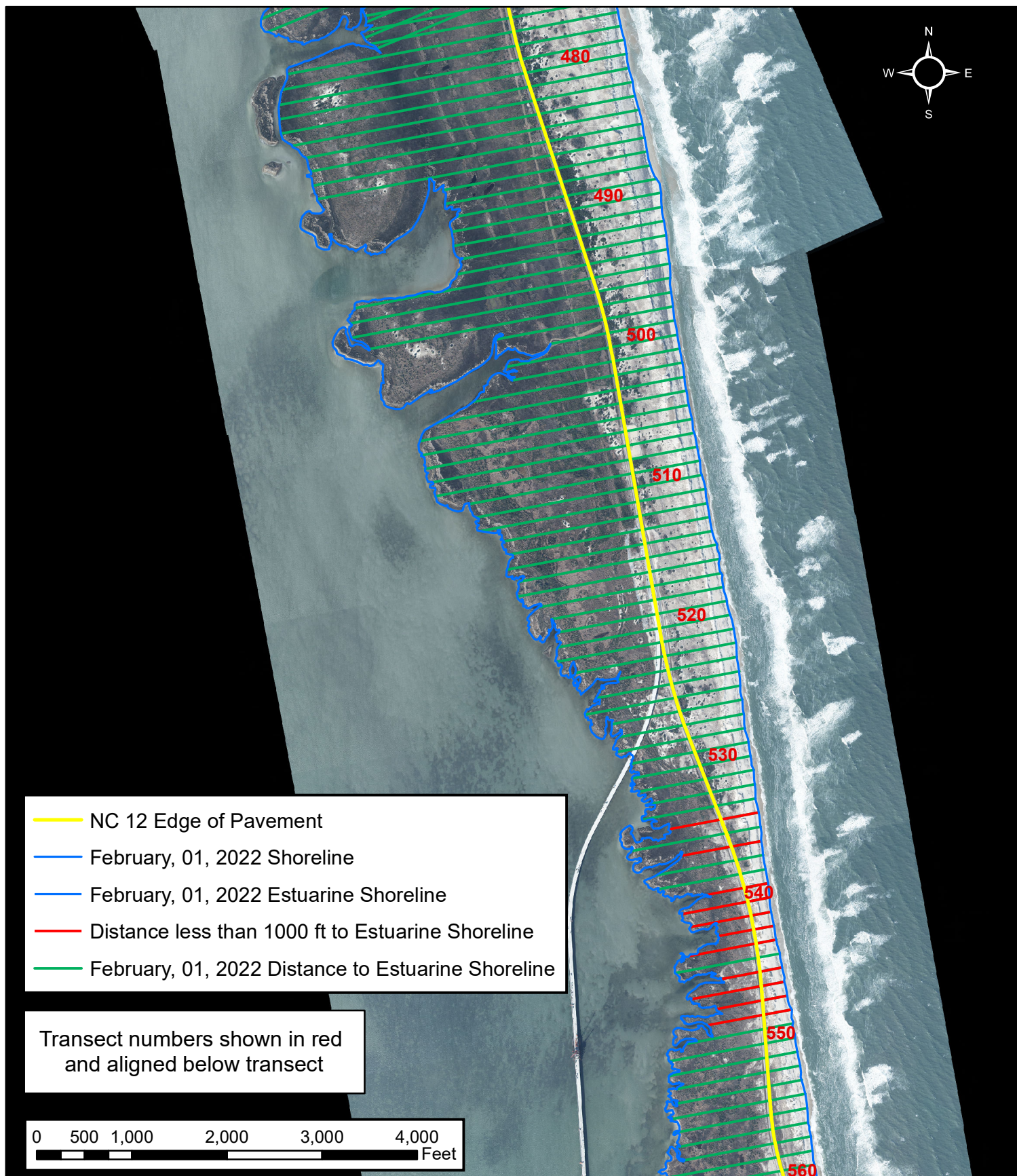
Figure 10

(View 5 of 6)

Pea Island - Distance from Ocean to Estuarine Shoreline

Prepared for the North Carolina Department of Transportation
Horizontal Datum: North Carolina State Plane Feet 1983 FIPS 3200
Orthophoto Date: February 01, 2022; Map Created: March 31, 2022

Legend:
- NC 12 Edge of Pavement
- February, 01, 2022 Shoreline
- February, 01, 2022 Estuarine Shoreline
- Distance less than 1000 ft to Estuarine Shoreline
- February, 01, 2022 Distance to Estuarine Shoreline

Transect numbers shown in red and aligned below transect
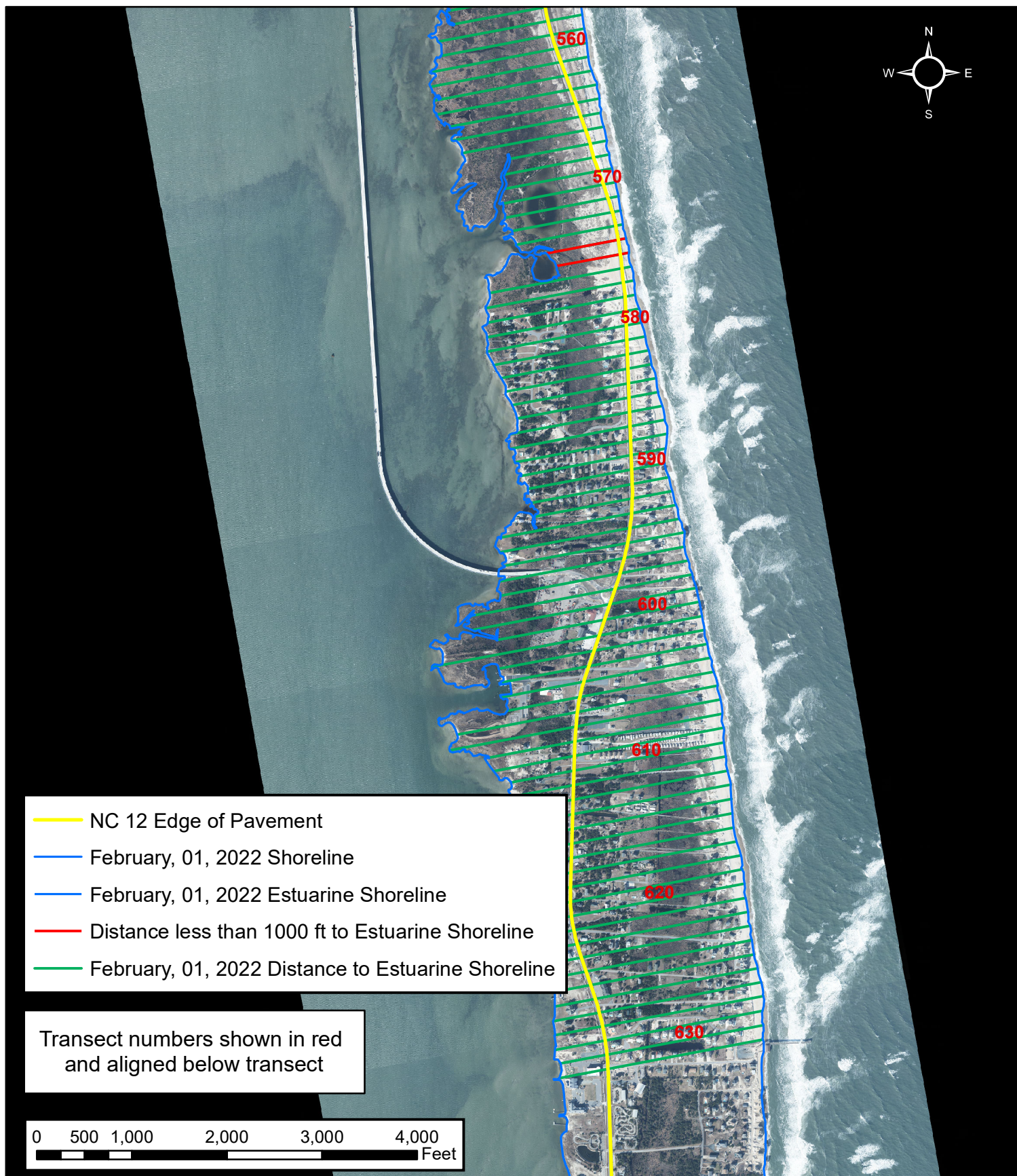
Figure 11

(View 6 of 6)

Pea Island - Distance from Ocean to Estuarine Shoreline

Prepared for the North Carolina Department of Transportation
Horizontal Datum: North Carolina State Plane Feet 1983 FIPS 3200
Orthophoto Date: February 01, 2022; Map Created: March 31, 2022

Legend:
- NC 12 Edge of Pavement
- February, 01, 2022 Shoreline
- February, 01, 2022 Estuarine Shoreline
- Distance less than 1000 ft to Estuarine Shoreline
- February, 01, 2022 Distance to Estuarine Shoreline

Transect numbers shown in red and aligned below transect

Scale: 0 500 1,000 2,000 3,000 4,000 Feet

Island Elevation and Dune Morphology

Dune Crest/Maximum Elevation between NC 12 and Ocean Shoreline

The maximum elevation between the NC 12 EOP and the ocean shoreline was determined at each transect for the 2021 digital terrain models (February 6, April 16, August 12 and September 30, 2021); for the purpose of this analysis, the maximum elevation is identified as the dune crest. Changes in the maximum elevation from date to date are shown in this section to illustrate the variability. Negative change means the elevation of the later date was lower than that of the earlier date (decrease in maximum elevation); positive change means that the maximum elevation increased between the two dates. Figure 12 illustrates the changes from February 6 to April 12, 2021. The average change in maximum elevation over the entire study area during this time frame was approximately 0.7 ft (computed using the absolute value of the difference). The largest change was an increase of just under 5 ft at Transect 214 near mile 1.25. The largest decrease was just over 7 ft at Transect 188 near mile 0.5. As in past reports, the majority of the elevation changes were in the Canal Zone area.
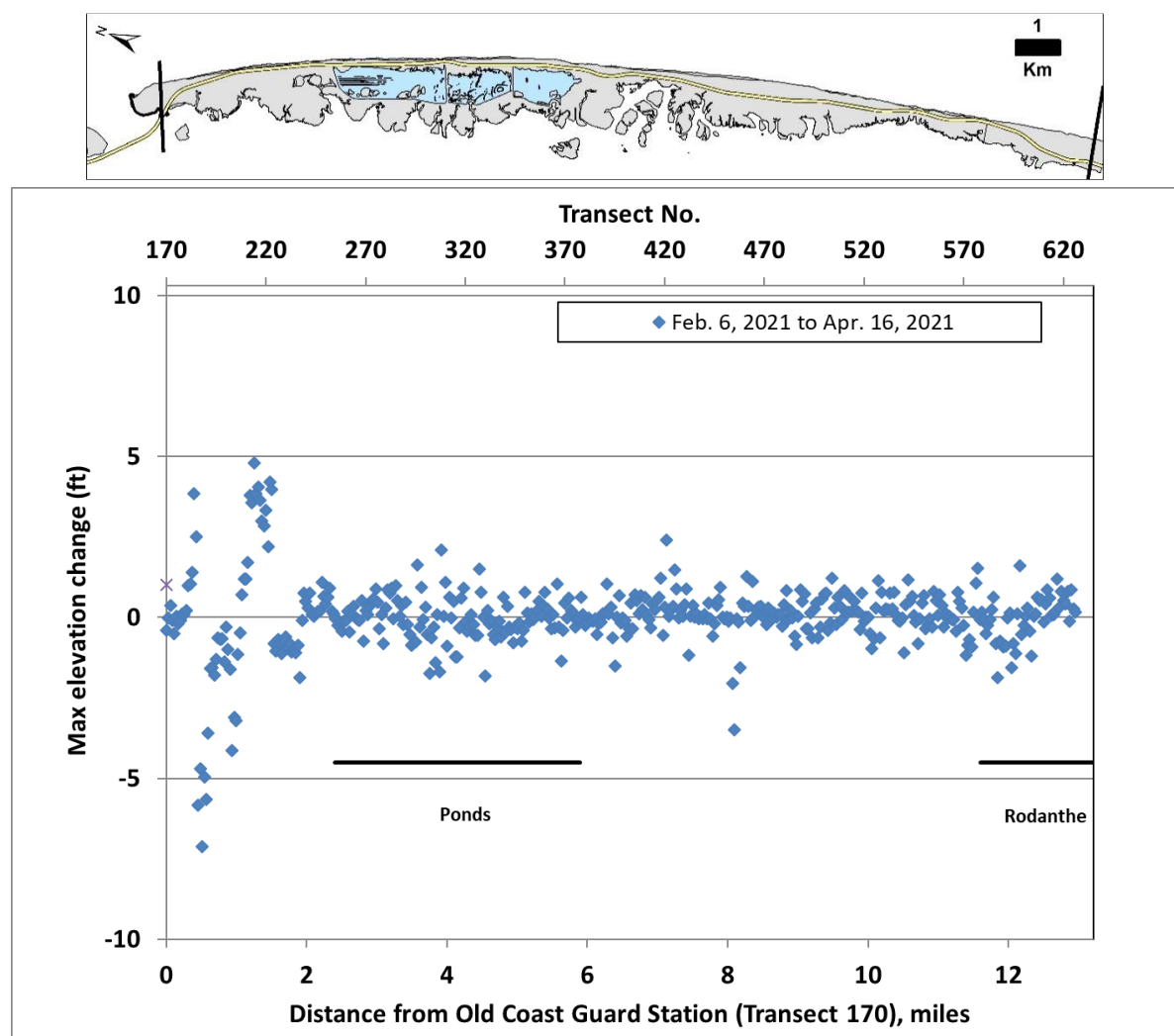
Figure 12. Maximum elevation change from February 6, 2021 to April 16, 2021 at each transect, displayed from north to south along the study area. Note that transects are spaced 150 ft apart.

Changes occurring between April 16 and August 12, 2021 are shown in Figure 13. The average change was 0.85 ft (considering the absolute value of the difference). The largest increase was approximately 2.2 ft near mile 12.3 (Transect 604), and the largest decrease approximately 6 ft near mile 0.85 (Transect 200). It is noted that the region (Canal Zone) that showed high variability in the February-April time period showed an overall decrease during the summer months.
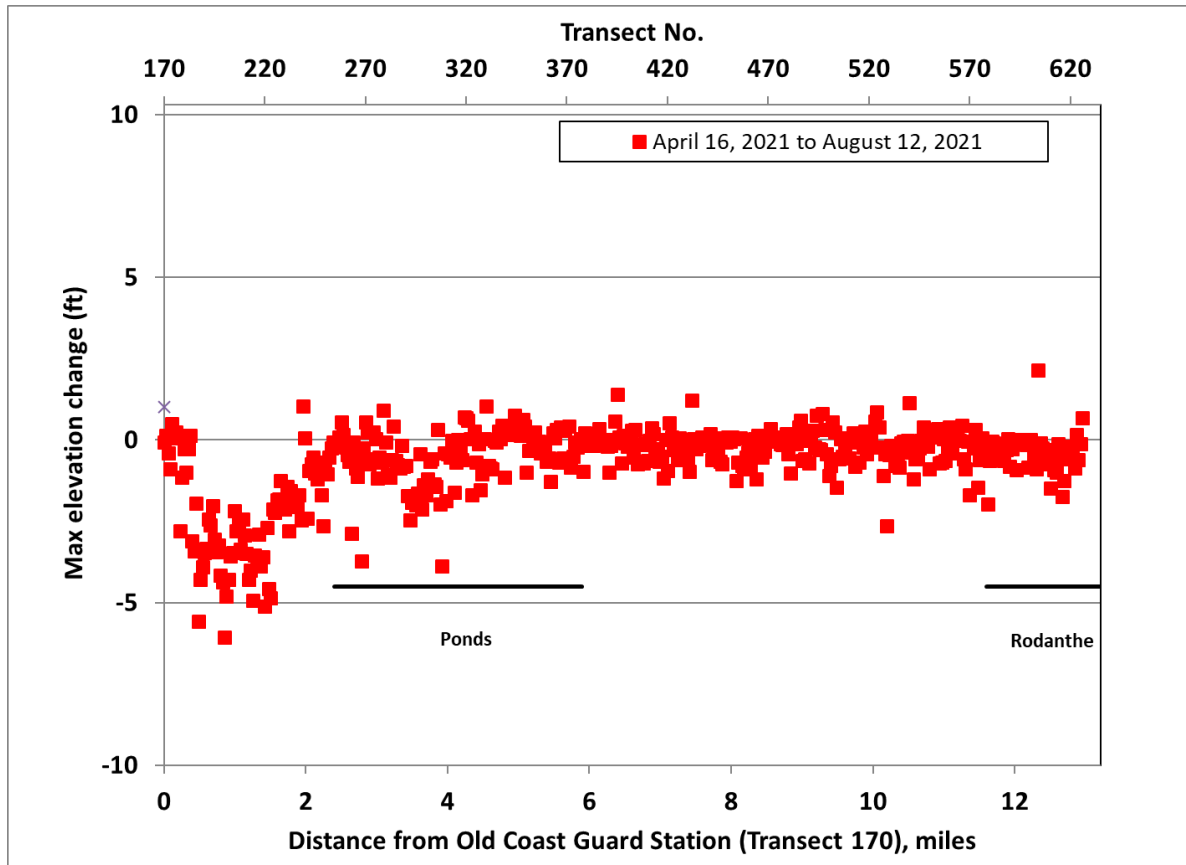
Figure 13. Maximum elevation change from April 16, 2021 to August 12, 2021 at each transect, displayed from north to south along the study area. Note that transects are spaced 150 ft apart.

Changes in maximum elevation from August 12 to September 30, 2021 are shown in Figure 14. This time period had the least observed change during the 2021 study year. Average change during this time period was 0.2 ft. The largest increase was 1.3 ft at Transect 579 (approximately mile 11.6), and the largest decrease was 1.6 ft at approximately mile 1.7 (Transect 228).

23
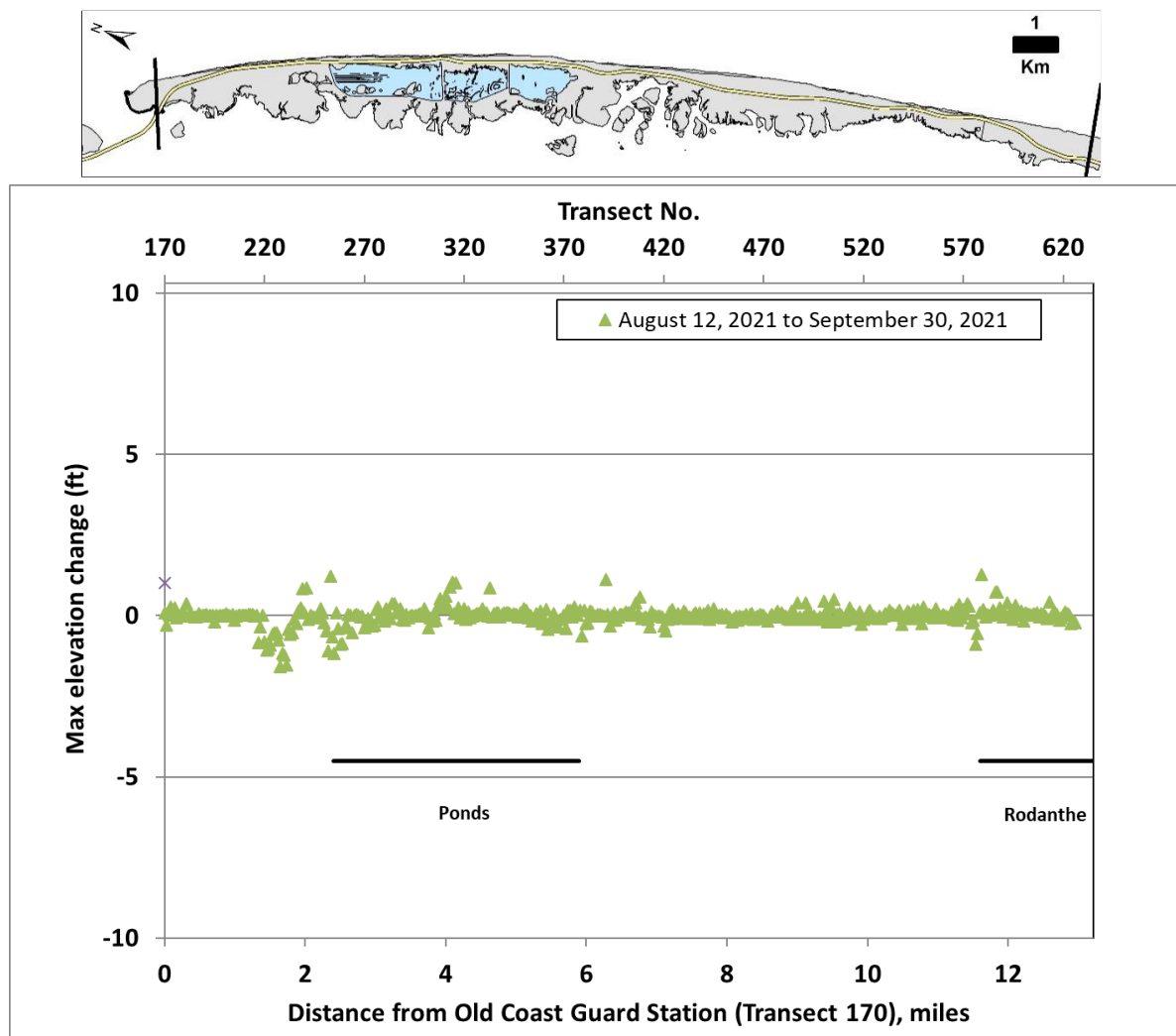
Figure 14. Maximum elevation change from August 21, 2021 to September 30, 2021 at each transect, displayed from north to south along the study area. Note that transects are spaced 150 ft apart.

The combination of wind-blown and water-borne transport and human intervention on the degraded dune field on Pea Island contributes to the high degree of variability observed over the study year, which for 2021 was primarily observed in the Canal Zone where high rates of sand transport and earth moving operations are frequent.

To assess the state of the dunes at the final topographic data collection date of the 2021 study year, the dune crest heights (or simply the maximum elevation along the profile east of the road where no distinct dune was present) along the study area as of September 30, 2021 were plotted (see Figure 15). General trends remain the same as those observed in previous reports. The lowest dunes along the study area are found in three sections: along the Canal Zone and northern side of the freshwater ponds region, adjacent to the Pea Island Breach, and at the south end of the Pea Island National Wildlife Refuge into Rodanthe.

Peak profile elevations (referenced to NAVD 88) ranged from a minimum of approximately 9 ft at Transect 386 adjacent to the Pea Island Breach to a maximum of 43 ft at Transect 482 in a wide dune field about 3 miles north of Rodanthe. As shown in Figure 15, there is a high degree of variability in the maximum elevation at each transect, due to the non-uniform degradation and buildup of the dune system. A 0.5-mile running average is also plotted to illustrate the overall alongshore trend. In the northern six miles of the study area, the average elevation of the dunes ranges from approximately 15 to 25 ft. Just south of the ponds the dunes were removed by the Pea Island Breach in 2011 and are gradually recovering. From miles 7 to 10, most dunes were greater than 20 ft in elevation; moving south from this area toward Rodanthe, the dune field is substantially degraded. In many parts of this stretch a narrow artificial dune was previously constructed over sandbags; these dunes were augmented by a beach nourishment project in August-September 2014, although the area has since returned to pre-project or further eroded conditions. As described in the methodology section, the maximum elevation was compared to the elevation of the road at each transect. The trends are similar to those described in previous reports.
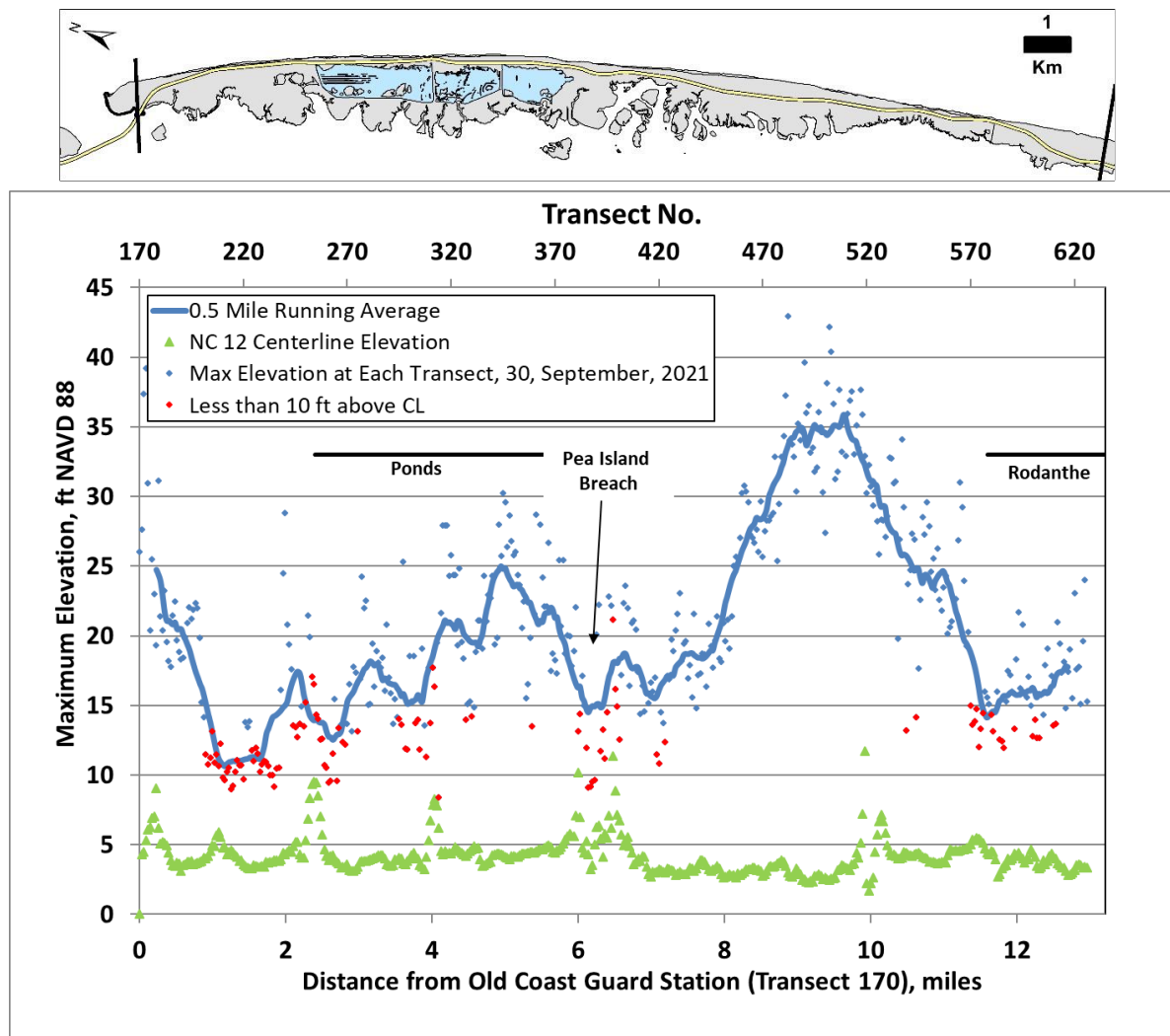
Figure 15. Maximum elevation at each transect, displayed from north to south along the study area for the September 30, 2021 topographic data set. Blue points are > 10 ft above the CL elevation, red points are <= 10 ft above the CL elevation. Note that transects are spaced 150 ft apart.

Dune Toe Position and Elevation

Dune toe position and elevation for the September 30, 2021 topographic data were evaluated. Figure 16 shows the horizontal dune toe position relative to the NC 12 edge of pavement as well as the shoreline and maximum dune elevation position. The position of the shoreline and maximum elevation as of October 5, 2020 are presented as well, for reference. The position of the dune toe is similar to that in 2020, as were the general patterns across the study area. Dunes along miles 1 through 4 and south of mile 11 have been reconstructed multiple times. It is noted that NCDOT is restricted in where and how high the dunes could be constructed due to the location of the current NC 12 highway easement within the PINWR. NCDOT was required to stay within its existing easement unless otherwise authorized. This is why the dunes in these areas are so close to the roadway.
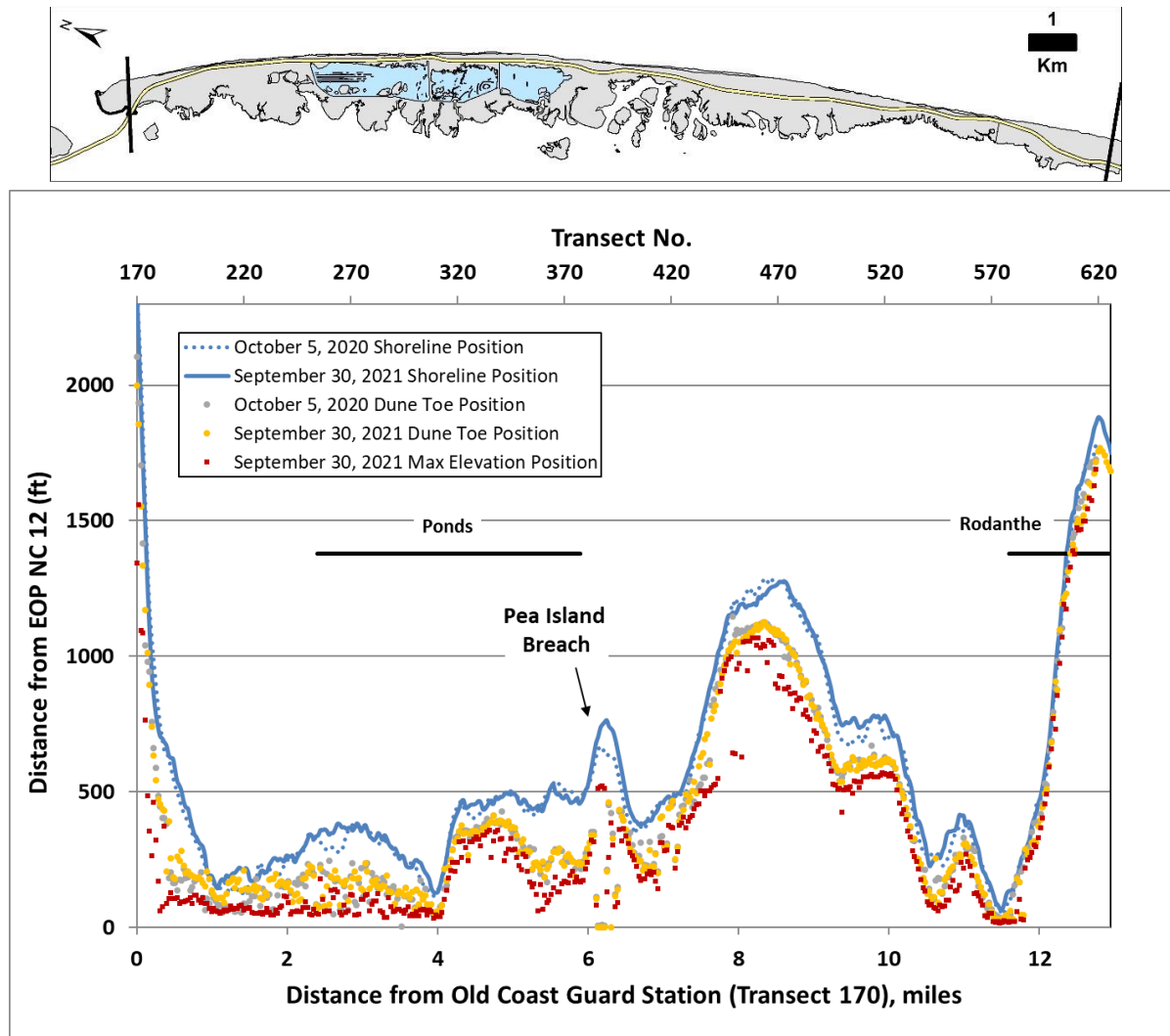
Figure 16. Dune toe, shoreline, and maximum elevation positions as of September 30, 2021, measured as distance from the NC 12 edge of pavement, compared with dune toe and shoreline positions as of October 5, 2020.

Figure 17 shows the elevation of the dune toe as of September 30, 2021, with the NC 12 centerline elevation for comparison as well as the dune toe elevation as of October 5, 2020. The average toe elevation along the study area was 8.9 ft NAVD, about half a foot lower than than the average elevation of 9.5 ft NAVD as of October 5, 2020.
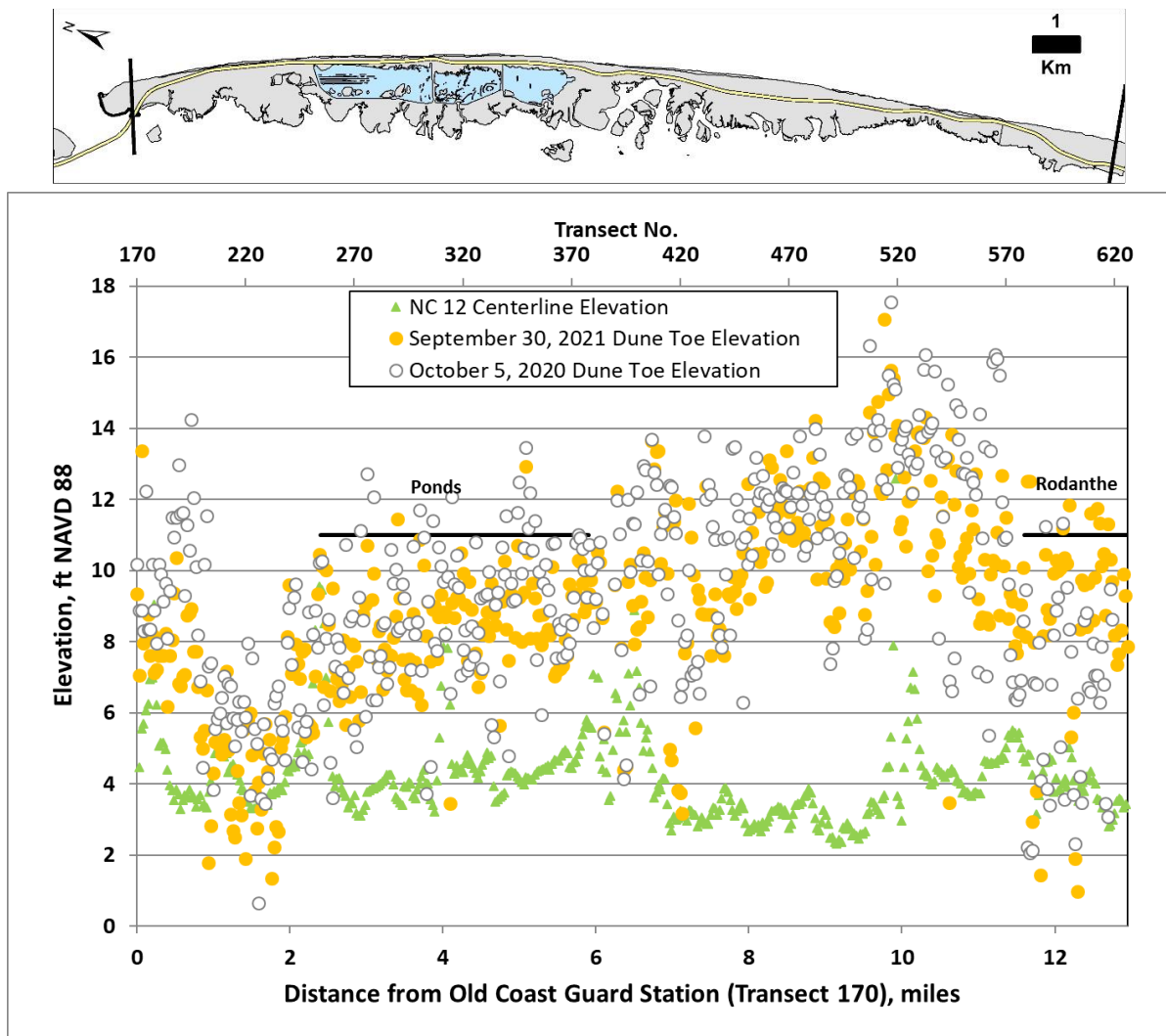
Figure 17. Dune toe elevation as of September 30, 2021, compared with elevation of the NC 12 centerline and dune toe elevations as of October 5, 2020.

Beach Width

Beach width, determined as the distance between the dune toe and ocean shoreline, as of September 30, 2021 is shown in Figure 18, with the beach width as of October 5, 2020 for comparison purposes. As discussed in the methodology section, a beach width of less than 100 ft is considered to increase vulnerability of the dune field to wave impact. In areas where dunes are already degraded, narrow beaches increase the likelihood of further dune erosion and/or overwash. In 2021, 121 transects had beach widths less than 100 ft; in 2020, this number was 181. The average beach width across the study area as of September 2021 was 150 ft, whereas in October 2020 it was 142 ft, and in October 2019 it was 130 ft. The pattern of beach widths as of September 30, 2021 was similar to that from the 2020 report. At this point in time, seven years after placement, the beach width in the area of the Rodanthe beach nourishment project is narrower than pre-project conditions. This was expected as the project was designed to mitigate erosion for three years (see the 2014 Report for further details on the project).

28
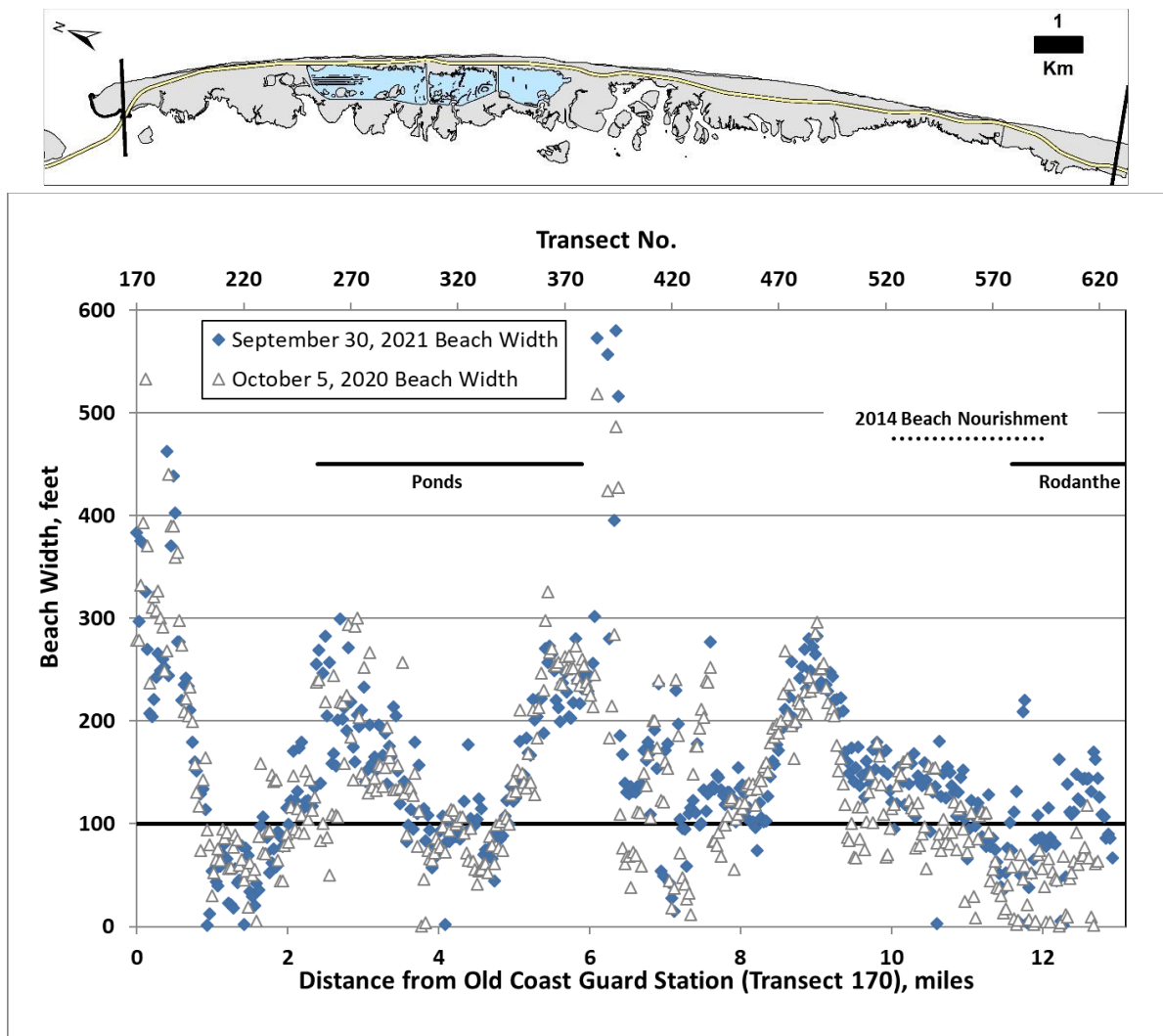
Figure 18. Beach width as of September 30, 2021 (blue), compared with beach width on October 5, 2020 (gray).

Beach Volume above MHW from EOP to Shoreline

The changes in beach volumes above MHW from October 5, 2020 to September 30, 2021 are presented in Figure 19. The volume per unit distance alongshore from the NC 12 EOP to the MHW elevation was computed at each transect. The numbers reflect both dune size and the distance from the road to the shoreline. Also included on the figure is the comparison between October 1, 2019 to October 5, 2020. When the two change rates are compared, it is noted that in several places a loss from 2019 to 2020 is mirrored by a gain from 2020 to 2021 or vice versa. The beach volume data inherently reflect variability due to storm impacts and recovery. It is noted that as detailed in the 2019 Report, Appendix B, there was a change in the edge of pavement reference line for the volume computations in 2019; some of the volume changes from 2018 to 2019 were attributed to this reference change. From transects 376 to 404, the EOP shifted west, causing an average increase of 3.2 cy/ft in that area, and from transects 513 to 526, the EOP shifted east, causing an average decrease of 4.6 cy/ft at those transects.
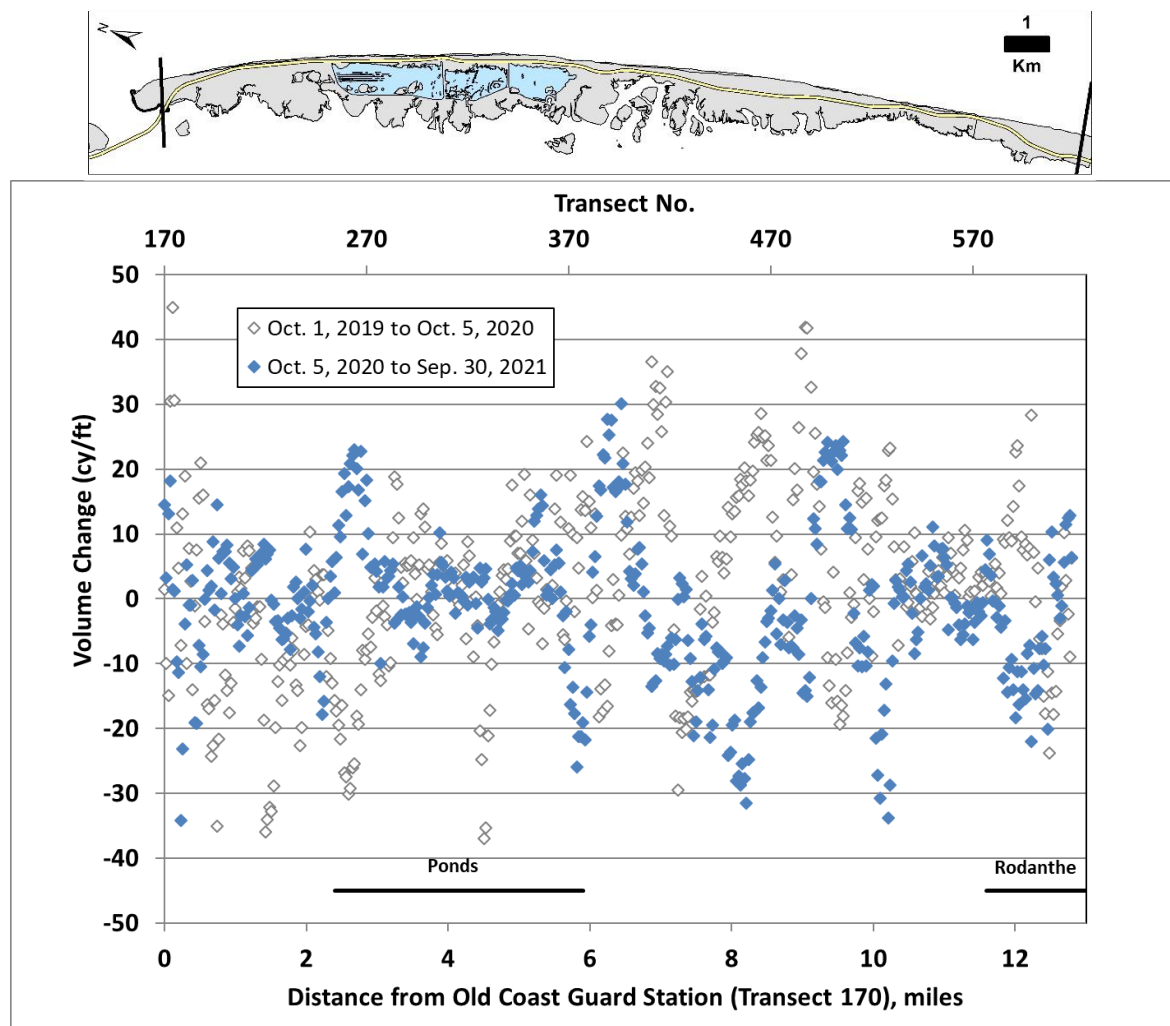
Figure 19. Changes in volume from October 2020 to September 2021, measured from the NC 12 EOP to the shoreline above the MHW elevation (displayed from north to south along the study area). Changes from October 2019 to October 2020 are also shown for reference.

The alongshore profile volumes observed in the region of the beach nourishment project (southern PINWR/ northern Rodanthe) from pre-project, post-project, at the end of 2020 and for dates during 2021 are shown in Figure 20. Volume changes between pre-project and post-project (April 2, 2014 and October 9, 2014) were on the order of 20-35 cy/ft increases in the sub-aerial volume alongshore for the main part of the project. From October 9, 2014 to February 4, 2015 there were some initial losses on the order of 10 cy/ft, after which the volumes remained relatively stable until October 2015 when volumes returned to near pre-project levels; this volume loss was thought to be due to the weather conditions immediately prior to the October 2015 data collection. By April 10, 2016, the area had recovered an average of 17 cy/ft with profile volumes similar to August 2015. From April to August 2016 average profile volume had decreased by about 8 cy/ft. In October 2016, the volumes had again decreased to

values similar to those in October 2015, likely due to effects of Hurricane Matthew. By February 2017, the area had recovered an average of 9 cy/ft, and by April had accumulated another 4 cy/ft on average. The profile volume remained relatively stable between April and early September. After the passage of Hurricanes Jose and Maria in mid to late September, the area had lost an average of 4 cy/ft as of October 2017. The volumes in the area of the beach nourishment project remained relatively stable in 2018. As of November 2018, about 14 cy/ft on average remained in the study area as compared to the April 2014 pre-project conditions. The northern area remained relatively stable in 2019, with additional losses observed just north of Rodanthe near Mile 11.5-12. As of October 2019, about 8.6 cy/ft on average remained in the study area as compared to the April 2014 pre-project conditions. In 2020, profile volumes increased in the northern part of the beach nourishment area, remained relatively stable near mile 11.5, and increased slightly towards Rodanthe. As of October 2020, an average of 14.2 cy/ft more than the April 2014 pre-project conditions remained in the study area. During 2021, the northern part of the nourishment area decreased in volume, while the rest of the study area remained relatively stable. From mile 11.4 to 12.0 the volume remained similar to pre-project conditions. As of September 2021, an average of 11 cy/ft more than the pre-project condition remained in the study area, primarily in the northern portion.

To compare volumetric conditions across the entire study area since the inception of the coastal monitoring program, a comparison of total sub-aerial volume change between the edge of pavement and the shoreline is shown in Figure 21. Dates of sand placement (2013 dredge material disposal near Oregon Inlet and the 2014 beach nourishment project) and significant storms are also indicated. The total volume was calculated by multiplying each of the profile volumes by 150 ft (the distance between the profiles) and summing the total across transects 170 to 626. Significant events affecting the volumes are highlighted by vertical red lines (Hurricane Irene, Hurricane Sandy, the October 2015 "Joaquin-easter" event, Hurricane Matthew in October 2016, Hurricanes Jose and Maria in September 2017, Winter Storm Riley and Hurricane Florence in 2018, Hurricane Dorian in 2019, Hurricane Isaias in 2020, and a severe nor'easter in November 2021. As of September 30, 2021, there was an estimated approximately 1.3 million cubic yards less volume between the road and the shoreline than there was under baseline conditions (January 2011).
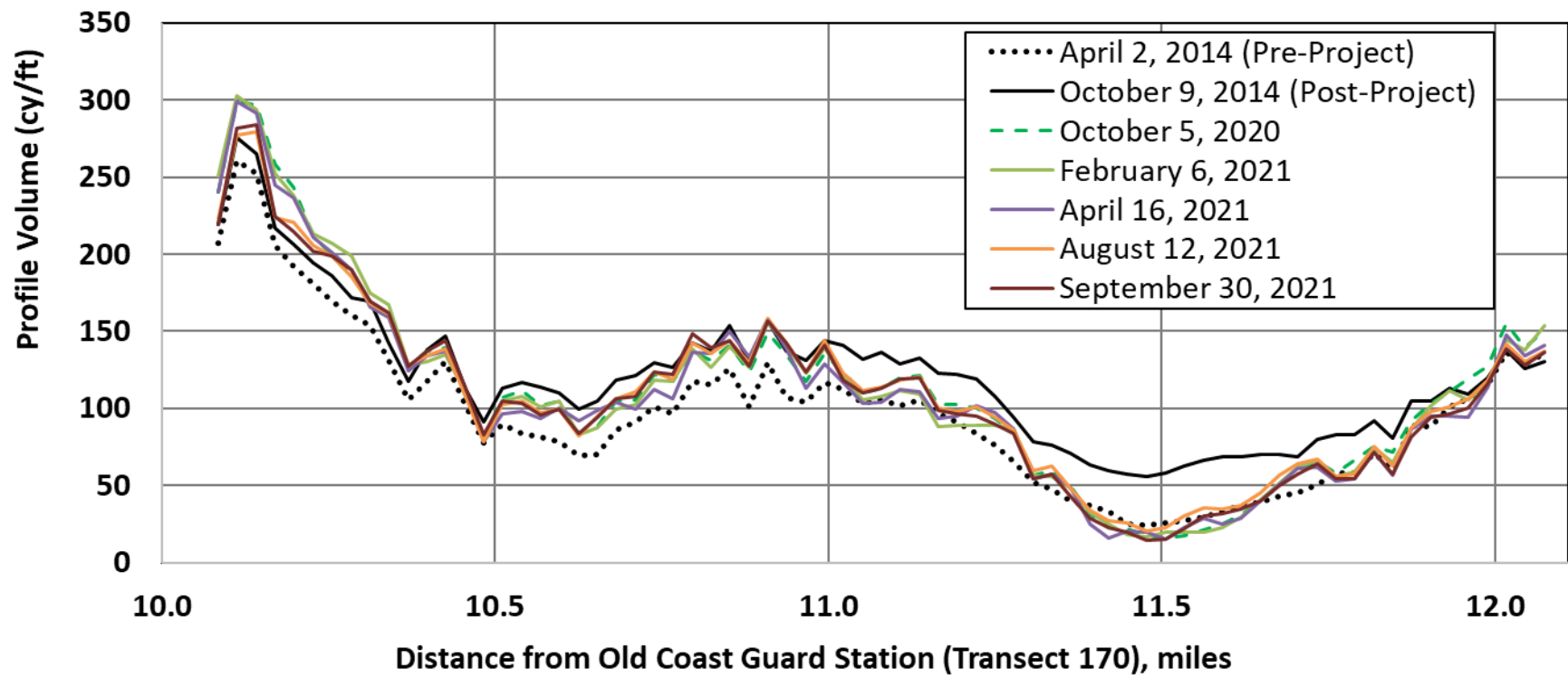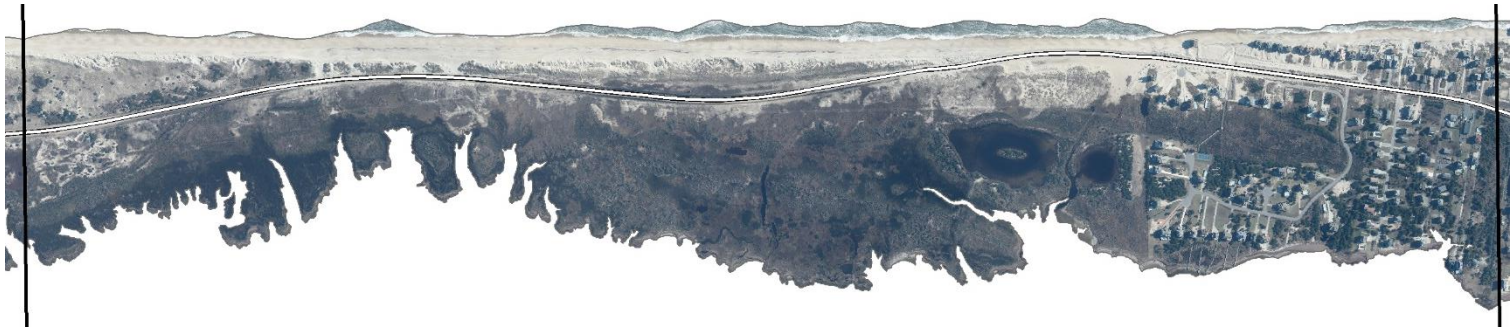
Figure 20. Profile volume from edge of pavement to shoreline, above the MHW elevation, by transect in region of the beach nourishment project.
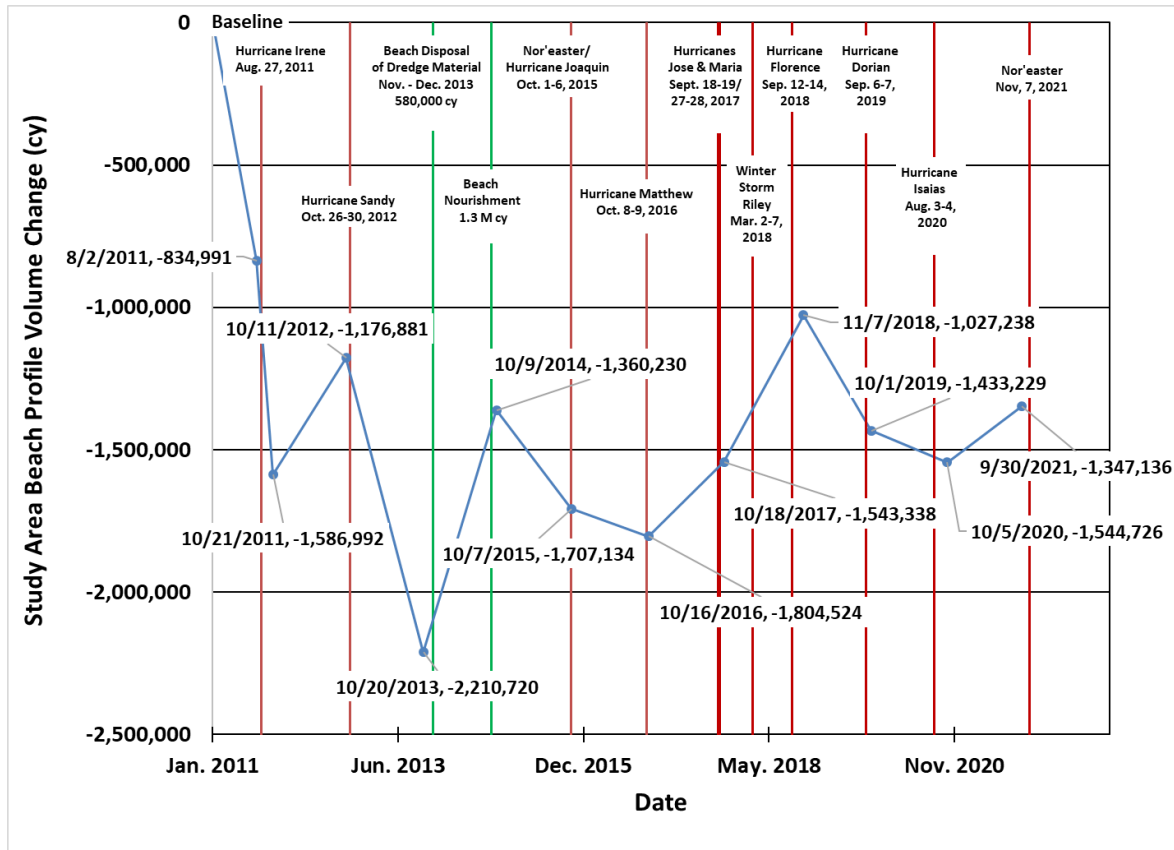
Figure 21. Total beach volume change (EOP to shoreline) across the study area, with respect to baseline conditions.

To assess conditions as of the last available topographic data of 2021, the computed volumes for September 30, 2021 are presented in Figure 22 with the running average of dune height included for comparison. The minimum measured value was approximately 15 cy/ft at Transect 574 at mile 11.5 north of Rodanthe. The average volume from the edge of pavement to the shoreline in September 2021 was approximately 166.5 cy/ft (in 2020 it was 166.2 cy/ft). Low values along the Canal Zone and freshwater ponds sections reflect the smaller dunes as well as the proximity of the road to the shoreline. From miles 7 to 10 the larger volumes correspond with higher dunes and the position of NC 12, which is set back further from the shoreline. In general, the spatial variation in profile volumes are similar to those observed in previous reports.
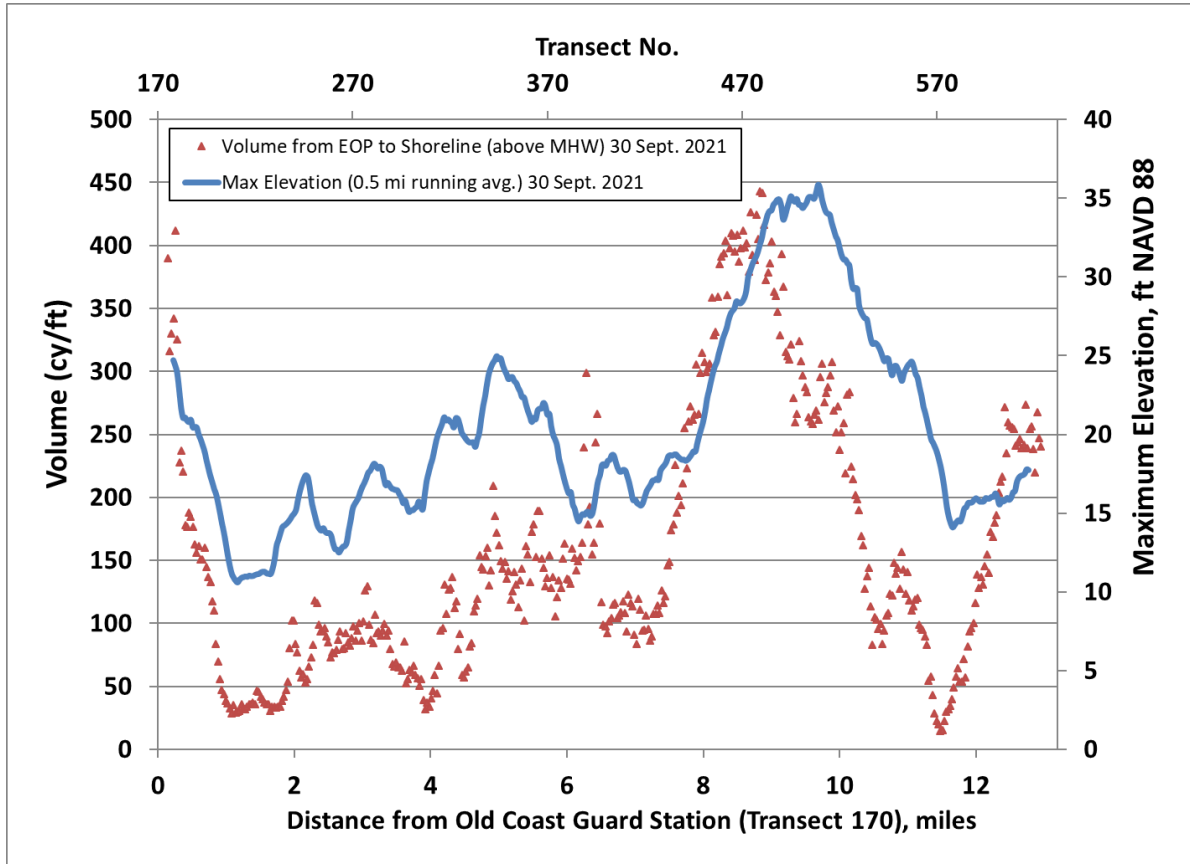
Figure 22. Computed volume as of September 30, 2021, from the NC 12 edge of pavement (EOP) to the shoreline above the MHW elevation displayed from north to south along the study area. The volume follows a trend similar to the running average of the maximum dune crest height, also shown.

Land Cover/Habitat Mapping

Results of the land cover/habitat mapping efforts are presented in this section. Table 5 and Figure 23 show the total areas in acres each year from 2012 to 2021. Overall, marsh is the dominant habitat in PINWR, followed by managed wetlands, shrub, bare sand dune and beach. The variation of total area is, for the most part, a consequence of variation in ocean shoreline positions. Figure 24 shows the mapping for 2020 and 2021.

Table 5. Area (acres) for each habitat class from 2012 to 2021

Class	2012	2013	2014	2015	2016	2017	2018	2019	2020	2021
Bare Sand	154.4	211.8	175.8	181.2	129.9	108.2	140.2	106.5	151.3	133.7
Estuarine Pond	65.3	70.0	61.7	83.0	77.4	67.8	77.5	81.8	117.9	99.4
Salt Flat	168.7	232.8	177.1	163.1	169.7	216.4	140.4	93.9	81.2	93.3
Shrub	534.0	361.6	404.0	388.1	579.1	620.8	403.8	308.2	386.7	472.3
Marsh	1932.2	2143.0	2123.4	2173.5	1992.4	1979.5	2162.9	2300.1	2094.2	2023.6
Vegetated Dune	167.4	104.0	141.2	121.3	129.9	136.2	122.3	158.2	146.7	195.2
Bare Sand Dune	284.9	318.7	277.6	310.9	288.9	284.7	282.2	243.7	250.0	200.8
Infrastructure	43.0	42.8	42.8	51.4	50.0	56.3	46.8	51.4	53.6	52.4
Maritime Brush	139.5	97.1	116.7	123.9	129.4	126.9	102.4	122.5	118.3	118.1
Managed Wetland	792.2	784.6	783.5	781.3	779.7	778.9	781.5	778.8	772.8	767.6
Beach	264.6	283.1	238.2	279.0	265.2	288.7	280.1	249.0	151.0	236.0
Groin	4.6	4.6	4.4	4.4	4.2	4.2	4.4	4.3	4.2	4.1
Total	4550.9	4654.0	4546.5	4660.9	4595.7	4668.6	4544.5	4498.2	4328.1	4396.5
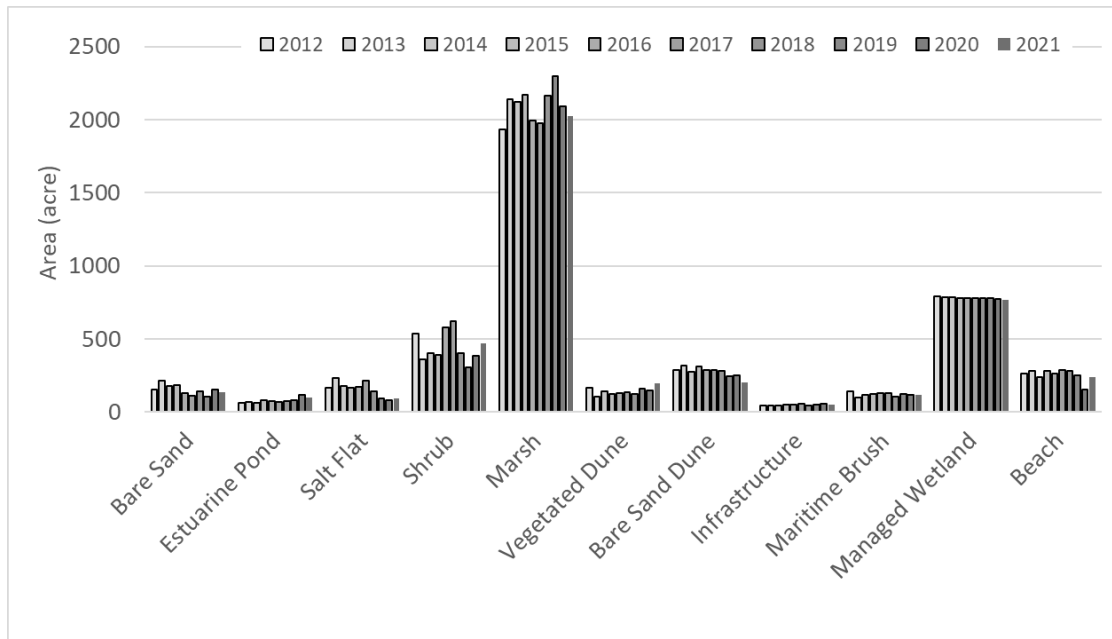
Figure 23. Area for each habitat class from 2012 until 2021
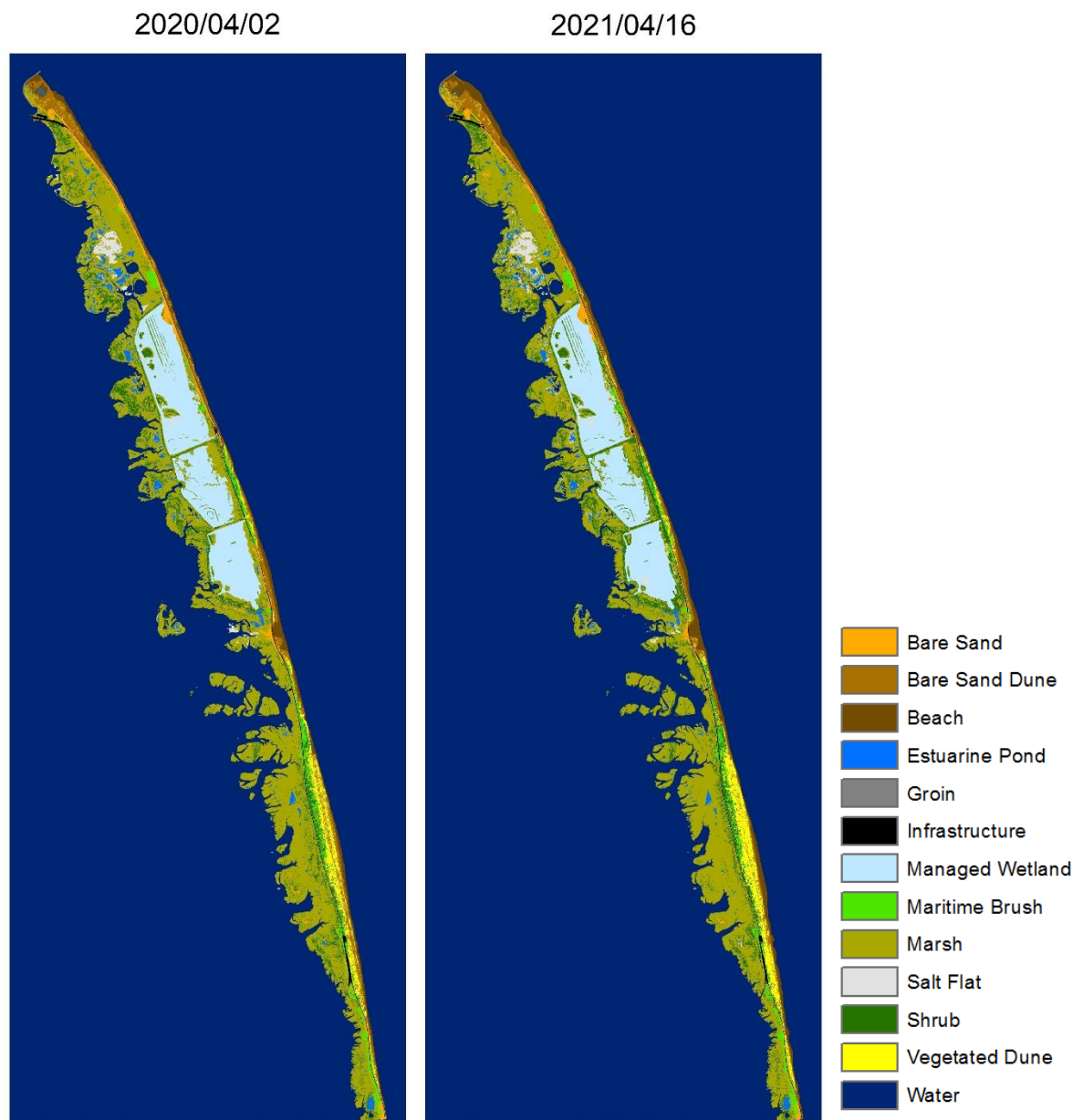
Figure 24. Habitat maps for 2020 and 2021

Evolution of habitat classes is highly variable and dependent on physical, biological, and management factors. Figure 25 shows linear trends for each habitat class. It should be noted that most habitats do not display a linear behavior, however, these trends provide a general idea of whether a given habitat class tends to increase or decrease over time. All classes with the exception of estuarine pond and infrastructure experienced significant changes between 2012 and 2013; this is a consequence of the effects of Hurricane Sandy on the island. Other abrupt changes in bare sand, salt flat, shrub, marsh, and maritime brush occurred between 2017 and 2018. The potential cause for the latter changes are three storms that impacted the Outer Banks in that period, including Hurricane Jose and Maria in mid and late September 2017 and Winter Storm Riley in March 2018, just a few weeks before the CIR image was taken.

Between 2018 and 2019, an increase in marsh was observed in contrast to a decrease in shrub. This is attributed to controlled burn management activities in areas with high shrub density. During the April 2020 imagery, the water levels were elevated due to an ongoing nor'easter, which is reflected in the decrease in beach and total island area. Estuarine ponds also increased sharply in 2020 as salt flats decreased, at least partly due to the elevated water levels. By 2021, the beach had recovered due to water levels being back to normal conditions. Marsh decreased with a corresponding increase in shrub.

The panel in the bottom left corner of Figure 25 shows the total area of the island computed as the sum of all classes different from water. The annual variability in this plot is primarily caused by the variability of the ocean shoreline position, which shifts depending on short-term storm impacts (erosion) and recovery (accretion) as well as on the water level when the images were taken. The data indicates that in the past nine years the area of the island has varied between approximately 4,300 to 4,700 acres. However, such variation follows a cyclical pattern that does not confirm gain or loss of the island's horizontal area. The total horizontal area of dunes (vegetated + bare sand dune) has been decreasing over time from 450 acres to near 400 acres. The observed behavior of each habitat class from 2012 to 2021 is described below:

- Bare Sand: Overall decreasing trend, significant increase after major ocean-side storms.
- Estuarine Pond: Highly variable with generally increasing trend. The number of enclosed bodies of water and their spatial extent depends on the water levels, rainfall, and the water table when the images were taken.
- Salt Flat: Also highly variable and dependent on water levels. Linear trend indicates a decrease over time; much of this is due to vegetation of the emergent salt flats adjacent to the Pea Island Breach.
- Shrub and Marsh: These two classes display an inverse behavior and linear trends for marsh indicates slight increase, shrub stable to slight decrease.
- Dune: Bare sand dune has a decreasing trend. Vegetated dune has a stable linear trend but fluctuations are observed. As expected, both classes show a strong sensitivity to ocean-side storms.
- Groin: Changes in groin area are a result of sand deposition over the structure and varying water levels. Overall, groin area visible in the photography has remained within 4.1 and 4.6 acres.
- Infrastructure: Increase from 2012 until 2017 due to the construction of the Basnight Bridge in the north and other NC 12 improvements near Pea Island Breach. Although the linear trend indicates increase in infrastructure over time, the data point in 2018 reflects less construction areas on the island due to completion of two bridge projects. Continued work on the Rodanthe bridge slightly increased infrastructure in 2019 and 2020, as the bridge neared completion there was a slight decrease in infrastructure in 2021.
- Maritime Brush: Depicts vegetation growth in overwash fans and the landward side of the dunes. Significant decrease after ocean-side storms with recovery generally within a year.
- Managed Wetlands: Slight decreasing trend. From 2012 to 2021 lost over 20 acres, most of that area was lost to overwash fans from ocean-side storms that reached the ponds.
- Beach: Highly variable and dependent on storm activity and water levels. 2020 data shows a large decrease in beach area primarily due to the observed elevated water levels in April 2020. April 2021 water levels were more normal conditions showing a rebound in beach area.
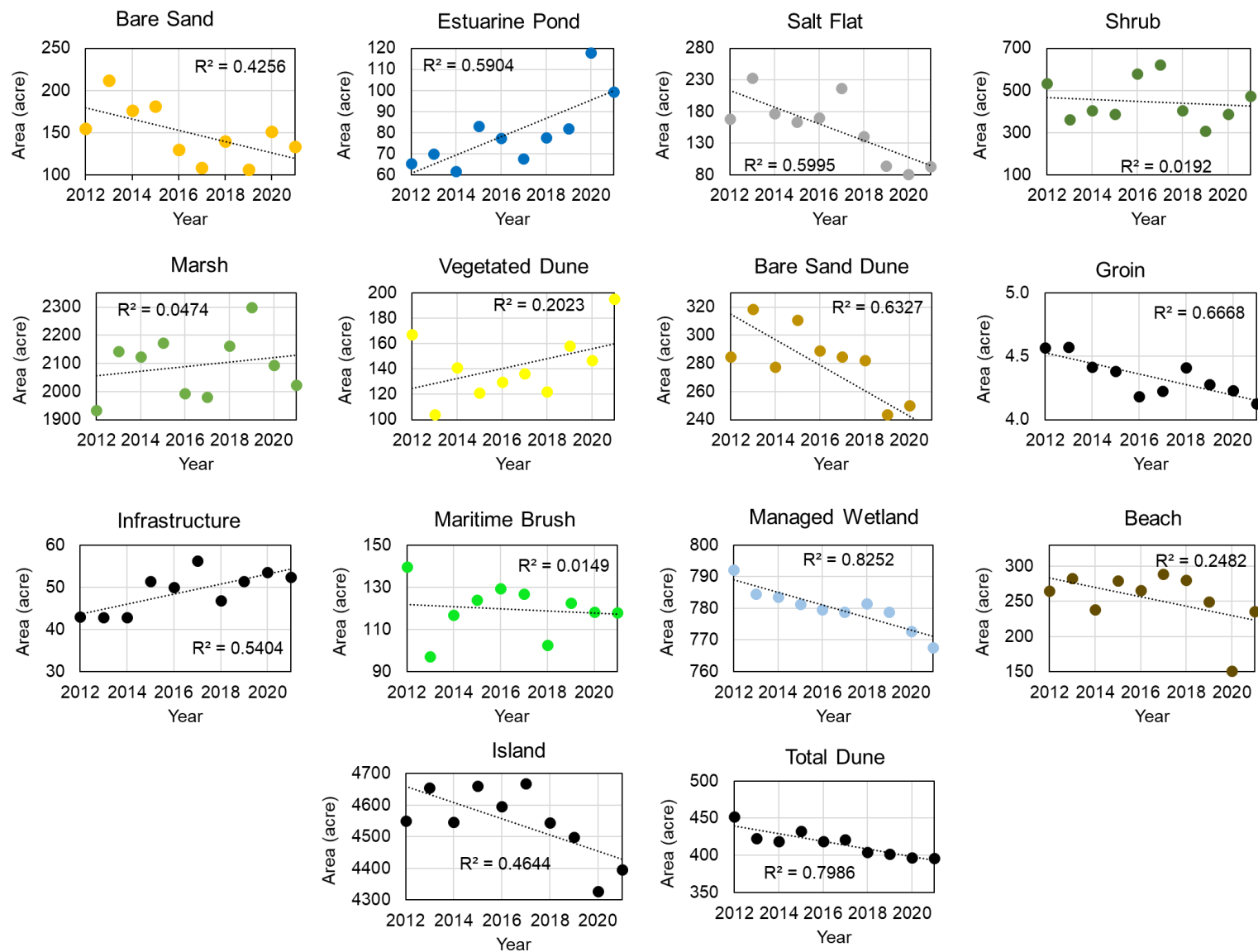
Figure 25. Linear trends for each habitat class.

A change matrix was created to identify changes from one habitat class to another from 2020 to 2021 (Figure 26). (Details of changes between prior years are found in Appendix B of the 2018 report and in the body of the 2019 and 2020 reports). Green cells in the diagonal of the matrix indicates the stable areas that remained within the same habitat. Warm colors indicate different levels of change with the most significant habitat changes (> 50 acres) in red cells.

The largest changes were from marsh to shrub, shrub to marsh and from water to beach. The shrub to marsh and marsh to shrub changes are attributable to succession and some management activities (controlled burns which reduce shrub, see Appendix B for burn areas and dates). The beach to water changes are attributed to the fact that there was an elevated water level condition in the April 2020 imagery which resulted in an apparent 'loss' of beach (108.86 acres from 2019 to 2020); the April 2021 imagery then showed a 'gain' of 98.35 acres from 2020. Overall from 2019 to 2021, there was a net loss of 10.51 acres of beach (converted to water).

.

2020 \ 2021	Bare Sand	Estuarine Pond	Salt Flat	Shrub	Marsh	Vegetated Dune	Bare Sand Dune	Water	Groin	Infrastructure	Maritime Brush	Managed Wetlands	Beach
Bare Sand	93.68	0.08	0.97	5.79	32.00	1.30	1.52	0.65	0.00	1.02	14.21	0.05	0.02
Estuarine Pond	0.13	89.73	15.12	0.32	8.03	0.00	0.00	3.14	0.00	0.00	0.09	0.01	1.28
Salt Flat	0.45	2.61	45.98	2.29	14.71	0.00	0.00	13.92	0.00	0.00	0.52	0.70	0.00
Shrub	1.25	0.04	0.26	241.47	134.15	2.04	0.21	0.03	0.00	0.07	6.81	0.17	0.02
Marsh	22.25	6.68	24.34	190.37	1828.74	0.00	0.00	12.50	0.00	0.68	6.20	1.72	0.17
Vegetated Dune	0.20	0.00	0.00	10.55	0.00	117.23	16.22	0.00	0.00	0.00	1.76	0.00	0.67
Bare Sand Dune	6.58	0.00	0.00	1.30	0.00	70.15	161.78	0.03	0.00	0.00	0.51	0.00	9.55
Water	0.20	0.18	0.28	0.11	3.36	0.00	1.20	27542.50	0.06	0.00	0.00	0.00	98.35
Groin	0.00	0.00	0.00	0.00	0.00	0.00	0.00	0.17	4.06	0.00	0.00	0.00	0.00
Infrastructure	1.33	0.00	0.00	0.60	1.07	0.00	0.00	0.02	0.00	50.56	0.04	0.00	0.00
Maritime Brush	6.84	0.06	0.00	19.28	0.14	3.71	0.30	0.00	0.00	0.00	87.92	0.00	0.00
Managed Wetlands	0.04	0.06	6.37	0.19	1.26	0.00	0.00	0.00	0.00	0.00	0.00	764.91	0.00
Beach	0.75	0.00	0.00	0.03	0.15	0.74	19.57	3.85	0.00	0.00	0.00	0.00	125.93

No change in class | Area (Acre): | < 0.1 | 0.1 - 1 | 1 - 10 | 10 - 50 | > 50

Shrub to Marsh

Water to Beach

Marsh to Shrub

0   1   2 Miles
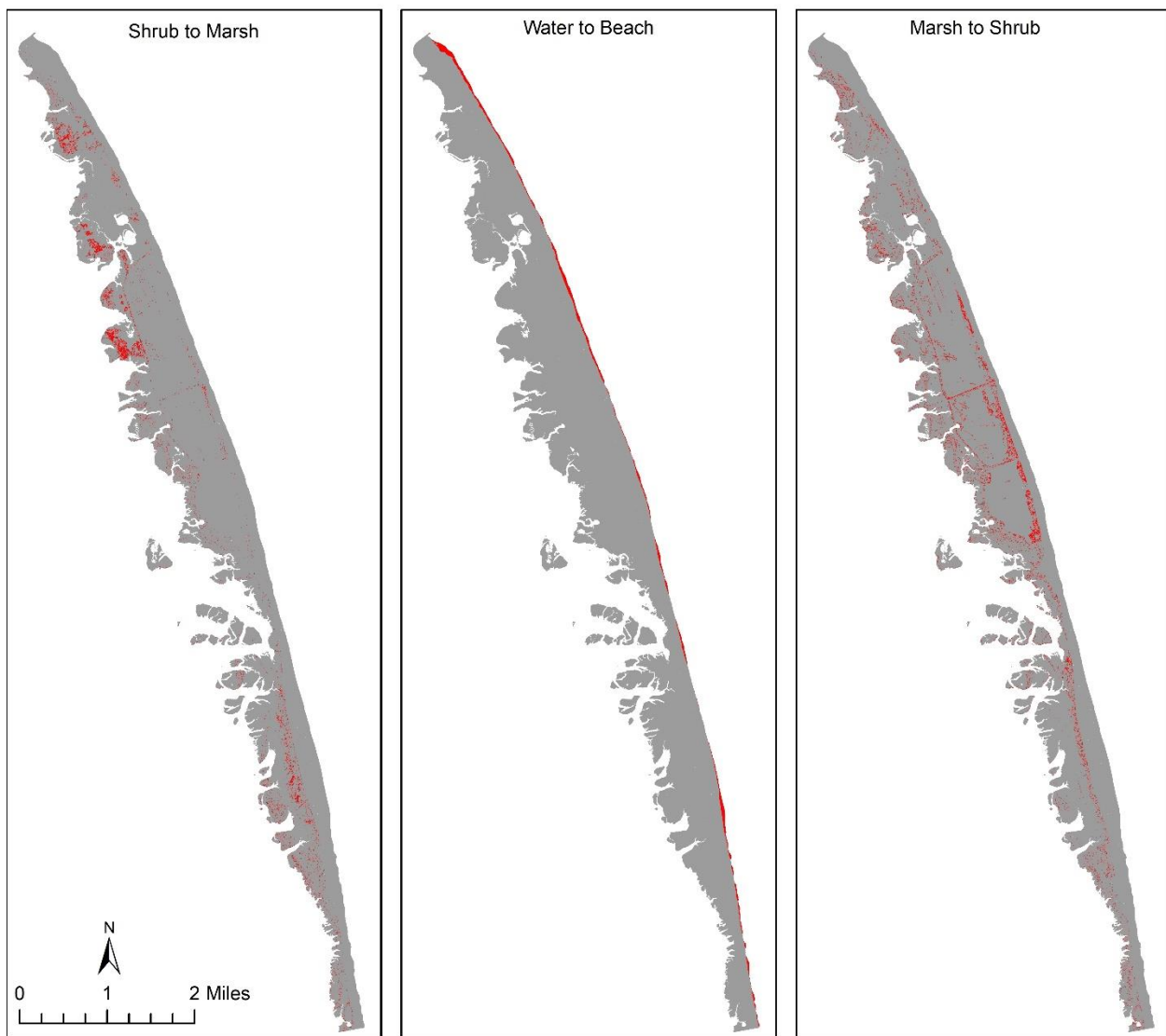
Figure 26. Habitat changes from 2020 to 2021. Top: Change matrix. Bottom: Spatial distributions of the three larger habitat changes enclosed in bold rectangles in the change matrix are shown in red.

Erosion Rate Update

With the recent shoreline position data from 2021 through February 2022 (this date was used because there was no December 2021 flight) added, the linear regression long-term shoreline change rates for the study area changed very little from the 2020 update conditions, as shown in Figure 27. Note that in this figure, "positive" shoreline change rates indicate erosion. In order to see more clearly the trends since the Baseline Report (conditions as of January 2011), Figure 28 shows each of the erosion rates reported yearly since December 2011. While the rates have not changed significantly year to year, it is apparent that there are some trends in the changes. In the first mile, while accretion has been present, the rates of accretion have been decreasing. In the Canal Zone, rates of accretion have been transitioning to rates of erosion (generally less than 2 ft/year). Over the remainder of the study area, trends have remained similar since the Baseline Report, with an average slight decrease in the rates of erosion in most areas. An accretionary area near Transect 470 has shifted slightly to the south over the past three to four years.
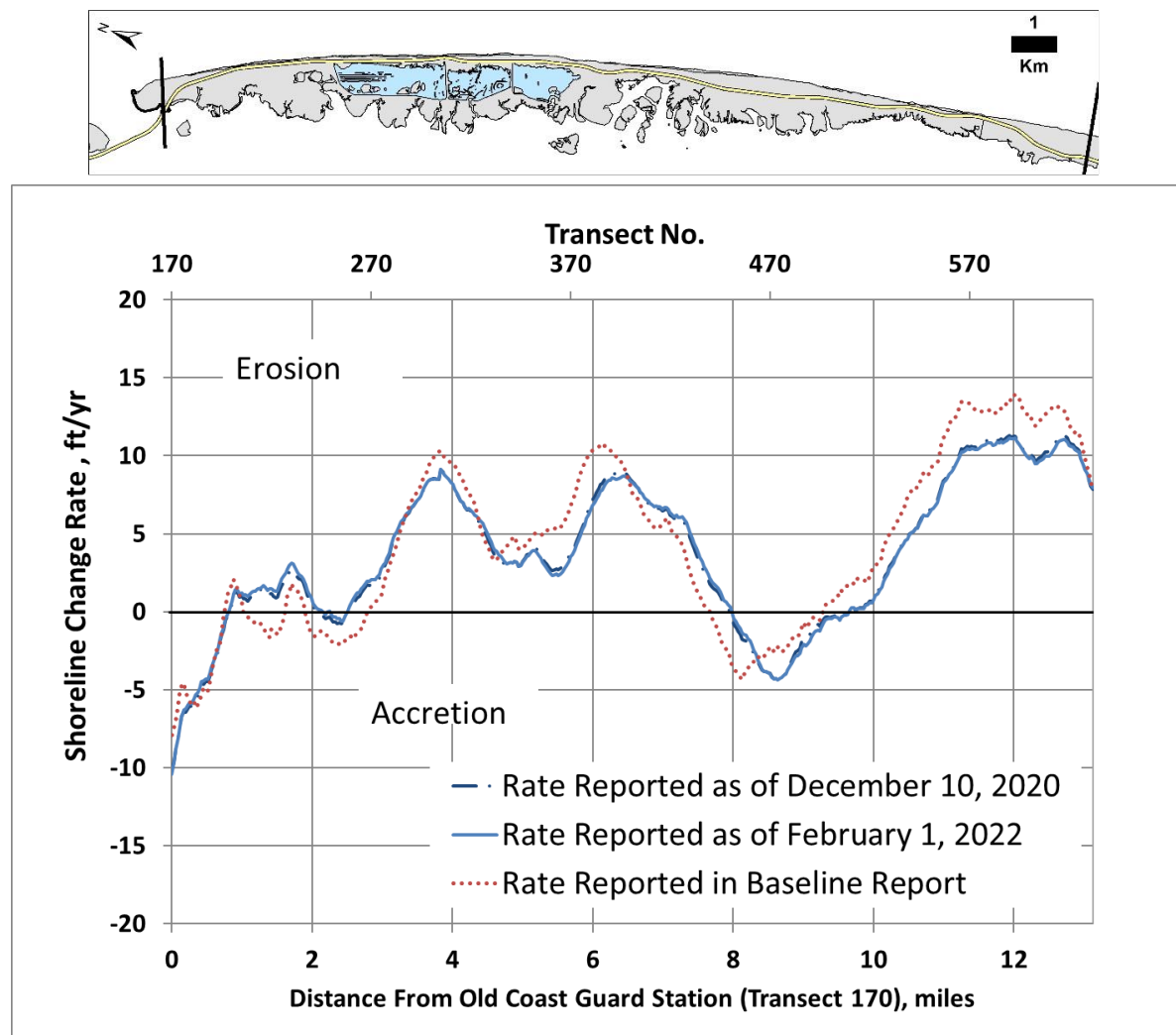
Figure 27. Updated erosion rates through February 1, 2022, compared with 2020 update conditions (as of December 10, 2020) and baseline report conditions.
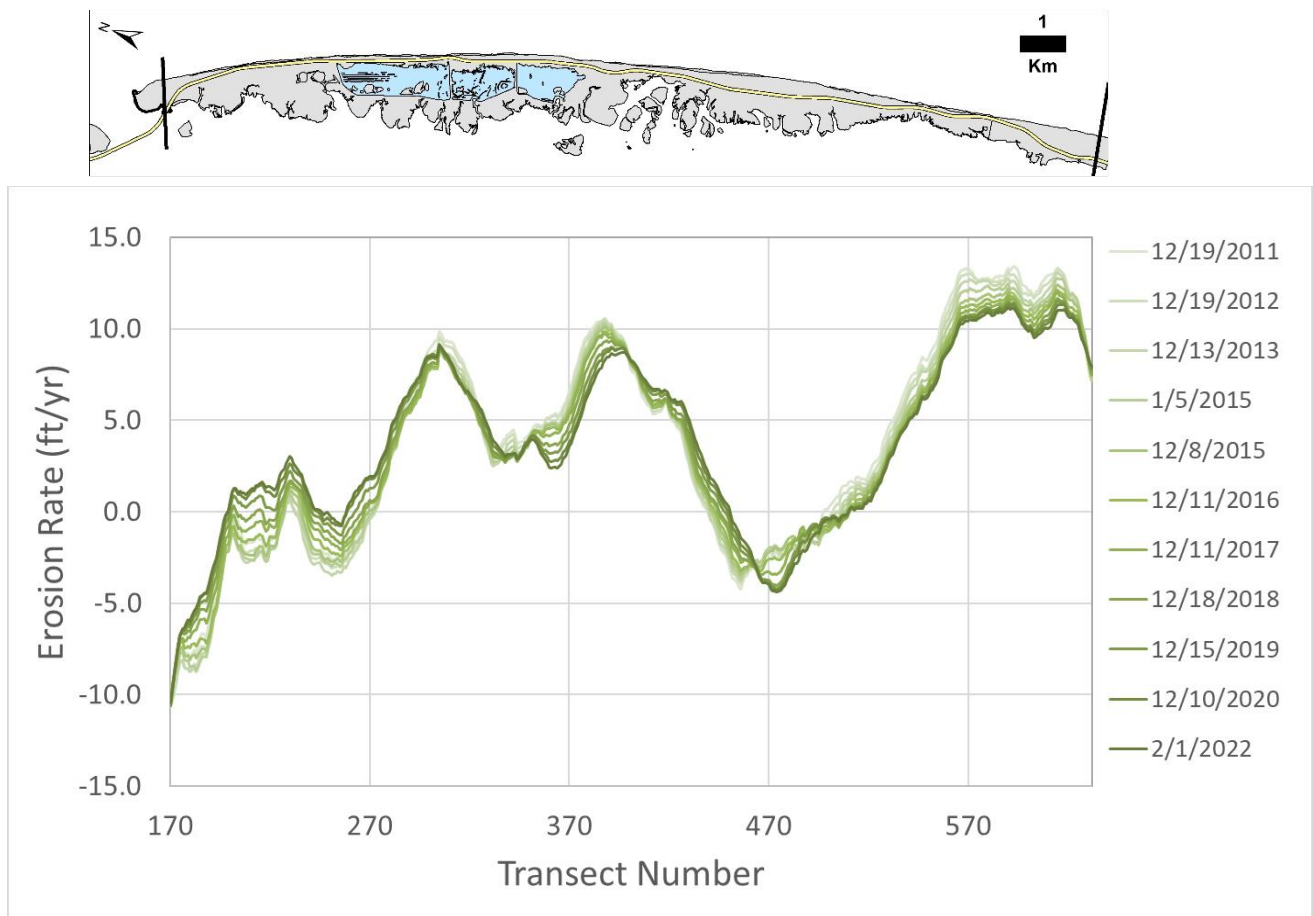
Figure 28. Erosion rate changes from December 2011 to February 2022.

Critical Buffer and Vulnerability: Present and Future

Baseline and 5-Year Vulnerability

Figure 29 to Figure 34 illustrate the location of the 230-foot buffer offset from the NC 12 edge of pavement at the conclusion of the 2021 study year. Because there was no photography in December 2021, the photography dated February 1, 2022 is used to represent the conditions at the conclusion of the 2021 study year. The lengths of NC 12 where the shoreline falls within this buffer or would be expected to fall within the buffer within 5 years, using the linear regression predicted average position, are highlighted on these maps. The average predicted position is used for the 5-year forecast to provide an indication of the areas most likely to be immediately impacted. It is noted that if the 5-year forecast from the present report (2026) is compared to 2020 forecast maps from early reports, vulnerable areas are substantially longer in the prior 2020 forecast maps than those shown on the current (2021) and 5-year (2026) vulnerability maps. This is due to the inclusion of the prediction interval bands (i.e., the "worst-case" high-erosion shoreline position) on the previous 2020 maps. This essentially shows the

uncertainty associated with the shoreline prediction, which makes the potentially vulnerable section larger.

Areas of current and 5-year vulnerability as determined by the 230-foot buffer include a section along the Canal Zone, a section in the middle of the freshwater ponds stretch near the PINWR visitors center, a narrow region just south of the wide dune field area, and along the shoreline segment just north of and into Rodanthe. The lengths of the vulnerable sections shown on the maps are presented in Table 6.

The section termed A in Table 6 and Figure 29 was identified as vulnerable in the 2020 report, and the length of the vulnerable area has increased by 489 ft since that report. Section B identified in Table 6 and Figure 30 are located along the section of NC 12 near the parking access at the juncture of the northernmost and middle ponds (this section corresponds approximately to the section identified as B in the 2020 report) with a similar length. Figure 33 shows Sections C, D, and E in another previously identified vulnerable area in a narrow section of the island just south of the start of the Rodanthe Bridge (construction shown in the figure). Section C in Table 6 and Figure 33 corresponds approximately to Section C in the 2020 report. Section D corresponds to Sections D, E , and F of the 2020 report, and Section E corresponds to Sections G, H, and I of the 2020 report. The length of this entire stretch has increased from 1,063 ft in 2020 to 1,145 ft in 2021. Sections F, G, and H in Table 6 and Figure 34 correspond with sections J, K, and L in the 2020 report and are located in the S-curves area at the north of Rodanthe. The total length of the 5-year and current vulnerable sections of NC 12 at the end of the 2021 study year was 14,545 ft, compared to 14,104 ft in 2020. Most of the change was due to the increases in the vulnerable areas within the Canal Zone.

Table 6. Current and 5-year vulnerable sections of NC 12

Map Location (refer to Figure 29-Figure 34)	Designation in 2020 Report	Vulnerability Timeframe	Length (ft)	Approximate Transect Span	Location Description
A	A	Current	6,408	200-242	Canal Zone
B	B	Current	3,404	294-316	Adjacent to PINWR Visitors Center (Freshwater Ponds)
C	C	5-year	136	541	Narrow area north of Rodanthe
D	D, E, F	Current	637	542-545	
E	G,H,I	5-Year	372	546-548	
F	J	Current	372	563-565	Just north of refuge boundary into Rodanthe (S-Curves)
G	K	5-Year	2,678	566-583	
H	L	Current	537	583-586	
TOTAL Current			**13,127**		
TOTAL 5-Year			**1,417**		
OVERALL TOTAL			**14,545**		

Legend:
- NC 12 Edge of Pavement
- Current Vulnerability
- 5-Year Vulnerability
- 230 Foot Critical Buffer Zone

0 500 1,000 2,000 3,000 4,000
Feet

A

Figure 29

(View 1 of 6)

Current and 5-Year NC 12 Vulnerability

Prepared for the North Carolina Department of Transportation
Horizontal Datum: North Carolina State Plane Feet 1983 FIPS 3200
Orthophoto Date: February 1, 2022; Map Created: October 6, 2022

A

B

N
W · E
S

Legend:
- NC 12 Edge of Pavement
- Current Vulnerability
- 5-Year Vulnerability
- 230 Foot Critical Buffer Zone

0   500 1,000   2,000   3,000   4,000
Feet

Figure 30

(View 2 of 6)

Current and 5-Year NC 12 Vulnerability

Prepared for the North Carolina Department of Transportation
Horizontal Datum: North Carolina State Plane Feet 1983 FIPS 3200
Orthophoto Date: February 1, 2022; Map Created: October 6, 2022

Figure 31

(View 3 of 6)

Current and 5-Year NC 12 Vulnerability

Prepared for the North Carolina Department of Transportation
Horizontal Datum: North Carolina State Plane Feet 1983 FIPS 3200
Orthophoto Date: February 1, 2022; Map Created: October 6, 2022

Legend:
- NC 12 Edge of Pavement
- Current Vulnerability
- 5-Year Vulnerability
- 230 Foot Critical Buffer Zone
- Interim Bridge

Scale: 0 500 1,000 2,000 3,000 4,000 Feet

B

Legend:
- NC 12 Edge of Pavement
- Current Vulnerability
- 5-Year Vulnerability
- 230 Foot Critical Buffer Zone
- Interim Bridge

Scale: 0 500 1,000 2,000 3,000 4,000 Feet

Figure 32

(View 4 of 6)

Current and 5-Year NC 12 Vulnerability

Prepared for the North Carolina Department of Transportation
Horizontal Datum: North Carolina State Plane Feet 1983 FIPS 3200
Orthophoto Date: February 1, 2022; Map Created: October 6, 2022

Legend:
- NC 12 Edge of Pavement
- Current Vulnerability
- 5-Year Vulnerability
- 230 Foot Critical Buffer Zone

0 500 1,000 2,000 3,000 4,000 Feet

Figure 33

(View 5 of 6)

Current and 5-Year NC 12 Vulnerability

Prepared for the North Carolina Department of Transportation
Horizontal Datum: North Carolina State Plane Feet 1983 FIPS 3200
Orthophoto Date: February 1, 2022; Map Created: October 6, 2022

F

G

H

N
W — E
S

NC 12 Edge of Pavement
Current Vulnerability
5-Year Vulnerability
230 Foot Critical Buffer Zone

0   500 1,000   2,000   3,000   4,000
                                              Feet

Figure 34

(View 6 of 6)

Current and 5-Year NC 12 Vulnerability

Prepared for the North Carolina Department of Transportation
Horizontal Datum: North Carolina State Plane Feet 1983 FIPS 3200
Orthophoto Date: February 1, 2022; Map Created: October 6, 2022

<u>Predicted Shoreline Positions: 2030 and 2060</u>

Figure 35 through Figure 40 show the prediction of the expected average shoreline position in 2030 (referred to as "Predicted 2030 Shoreline" in the figures) based on the linear regression of shoreline position including data through February 1, 2022. For these predictions, a band showing the potential high-erosion and low-erosion position of the shoreline is also presented, determined using the 95% confidence prediction intervals for the position data (this band is referred to as "95% Prediction Interval Range" in the figures). Red highlights the areas along NC 12 where, at a minimum, the high-erosion shoreline (the western edge of the band) encroaches on the 230 ft critical buffer. These areas are considered to be potentially vulnerable roadway. The length and approximate transect span of these locations is summarized in Table 7.

By 2030, the average shoreline position (represented by the mid-point of the band) reaches the 230-foot critical buffer throughout the Canal Zone near Oregon Inlet (Figure 35), north of the freshwater ponds. [It is noted that a portion of this area is already showing vulnerability in the current year making this an area of immediate concern.] The average 2030 shoreline position again reaches the buffer near the center of the freshwater ponds near the Visitor's Center, while the high-erosion shoreline falls within the buffer north of this area along North Pond (Figure 36). Figure 37 shows the 2030 high-erosion shoreline encroaching on the buffer along the southernmost freshwater pond and adjacent to the Pea Island Breach. It is also within the buffer along a small section south of the breach (Figure 38). The 2030 high-erosion shoreline is well within the critical buffer zone and encroaches onto the road along the S-Curves section of NC 12 north of Rodanthe and into the northern section of Rodanthe, as shown in Figure 39 and Figure 40.

The potentially vulnerable sections in the 2030 prediction were similar overall to those in previous reports, with small differences from the 2020 report. Sections A and B were slightly longer than the corresponding sections in the 2020 report. Sections C and D correspond to Section C in the 2020 report and are discontinuous with a smaller total length, and a slightly smaller length of the interim bridge span was identified as potentially vulnerable in the 2021 report when compared to the 2020 report. The total length of potentially vulnerable roadway with the 2030 forecast is 26,736 ft, compared with 27,169 ft in the 2020 report. Note that a portion of the length of the Interim Bridge span is included in this estimate, because this bridge is considered a temporary solution to the vulnerability in that area.

Table 7. 2030 potentially vulnerable sections of NC 12

Map Location (refer to Figure 35-Figure 40)	Designation in 2020 Report	Length (ft)	Approximate Transect Span	Location Description
A	A	8,347	196-250	Canal Zone
B	B	6,048	278-318	North of, Adjacent to, and South of Pea Island Visitors Center (Freshwater Ponds)
C	C	903	359-364	Adjacent to South Pond and just north of Pea Island Breach
D	C	1,994	367-379	
Interim Bridge	Interim Bridge	400	380-382	Portion of Interim Bridge Span
E	D	224	403-404	Small section south of the Interim Bridge
F	E	8,822	535-593	Narrow area north of Rodanthe, past refuge boundary into Rodanthe (S-Curves)
TOTAL		26,736		

Legend:
- NC 12 Edge of Pavement (yellow)
- 2030 Potentially Vulnerable Roadway (red)
- 230 Foot Critical Buffer Zone (black)
- Predicted 2030 Shoreline (blue)
- 95% Prediction Interval (blue hatched)

Scale: 0, 500, 1,000, 2,000, 3,000, 4,000 Feet
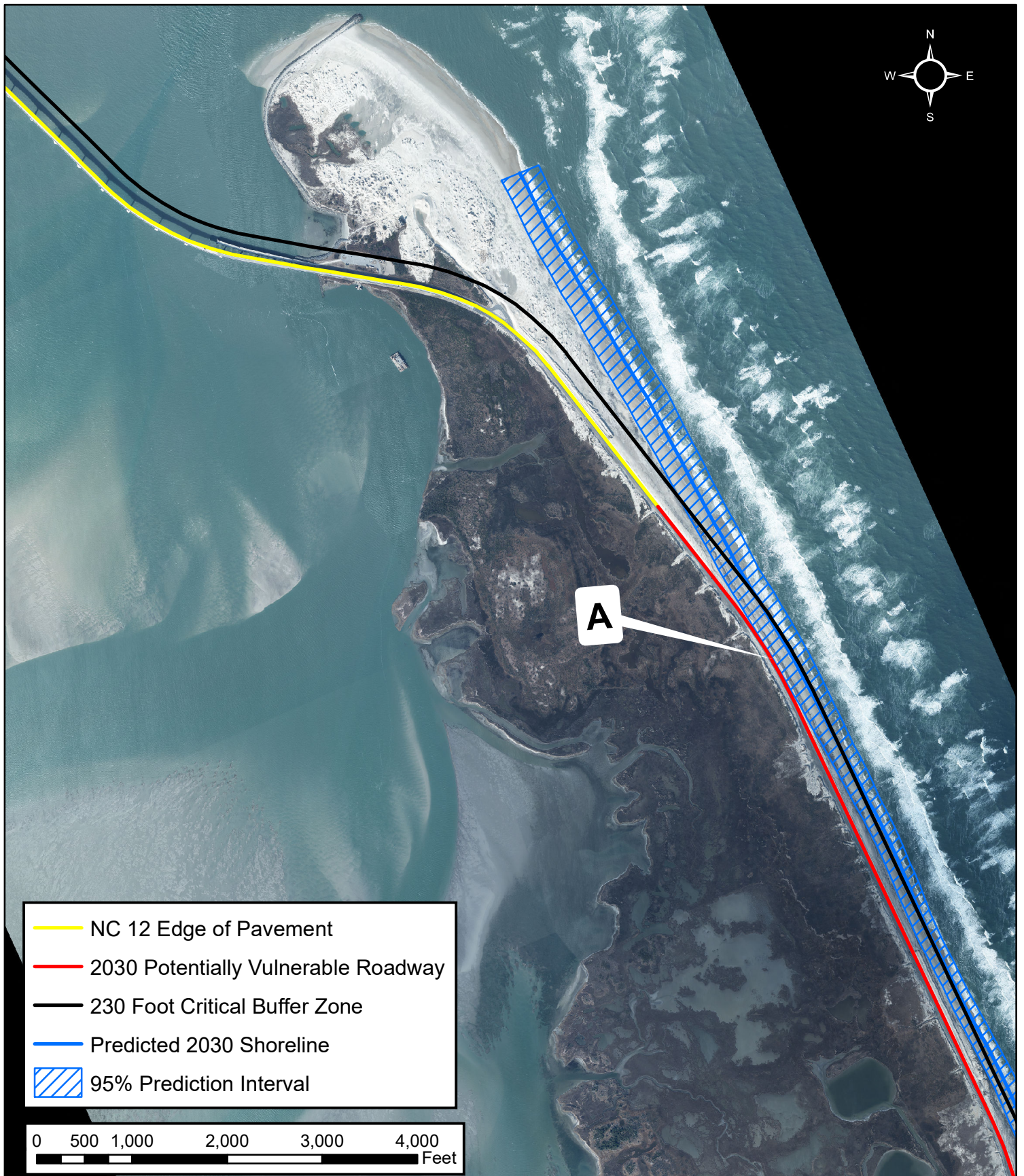
Figure 35

(View 1 of 6)

2030 Projected Shoreline and 95% PI

Prepared for the North Carolina Department of Transportation
Horizontal Datum: North Carolina State Plane Feet 1983 FIPS 3200
Orthophoto Date: February 1, 2022; Map Created: July 6, 2022

Legend:
- NC 12 Edge of Pavement
- 2030 Potentially Vulnerable Roadway
- 230 Foot Critical Buffer Zone
- Predicted 2030 Shoreline
- 95% Prediction Interval

0 500 1,000 2,000 3,000 4,000 Feet

Figure 36

(View 2 of 6)

2030 Projected Shoreline and 95% PI

Prepared for the North Carolina Department of Transportation
Horizontal Datum: North Carolina State Plane Feet 1983 FIPS 3200
Orthophoto Date: February 1, 2022; Map Created: July 6, 2022

Legend:
- NC 12 Edge of Pavement
- 2030 Potentially Vulnerable Roadway
- 230 Foot Critical Buffer Zone
- Predicted 2030 Shoreline
- 95% Prediction Interval
- Interim Bridge

Figure 37

(View 3 of 6)

2030 Projected Shoreline and 95% PI

Prepared for the North Carolina Department of Transportation
Horizontal Datum: North Carolina State Plane Feet 1983 FIPS 3200
Orthophoto Date: February 1, 2022; Map Created: July 6, 2022

E

Legend

— NC 12 Edge of Pavement

— 2030 Potentially Vulnerable Roadway

— 230 Foot Critical Buffer Zone

— Predicted 2030 Shoreline

▨ 95% Prediction Interval

▨ Interim Bridge

0 500 1,000 2,000 3,000 4,000 Feet

Figure 38

(View 4 of 6)

2030 Projected Shoreline and 95% PI

Prepared for the North Carolina Department of Transportation
Horizontal Datum: North Carolina State Plane Feet 1983 FIPS 3200
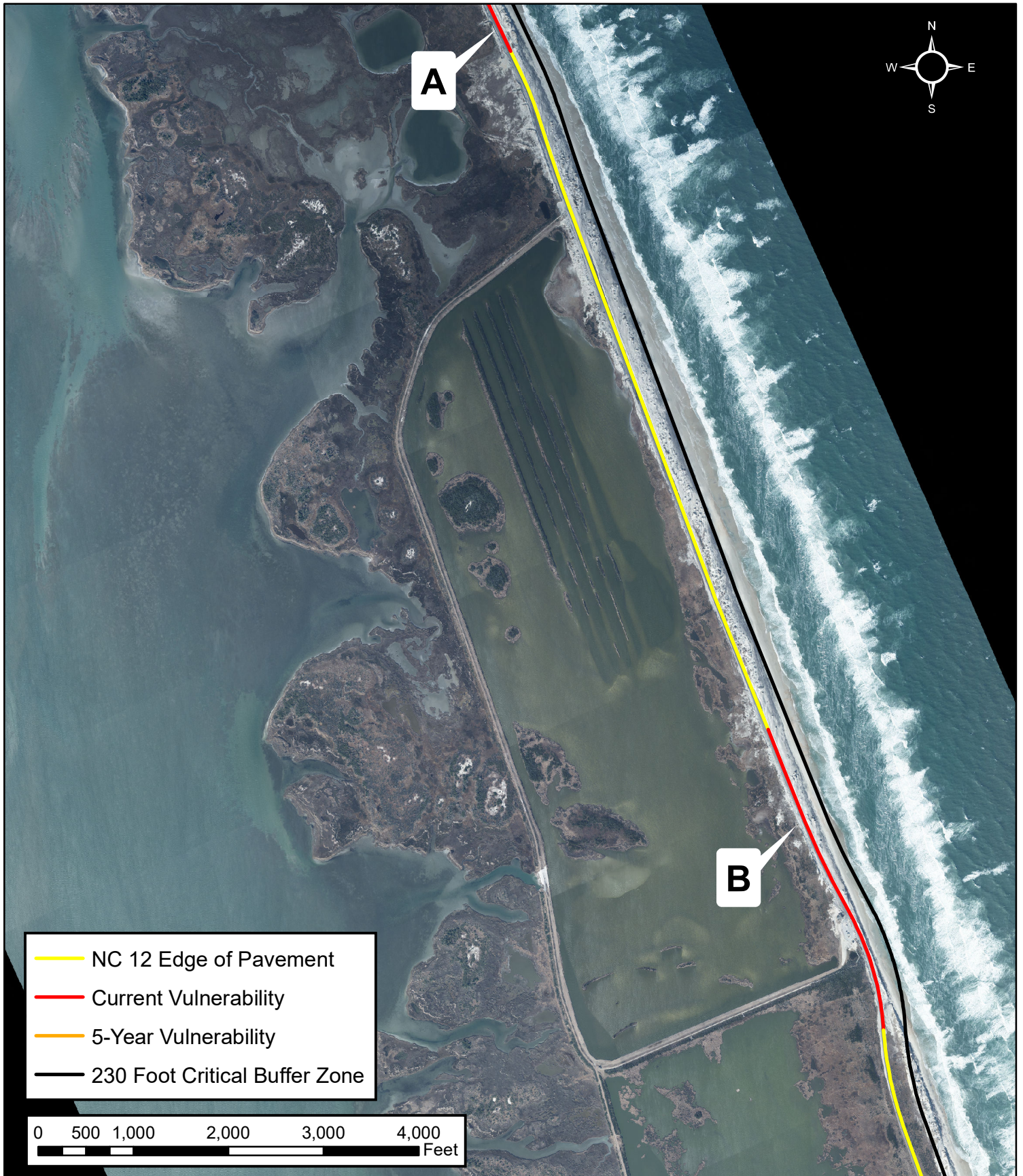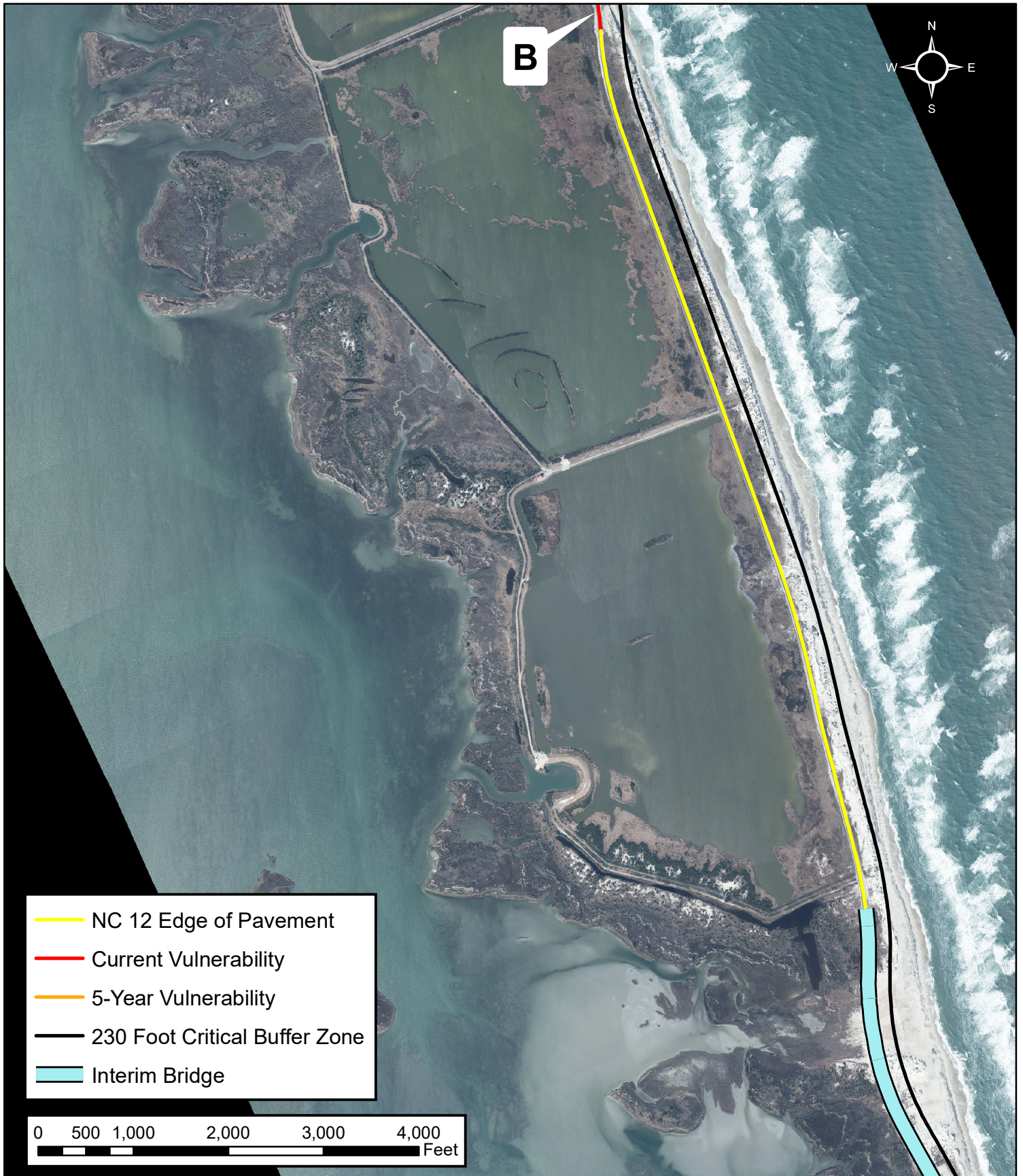Orthophoto Date: February 1, 2022; Map Created: July 6, 2022

F

Legend

— NC 12 Edge of Pavement

— 2030 Potentially Vulnerable Roadway

— 230 Foot Critical Buffer Zone

— Predicted 2030 Shoreline

▨ 95% Prediction Interval

Scale: 0 500 1,000 2,000 3,000 4,000 Feet

Figure 39

(View 5 of 6)

2030 Projected Shoreline and 95% PI

Prepared for the North Carolina Department of Transportation
Horizontal Datum: North Carolina State Plane Feet 1983 FIPS 3200
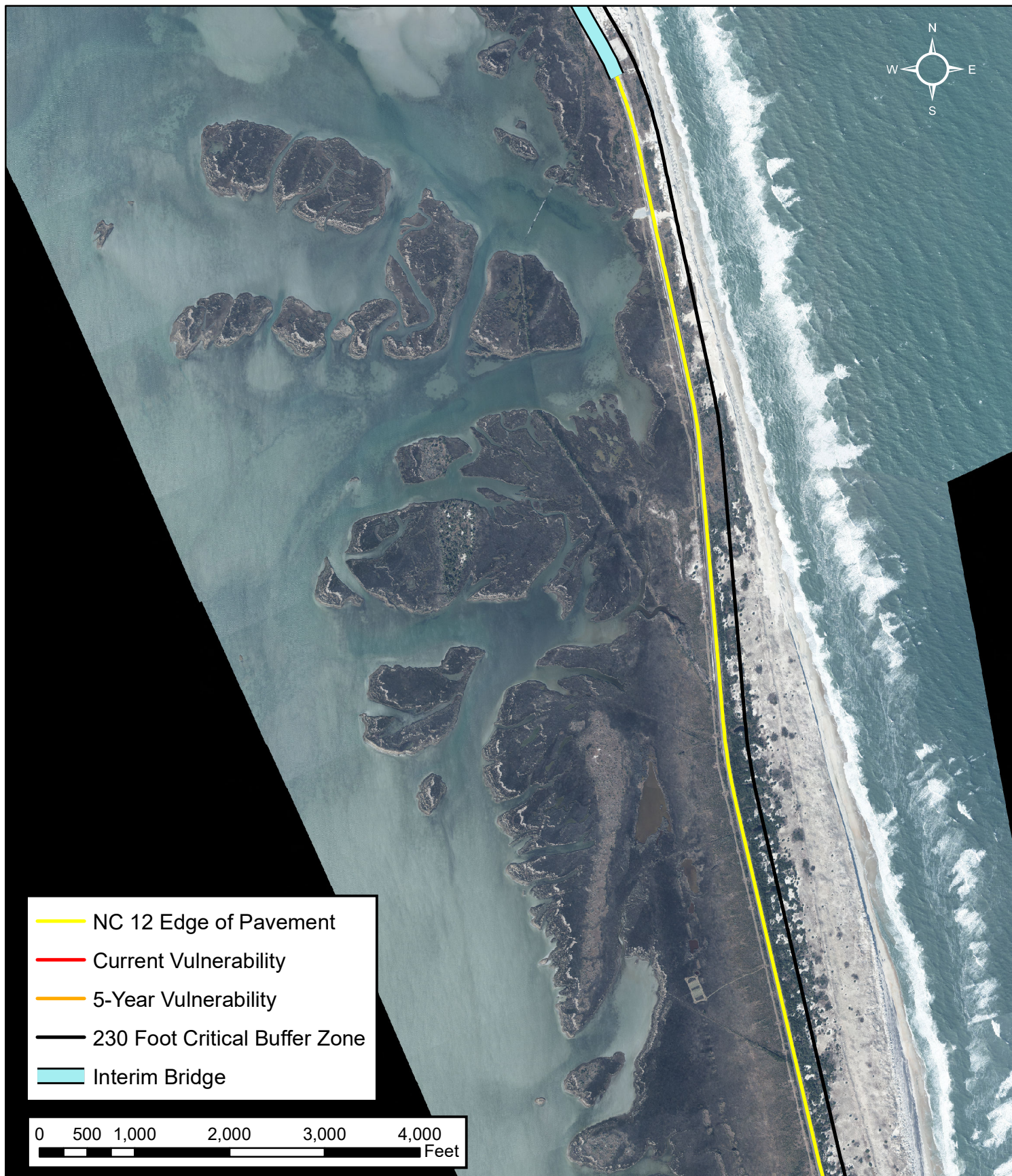Orthophoto Date: February 1, 2022; Map Created: July 6, 2022

F

Legend:
- NC 12 Edge of Pavement
- 2030 Potentially Vulnerable Roadway
- 230 Foot Critical Buffer Zone
- Predicted 2030 Shoreline
- 95% Prediction Interval

0   500 1,000   2,000   3,000   4,000
Feet

Figure 40

(View 6 of 6)

2030 Projected Shoreline and 95% PI

Prepared for the North Carolina Department of Transportation
Horizontal Datum: North Carolina State Plane Feet 1983 FIPS 3200
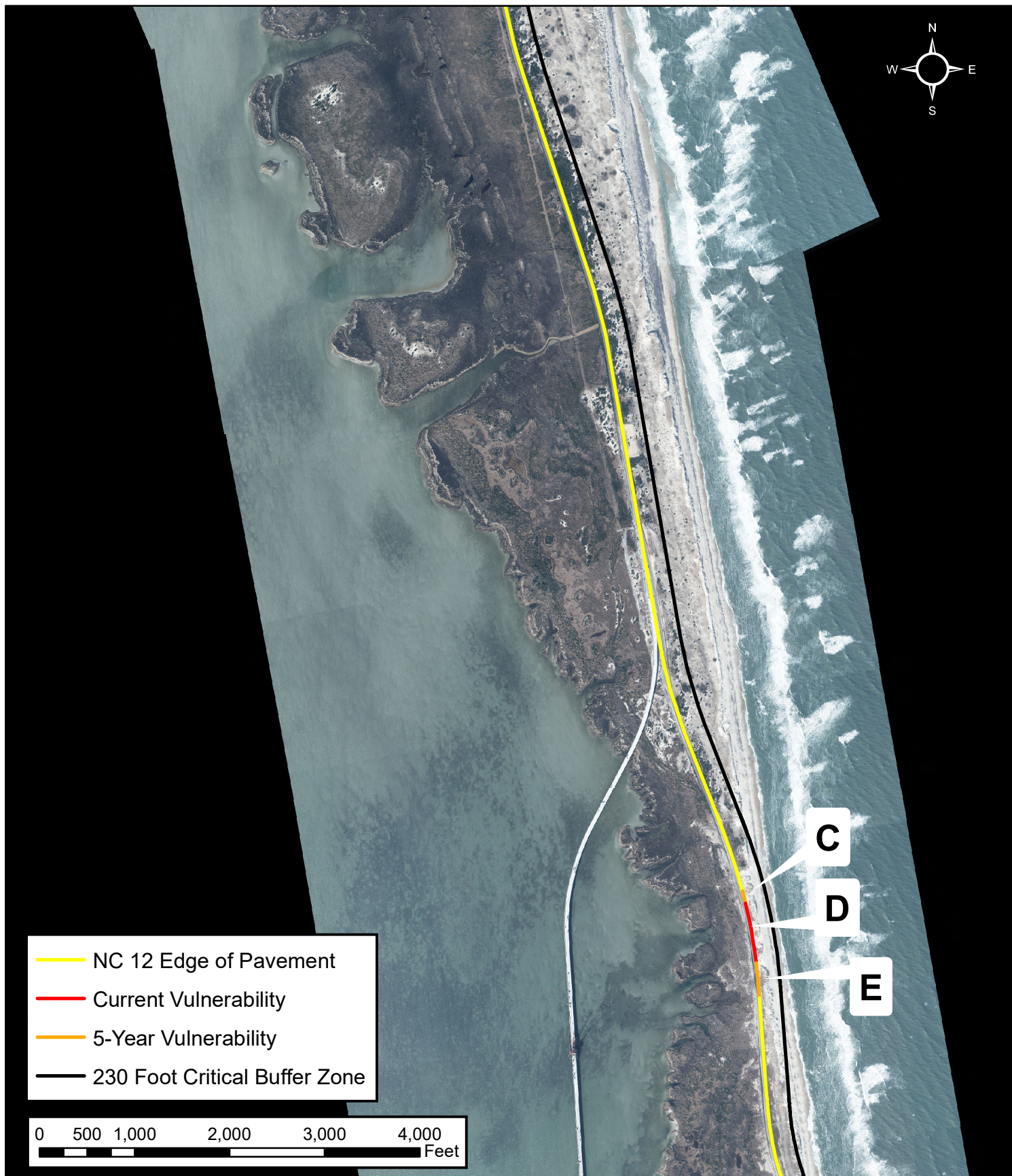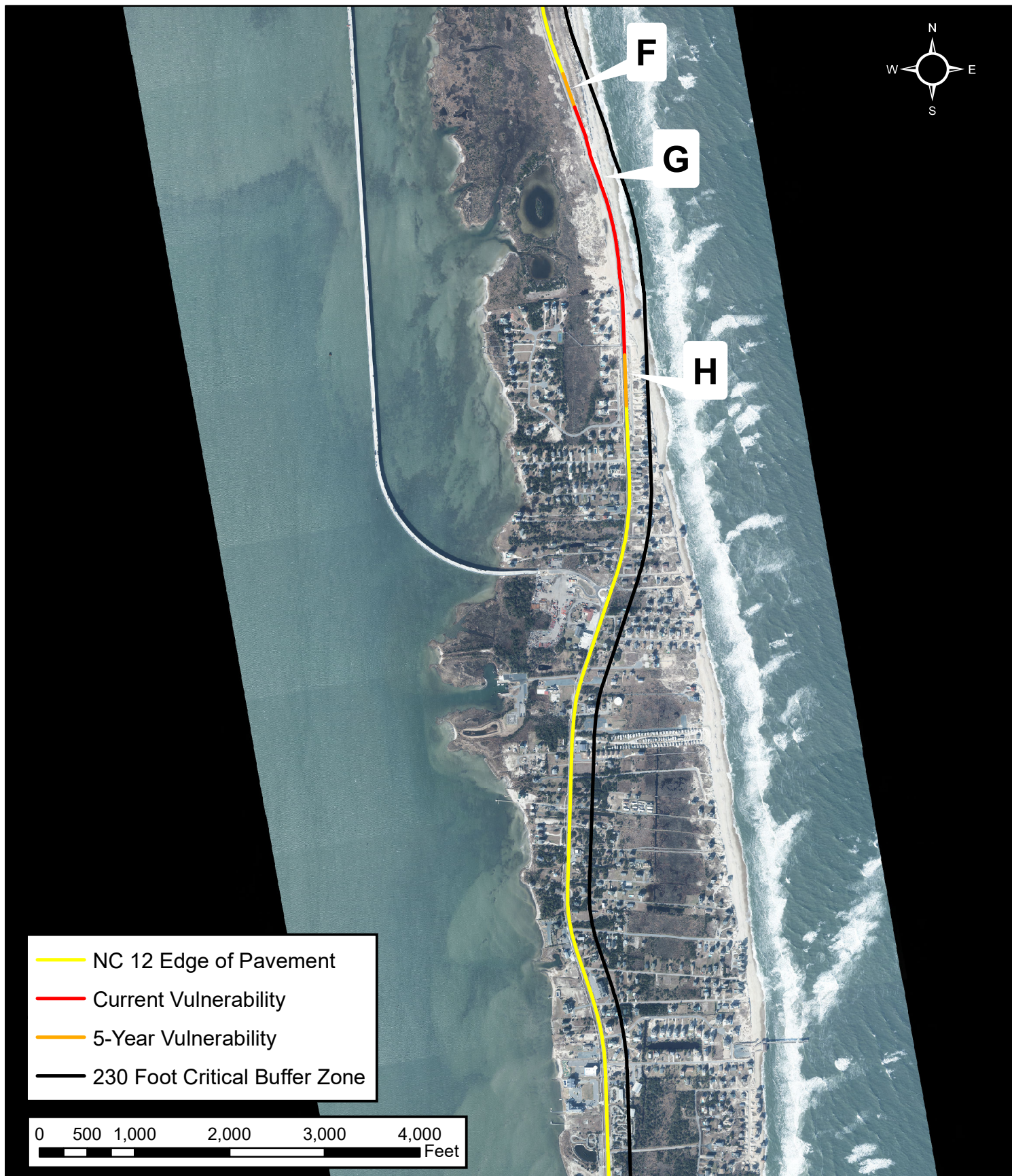Orthophoto Date: February 1, 2022; Map Created: July 6, 2022

The prediction of the expected average shoreline position in 2060 (referred to as "Predicted 2060 Shoreline"), along with a band showing the potential high-erosion and low-erosion shoreline positions (referred to as "95% Prediction Interval Bounds") is presented in Figure 42 through Figure 47. The length and approximate transect span of the areas where the band encroaches on the 230 ft buffer is summarized in Table 8.

As shown in Figure 42, the 2060 average shoreline reaches the critical buffer along a stretch of NC 12 just south of Oregon Inlet. This area is currently showing very slight accretion in the long-term rates (see Figure 27); therefore Area A in this figure is slightly smaller than Area A (along the same stretch of roadway) shown in Figure 35. In the shadow of the terminal groin and north of the ebb shoal bar attachment point, the shoreline is essentially stabilized, fluctuating around an average position with cyclic periods of erosion and accretion. This cyclic fluctuating shoreline behavior is a function of the presence of the terminal groin that traps sand, the ebb shoal bar which tends to refract the waves and reverse the direction of alongshore transport (to the north) and the occasionally episodic supply of sand provided by the dredge disposal activities of the USACE. Figure 41 shows the approximate location of the ebb shoal bar, and provides an example of a period of sediment transport to the north such that sand accumulated on the inlet side of the terminal groin. A linear analysis of these kinds of data typically results in a small shoreline change rate (either erosion or accretion) and a large prediction interval reflecting the uncertainty of the trend. In this area at the present time, accretion is indicated by the linear regression analysis. *It is noted that there is a limit to how much accretion will be maintained before the shoreline position oscillates back to an erosion condition*. Future monitoring will determine if the shoreline change rate reverses trend in the future, and subsequent shoreline position predictions will be adjusted accordingly.

Along the freshwater ponds and adjacent to the Pea Island Breach, even the low-erosion 2060 shoreline moves landward of NC 12 in some areas and most of the roadway adjacent to the ponds is identified as potentially vulnerable (Figure 43 and Figure 44). Just south of the ponds, the low-erosion 2060 shoreline is within the critical buffer area, and the average-erosion shoreline approaches the road (Figure 45). South of that section, all predicted shorelines lie east of the buffer for approximately three miles until a narrow section north of Rodanthe (and just south of the under-construction Rodanthe Bridge) where the high erosion predicted shoreline transitions to a position landward of NC 12 (Figure 46). All predicted shorelines are landward of the road from that area south to the northernmost portion of Rodanthe (Figure 47), just north of the roundabout where the Rodanthe Bridge ties into the existing NC 12 roadway.

The total length of potentially vulnerable roadway for the 2060 prediction is 40,655, slightly longer than the total length of potentially vulnerable roadway for the 2060 prediction in the 2020 report, 39,657 ft. Note that the length of the Interim Bridge span is included in this estimate, because this bridge is considered a temporary solution to the vulnerability in that area.

Table 8. 2060 potentially vulnerable sections of NC 12

Map Location (refer to Figure 42-Figure 47)	Approximate Corresponding Section in 2030 Maps (Figure 35-Figure 40)	Designation in 2020 Report	Length (ft)	Approximate Transect Span	Location Description
A	A	A	8,255	196-250	Canal Zone
B	B	B	10,392	262-330	North of, Adjacent to, and South of Pea Island Visitors Center (Freshwater Ponds)
C	C, D	C	5,021	347-379	Adjacent to South Pond to north of Interim Bridge
Interim Bridge	Interim Bridge	Interim Bridge	3,205	380-400	Span of Interim Bridge
D	E	D	3,740	401-425	South of Interim Bridge
E	F	E	10,041	533-598	Narrow area north of Rodanthe, past refuge boundary into Rodanthe (S-Curves)
TOTAL			40,655		
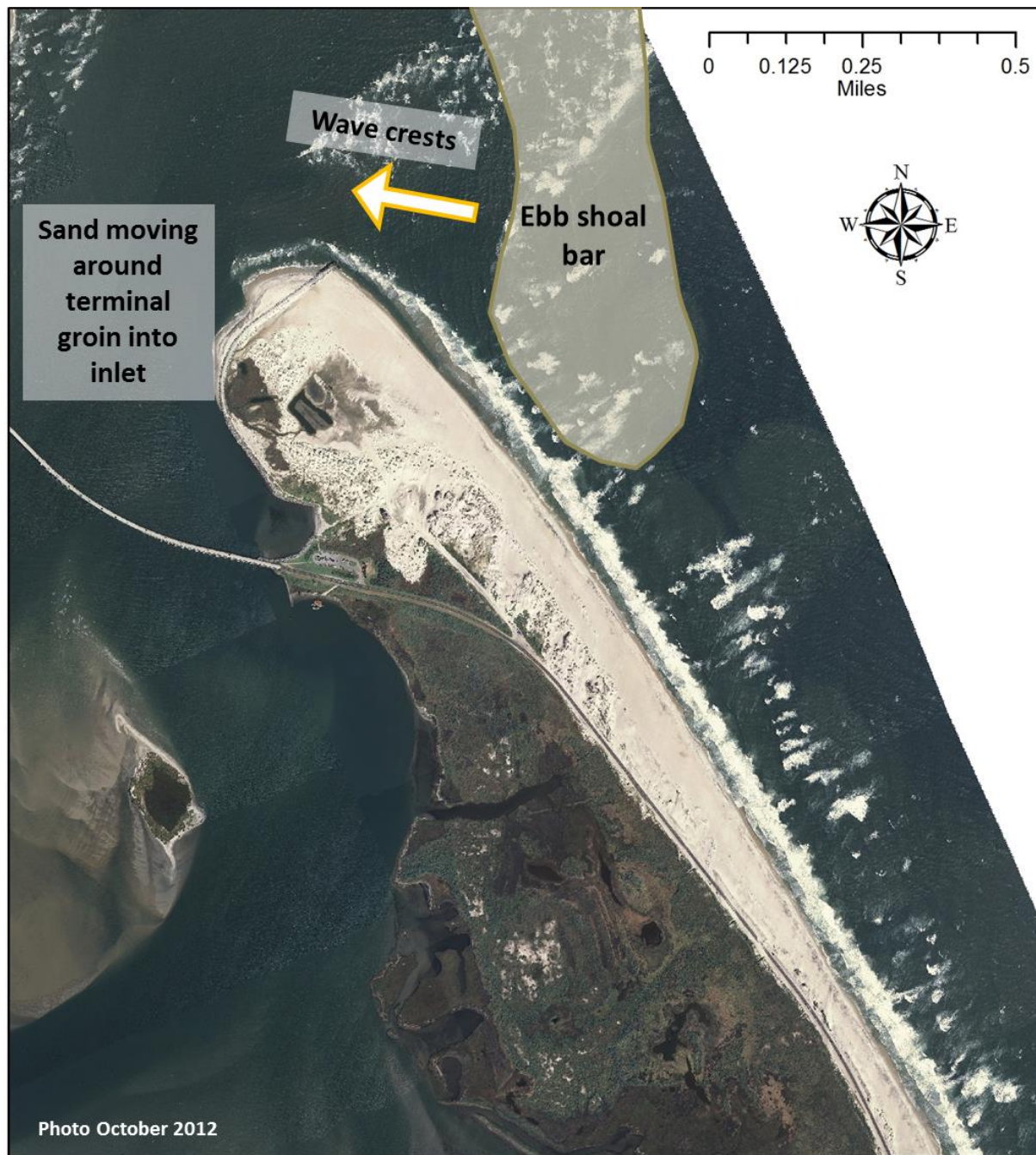
Figure 41. Diagram showing approximate location of the ebb shoal bar (visible due to waves breaking over the shallower areas of the bar) and local reversal of sediment transport, leading to sand deposition on the inlet side of the terminal groin.

NC 12 Edge of Pavement

2060 Potentially Vulnerable Roadway

230 Foot Critical Buffer Zone

Predicted 2060 Shoreline

95% Prediction Interval

0   500 1,000   2,000   3,000   4,000
                                              Feet

A
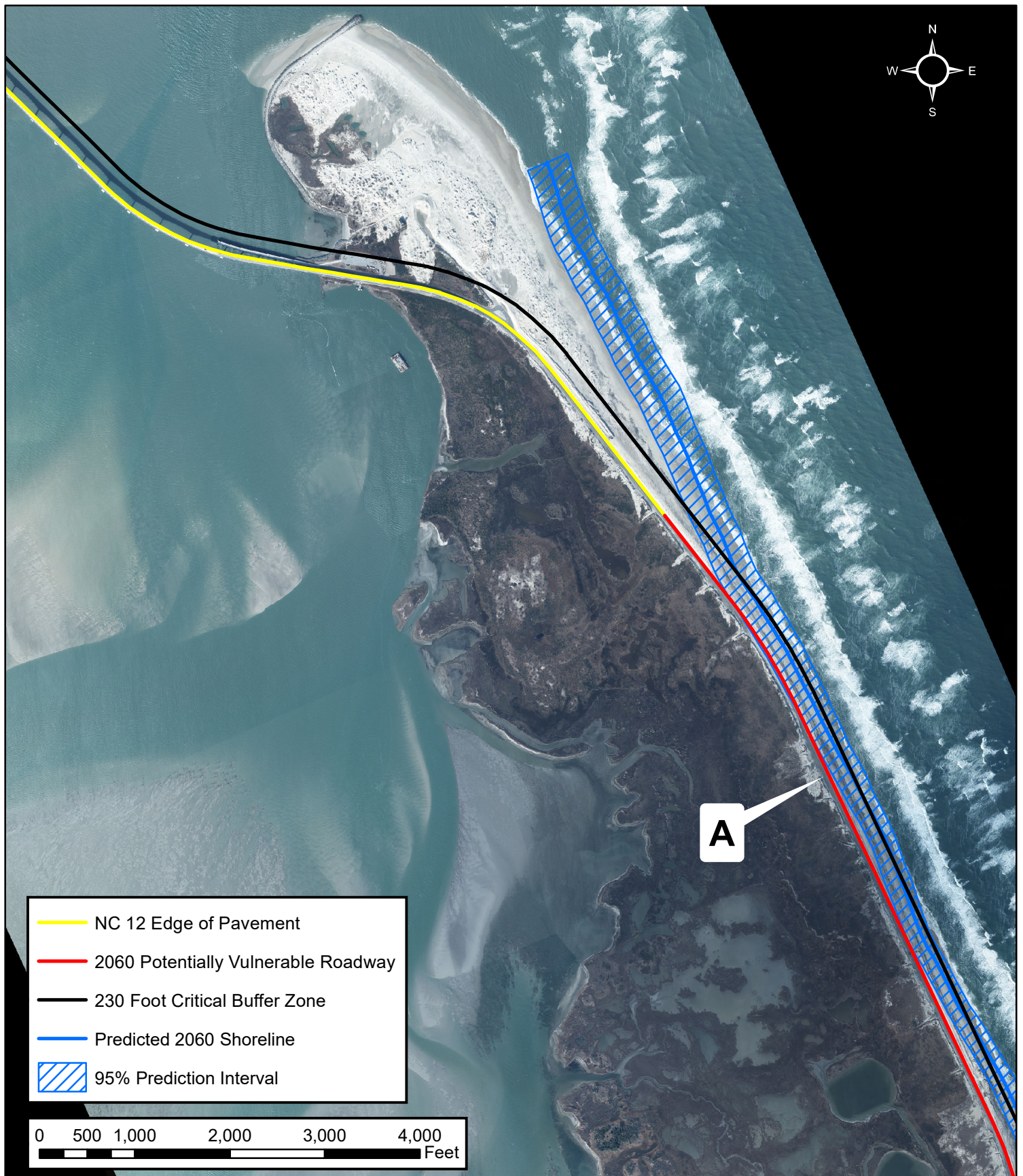
Figure 42

(View 1 of 6)

Projected 2060 Shoreline with 95% PI

Prepared for the North Carolina Department of Transportation
Horizontal Datum: North Carolina State Plane Feet 1983 FIPS 3200
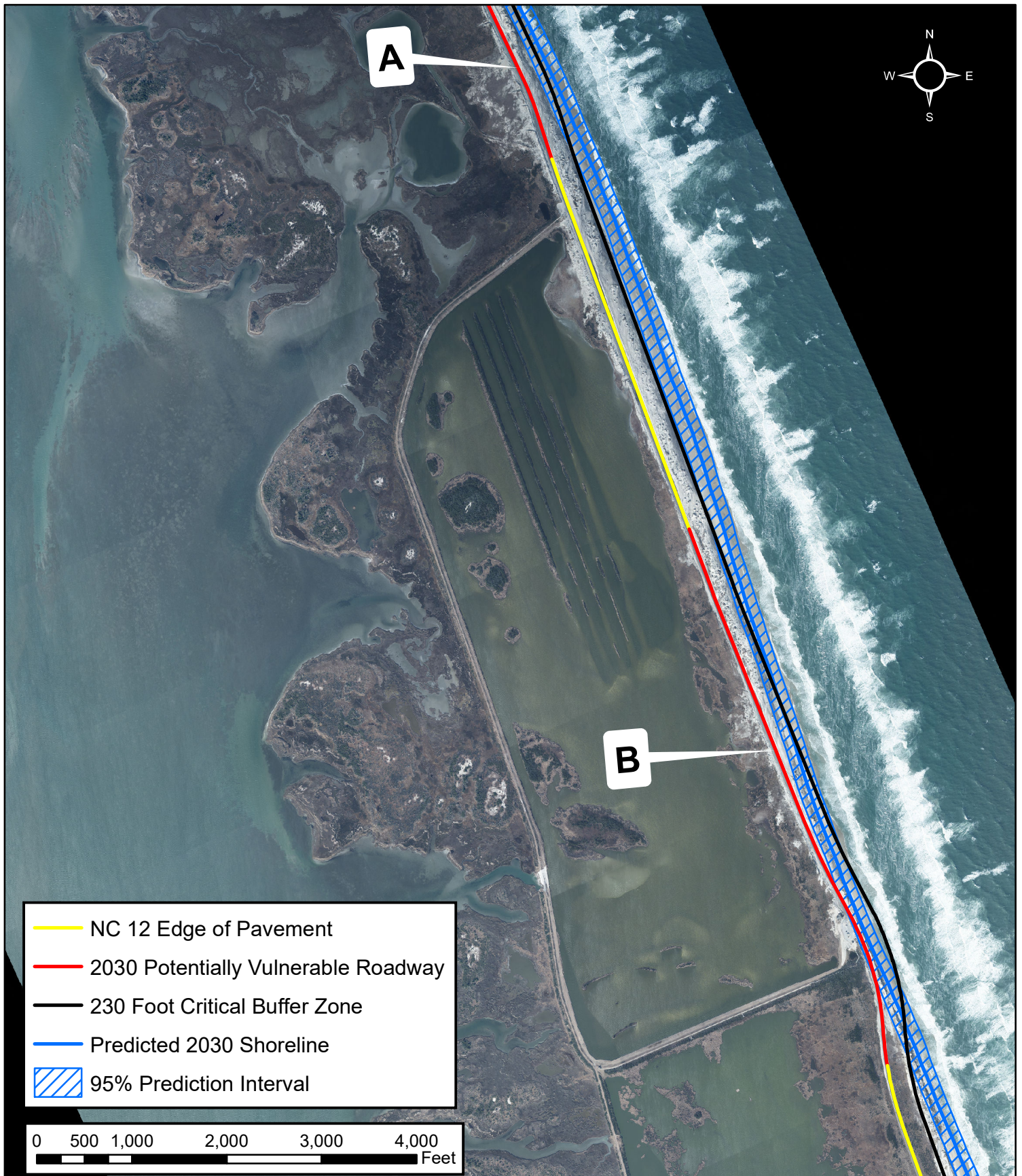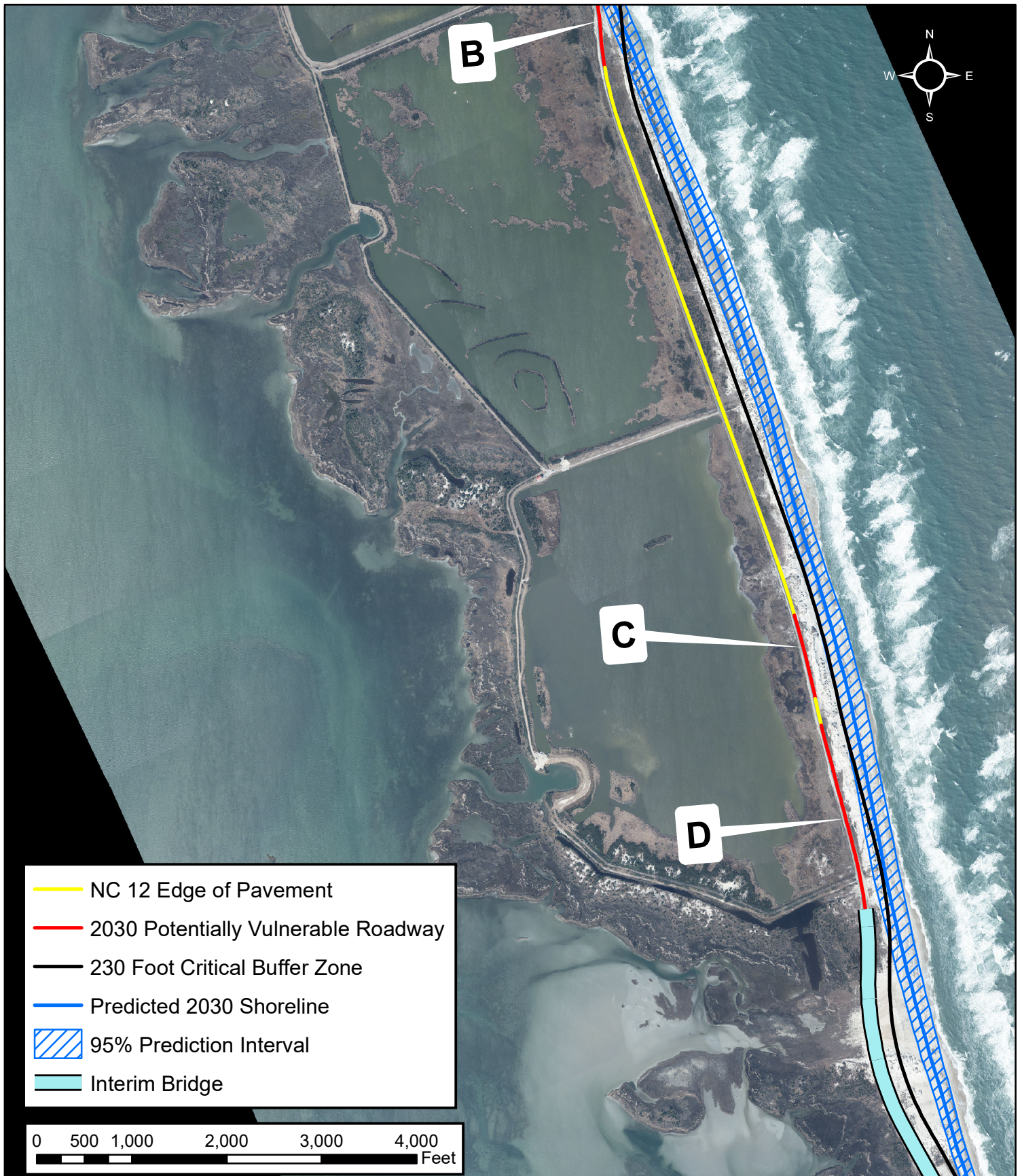Orthophoto Date: February 1, 2022; Map Created: October 10, 2022

Legend:
- NC 12 Edge of Pavement
- 2060 Potentially Vulnerable Roadway
- 230 Foot Critical Buffer Zone
- Predicted 2060 Shoreline
- 95% Prediction Interval

0 500 1,000 2,000 3,000 4,000 Feet
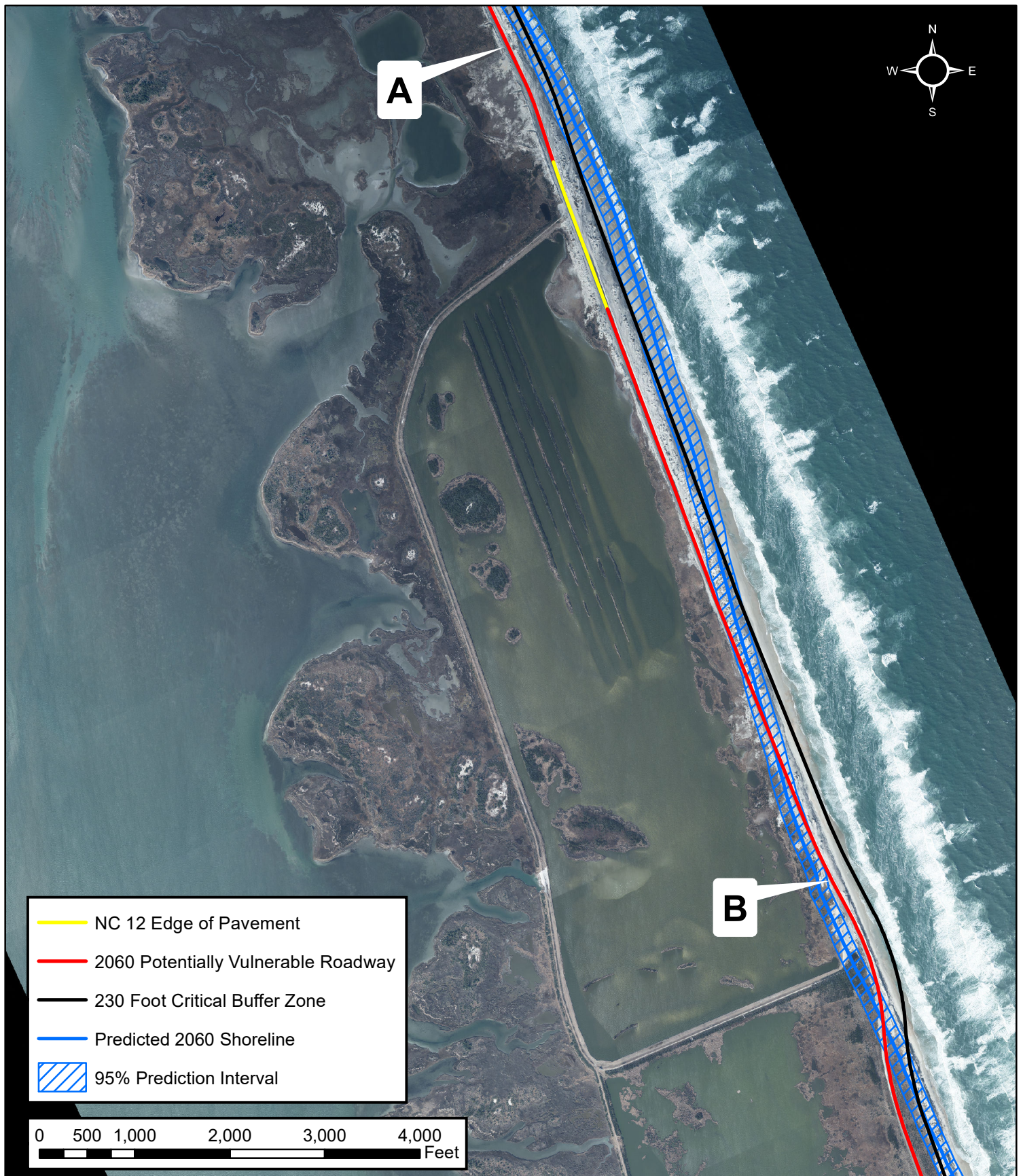
Figure 43

(View 2 of 6)

Projected 2060 Shoreline with 95% PI

Prepared for the North Carolina Department of Transportation
Horizontal Datum: North Carolina State Plane Feet 1983 FIPS 3200
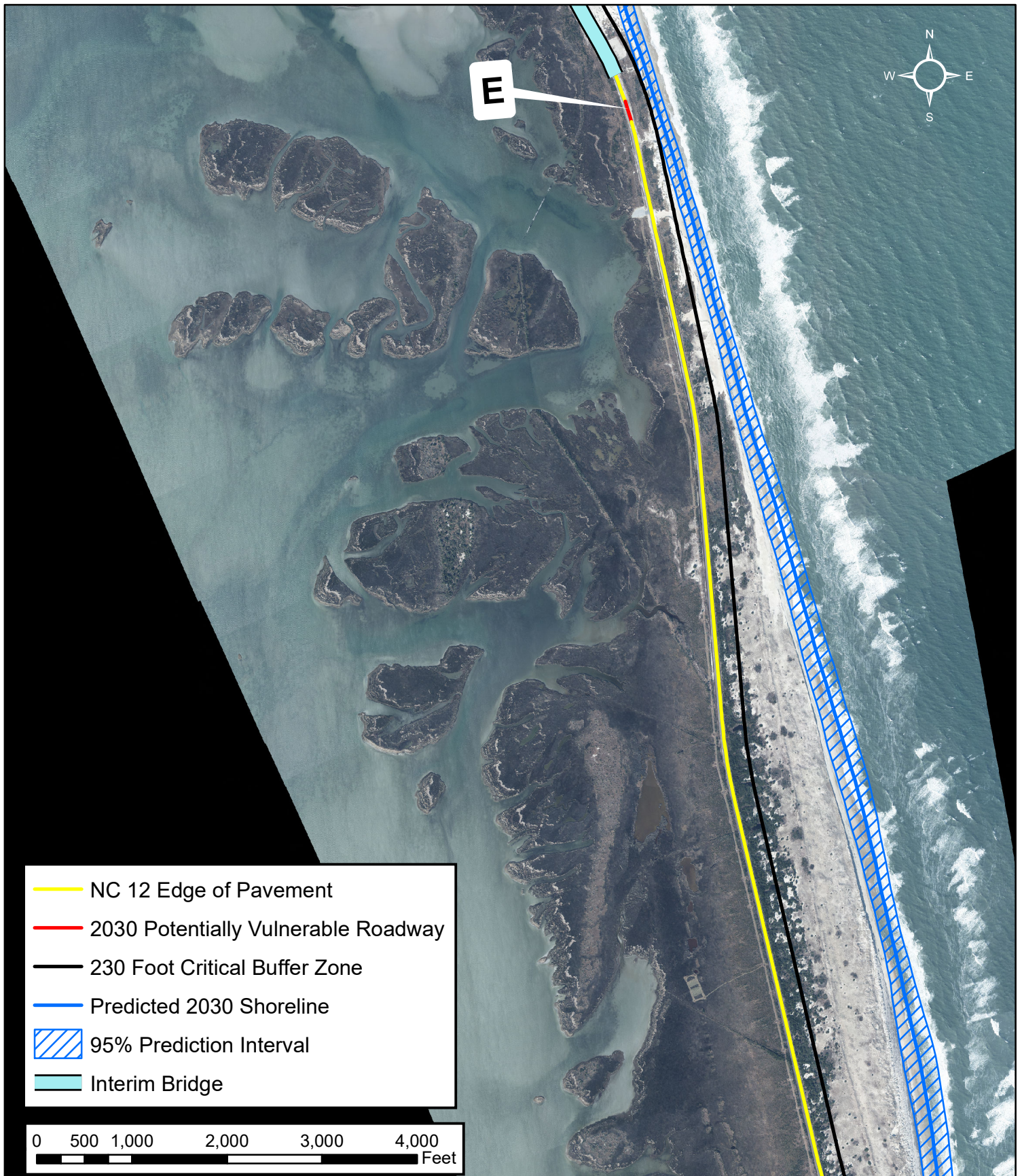Orthophoto Date: February 1, 2022; Map Created: October 10, 2022

Legend:
- NC 12 Edge of Pavement
- 2060 Potentially Vulnerable Roadway
- 230 Foot Critical Buffer Zone
- Predicted 2060 Shoreline
- 95% Prediction Interval
- Interim Bridge

Scale: 0 500 1,000 2,000 3,000 4,000 Feet
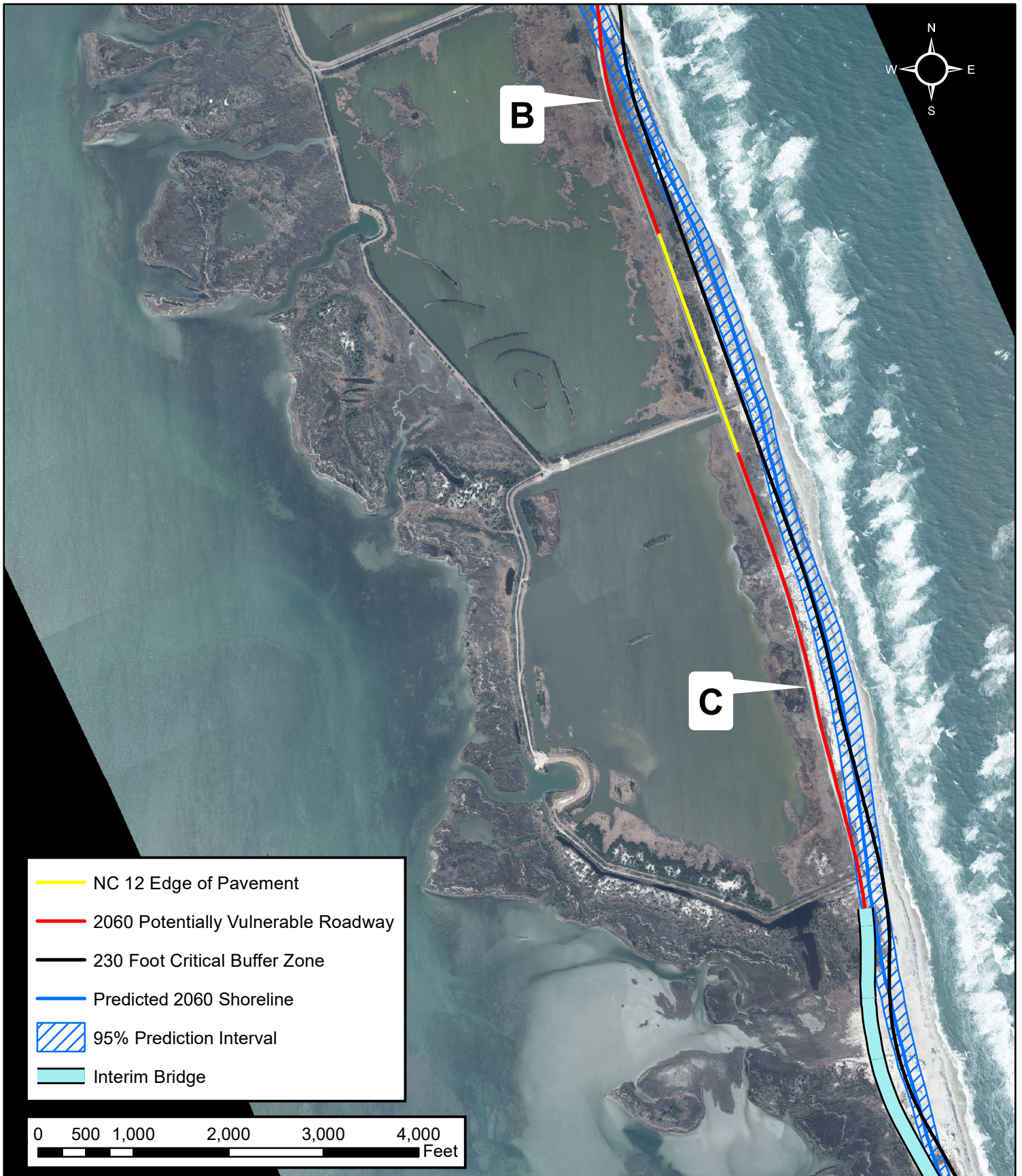
Figure 44

(View 3 of 6)

Projected 2060 Shoreline with 95% PI

Prepared for the North Carolina Department of Transportation
Horizontal Datum: North Carolina State Plane Feet 1983 FIPS 3200
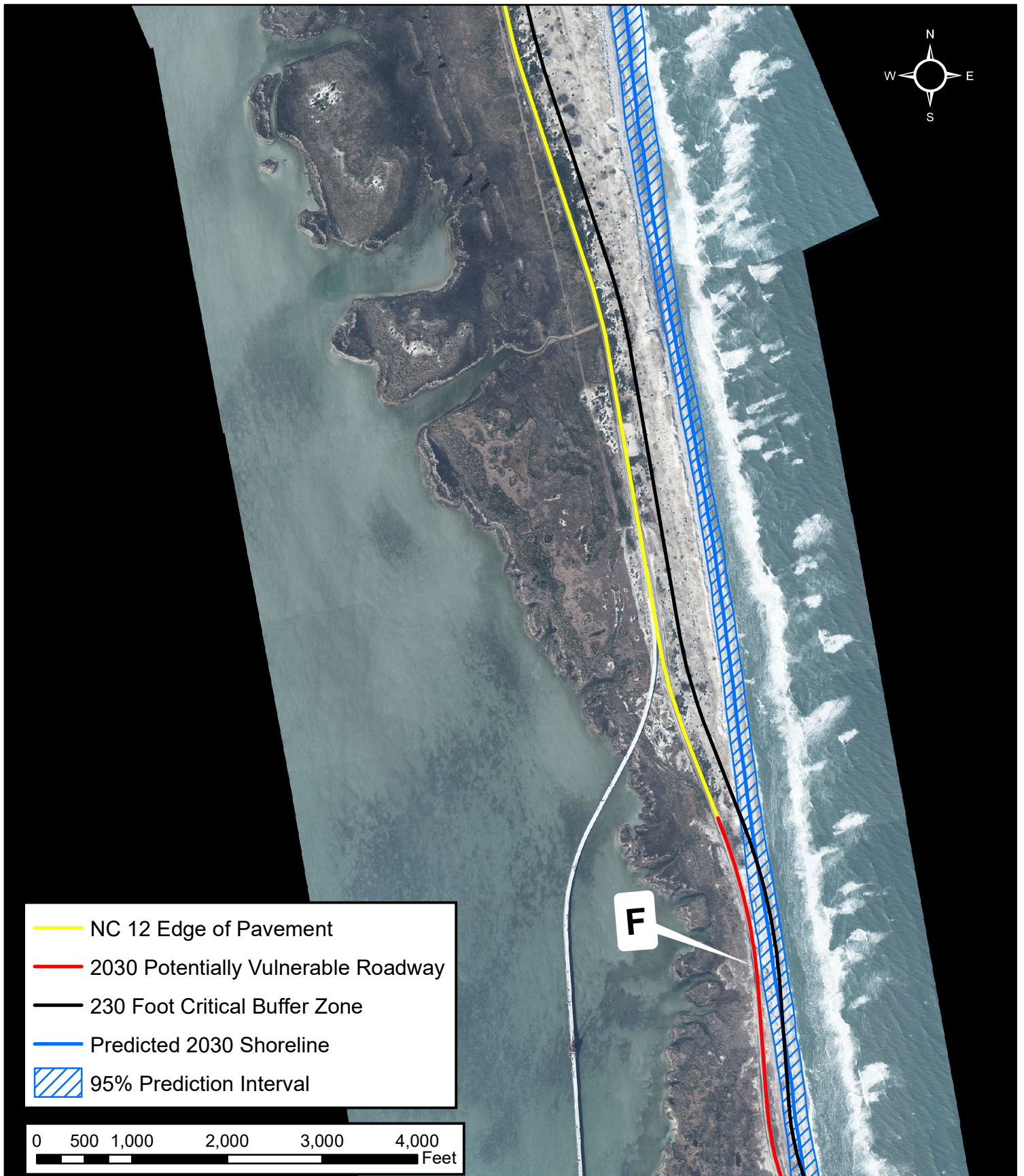Orthophoto Date: February 1, 2022; Map Created: October 10, 2022
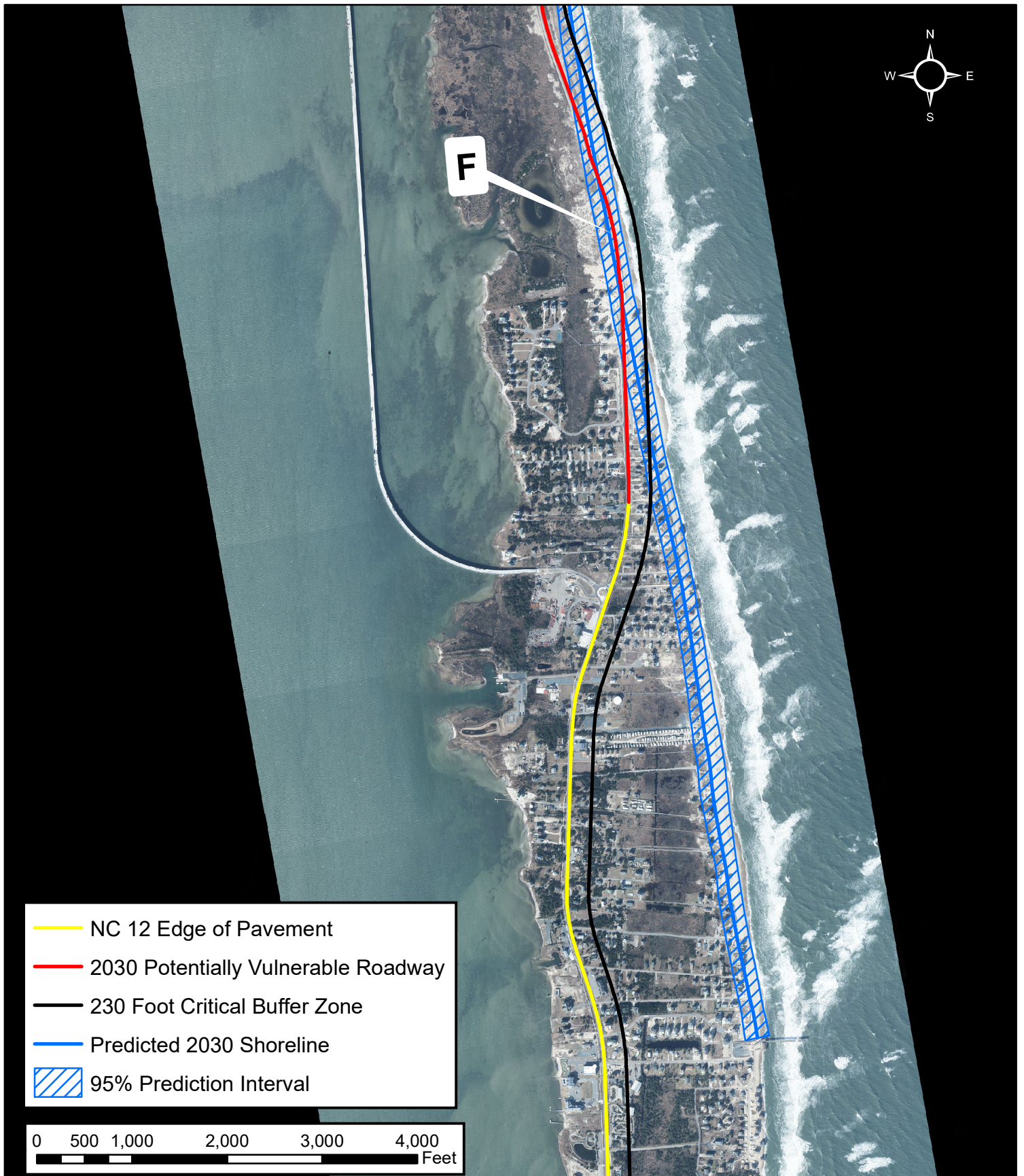
Legend:
- NC 12 Edge of Pavement
- 2060 Potentially Vulnerable Roadway
- 230 Foot Critical Buffer Zone
- Predicted 2060 Shoreline
- 95% Prediction Interval
- Interim Bridge

0 500 1,000 2,000 3,000 4,000 Feet
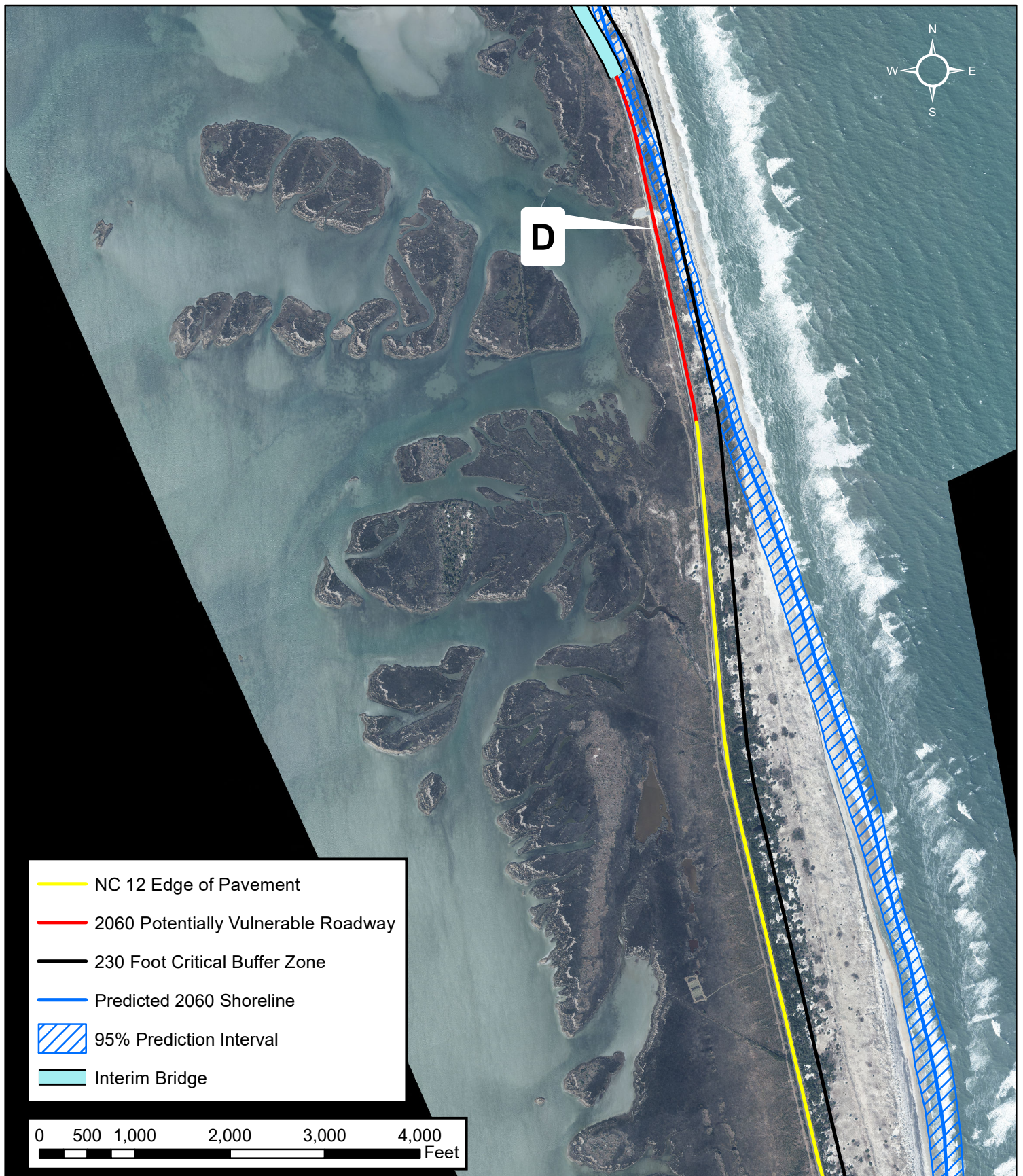
Figure 45

(View 4 of 6)

Projected 2060 Shoreline with 95% PI

Prepared for the North Carolina Department of Transportation
Horizontal Datum: North Carolina State Plane Feet 1983 FIPS 3200
Orthophoto Date: February 1, 2022; Map Created: October 10, 2022

Legend

- NC 12 Edge of Pavement
- 2060 Potentially Vulnerable Roadway
- 230 Foot Critical Buffer Zone
- Predicted 2060 Shoreline
- 95% Prediction Interval

E

0 500 1,000 2,000 3,000 4,000 Feet
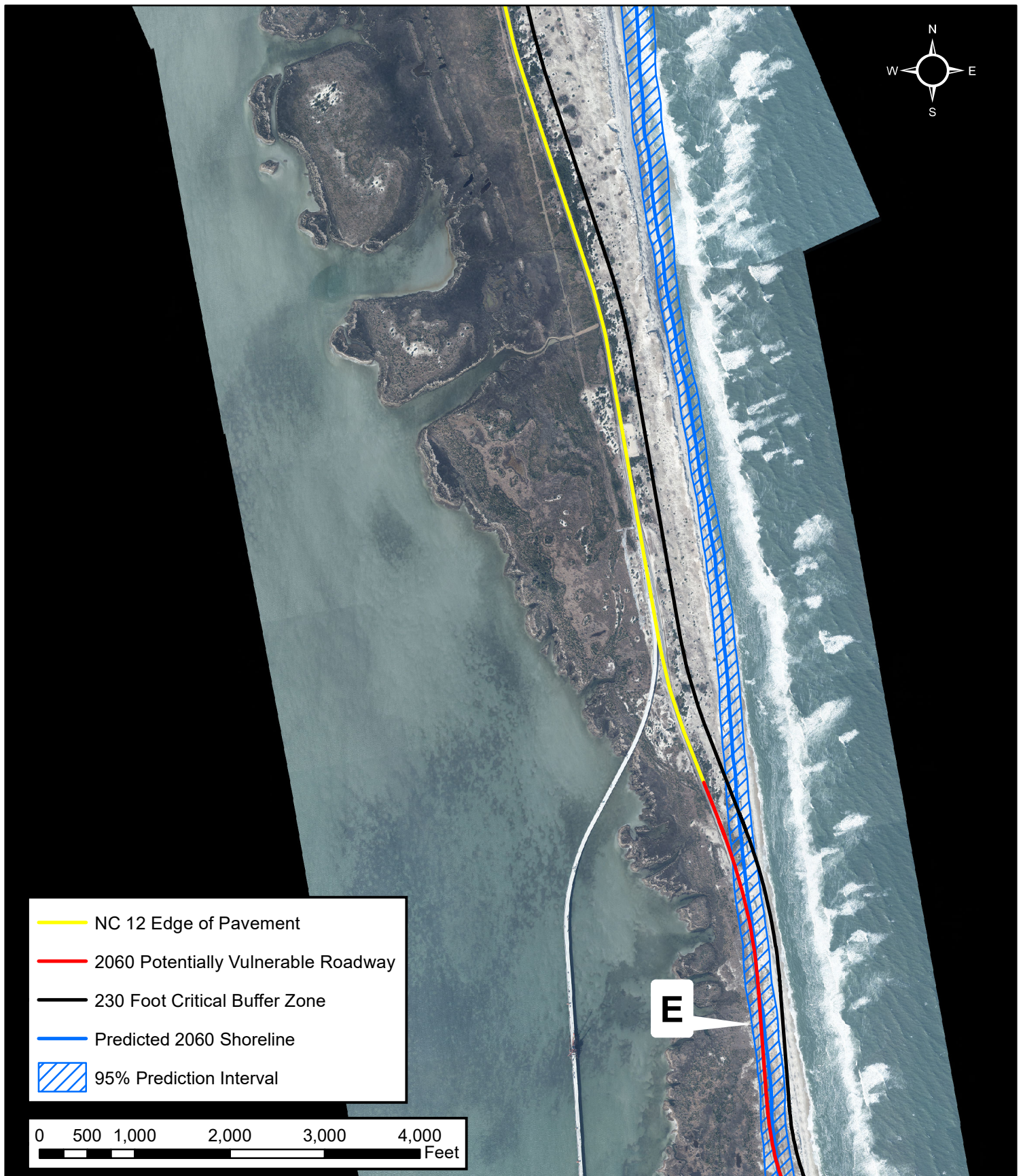
Figure 46

(View 5 of 6)

Projected 2060 Shoreline with 95% PI

Prepared for the North Carolina Department of Transportation
Horizontal Datum: North Carolina State Plane Feet 1983 FIPS 3200
Orthophoto Date: February 1, 2022; Map Created: October 10, 2022

E

Legend:

- NC 12 Edge of Pavement
- 2060 Potentially Vulnerable Roadway
- 230 Foot Critical Buffer Zone
- Predicted 2060 Shoreline
- 95% Prediction Interval

0 500 1,000 2,000 3,000 4,000 Feet
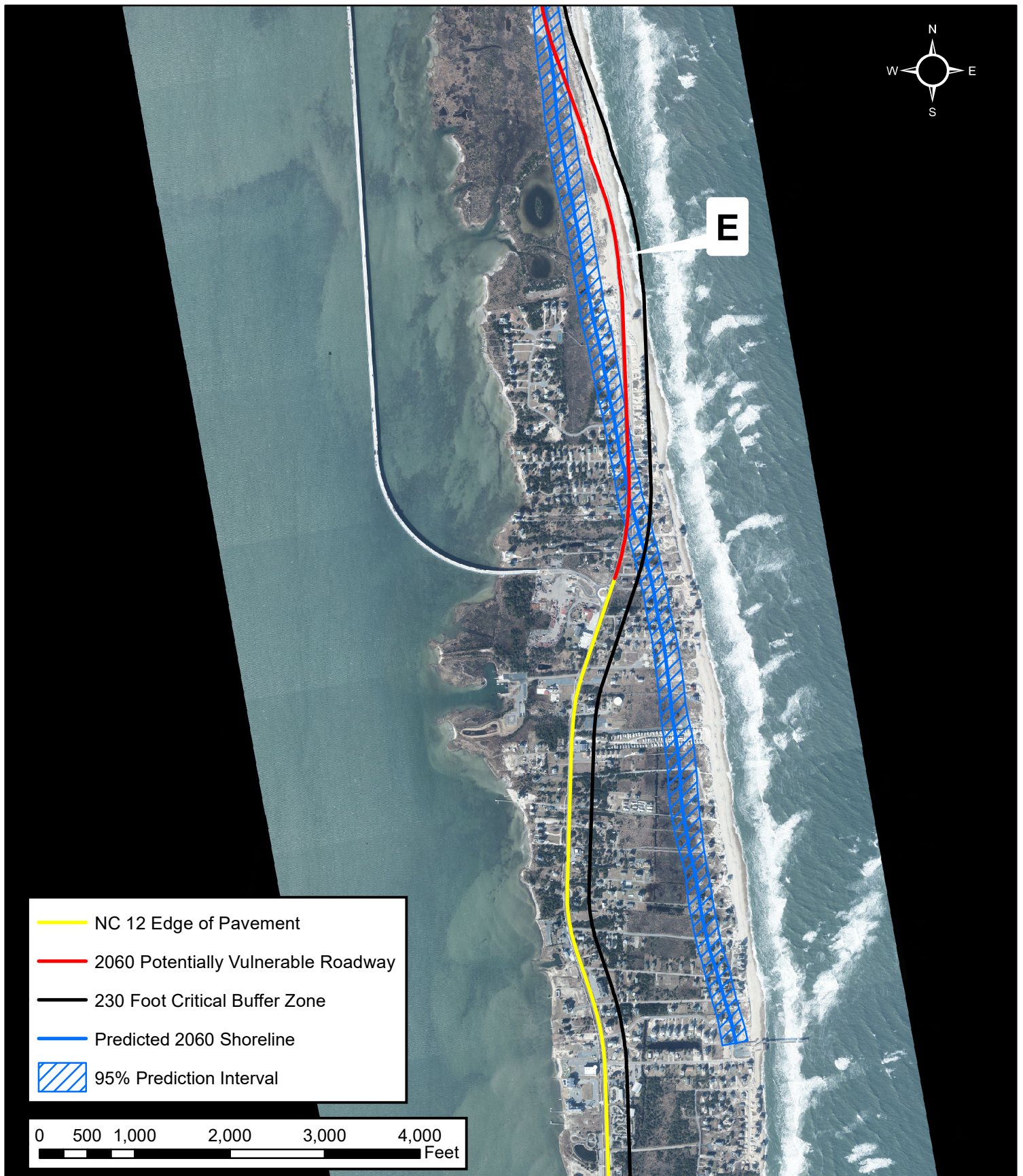
Figure 47

(View 6 of 6)

Projected 2060 Shoreline with 95% PI

Prepared for the North Carolina Department of Transportation
Horizontal Datum: North Carolina State Plane Feet 1983 FIPS 3200
Orthophoto Date: February 1, 2022; Map Created: October 10, 2022

Storm Events

Table 9 presents the storm events compiled from the USACE Duck Field Research Facility for the calendar year 2021. The maximum water level was the maximum elevation measured over the storm time frame from the hourly data. Maximum storm surge was the maximum of the difference between the observed and predicted water levels. Table 10 shows dates when NC 12 on Pea Island was hazardous or closed according to the NCDOT Traveler Information Management System. There was a relatively quiet tropical season during 2021, but several coastal storms led to impacts and closures. The most extensive closures documented in 2021 were November 7 to 9 due to a strong coastal storm, according to the NCDOT Traveler Information Management System.

Table 9. Storm events, 2021, as measured at the Duck Field Research Facility 17 m waverider (waves) and pier (water levels) (events had a maximum wave height greater than 6.6 ft for a sustained duration greater than 8 hours.) Date and time shown in EST.

Start Date	End Date	Max Hmo (ft)	Duration (hr)	Max Water Level (ft NAVD)	Max Storm Surge (ft)
1/28/2021 9:26	1/29/2021 2:26	9.3	17.0	3.4	2.4
2/12/2021 3:56	2/12/2021 16:26	9.1	12.5	3.1	1.7
2/13/2021 6:56	2/13/2021 17:56	7.4	11.0	2.6	1.6
2/15/2021 3:26	2/15/2021 13:56	7.5	10.5	2.3	2.0
3/19/2021 10:26	3/21/2021 5:56	12.3	43.5	3.0	2.7
10/10/2021 0:56	10/11/2021 19:56	11.0	43.0	4.2	2.2
10/29/2021 7:56	10/29/2021 21:26	8.5	13.5	3.0	2.2
11/6/2021 5:26	11/9/2021 2:56	13.1	69.5	4.4	2.4
11/23/2021 0:56	11/23/2021 15:56	8.9	15.0	2.9	1.6

Figure 48. Coastal storm impacts north of Rodanthe, November 8, 2021 (Photo NCDOT NC 12 Twitter).

Table 10. Traveler Information Management System NC 12 closure data for 2021, Pea Island

StartTime (EST)	EndTime (EST)	City	Condition	Reason
2/15/2021 10:54:00 AM	2/24/2021 3:00:00 PM	Rodanthe	Lanes Narrowed	Maintenance is performing routine maintenance to the NC12 protective dunes in the Mirlo S-Curve area. One lane may be closed for short periods.
8/5/2021 9:05:00 AM	8/9/2021 10:05:00 AM	Near Rodanthe	Lanes Narrowed	Standing water remains on portions of NC12 from south of the Basnight Bridge to Hatteras. Areas impacted include Pea Island, Rodanthe, Waves, Salvo, and Ocracoke Island. N.C. 12 is passable, but motorists should slow down and use caution in areas where there is standing water.
10/29/2021 8:41:00 PM	10/30/2021 10:00:00 AM	Near Wanchese	Congestion	There is standing water from the Oregon Inlet Bridge to Hatteras Island. Motorists are advised to use caution when traveling through the area.
11/7/2021 9:21:00 AM	11/9/2021 1:00:00 PM	Rodanthe	Road Closed	Officials plan to reopen N.C. 12 between Marc Basnight Bridge and Rodanthe at 1 p.m. after N.C. Department of Transportation crews were able to clear much of the sand covering the Outer Banks highway.N.C. 12 was closed just after high tide at 9 a.m. Sunday and remained closed the past few days as heavy winds and ocean overwash from a coastal storm made the highway unsafe for travel on Hatteras Island. Drivers should use caution on N.C. 12 as standing water and sand are still present on parts of the road.
11/11/2021 9:21:00 AM	11/13/2021 10:21:00 PM	Rodanthe	Lane Closed	NCDOT crews are repairing the protective dunes just north of the Village of Rodanthe. One lane will be closed for this operation follow temporary traffic signs and watch out for moving equipment and maintenance workers in the area.
11/19/2021 7:25:00 AM	11/23/2021 5:00:00 PM	Rodanthe	Lane Closed	One Lane Closed for Alternating Traffic for Dune Reconstruction. Watch for Flaggers and Pilot Car
February: Coastal storms in late January and early February led to need for dune maintenance. August: Standing rainwater. October: Rain and soundside flooding (reference NCDOT NC12 Twitter 10/29/2021). November: Coastal storm November 6-9 and subsequent dune restoration.				

USACE Dredge and Disposal Records

The USACE has historically dredged and placed material within the project monitoring area on a near-annual basis as described in the baseline report. However, in recent years dredging and placement events have been sparse. Data are gathered from the USACE Navigation Data Center databases (https://www.iwr.usace.army.mil/About/Technical-Centers/NDC-Navigation-and-Civil-Works-Decision-Support/NDC-Dredges/). Because the data sets were not available at the time of the 2020 update due to

changes in the USACE web file structure, dredging information for both Fiscal Year 2020 and Fiscal Year 2021 are included in the present report (Table 11). There were no private contract dredging operations in Oregon Inlet during either of these fiscal years, with the USACE conducting all of the operations using the dredges Currituck (special purpose small hopper dredge), Merritt (sidecaster), and Murden (special purpose small hopper dredge). The amounts dredged were relatively small with totals of 144,323 cubic yards in FY2020 and 142,947 cubic yards in FY2021 (for comparison, beach nourishment in Buxton completed in August 2022 placed 1.2 million cubic yards of sand over 2.9 miles of shoreline). The sidecaster operations do not remove material from the inlet system and the small hopper dredges generally place dredged material as close as possible to the surf zone at the north end of Pea Island.

Table 11. Dredging in the vicinity of Oregon Inlet in Fiscal Years 2020 and 2021.

DREDGE NAME	FY	JOB NAME	START DATE	STOP DATE	ACTUAL CUBIC YDs	ACTUAL COST
CURRITUCK	2020	OREGON INLET, NC	10/9/2019	10/17/2019	4,360	$156,000.00
CURRITUCK	2020	OREGON INLET, NC	10/26/2019	10/29/2019	2,080	$45,000.00
MERRITT	2020	OREGON INLET, NC	10/31/2019	11/9/2019	14,208	$275,000.00
MERRITT	2020	OREGON INLET, NC	11/27/2019	12/8/2019	14,328	$220,000.00
MERRITT	2020	OREGON INL, NC -NCDOT	2/14/2020	3/8/2020	45,900	$660,000.00
CURRITUCK	2020	OREGON INLET, NC	4/15/2020	5/6/2020	16,040	$580,500.00
CURRITUCK	2020	OREGON INLET, NC	5/14/2020	5/20/2020	4,790	$180,000.00
MERRITT	2020	OREGON INLET, NC	6/15/2020	7/5/2020	32,490	$375,809.00
MERRITT	2020	OREGON INLET, NC	7/19/2020	7/22/2020	5,442	$88,000.00
CURRITUCK	2020	OREGON INLET, NC	9/4/2020	9/16/2020	4,685	$150,000.00
				Totals FY 2020	**144,323**	**$2,730,309.00**
DREDGE NAME	FY	JOB NAME	START DATE	STOP DATE	ACTUAL CUBIC YDs	ACTUAL COST
MERRITT	2021	OREGON INLET, NC	11/16/2020	11/30/2020	16,985	$198,152.00
MURDEN	2021	OREGON INLET, NC	11/30/2020	1/6/2021	27,335	$619,400.00
CURRITUCK	2021	OREGON INLET, NC	12/14/2020	12/18/2020	550	$105,000.00
MERRITT	2021	OREGON INLET, NC	2/10/2021	3/1/2021	31,932	$403,160.00
MURDEN	2021	OREGON INLET, NC	2/15/2021	2/25/2021	12,580	$292,600.00
MERRITT	2021	OREGON INLET, NC	5/9/2021	5/19/2021	12,995	$205,000.00
MERRITT	2021	OREGON INLET, NC	6/17/2021	6/23/2021	9,425	$140,080.00
MERRITT	2021	OREGON INLET (WEST), NC	7/1/2021	7/14/2021	17,515	$273,328.00
MURDEN	2021	OREGON INLET, NC	8/26/2021	8/30/2021	8,500	$182,400.00
MURDEN	2021	OREGON INLET, NC	9/26/2021	9/30/2021	5,130	$273,600.00
				Totals FY 2021	**142,947**	**$2,692,720.00**

NCDOT Maintenance Records

NCDOT provided information on NC 12 roadway maintenance activities in 2021. Table 12 lists the maintenance activities undertaken within the monitoring program study area in the year 2021. This list does not include any work associated with removal of the Herbert C. Bonner Bridge, the Basnight Bridge, the Rodanthe Bridge, nor any work reported on NC 12 outside of the study area. As shown, maintenance expenditures in 2021 were approximately $771,000 with most of the expenses related to sand removal and response to the November 7, 2021 coastal storm (see discussion in the Storm Events section).

Table 12. NCDOT Highway 12 Maintenance, 2021 Expenditures.

Dates/Event	Description	Labor & Material	Equipment	Other	Total
8/31/2021	Repair Pipe Pea Island NC 12	$1,978 L $708.38 M	$819		$3,505.38
7/12/2021	Patching NC 12 South	$17,421 L $11.81 M	$4,426	$3,441.96	$25,300.65
1/1/2021-12/31/21	Pea Island Removal of Sand	$240,513.47 L	$100,882.60	$362,446.12	$463,328.72
November 7th 2021 Coastal Storm	NC 12-Canal Area	$6,891.2 L	$534.75	$217,992.93	$218,527.68
November 7th 2021 Coastal Storm	NC 12-Canal Area	$4,294.74 L	$629.25	$60,041.61	$60,670.86
				Total	$771,333.29

Barrier Island Breaches

In two locations, the barrier island was breached by Hurricane Irene in August 2011: just south of the freshwater ponds (Pea Island Breach) and at the north end of the town of Rodanthe (Rodanthe Breach). The evolution of these breaches during 2021 is shown in Figure 49 and Figure 50. The original breach configurations following Hurricane Irene are shown as dashed lines on the figures. Figure 49 shows Pea Island Breach shorelines digitized from available photography over the February 1, 2022 photograph. Similarly, Figure 50 presents the Rodanthe Breach shorelines digitized, over the February 1, 2022 photography. The Pea Island Breach was closed for all of 2021, with the most seaward shoreline position measured in August 2021. The majority of the Rodanthe Breach (within the right of way) was filled by NCDOT shortly after its formation in order to repair the roadway, and the area is continuing to be monitored. The most seaward positions in this area were also observed in August 2021.

2021 Shorelines

- ——— February 1, 2022
- ——— September 30, 2021
- ——— August 12, 2021
- ——— June 18, 2021
- ——— April 16, 2021
- ——— February 6, 2021
- ——— December 10, 2020
- ╌╌╌ August 28, 2011

0   125   250   500 Feet
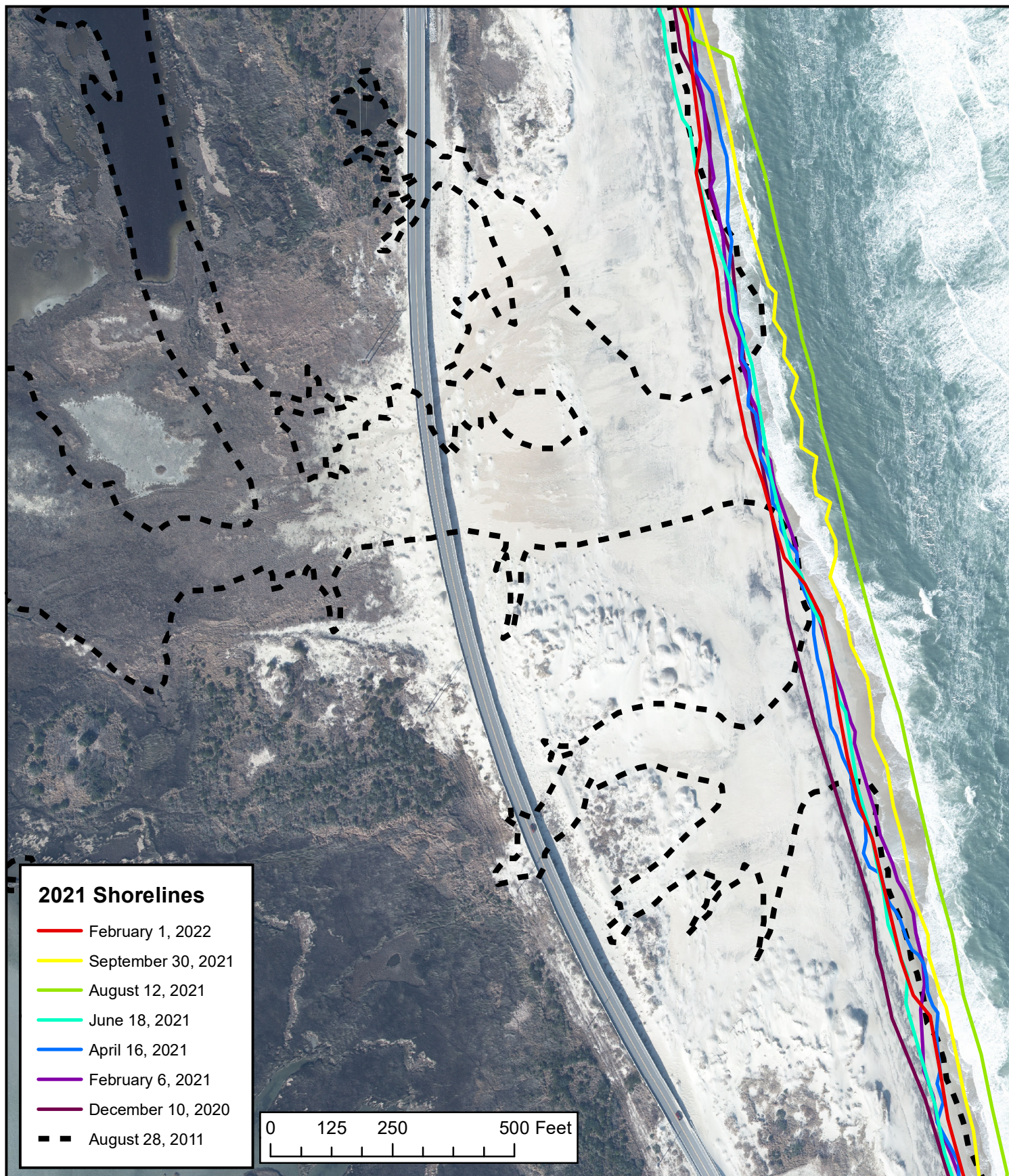
Figure 49

(Image 1 of 1)

Evolution of the Pea Island Breach

Prepared for the North Carolina Department of Transportation
Horizontal Datum: North Carolina State Plane Feet 1983 FIPS 3200
Orthophoto Date: February 1, 2022; Map Created: October 11, 2022

2021 Shorelines

— February 1, 2022
— September 30, 2021
— August 12, 2021
— June 18, 2021
— April 16, 2021
— February 6, 2021
— December 10, 2020
- - - August 28, 2011

0   125   250   500 Feet
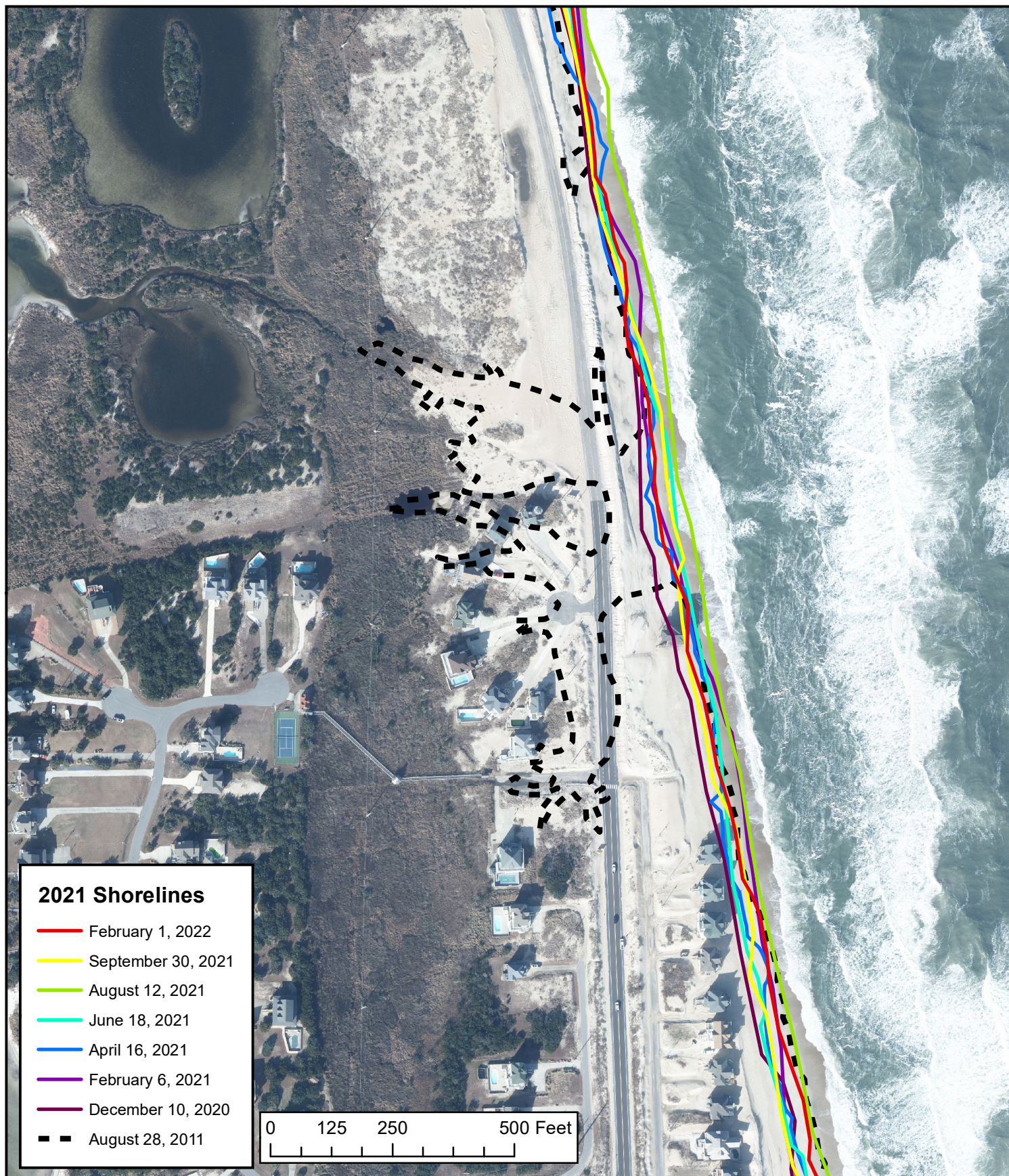
Figure 50

(Image 1 of 1)

Evolution of the Rodanthe Breach

Prepared for the North Carolina Department of Transportation
Horizontal Datum: North Carolina State Plane Feet 1983 FIPS 3200
Orthophoto Date: February 1, 2022; Map Created: October 11, 2022

4. TERMINAL GROIN MONITORING

A subset of the Coastal Monitoring Program is the specific analysis of shoreline data as required by the easement (permit) for the Oregon Inlet Terminal Groin. Two permits have been issued for the groin, one in 1989 and a second in 2012.

In 1989, prior to construction, a monitoring program was proposed and accepted to meet the requirements of the permit. Key elements of the program were: 1) the establishment of a historical shoreline change rate, 2) the determination of a project shoreline change rate every two months and 3) a comparison of the project rate to the historical rate to determine possible adverse impact. If the monitoring program determines that there is an increase in shoreline erosion above the background historical rates, then two thresholds for corrective beach nourishment have been established.

These criteria are, in summary:

1) If the erosion, in volume of sand (1 sq ft = 1 cu yd), exceeds the predicted loss in the amount of 250,000 cu yd in any one mile segment of the Pea Island monitoring area, or

2) If the volume of erosion in any three mile segment of the monitoring area exceeds the predicted loss by 500,000 cu yd, and

3) If either of these losses is confirmed through two consecutive two-month cycles of the monitoring program, then

4) Beach nourishment will be scheduled by NCDOT with the minimum volume equaling that which is necessary to replace the excess erosion at the time of confirmation of need.

A conversion of 1 square ft of beach surface to 1 cubic yd of beach volume is commonly used in coastal engineering design and reflects a vertical distance from the beach berm to a depth of closure of 27 ft.

Under the conditions of the new terminal groin easement signed in August 2012, the historical rate must be reviewed in order to validate or update in light of climate change and related coastal processes. This review has been presented in a separate report to NCDOT (Overton 2014) and discussed at a number of meetings with NCDOT and US Fish and Wildlife Service. On April 6, 2018, a memo was received from the US Fish and Wildlife Service (included in the 2018 report) confirming the new methodology to determine the historical and project rates.

The historical rate is now determined as a linear regression rate using shoreline data between October 1968 and October 1988. The project rate is determined as a linear regression rate using shoreline data beginning in August 1992 to present. These rates are used along with the established methodology for determination of adverse impact.

Unlike the previous sections, the terminal groin monitoring focuses on the first six miles of Hatteras Island immediately south of Oregon Inlet (Transects 170 to 381).

Completed per the conditions of the August 2012 USFWS easement, the terminal groin monitoring results are presented in this section.

Historical Analysis

The dates selected for the historical analysis are October 3, 1968 to October 9, 1988, inclusive of intermediate dates presented in Table 13. These dates have been selected following analysis (Overton 2014) and multiple discussions with NCDOT and USFWS representatives. The early date of October 3, 1968 was selected because it was in the 1960s as mentioned in the 2012 easement, and was also 6 years after the 1962 "Ash Wednesday" nor'easter, which had a dramatic impact on the barrier island morphology. The more recent date, October 9, 1988, was chosen because it is the most recent set taken prior to the March 1989 nor'easter, a storm that caused considerable erosion. The use of photography just after this storm had the potential to bias the historical erosion rate analysis to higher values.

Table 13. Shoreline position data used for computation of historical shoreline change rate

Date	Shoreline Position Data Source
10/3/1968	COASTS database
6/4/1974	COASTS database
12/2/1978	CERC-UVA Rectified photos
10/21/1980	COASTS database
9/19/1984	NCDOT Archive
10/1/1986	COASTS database
7/10/1987	CERC- UVA Rectified photos
10/9/1988	NCDOT Archive

Figure 51 shows the annual historical erosion rate based upon linear regression of shoreline position at each transect from October 1968 to October 1988. Transect 170 corresponds to mile zero reported in Figure 51, and Transect 381 corresponds to mile 6 (see Figure 1 for transect locations). In general, the historical erosion rate along this portion of Pea Island was relatively high, with a mean value of about 12.7 ft/yr. The portion of the shoreline within the first mile of the old Coast Guard Station (closest to the inlet) was clearly the area of highest erosion, as one would expect near the inlet. In this area, the erosion rate has a maximum value of 36 ft/yr, and decreases to about 12 ft/yr approximately 1 mile south of the old Coast Guard Station. Rates increase to over 20 ft/year at the northernmost pond (mile 2.6), with lower rates further south.
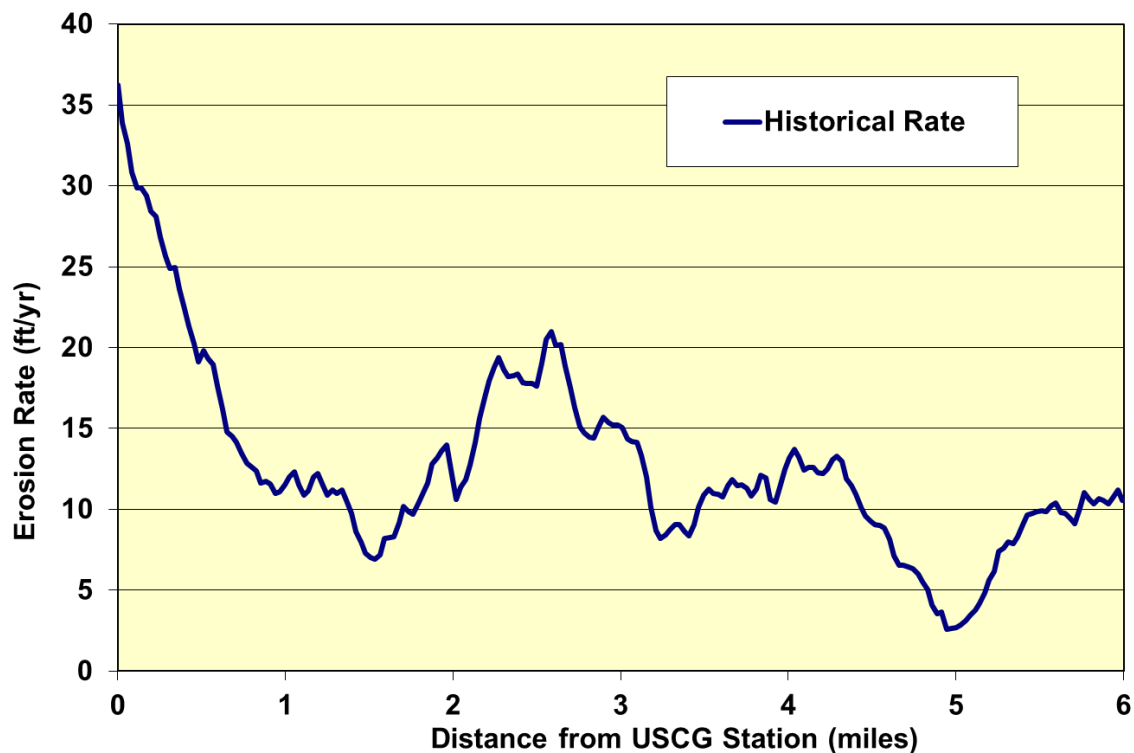
Figure 51. Annual Historical Erosion Rate: October 3, 1968 to October 9, 1988.

Dates of Aerial Photography

Shorelines digitized from the 2021 aerial photography (Table 1) were used along with other historical data in the following analysis. It is noted that the February 1, 2022 shoreline position was used in this analysis because there was no photography in December 2021.

Shoreline Change Adjacent to the Terminal Groin

An enlargement of the map of the northern end of Pea Island is shown in Figure 52 and Figure 53. Each figure shows the shoreline differences over a six month time span (December 2020 to June 2021, Figure 52, and June 2021 to February 2022, Figure 53). Three shoreline positions are presented in each figure: the two between which differences are noted and the initial position prior to terminal groin construction (October 5, 1989). For the purpose of monitoring the impact of the terminal groin, the study area begins at Transect 170, which cuts through the old US Coast Guard Station. However,

approximately 2,000 ft of shoreline lies between the groin and Transect 170. While the change in shoreline in the vicinity of the groin is not included in the standard analysis of shoreline change, it is documented each survey period. Using Transect 170, the terminal groin, the October 5, 1989 shoreline, and the current shoreline as boundaries, it is possible to determine the net change in beach area since construction of the groin. The beach area between the terminal groin and transect 170 was essentially filled in by October 1992. At that time the area was approximately 51 acres. Since then, the beach area has varied, for the most part, between 50 and 70 acres, as seen in Figure 54. As of February 2022, the area between the groin and transect 170 was approximately 57 acres, while the greatest area in 2021 was observed in August and September and was approximately 69 acres (in both months).

Method of Analysis

The method used to determine shoreline change rate has changed from endpoint in reports prior to 2018, to linear regression. At each transect, the locations of all shoreline positions in the dataset from August 8, 1992 to present are used in a linear regression analysis. The shoreline change rate is the slope of the linear regression line at each transect. This establishes what is referred to as the "project rate," which is then compared to the historical shoreline change rate. This allows for a comparison of the shoreline change observed during the project period (in this case, from August 8, 1992 through the end of calendar year 2021) as compared to the rate of the shoreline change during the period established for historical reference (between October 1968 and October 1988).

In order to determine if there is any significant increase in erosion along the northern end of Pea Island, the one-mile and three-mile criteria have been established, as discussed previously. The one-mile threshold is 250,000 cu yd, while the three-mile threshold is 500,000 cu yd. The one-mile volume is calculated using 35 transects (approximately 5,250 ft), and the value is assigned to the transect at the mid-point of the section. Thus, the first value reported is for transect 187 (170 + 17).

The three-mile volume calculations are made in a manner similar to the one-mile, with 106 transects (15,900 ft, or 3.01 miles) used as the distance. Again, the value used in reporting is assigned to the transect at the mid-point of the section. Therefore the first value is assigned to transect 223 (170+53).
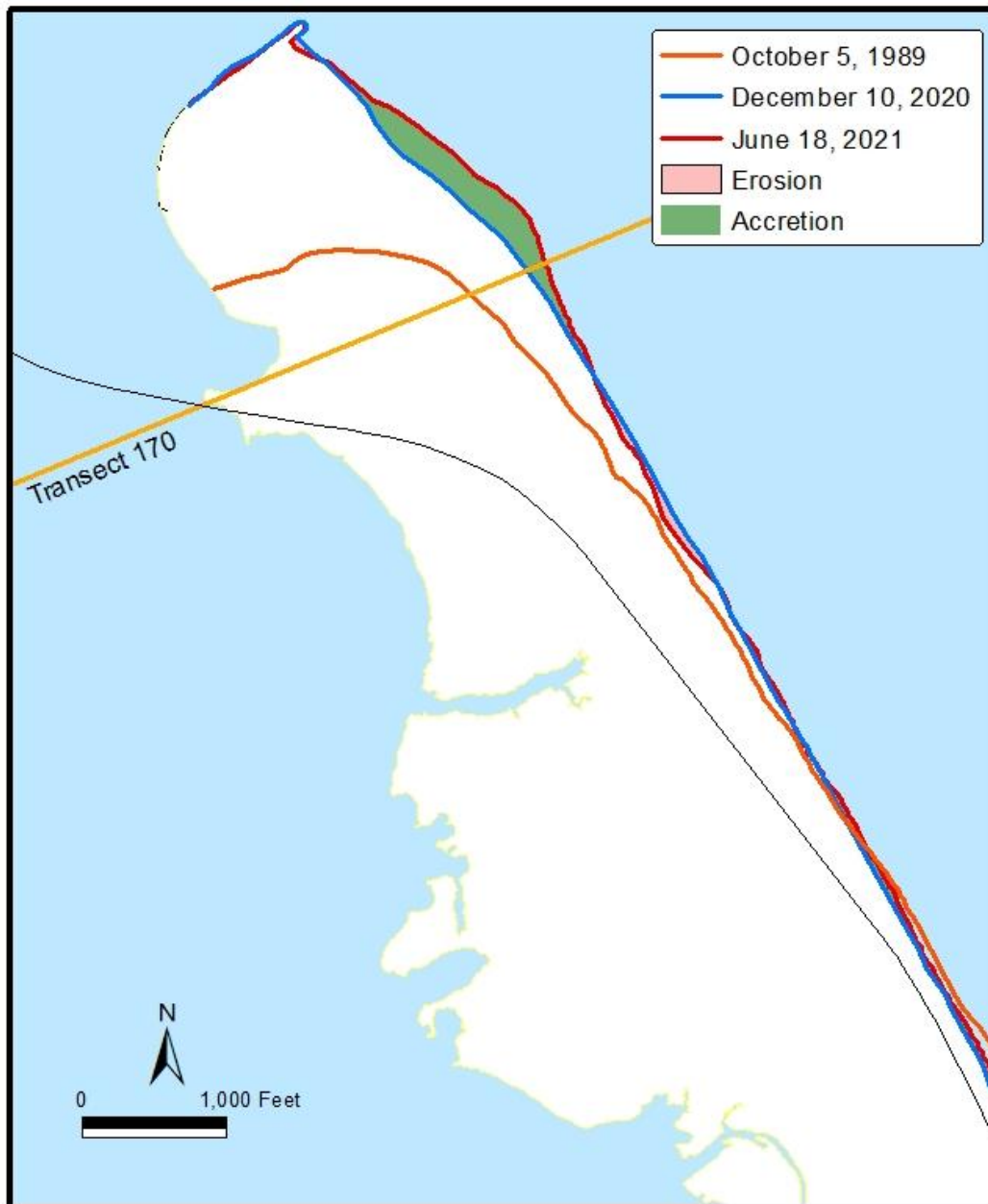
Figure 52. Shoreline Change near the Terminal Groin, December 2020 to June 2021
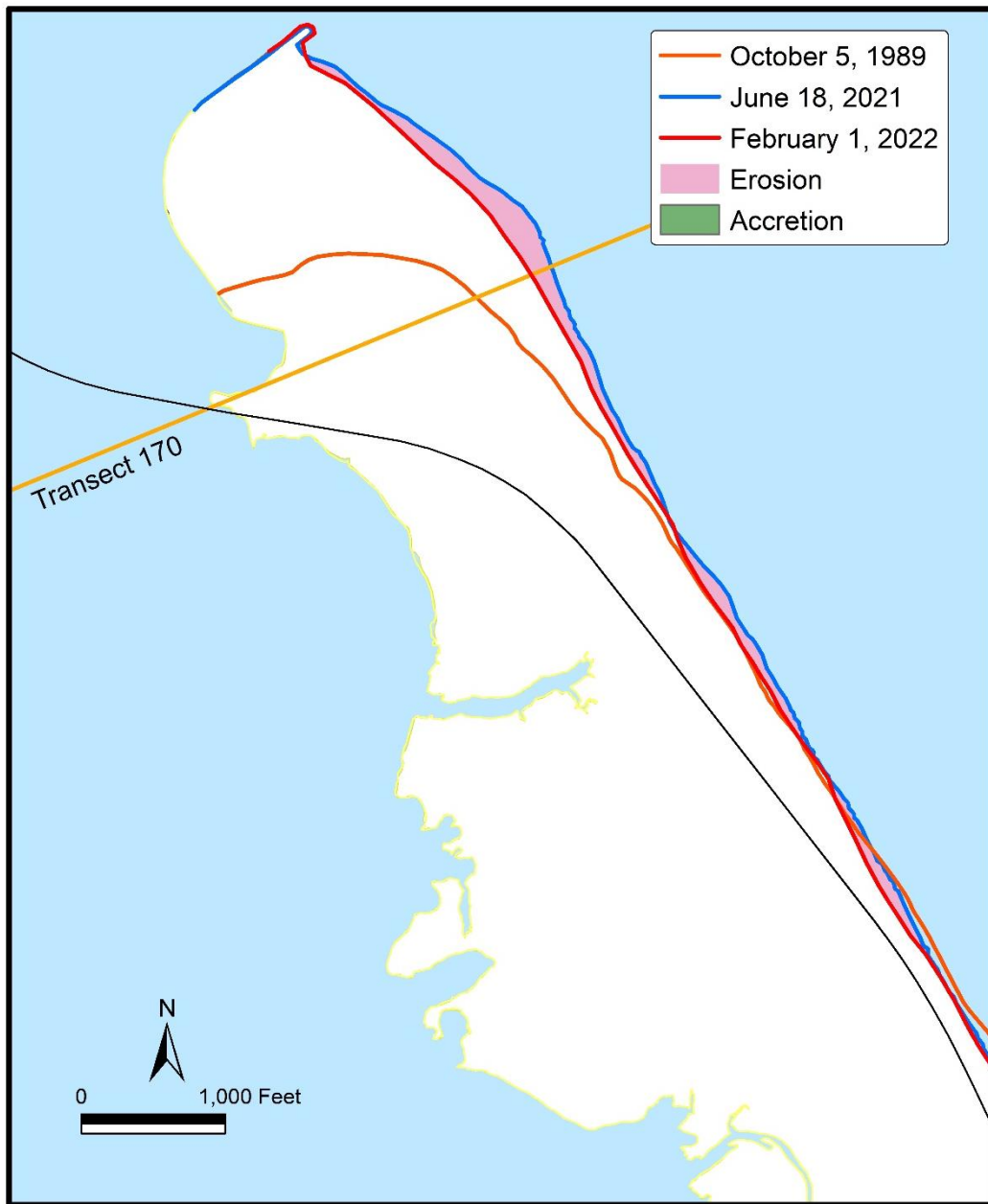
Figure 53. Shoreline Change near the Terminal Groin, June 2021 to February 2022
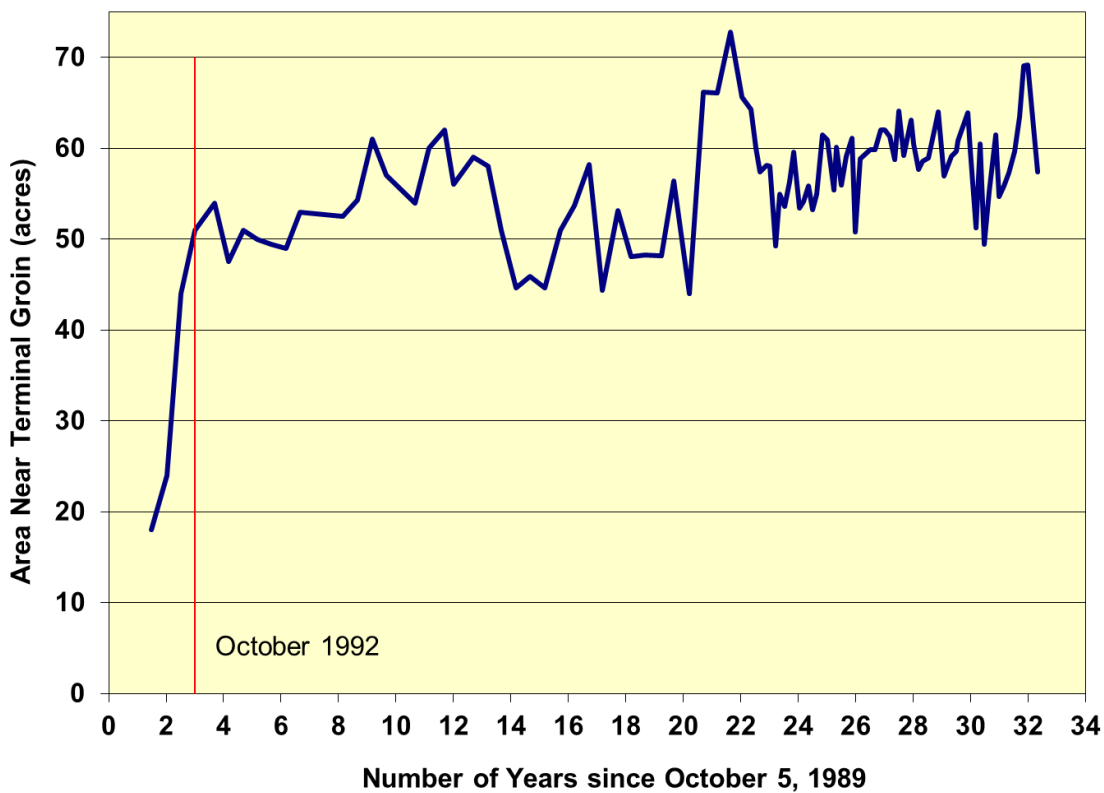
Figure 54. Area of Accretion between Transect 170 and the Terminal Groin

Project Erosion Rate

Using the August 8, 1992 to February 1, 2022 data, the current project erosion rate is computed and compared with the previously reported historical erosion rate in

Figure 55. The historical rate can be characterized by trends in three sections: in the first mile, the erosion rate was high with a peak of 36 ft/yr and an average of 21 ft/yr. In the next three miles, the rate was approximately 13 ft/yr; in the last two miles, the average rate was 9 ft/yr. The trends of the current project rate can also be examined according to spatial variation along the project area. Within the first mile of the study area, the project rate and hence, shoreline position, is clearly influenced by the groin and any dredge disposal activity that has taken place. The project rate in this section is, on average, 2.8 ft/yr of accretion. In the next three miles of the study area, the current project rates are also less than the historical rates. The average project rate from mile 1 to 4 is 2.9 ft/yr of erosion. In the last two miles the average erosion rate is 3.0 ft/yr. The lower rates closer to the groin are due to the cyclic fluctuating shoreline caused by the presence of the terminal groin that traps sand, the ebb shoal bar which tends to refract the waves and reverse the direction of alongshore transport (to the north) and the occasional episodic supply of sand provided by the dredge disposal activities of the USACE. The project rate does not exceed the historical rate at any transect in the study area for 2021.
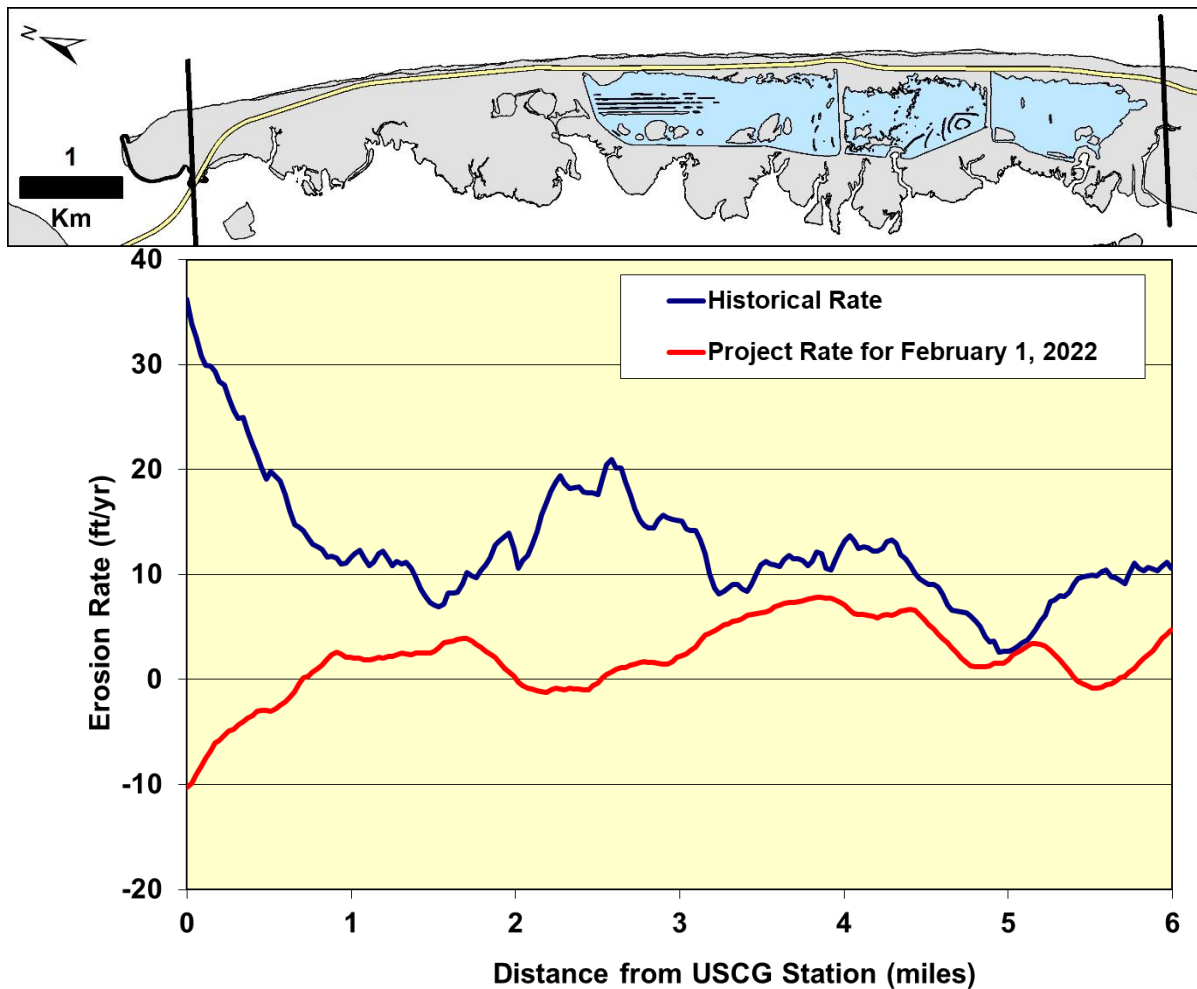
Figure 55. Comparison: Historical Erosion Rate and Project Erosion Rate for February 1, 2022

One-Mile Volume Change Analysis

The one-mile volume analyses for February 2021 through February 2022 are presented in Figure 56. The values are different from those in reports prior to 2018 because of the change in methodology for calculating the historical and project rates as of the 2018 report. Additionally, the values are similar from date to date because the linear regression project erosion rate does not change substantially during the year. The volume change everywhere is less than that predicted by the historical rates.

Three-Mile Volume Change Analysis

The three-mile volume analyses for February 2021 through February 2022 are presented in Figure 57. The values are different from those in earlier reports because of the change in methodology for calculating the historical and project rates, and volume change everywhere is less than that predicted by historical rates.
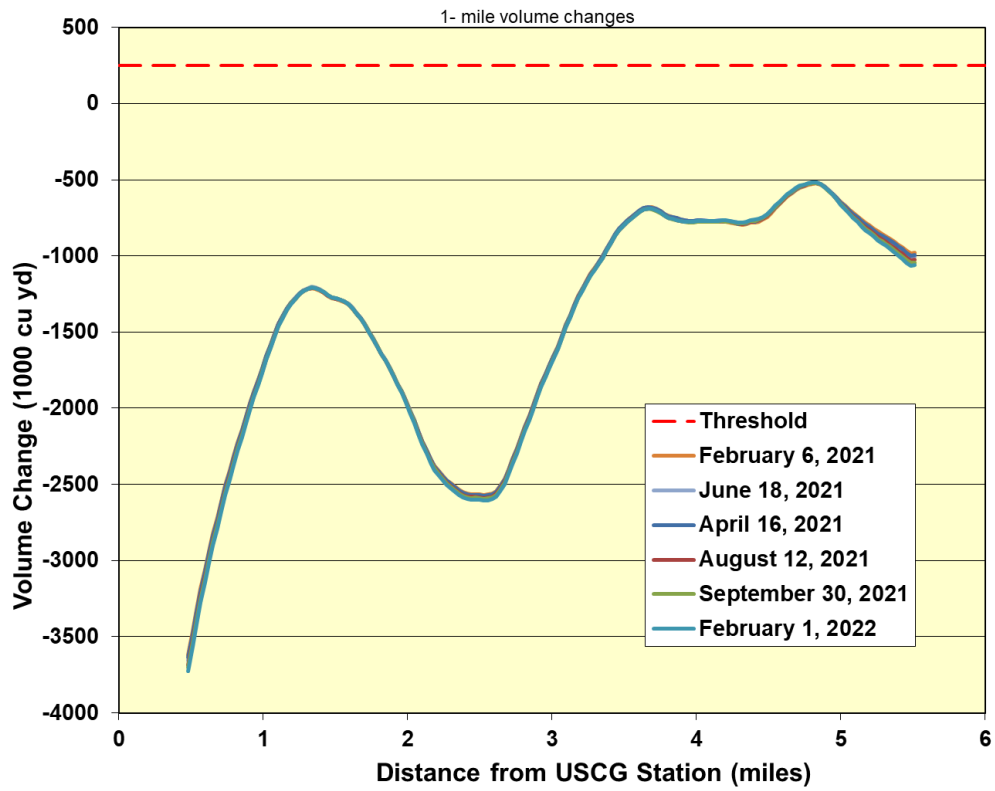
Figure 56. One-Mile Volume Change for 2021.
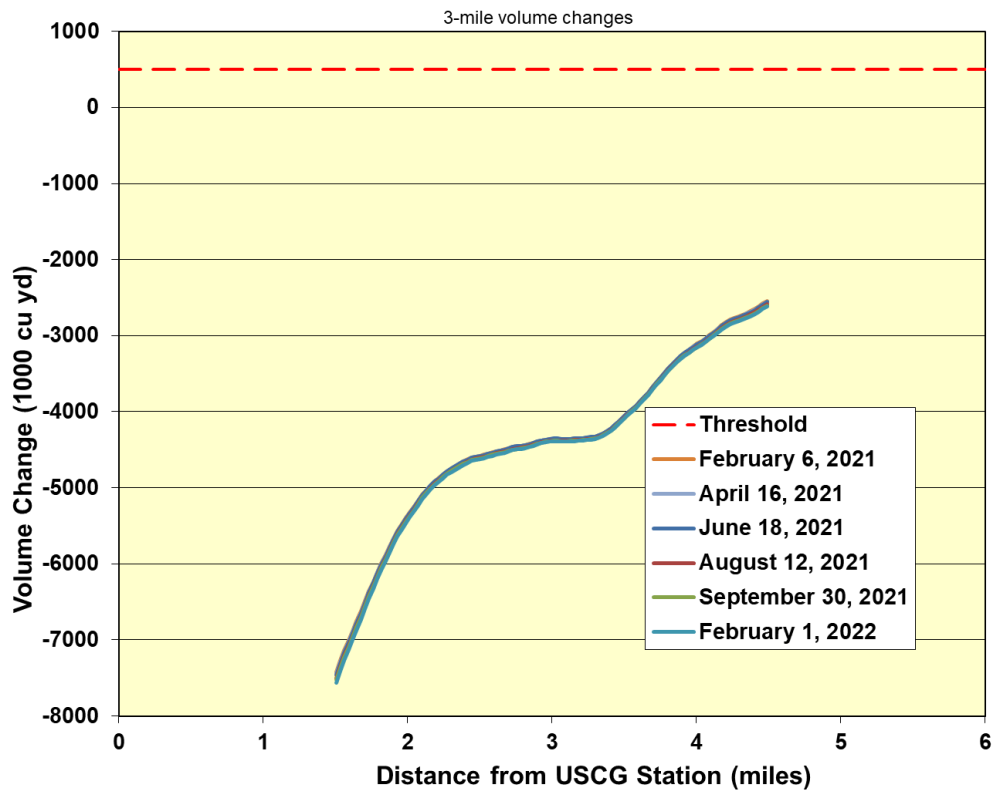
Figure 57. Three-Mile Volume Change for 2021.

Terminal Groin Monitoring Summary and Conclusions

As of February 1, 2022, the project erosion rate does not exceed the historical rate at any point in the first six miles south of the Oregon Inlet terminal groin. The one and three mile volume calculations are well below that which would be expected using the historical erosion rate. In summary, the construction of the groin does not appear to have caused an adverse impact to the shoreline over the six-mile study area.

5. HIGHWAY VULNERABILITY CONCLUSIONS

Figure 58 illustrates the changes in vulnerability throughout 2021, including values for each indicator as well as a composite of the three at each photo date. For the dates when no topographic data were obtained, the dune crest height corresponding to the previous photo date was used.

In order to assess overall vulnerability at each transect during 2021, a composite of three of the primary criteria discussed in this report was created, and it is shown in Figure 59. The summary criteria were: 1) Island width (measured as distance from ocean to estuarine shoreline) less than 1000 ft; 2) Dune crest elevation less than 10 ft above NC 12; and 3) The critical buffer, where the NC 12 edge of pavement was within 230 ft of the present shoreline. In a change from previous reports, and based on feedback from meetings with NC DOT and US FWS, this figure shows the composite vulnerability based on the transect meeting the criterion at any point during the study year (i.e., if one transect met the island width criterion in February and the critical buffer criterion in December, it would be reported as having met two criteria during the study year). This change has led to an overall increase in the reported numbers of vulnerable transects.

In reports between 2011 and 2017, the four transects within the original Pea Island Breach (and the associated temporary bridge) were excluded from the vulnerability analysis. NCDOT completed construction of a 0.5-mile interim structure in late 2017. Because the new structure is not intended as a long-term solution for the maintenance of NC 12, this analysis will continue to assess the distance between the edge of pavement (bridge) and the ocean shoreline within the interim bridge area. All transects are now being included in the composite vulnerability plots from the 2018 report and moving forward.
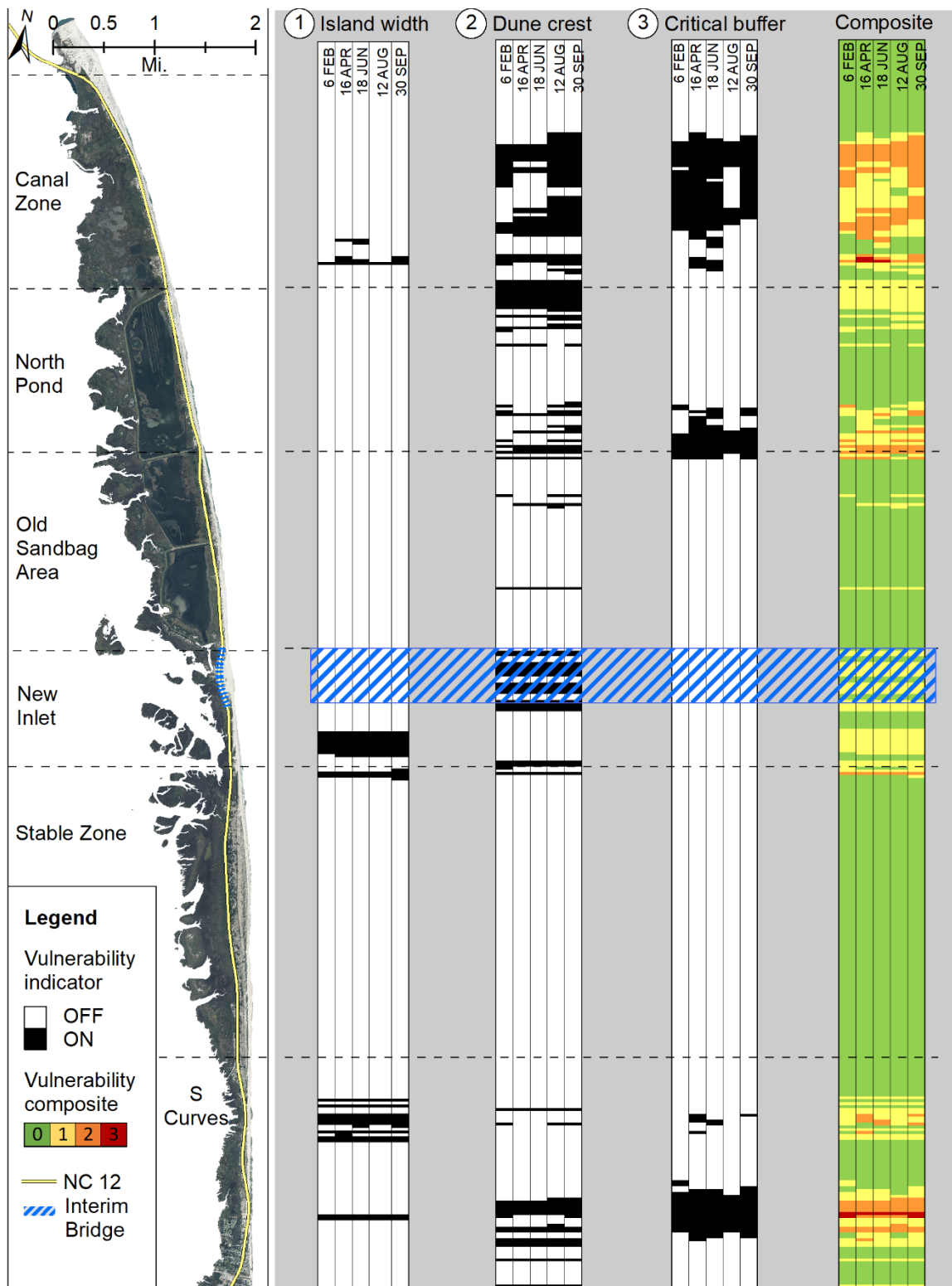
Figure 58. Composite NC 12 vulnerability along the study area at each photo date; note that for the June imagery, the dune crest height at the previous date was used because no topographic data were obtained.
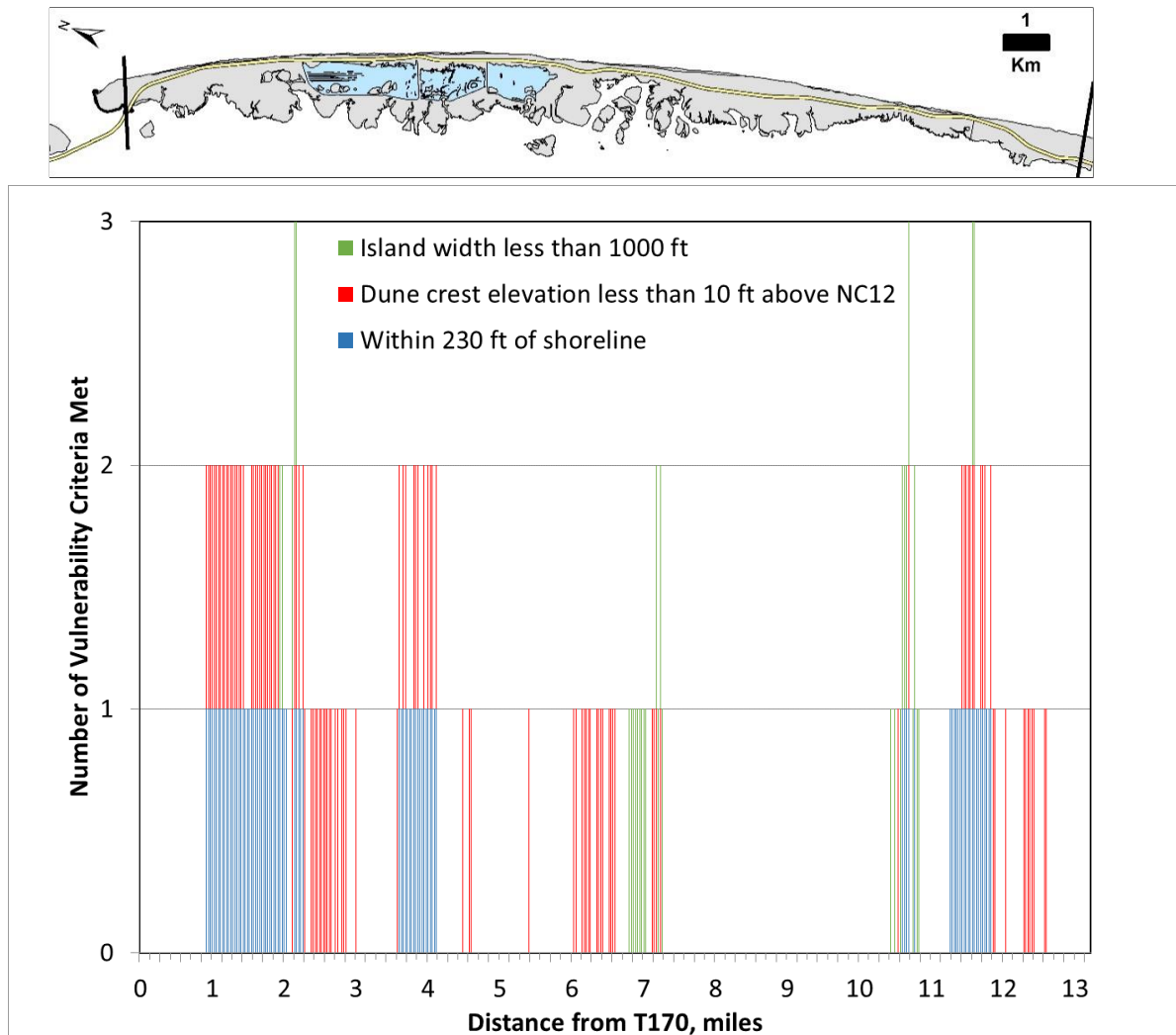
Figure 59. Composite NC 12 vulnerability along the study area, considering criteria met during any of the photo dates in 2021.

As determined by the established 230 ft critical buffer vulnerability criteria, there were 90 transect locations along NC 12 that were vulnerable in 2021, a decrease from the number reported at the end of 2020. The transects where the shoreline was located within the 230 ft buffer were Transects 202-241, 245-249, 296-314, 541-544, 547, and 564-584.

There were 31 transects at which the island widths were less than 1000 ft during the 2021 study year: Transects 238-239 and 244-246 in the Canal Zone, Transects 408-416 and 421-424 south of the Pea Island Breach, and 11 transects distributed between Transects 535 and 549 narrow area north of Rodanthe, approximately miles 10.4 - 10.8); and Transects 575 and 576 (approximately mile 11.5 near the southern refuge boundary).

There were 115 transects with dune crest elevations less than 10 ft above the NC 12 centerline elevation at some point in 2021. The transects with dune crest elevations less than 10 ft above the NC 12 elevation are widely distributed over the study area, with the exception of the well-developed dune field in place from approximately miles 7.5 to 10.5 south of the Old Coast Guard Station.

The areas of primary concern (meeting more than one of the criteria) as shown on Figure 59 were located in the Canal Zone, near the Pea Island Visitors Center between the north and center ponds, south of the Pea Island Breach, and in northern Rodanthe. This result is similar to results reported in past updates.

Figure 60 presents a comparison of the vulnerability from the baseline report to the present (2021) report. These conditions are the conditions at the end of each study year. The transects that have been the most vulnerable throughout the study period are highlighted in red (Transects 244-245 and Transects 575-576).
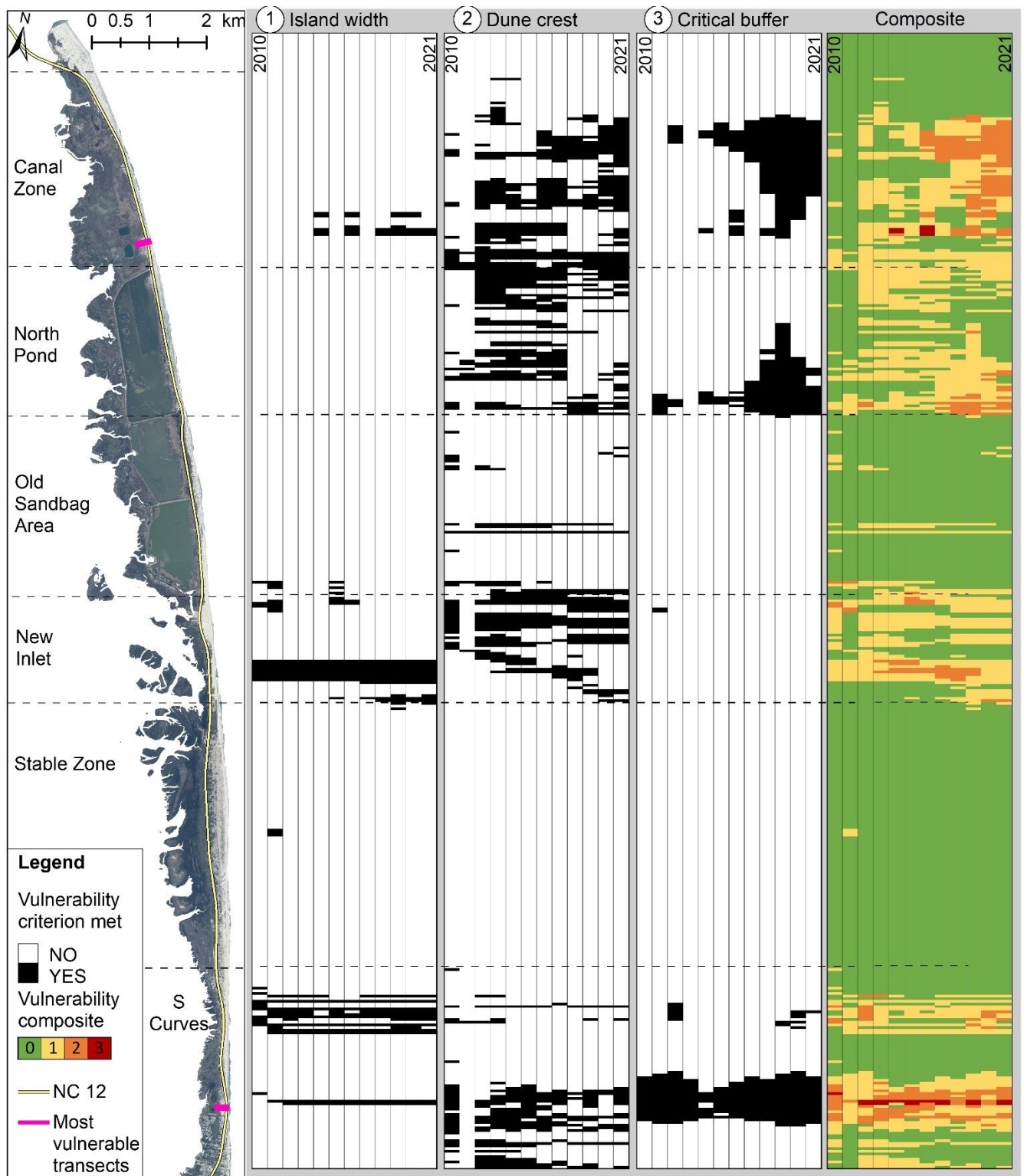
Figure 60. Comparison of vulnerability from the baseline report to the 2021 report. Vulnerabilities reported at the end of each study year.

6. REFERENCES

Dolan, R., Hayden, B. P., May, P., and May, S., 1980. The reliability of shoreline change measurements from aerial photographs. *Shore and Beach*, 48(4), 22–29.

Lillesand, T. M., R. W. Keifer and J. W. Chipman, 2004. *Remote Sensing and Image Interpretation*. 5th ed., New York: Wiley.

National Oceanographic and Atmospheric Administration (NOAA), 2012. Vertical Datum Transformation Tool (VDATUM) website < http://vdatum.noaa.gov/>, last accessed 5/8/2012.

Overton, M.F., 2012. Coastal Monitoring Program, NC 12 Transportation Management Plan, TIP Project B-2500, Baseline Report.

Overton, M.F., 2013. Coastal Monitoring Program, NC 12 Transportation Management Plan, TIP Project B-2500, Update Report.

Overton, M.F., 2014. Coastal Monitoring Program, NC 12 Transportation Management Plan, TIP Project B-2500, Update Report.

Overton, M.F., 2014. Historical Erosion Rates in the Vicinity of the Oregon Inlet Terminal Groin, NC 12 Transportation Management Plan, TIP Project B-2500, 9/10/2014.

Overton, M.F., and E.J. Sciaudone, 2015. Coastal Monitoring Program, NC 12 Transportation Management Plan, TIP Project B-2500, Update Report.

Overton, M.F., and E.J. Sciaudone, 2016. Coastal Monitoring Program, NC 12 Transportation Management Plan, TIP Project B-2500, Update Report.

Overton, M.F., and E.J. Sciaudone, 2017. Coastal Monitoring Program, NC 12 Transportation Management Plan, TIP Project B-2500, Update Report.

Overton, M.F., and E.J. Sciaudone, 2018. Coastal Monitoring Program, NC 12 Transportation Management Plan, TIP Project B-2500, Update Report.

Sciaudone, E.J. and M.F. Overton, 2019. Coastal Monitoring Program, NC 12 Transportation Management Plan, TIP Project B-2500, Update Report.

Sciaudone, E.J. and M.F. Overton, 2020. Coastal Monitoring Program, NC 12 Transportation Management Plan, TIP Project B-2500, Update Report.

Overton, M.F. and J.S. Fisher, 2005. Bonner Bridge Replacement, Parallel Bridge Corridor with NC 12 Maintenance. Shoreline Change and Stabilization Analysis. Prepared for URS Corporation – North Carolina, June 2005, Task Orders 18 and 20, TIP No. B-2500.

Stone, J., Overton, M.F. and J.S. Fisher, 1991. Options for North Carolina coastal highways vulnerable to long term erosion, NCSU Research Report prepared for the NC Department of Transportation.

APPENDIX A: NCDOT Physical and Biological Monitoring Reports – 2021

STATE OF NORTH CAROLINA
DEPARTMENT OF TRANSPORTATION

ROY COOPER
GOVERNOR

J. ERIC BOYETTE
SECRETARY

06/06/2022

Mr. Tyler Stanton
Biological Surveys Group Project Manager
NCDOT Environmental Analysis Unit
1598 MSC
Raleigh NC, 27699-1598

June 2022

Memorandum To:	John Conforti, REM, Senior Project Manager Michael Turchy, Environmental Program Consultant Environmental Analysis Unit
From:	Tyler Stanton, Environmental Supervisor Environmental Analysis Unit
Subject:	2021 Data Summary: Shoreline Monitoring of Physical and Biological Condition of the Beach Sand on Pea Island National Wildlife Refuge, Dare County

Introduction

This report summarizes and graphically presents the results of ten years (4 quarterly sampling events per year) of monitoring the physical and ecological condition of the beach on Pea Island National Wildlife Refuge (PINWR) from the Terminal Groin to Mirlo Beach.

In 2012, as a condition of the new easement for Retention and Maintenance of the Oregon Inlet Terminal Groin at Pea Island NWR, the North Carolina Department of Transportation Biological Surveys Group (NCDOT BSG), implemented a monitoring program to provide the US Fish and Wildlife Service (USFWS) with data on the physical and biological attributes of the beach sand on PINWR. This study encompasses the entire length of the Refuge beach, from the Terminal Groin to Rodanthe (Figure 1).

Mailing Address:
NC DEPARTMENT OF TRANSPORTATION
PROJECT DEVELOPMENT AND
ENVIRONMENTAL ANALYSIS
1548 MAIL SERVICE CENTER
RALEIGH, NC 27699-1548

Telephone: (919) 707-6000
Fax: (919) 250-4224
Customer Service: 1-877-368-4968

Website: www.ncdot.gov

Location:
1000 BIRCH RIDGE DRIVE
RALEIGH, NC 27610

The purpose of this multi-year study is to monitor the environmental effects of the Terminal Groin and any future beach nourishment or other activities on Pea Island National Wildlife Refuge in Dare County, NC.

Sampling was conducted quarterly; usually in January, April, July and October. There are 62 total transects beginning at the terminal groin (TG) and continuing south every 0.2 miles to the southern terminus of PINWR in Mirlo Beach. The first transect is located 0.1 mi south of the TG (numbered TG1), the 2nd 0.3 mi south of the TG (numbered TG2) and the third 0.5 mi south of the TG (numbered T1). Subsequent transects will continue with odd numbers through transect T29, so that they coincide with existing PINWR data points, and are located at 0.2 mi intervals. Beyond T29 transects are numbered in sequence (T30 - T74) to the southern boundary of the Refuge.
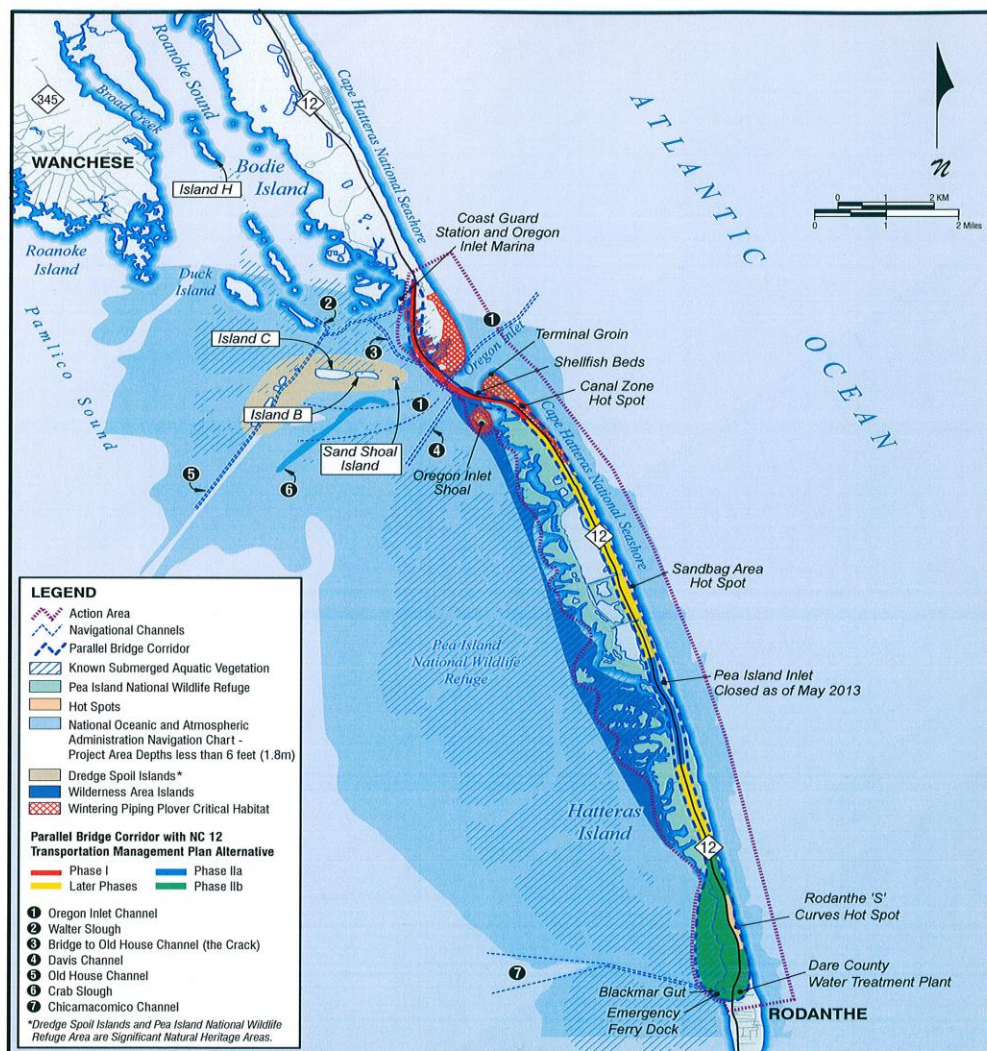
BIOLOGICAL ASSESSMENT ACTION AREA AND NATURAL RESOURCE-RELATED FEATURES

Figure 1

Meteorological and Other Activities Affecting the PINWR Beach

In August 2011 Hurricane Irene breached NC 12 in two locations in the project area – in northern Rodanthe (the "Rodanthe breach") approximately 12 miles south of Oregon Inlet and within the Pea Island National Wildlife Refuge (Refuge) approximately 6 miles south of Oregon Inlet (the new "Pea Island inlet") (see Figure 1). NCDOT repaired the section of NC 12 at the Pea Island inlet by installing a temporary bridge across the inlet. This temporary bridge was completed in October 2011. The Rodanthe breach was filled using sand sources from Hatteras Island, and the NC12 roadway was repaired within the existing easement. Since then, this bridge has been replaced by an interim bridge over the Pea Island breach to provide for interim safe and reliable transportation while the long-term solution is re-evaluated and constructed.

Hurricane Sandy, in October 2012, and two subsequent northeasters in November 2012 caused extensive shoaling near the mouth of the Pea Island inlet. Overwash during Hurricane Sandy resulted in more than three miles of dunes being lost or severely damaged between Oregon Inlet and Rodanthe. Repair work on NC 12 including rebuilding the sandbag dune at the S-curves occurred between November 2012 and January 2013. As of May 2013, the Pea Island Inlet closed as a result of naturally-occurring coastal processes.

From November to December 2013 sand was bypassed from a dredging operation in Oregon Inlet to the PINWR beach just south of the Terminal Groin. Approximately 581,000 cubic yards of sand were deposited on the Pea Island beach just south of the terminal groin.

From May through October 2014 a beach nourishment project was conducted on the southern 2 miles of PINWR and further onto National Park Service beach property. The sand sampling event occurred 1 week after the completion of the project and Transects 66 thru 73 occur in the nourishment area (Figure 2).

Hurricane Arthur, in July 2014, hit the outer banks, including Pea Island as a Category 2 Hurricane. Hurricane Arthur caused the Inlet, that was originally opened by Hurricane Sandy, to re-open; however, flow in subsequent weeks was reduced to limited sheet flow during high tides and the inlet closed again.

In the winters of 2015 and 2016, heavy Nor'easters hit Pea Island with 30-45mph winds and gusts in the upper 60+ mph range. The surf was approximately 12+ feet causing flooding and major washouts. Nor'easters are common during the winter, but many are not this intense.

In September 2016, Hurricane Hermine hit as a tropical storm, with heavy rainfall. Directly following in October 2016 Hurricane Matthew brings record rainfall and devastating flooding to the area. Hurricane Matthew brought approximately 9.4 inches of rain and wind speeds reached 74mph.

On September 18, 2017, Hurricane Jose passed the outer banks as a tropical storm with sustained winds of 85 mph, causing major flooding along PINWR and NC 12. Although

the strongest winds stayed offshore, with no direct hit to the outer banks, approximately 4 inches of standing water was reported causing closures of NC 12 through the PINWR.

On September 26 and 27, 2017, Hurricane Maria downgraded to a tropical storm with sustained winds of 70 mph before hitting the outer banks of NC, including the PINWR. Maria brought high storm surges with flooding which led to the temporary closure of many roads in the area. At the time, because of the predicted damage due to high winds and a water level rise of at least 2-4 ft, an evacuation was recommended in this area.

Winter Storm Riley affected the US East Coast in early March 2018 causing coastal flooding and beach erosion over multiple high tides prompting the closure of NC 12 through PINWR during these high tides.

Tropical Strom Chris formed off the coast of North Carolina in early July 2018. This storm caused heavy rain and erosion. High swells from the storm affected multiple areas along the Outer Banks.

Hurricane Florence, on September 14, 2018, brought winds up to 90 mph to the island with ocean overwash and a 13-foot storm surge. This contributed to dune erosion within PINWR. NCDOT closed NC 12 between Hatteras Village and the Bonner Bridge noting multiple locations were impassable including areas near PINWR.

Hurricane Michael was downgraded to a tropical storm as it passed through North Carolina on October 11 and 12, 2018. Gusts were observed as high as 74 mph in the northern Outer Banks including PINWR and water levels, from the storm surge, were 2-4 feet above ground level.

On September 6, 2019, Hurricane Dorian made landfall on Ocracoke Island and moved north over Hatteras Island causing severe beach erosion. This storm also resulted in a 7ft. storm surge on the sound.

October 11 and 13, 2019 Sub-Tropical storm Melissa hung offshore during a Harvest Moon tide for three to four days of high tide overwash of NC 12, burying the S-Curves area under approximately 5 ft of sand. The road was not compromised.

On November 16 and 17, 2019 heavy winds, up to 45 mph, and rain caused sand overwash and flooding: the storm compromised NC 12 causing closures from Marc Basnight Bridge (Oregon Inlet) to Rodanthe.

In April of 2020, an unnamed storm brought heavy overwash and flooding along NC 12.

On August 4, 2020 Isaias made landfall as a Category 1 hurricane in Ocean Isle, NC but brought tropical-storm-force winds (48 mph sustained, and 63 mph gusts) and a 2-4 ft storm surge to Oregon Inlet. Flooding was reported along NC 12. However, no overwash was reported.

On September 21, 2020, a triple threat hit PINWR including: seasonal high tides, strong northeast winds and long wave forms from Hurricane Teddy, which was hundreds of miles

off shore. These conditions caused overwash and dune losses along the refuge and closed several locations along NC 12.

On November 7, 2021, after the fall survey, NC 12 was closed between Rodanthe and Oregon Inlet due to moderate to major overwash in the Mirlo Beach area. Waves reached 15 to 20 ft. in the surf zone with wind gusts up to 60 mph, which led to dangerous beach conditions, flooding, and erosion

April 2020. Flooding reported along NC12 during unnamed storm event.

September 21, 2020. NC12 road closure in Mirlo Beach, NC.

September 21, 2020. NC 12 road closure from storm event overwash and King tide.

November 8, 2021. Highway 12 ("S" Turn) just north Rodanthe. Credit: NCDOT

SAMPLING METHODS

Macrobenthos

The swash zone of a beach is a constantly changing and complex habitat that supports many species of organisms unique to shorelines. Surf clams and mole crabs are two species that stand out as inhabitants of the surf zone. Both animals are extremely fast burrowers, able to rebury themselves almost as fast as they become exposed in shifting sands. The surf clam, also known as the coquina clam (*Donax variabilis*), is a filter feeder that uses its gills to filter microalgae, tiny zooplankton, and small particulates out of seawater. The mole crab (*Emerita talpoida*) is a suspension feeder that feeds by capturing zooplankton with its antennae. Further up the beach, somewhat removed from intense wave action, is where the ghost crab (*Ocypode quadrata*) makes its home by burrowing into the sand (Dolan, et al. 2004).

These organisms serve as excellent indicator species for estimating the overall physical conditions of sandy beaches as well as deviations from the natural state of these beaches. These two taxa (mole crabs and coquina clams) do not flourish when the beach sand is too coarse, too fine, or polluted. Both have adapted to rapid physical changes in the swash-zone in order to maintain their positions in the beach to optimize feeding efficiency. To ensure survival, these intertidal organisms must respond rapidly to the changes that beach nourishment introduces or perish. Any changes to the beach that impact coquina clams and mole crabs have ecological impacts far beyond the swash zone (Dolan, et al. 2004).

Finer sand with a heavier mineral content increases compaction which makes it harder for the clams and mole crabs to burrow in and out of the sand. Decreases in the abundances of these animals, as well as ghost crabs, results in a loss to the base of the food chain on PINWR.

Figure 2. Location of Transects, Pea Island National Wildlife Refuge, Dare County, NC Within the 2014 Beach Nourishment Area.

Benthos Field Methods
Three sand samples were taken from each transect at random locations within the swash zone. In addition, a ghost crab burrow count was made in the upper beach area at the foot of the dunes. To conduct these counts a 1-meter diameter hoop was randomly tossed three times in the area between the toe of the dune and the wrack line. The number of crab burrows were counted from each toss and combined. The benthic sand samples were taken using a cylindrical corer with internal diameter of 4" (PVC pipe), inserted 4" into the swash zone. The resulting sample was then filtered through a 1mm mesh sieve to isolate the macrofauna. The mole crab (Emerita spp.) individuals were measured for separation into size classes, enumerated and released. Donax spp., amphipods and worms were enumerated and released. The size classes for Emerita sp. are as follows: Small (1-4mm), Medium (4-8mm), and Large (>8mm). Physical data collected included water temperature, air temperature, wave height, salinity, sand bar distance offshore, and presence and height of erosion scarps on the beach face. Digital photographs were taken at each transect during each sampling occurrence.

SAMPLE TRANSECT
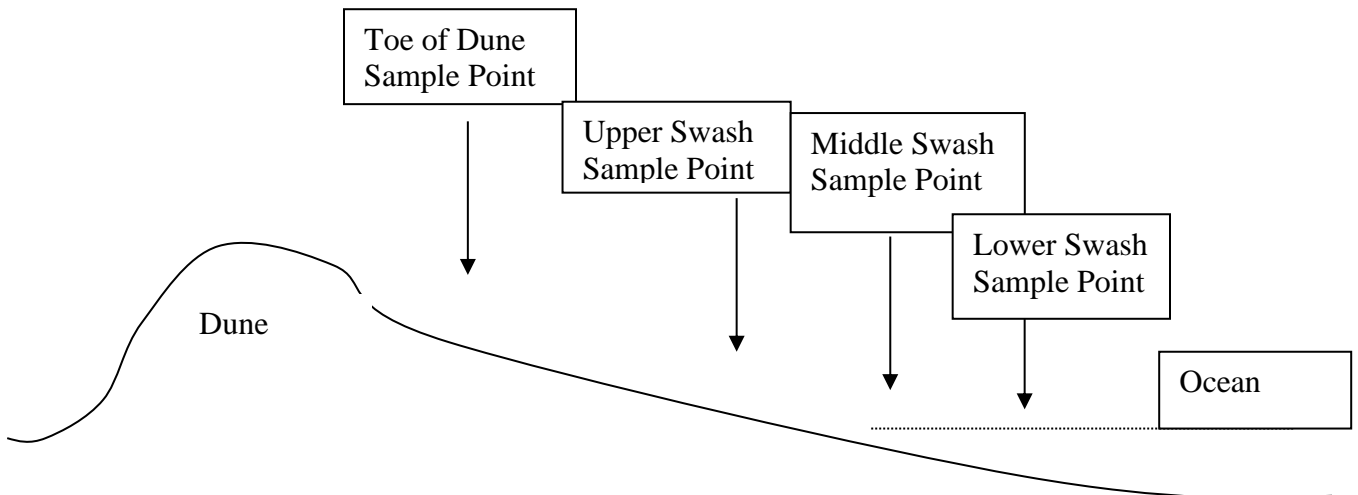
Collecting benthos sample in swash zone

Sand sample in sieve

Counting benthos

Emerita talpoidea

Coquina clams in the swash

Sand Sampling Introduction

Sediments that comprise the beaches and barrier islands of the Outer Banks of NC can be described in three size classes: Coarse, consisting of sands and gravel (0.5mm up to 2mm), medium (0.25mm to 0.5mm) and fine (grain size below 0.25mm) (Dolan et al, 2004). Changes to beach sand size or color (mineral content) can affect its biological and ecological processes. Darker sand will cause an increase in temperature that could affect turtle hatching and changes in sand coarseness will alter the distribution and density of the benthic community and could result in changes to beach slope and scarping if too much fine sand is deposited. The sand used to nourish the beach at the project location must be compatible with regards to grain size and mineralogy to the indigenous sand of Pea Island.

Sand Field Methods
Each of the 62 transects has 4 sample locations for a total of 248 samples. The upper beach sample was collected at the toe of the dune at a depth of 8-12 inches. The upper swash surface sample was collected at the wet line. The lower swash sample was collected half way between the upper and lower swash areas. All swash samples were collected within 6 inches of the surface. Samples and sample locations were identified by the site: Transect (1 through 74) and location (toe of dune=D, upper-swash=C, mid-swash=B, lower-swash=A).

Compaction and the slope of the beach were measured from each transect just above the upper swash zone. Each sand sample was analyzed for grain size and heavy mineral content.

Compaction measurements were collected just above the upper-swash zone from the surface to 12-inches deep with a DICKEY-john® Soil Compaction Tester. Compaction

measurements were recorded every three inches. According to United States Army Corp of Engineers personnel, this equipment (DICKEY-john® Soil Compaction Tester) is commonly used for compaction testing in similar studies. There is no ASTM method associated with the soil compaction tester. Slope measurements were made using a Brunton™ compass placed on a 12-inch board. The 12-inch board was oriented perpendicular to the water's edge.

Sand samples consisting of an amount equivalent to about ¼ cup of material were placed in sealable polyethylene bags for lab analysis. Samples were submitted to the NCDOT Materials and Test Unit Soils laboratory for sieve analysis and to the North Carolina Geologic Survey for heavy mineral analysis.

Collecting sand sample for grain size analysis

Laboratory Testing

Grain size analysis
Samples were delivered to the NCDOT Soil Laboratory for sieve analysis in accordance with 1995 Standard Specifications. The following sieve sizes were used for analysis. #4 (4.75mm), #10 (2mm), #18 (1mm), #25 (0.75mm), #35 (0.5mm), #60 (0.25mm), #100 (0.15mm), and #140 (0.106mm). The samples were dried, split evenly and approximately 200 grams was weighed for sieve analysis. Samples were washed over the # 200 sieve until the wash water ran clear, transferred to a sample container and placed in an oven to dry at a temperature of 230 degrees Fahrenheit. Dried samples were then poured into the nest of required sieves and shaken for a short period of time. The retained material on each individual sieve was weighed and recorded.

Mean grain size was determined by calculating the mean of the 25th and 75th percentiles of the % of sand passing through each size sieve. The 25th, 75th percentile were determined by graphing the % passing results of each sample per sieve size.

Measuring compaction

Laboratory Testing

Minerals analysis

The samples were analyzed by the North Carolina Geological Survey Lab. Each of the two hundred and forty-eight (248) samples, per sampling event, was washed over a sieve with 62.5 micron, (4 phi (Ø), openings to remove salt water and any mud. The samples were then placed in a warm oven overnight until dry. The samples were reduced in size, with a sample splitter until a reasonably sized sub sample was obtained. Each sample was transferred into a Pyrex dish, 88 mm in diameter, spread out until a single layer of mineral grains was obtained, and then examined with a binocular microscope at 10x. Nine (9) random views were examined under the binocular microscope for each sample. The number of heavy mineral grains in each of the nine views was counted and recorded. Volumetric estimates were performed on the percent of heavy minerals by comparing the views with standard area percentage diagrams. An average number of heavy minerals for each of the 248 samples was calculated. An average percent of heavy minerals for each of the 248 samples was also calculated. Five (5) samples were chosen at random and re-counted for quality control. The QC analyses were within 10% of the original counts. Two (2) samples, per sampling event, were chosen and the heavy mineral content was identified to individual mineral species. The following minerals were identified: epidote, staurolite, garnet, kyanite, ilmenite, magnetite, zircon, tourmaline, rutile, and pyroxene/amphibole. Pyroxene and amphibole are grouped together due to difficulty in differentiating the separate minerals.

RESULTS AND ANALYSIS

Physical parameters and biological data were entered to an Excel spreadsheet after each sampling event. Tabulated sample results and copies of the raw data were submitted to the Pea Island NWR biologist at the end of the sampling year. An annual report will be submitted in hard copy and electronic format.

Data will be analyzed according to methods in Dolan, 2004: Analysis of Changes in the Beach Sediment and Beach-face Organisms Associated with Sand Bypassing from the Oregon Inlet to Pea Island, North Carolina, 1990-2002.

The graphs represented at the end of this document summarize the data collected in 2012 through 2021. This section of the report will cover the analysis for the three "trouble spots" located on Pea Island.

Beginning in 2018, three areas identified by the ongoing Coastal Monitoring Program as problem areas: The Canal Zone, the PI Inlet area, and the Rodanthe S-Curves (Figures 3-7). These "trouble spots" were separated out and the data were analyzed to determine if these areas were exhibiting any changes that may have been masked by the overall island analysis. Graphs summarizing this data are presented after the overall analyses (Figures 19, 20, and 21).

Beginning in 2019, data was analyzed with a cubic function rather than a linear function. This function indicates an inverse relationship between grain size and species abundance. Generally, grain size distributions and species abundance across the study area were as expected with seasonal and long-term variations. The data also indicate that major storms have an influence over benthic numbers, but these numbers recover over time.

When the three "trouble spots" are analyzed separately, the data indicates seasonal and long-term variations in congruence with the overall analysis. Although the relationship between grain size and species abundance was different between each "trouble spot." After analyzing the data of the "trouble spots" for 2019-2021, there is a constant strong inverse relationship (5-year cycle) between average grains size and average species abundance in the PI Inlet area (Figure 20). Although the data indicates that there is a weak inverse relationship between the average grains size and average species abundance within the Canal Zone and the Rodanthe S-Curve (Figures 19 and 21). This relationship has fluctuated between a weak inverse relationship and a linear relationship, with the 2021 data indicating a long term (10-year cycle) weak inverse relationship between average grain size and average species abundance. In the Canal Zone this is currently a positive inverse relationship as the average number of species is continuing to increase. In the Rodanthe S-Curve this is currently a negative inverse relationship, where the average increase in grain size is decreasing the average number of species observed at this location. The immediate drop in the average grain size from summer of 2020 (1.08mm) to the fall of 2020 (0.56mm), along with only an increase to 0.75mm in the summer of 2021, resulted in a rising trend for average abundance of species within the Canal Zone. The S-Curve average grain size from spring of 2020 to the fall of 2021 averaged 0.81mm which resulted in a decreasing average species abundance trend while the trend for the average grain size is steadily increasing. Since 2012, the average grain size within the PI Inlet Zone has ranged from

0.5mm to 1.30mm with an overall average grain size of 0.8mm, with the average grain size currently on a downward trend. The decreasing trend in grain size at the PI Inlet Zone, for 2021, produced the second highest average species abundance (49 species per transect) since July of 2013 (73.5 species per transect).

In the Summer of 2020, the Canal Zone observed its first survey that recorded an average grain size of over 1.00mm (1.08mm), while the winter of 2020 was only the second occurrence of an average grain size over 1.00mm (1.15mm) for the S-Curve. The 2021 survey year resulted is the first occurrence since 2015 that the average grain size for all three "trouble spots" did not exceed 1.00mm. This resulted in an abundance of benthic species collected, averaging approximately 40 species per sample in the summer of 2021. Hurricanes and other major storms had little to no effects on the 2021 survey results.

T11-T30 "Canal Zone"

N
W · E
S

TG-1
TG2
T-1
T-3
T-5
T-7
T-9
T-11
T-13
T-15
T-17
T-19
T-21
T-23
T-25
T-27
T-29
T-30
T-31
T-32
T-33
T-34
T-35
T-36
T-37
T-38

0   0.15   0.3 Miles

PREPARED BY:

RK&K

NORTH CAROLINA
DEPARTMENT OF TRANSPORTATION

STATE OF NORTH CAROLINA
DEPARTMENT OF TRANSPORTATION

Monitoring NC-12
Dare County

Monitoring Locations Map TG1-T38   FIGURE 3

Source: NOAA, Esri

T-38
T-39
T-40
T-41
T-42
T-43
T-44
T-45
T-46
T-47
T-48
T-49
T-50
T-51
T-52
T-53
T-54

T47-T54 Narrow area
South of PI Inlet Area

T-55
T-56
T-57
T-58
T-59
T-60
T-61
T-62
T-63
T-64
T-65
T-66
T-67
T-68
T-69
T-70
T-71
T-72
T-73
T-74

T65-T74 Beach
nourishment area and
"S Curves"

0   0.25   0.5 Miles

PREPARED BY:

RK&K

NORTH CAROLINA
DEPARTMENT OF TRANSPORTATION

Monitoring NC-12
Dare County

Monitoring Locations Map T38-T74   FIGURE 4

Source: NOAA, Esri

N
W   E
S

T-11

T-13

T-15

T-17

T-19

T-21

T-23

T-25

T-27

T-29

T-30

0 205 410   820 Feet

PREPARED BY:
RK&K

NORTH CAROLINA
DEPARTMENT OF TRANSPORTATION

STATE OF NORTH CAROLINA
DEPARTMENT OF TRANSPORTATION

Monitoring NC-12
Dare County

T11-T30 "Canal Zone"   FIGURE 5

Source: NOAA, Esri

N
W — E
S

T-47

T-48

T-49

T-50

T-51

T-52

T-53

T-54

0 175 350   700 Feet

PREPARED BY:

RK&K

NORTH CAROLINA
DEPARTMENT OF TRANSPORTATION

Monitoring NC-12
Dare County

T47-T54 Narrow Area South of PI Inlet Area   FIGURE 6

Source: NOAA, Esri

N
W · E
S

T-65

T-73

T-66

T-74

T-67

T-68

T-69

T-70

T-71

T-72

T-73

T-74

0 200 400   800 Feet

PREPARED BY:

RK&K

NORTH CAROLINA
DEPARTMENT OF TRANSPORTATION

Monitoring NC-12
Dare County

T65-T74
Beach nourishment area and "S curves"

FIGURE 7

Source: NOAA, Esri
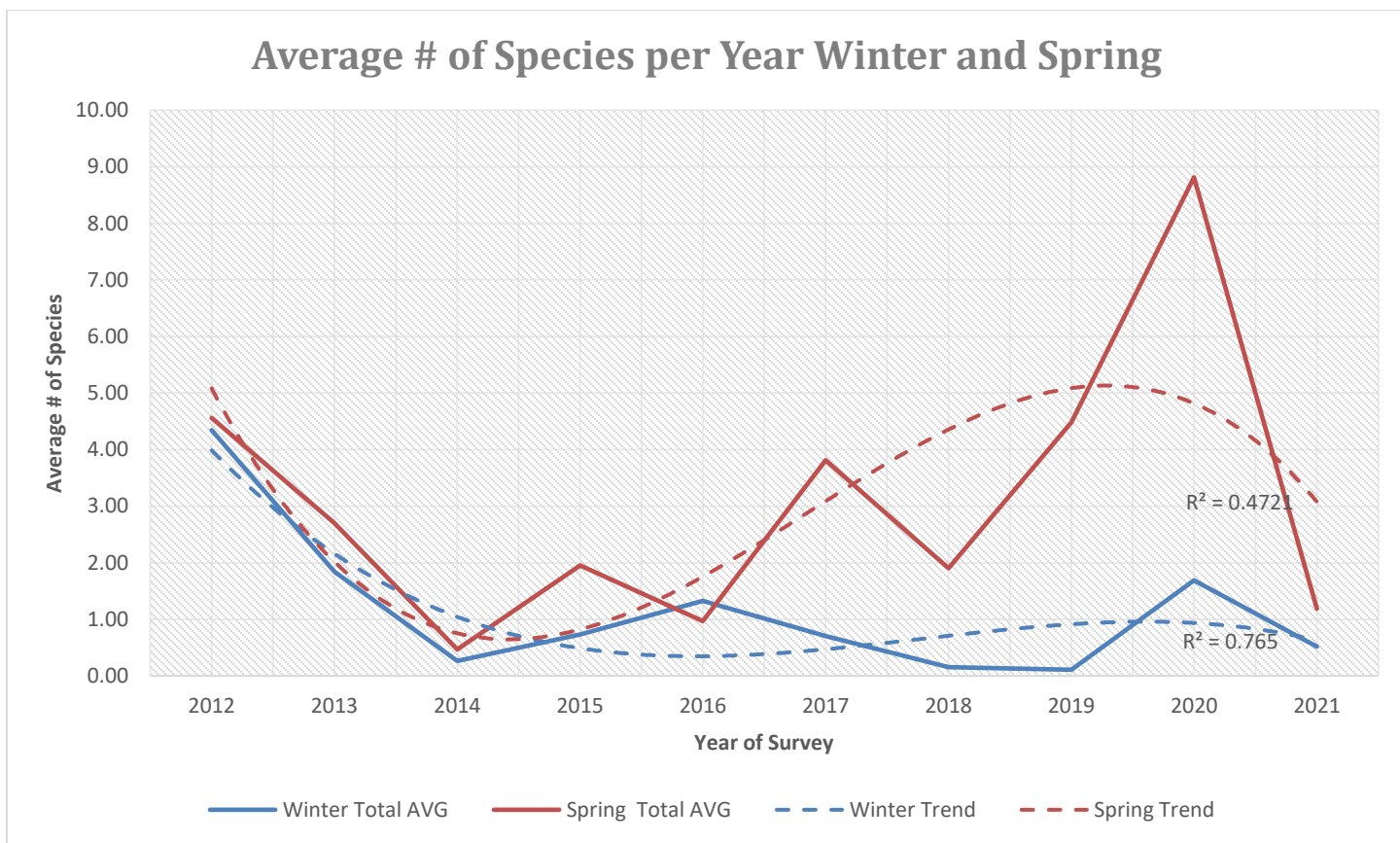
Fig.8 – Average number of species per season in the winter and spring of 2012-2021.
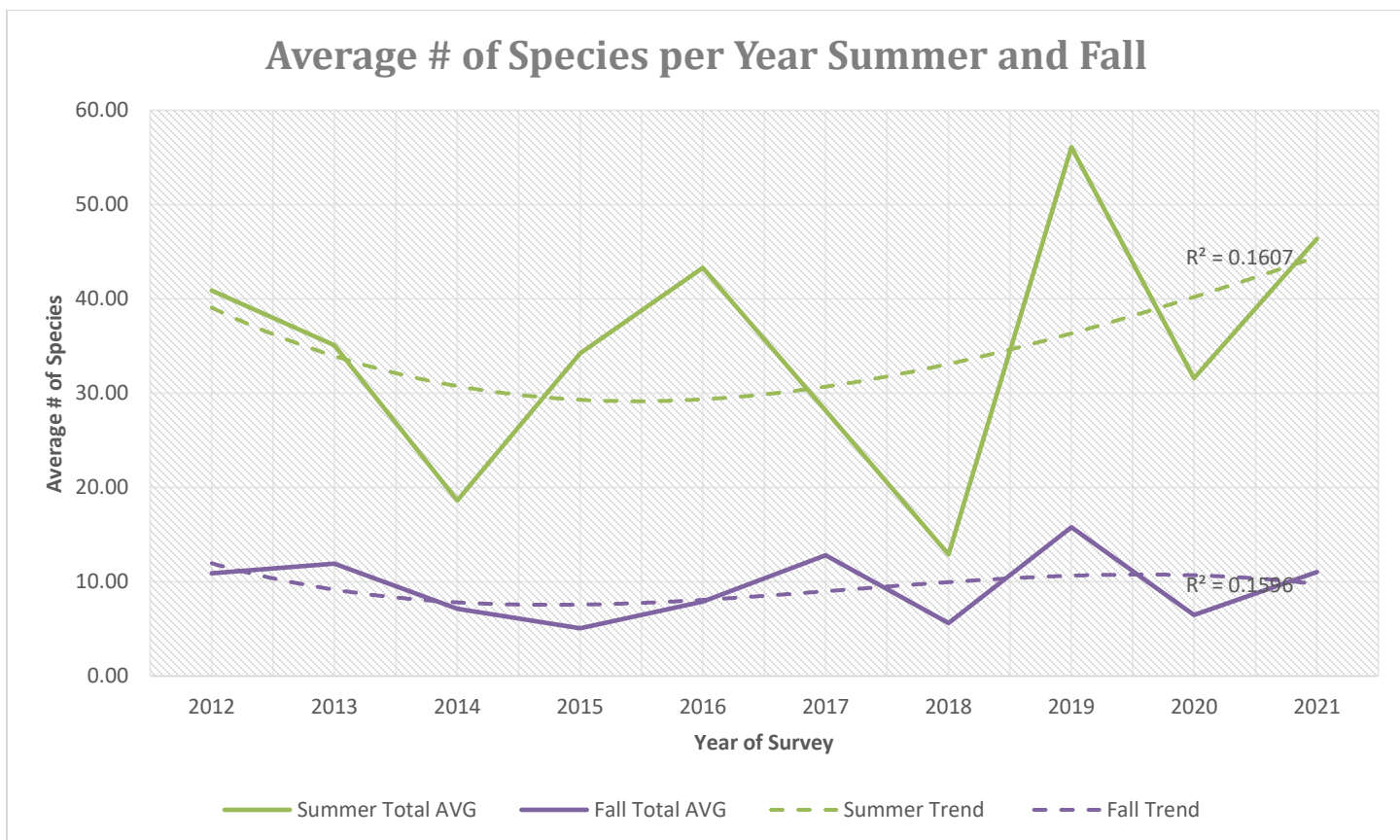
Fig.9 – Average number of species per season in the summer and fall of 2012-2021.
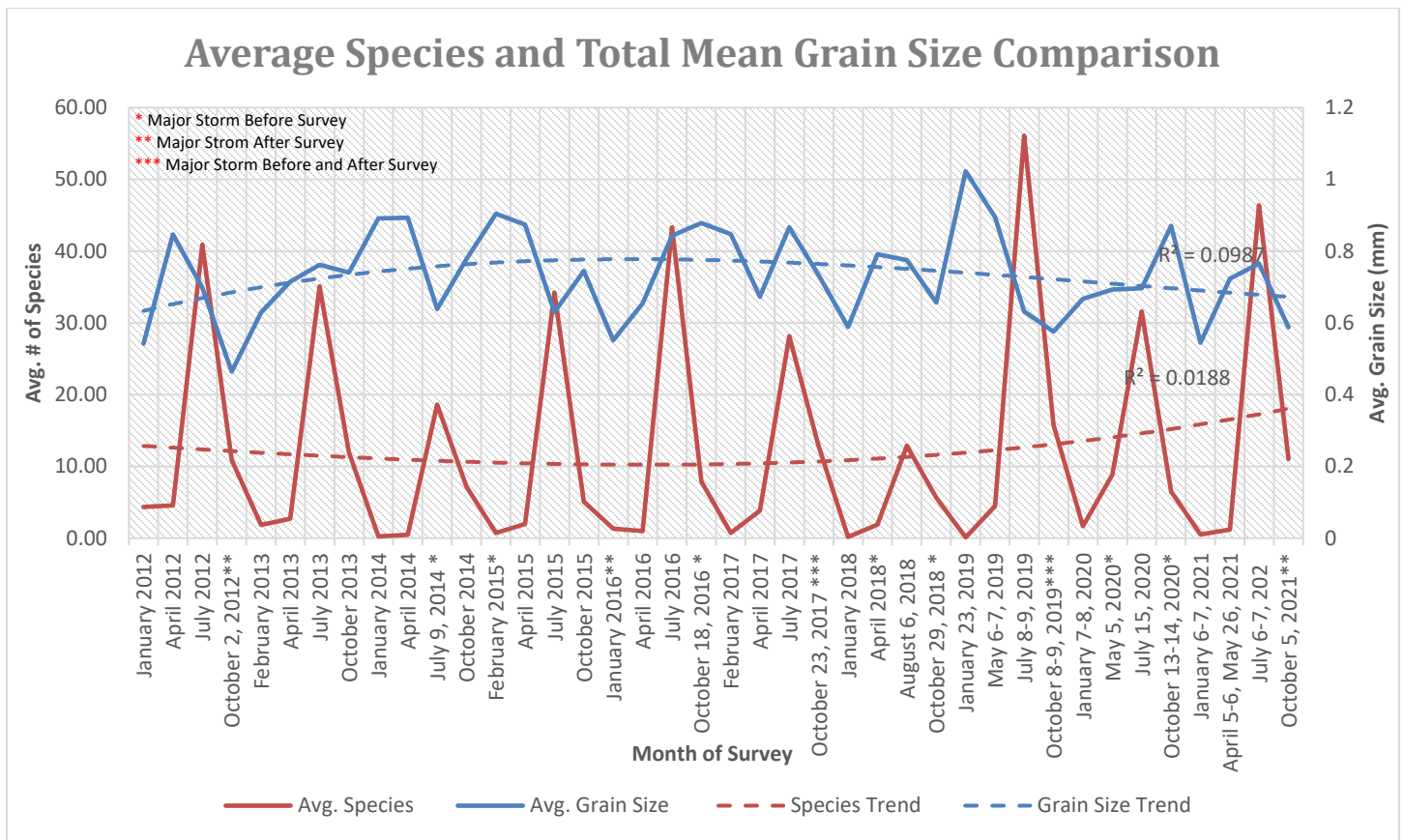
Fig.10 – Average species and total mean grain size comparison.
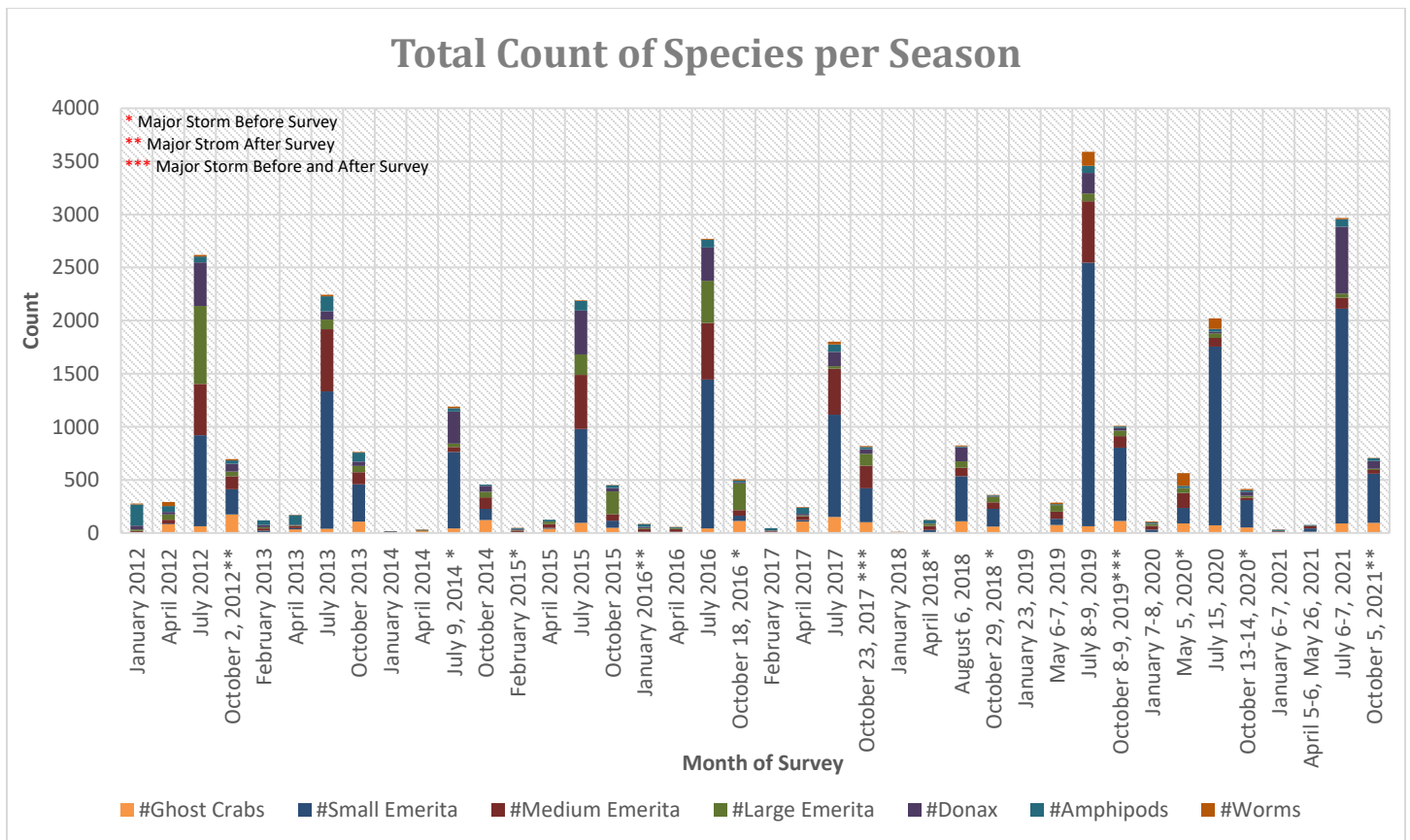
Fig.11 – Total number of species observed during each survey.
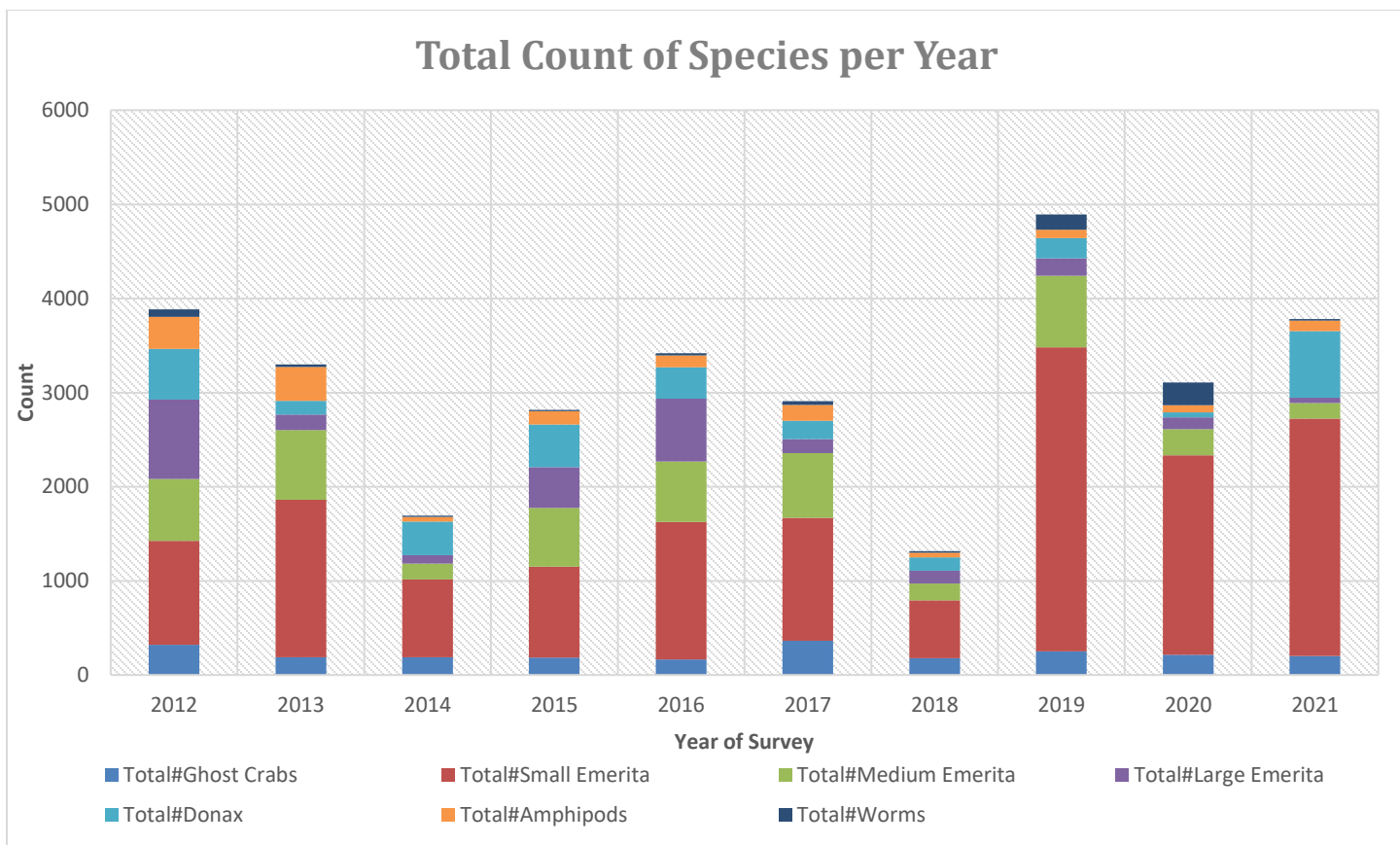
Fig.12 – Total number of species observed per year.
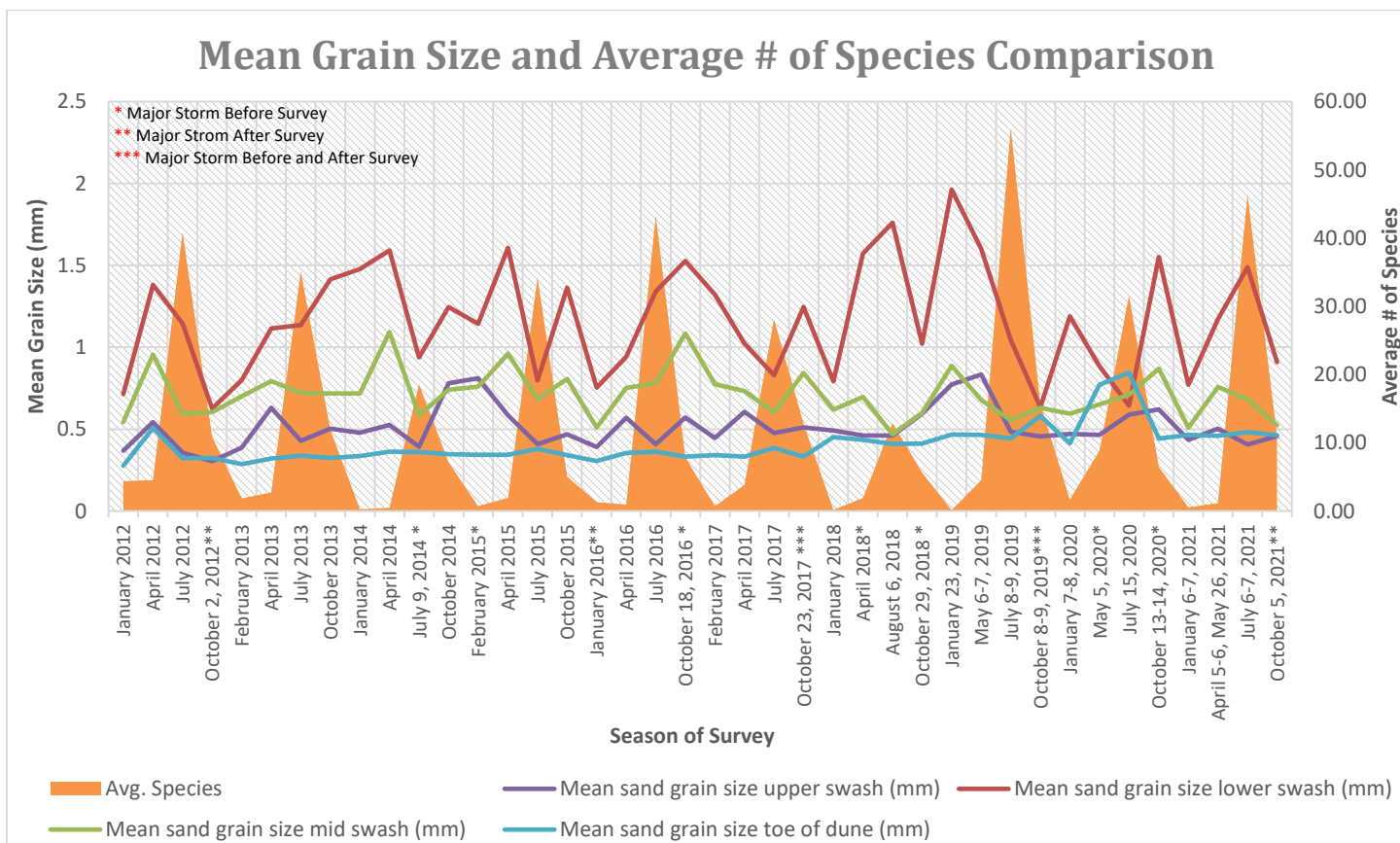
Fig.13 – The mean grain size compared to the average number of species observed per survey.
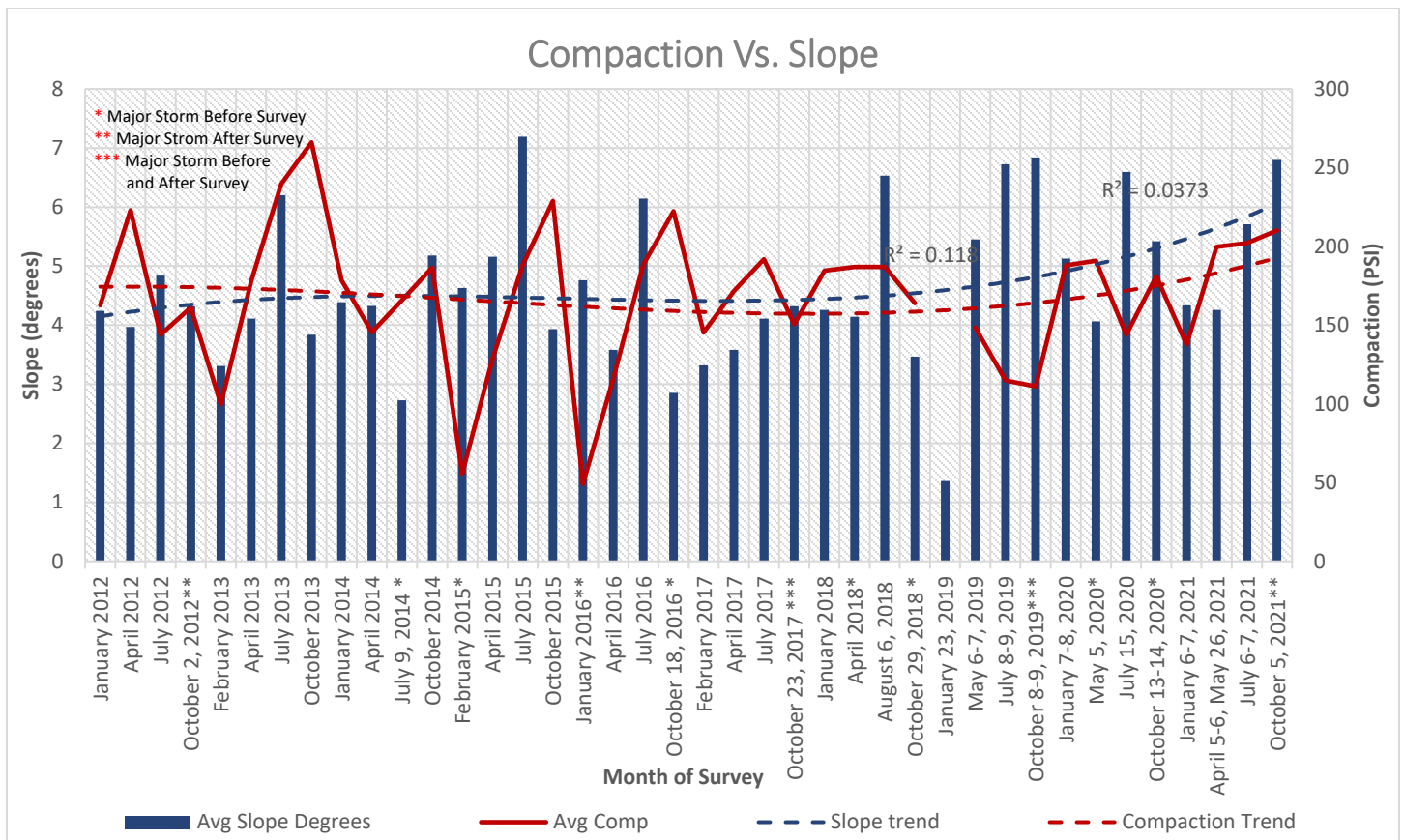
Fig.14 – The comparison between compaction and slope. Note: January 2019 compaction data not available.
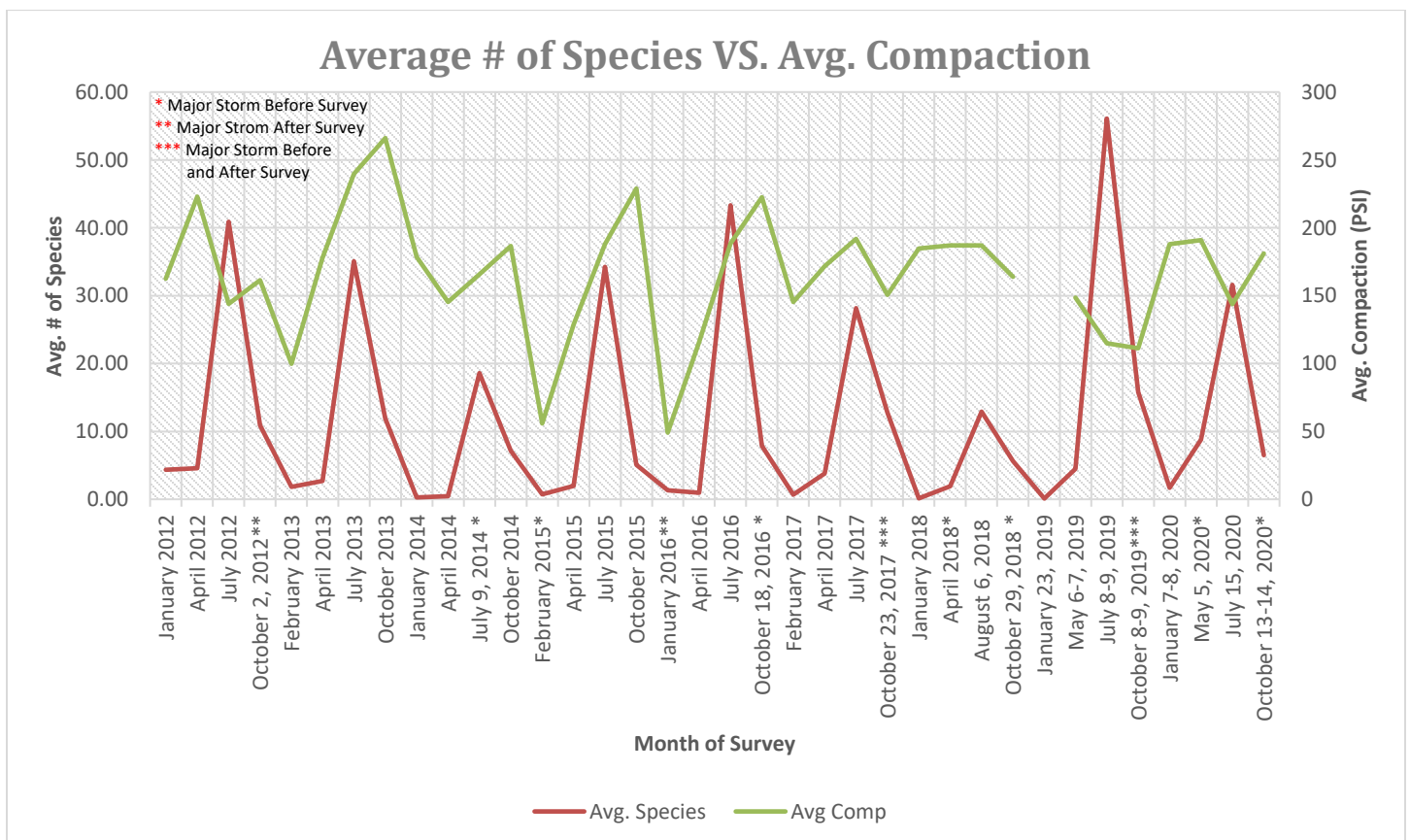
Fig.15 – The comparison between the average number of species observed per survey and average compaction. Note: January 2019 compaction data not available
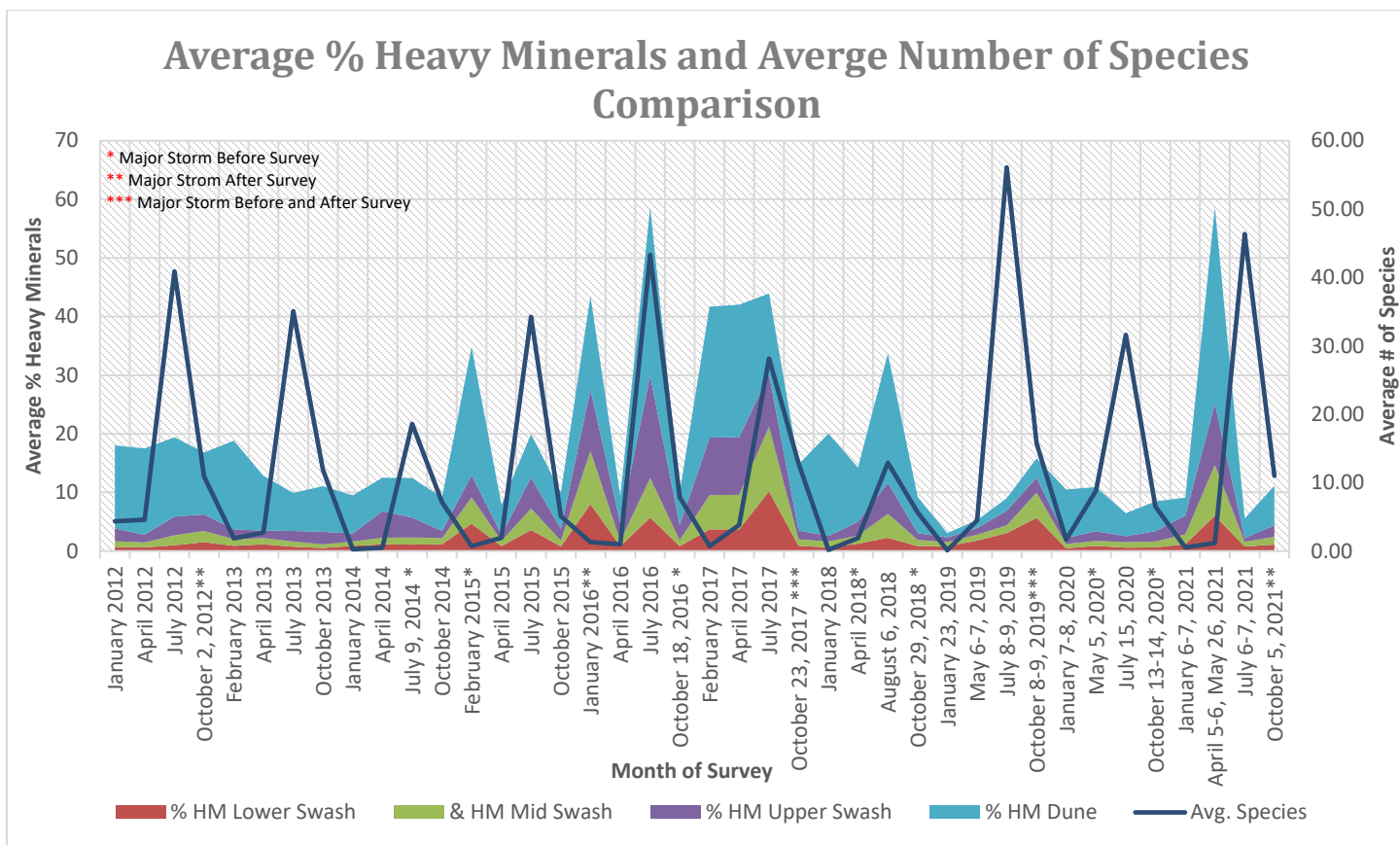
Fig.16 – The comparison between the average percent heavy minerals and the average number of species found per survey. Note: 2015-2019 heavy mineral sand analysis was performed using a different method.
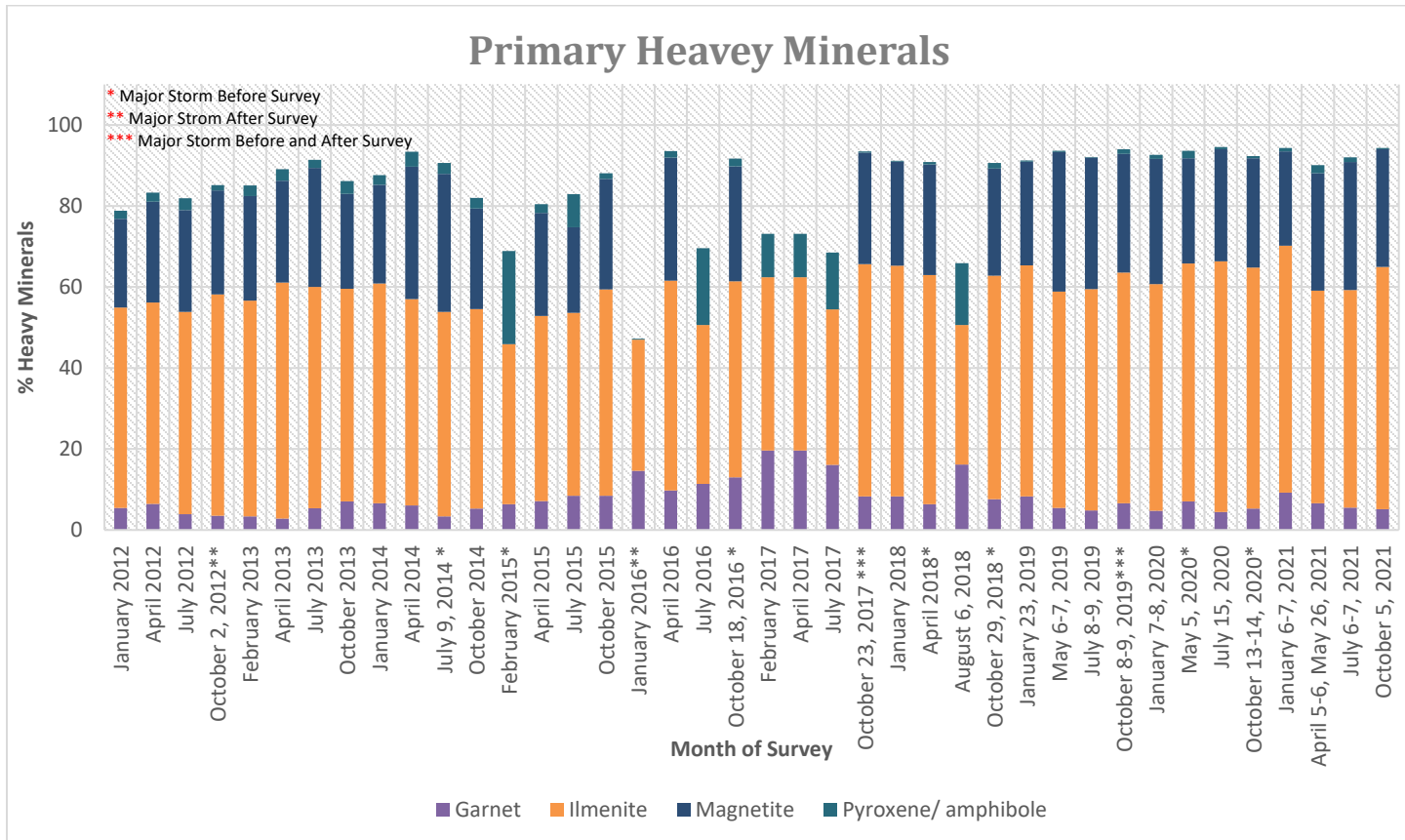
Fig.17 – The percent of primary heavy minerals observed in each survey.
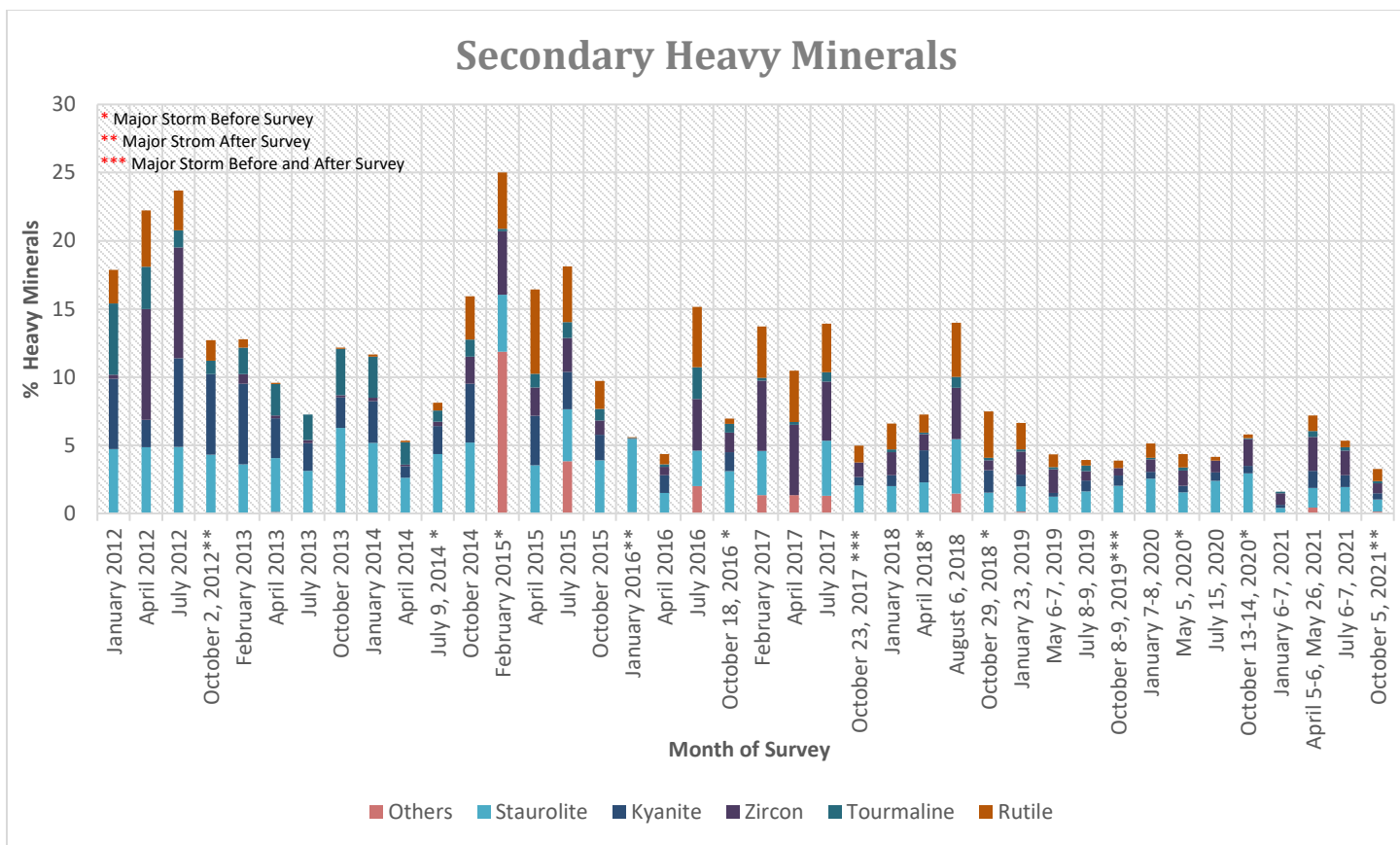
Fig.18 – The percent of secondary heavy mineral observed in each survey.
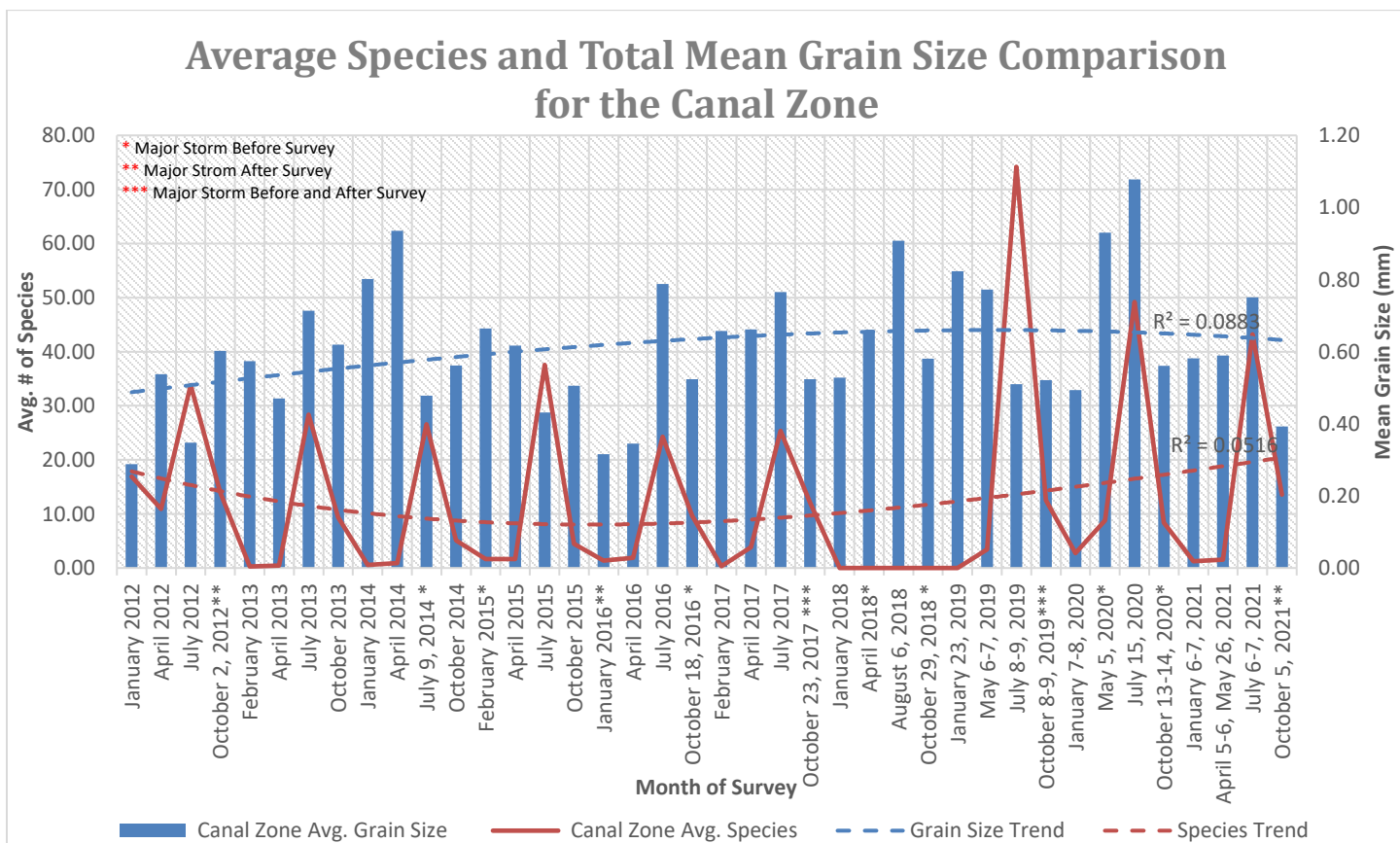
Fig.19 – Average species and total mean grain size comparison for the Canal Zone.
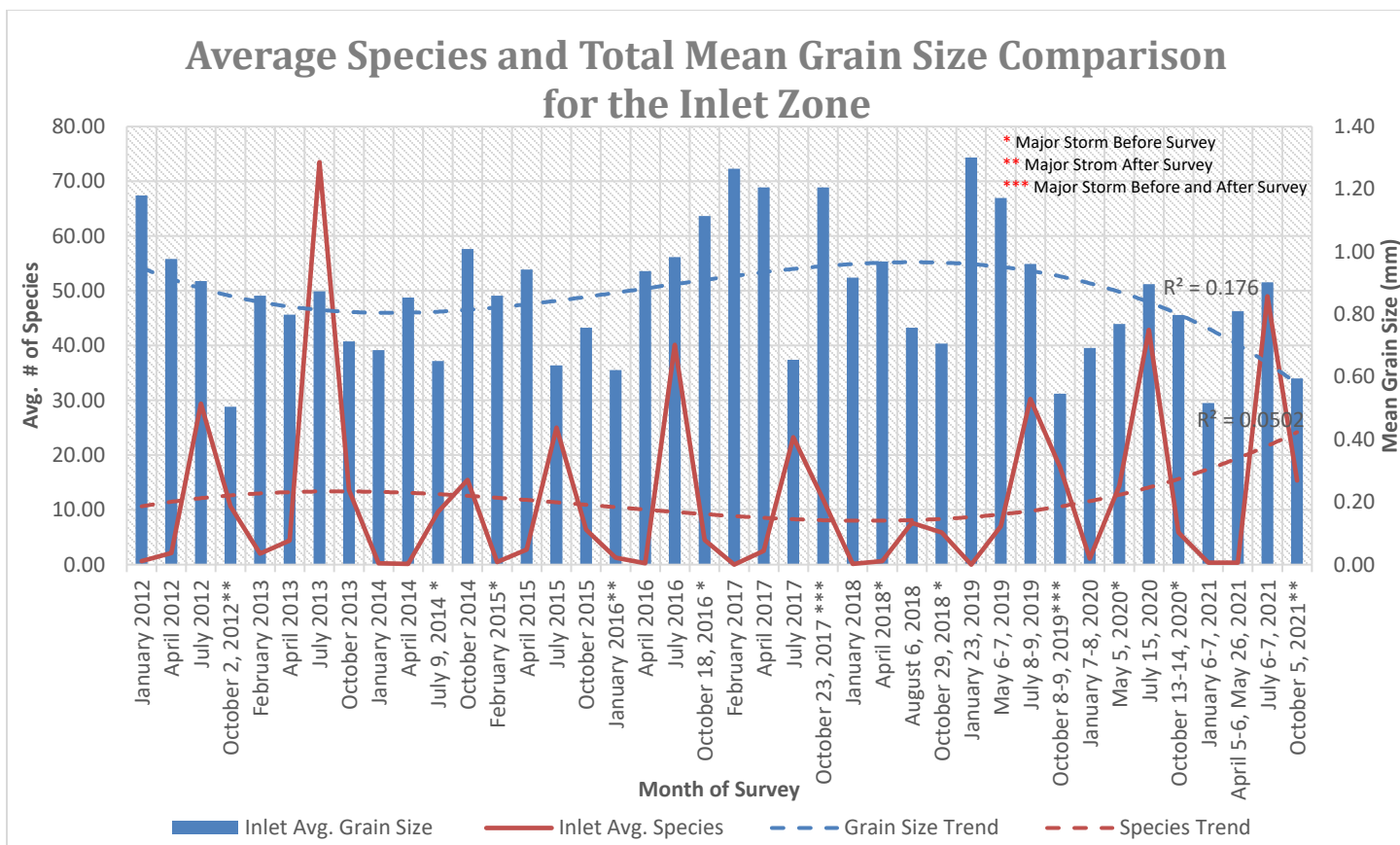
Fig.20 – Average species and total mean grain size comparison for the Pea Island Inlet Zone.
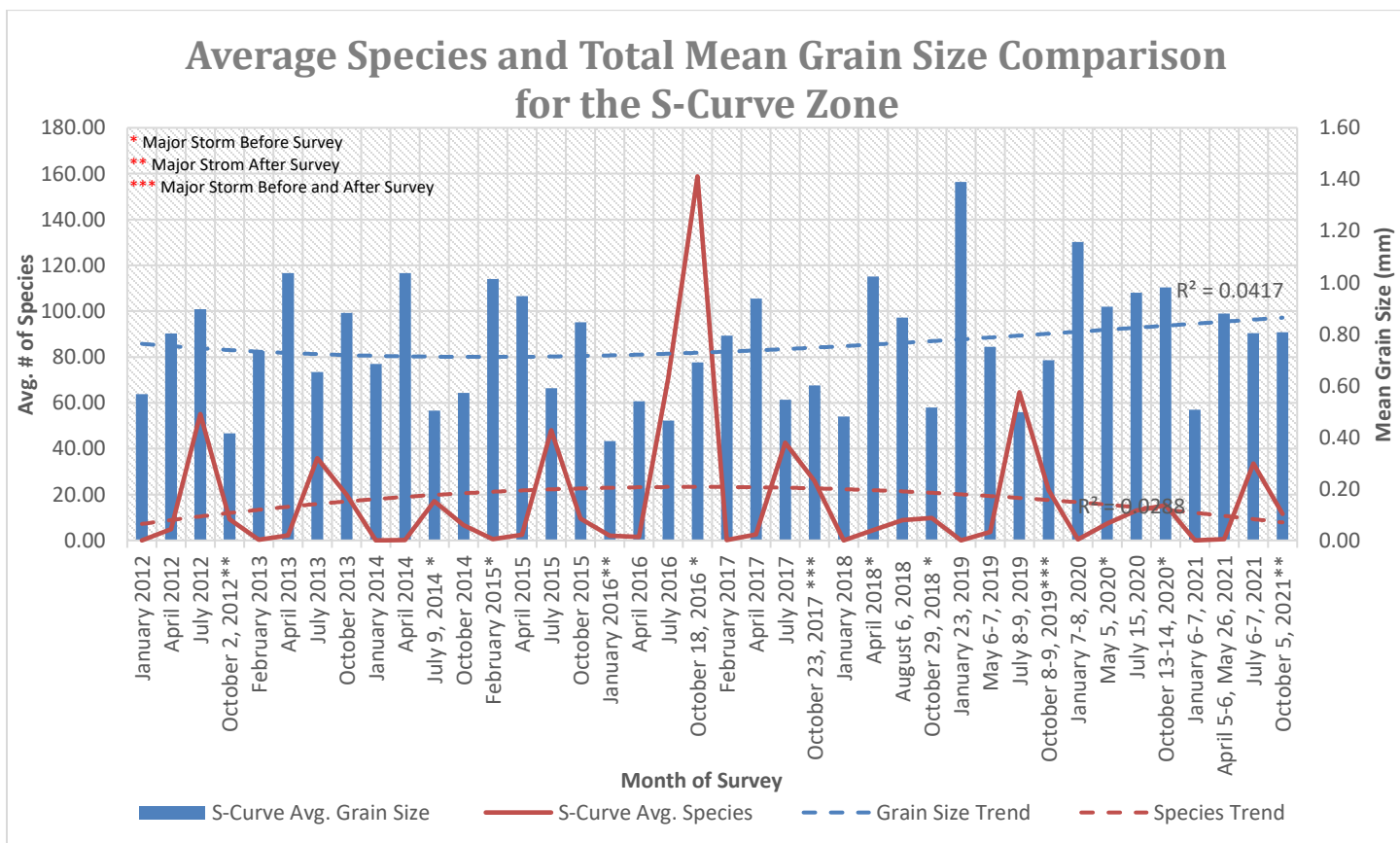
Fig.21 – Average species and total mean grain size comparison for the Rodanthe S-Curve Zone.

2012 Sand Survey Statistics

2012 Statistics						
	VAR	STD	STE	mean	Min	Max	Range
Avg. Grain Size	0.03	0.17	0.03	0.64	0.46	0.85	0.38
Mean sand grain size lower swash (mm)	0.13	0.36	0.06	0.97	0.63	1.38	0.76
Mean sand grain size mid swash (mm)	0.04	0.19	0.03	0.67	0.54	0.96	0.41
Mean sand grain size upper swash (mm)	0.01	0.10	0.02	0.39	0.30	0.54	0.24
Mean sand grain size toe of dune (mm)	0.01	0.10	0.02	0.36	0.28	0.51	0.23
Total Benthos	1242991.6	1114.9	185.8	971.3	278.0	2618.0	2340.0
Avg. Species	309.0	17.6	2.9	15.3	4.5	41.3	36.8
Avg Slope Degrees	0.13	0.36	0.06	4.34	3.97	4.84	0.87
Avg Comp	1193.26	34.54	5.76	172.73	144.04	222.97	78.93
% HM Lower Swash	0.16	0.40	0.07	0.95	0.63	1.50	0.88
& HM Mid Swash	0.29	0.54	0.09	1.37	0.82	1.95	1.13
% HM Upper Swash	0.65	0.80	0.13	2.38	1.34	3.19	1.85
% HM Dune	3.39	1.84	0.31	13.24	10.57	14.72	4.15
Average %HM	0.08	0.28	0.05	4.49	4.21	4.86	0.65

Table 1 – The 2012 statistics analyzing the variance, standard deviation, standard error, mean, minimum, maximum, and ranges of the mineral and benthic data collected from each survey (winter, spring, summer, fall).

2013 Sand Survey Statistics

2013 Statistics							
	VAR	STD	STE	mean	Min	Max	Range
Avg. Grain Size	0.00	0.06	0.01	0.71	0.63	0.76	0.13
Mean sand grain size lower swash (mm)	0.06	0.25	0.04	1.12	0.80	1.42	0.62
Mean sand grain size mid swash (mm)	0.00	0.04	0.01	0.73	0.70	0.79	0.09
Mean sand grain size upper swash (mm)	0.01	0.11	0.02	0.49	0.39	0.63	0.24
Mean sand grain size toe of dune (mm)	0.00	0.02	0.00	0.32	0.29	0.34	0.05
Total Benthos	981732.3	990.8	165.1	824.8	118.0	2245.0	2127.0
Avg. Species	239.0	15.5	2.6	13.0	1.9	35.1	33.2
Avg Slope Degrees	1.61	1.27	0.21	4.37	3.31	6.20	2.89
Avg Comp	5470.91	73.97	12.33	195.82	99.72	266.08	166.37
% HM Lower Swash	0.07	0.27	0.05	0.83	0.52	1.17	0.65
& HM Mid Swash	0.05	0.23	0.04	0.91	0.61	1.12	0.51
% HM Upper Swash	0.12	0.34	0.06	1.74	1.30	2.12	0.82
% HM Dune	14.65	3.83	0.64	9.68	6.46	15.15	8.69
Average %HM	0.98	0.99	0.17	3.29	2.48	4.71	2.23

Table 2 – The 2013 statistics analyzing the variance, standard deviation, standard error, mean, minimum, maximum, and ranges of the mineral and benthic data collected from each survey (winter, spring, summer, fall).

2014 Sand Survey Statistics

2014 Statistics							
	VAR	STD	STE	mean	Min	Max	Range
Avg. Grain Size	0.01	0.12	0.02	0.80	0.64	0.89	0.25
Mean sand grain size lower swash (mm)	0.08	0.29	0.05	1.31	0.94	1.59	0.65
Mean sand grain size mid swash (mm)	0.05	0.22	0.04	0.78	0.59	1.09	0.51
Mean sand grain size upper swash (mm)	0.03	0.17	0.03	0.54	0.39	0.78	0.39
Mean sand grain size toe of dune (mm)	0.00	0.01	0.00	0.35	0.34	0.36	0.03
Total Benthos	303399.0	550.8	91.8	423.5	17.0	1191.0	1174.0
Avg. Species	77.1	8.8	1.5	6.8	0.2	18.9	18.7
Avg Slope Degrees	1.06	1.03	0.17	4.16	2.73	5.18	2.45
Avg Comp	322.98	17.97	3.00	169.12	145.47	186.66	41.19
% HM Lower Swash	0.01	0.10	0.02	1.07	0.92	1.14	0.23
& HM Mid Swash	0.05	0.22	0.04	1.04	0.74	1.25	0.52
% HM Upper Swash	2.59	1.61	0.27	2.62	1.23	4.52	3.29
% HM Dune	0.27	0.52	0.09	6.18	5.74	6.75	1.01
Average %HM	0.21	0.46	0.08	2.73	2.29	3.13	0.84

Table 3 – The 2014 statistics analyzing the variance, standard deviation, standard error, mean, minimum, maximum, and ranges of the mineral and benthic data collected from each survey (winter, spring, summer, fall).

2015 Sand Survey Statistics

2015 Statistics							
	VAR	STD	STE	mean	Min	Max	Range
Avg. Grain Size	0.02	0.13	0.02	0.79	0.63	0.90	0.27
Mean sand grain size lower swash (mm)	0.12	0.34	0.06	1.23	0.80	1.61	0.81
Mean sand grain size mid swash (mm)	0.01	0.12	0.02	0.80	0.68	0.96	0.28
Mean sand grain size upper swash (mm)	0.03	0.18	0.03	0.57	0.41	0.81	0.40
Mean sand grain size toe of dune (mm)	0.00	0.02	0.00	0.35	0.34	0.38	0.04
Total Benthos	1039432.9	1019.5	169.9	671.8	47.0	2191.0	2144.0
Avg. Species	270.4	16.4	2.7	10.8	0.8	35.3	34.6
Avg Slope Degrees	1.97	1.40	0.23	5.23	3.93	7.19	3.26
Avg Comp	5664.01	75.26	12.54	150.30	55.81	228.91	173.09
% HM Lower Swash	3.89	1.97	0.33	2.46	0.76	4.66	3.90
& HM Mid Swash	3.39	1.84	0.31	2.53	0.91	4.53	3.61
% HM Upper Swash	3.50	1.87	0.31	3.03	1.05	5.29	4.24
% HM Dune	62.15	7.88	1.31	10.15	5.10	21.89	16.79
Average %HM	3.02	1.74	0.29	2.58	0.87	4.98	4.11

Table 4 – The 2015 statistics analyzing the variance, standard deviation, standard error, mean, minimum, maximum, and ranges of the mineral and benthic data collected from each survey (winter, spring, summer, fall).

2016 Sand Survey Statistics

2016 Statistics							
	VAR	STD	STE	mean	Min	Max	Range
Avg. Grain Size	0.02	0.16	0.03	0.73	0.55	0.88	0.33
Mean sand grain size lower swash (mm)	0.13	0.35	0.06	1.14	0.75	1.53	0.77
Mean sand grain size mid swash (mm)	0.06	0.23	0.04	0.78	0.51	1.08	0.57
Mean sand grain size upper swash (mm)	0.01	0.10	0.02	0.48	0.39	0.57	0.18
Mean sand grain size toe of dune (mm)	0.00	0.03	0.00	0.34	0.31	0.36	0.06
Total Benthos	1672001.7	1293.1	215.5	855.5	62.0	2771.0	2709.0
Avg. Species	434.4	20.8	3.5	13.8	1.0	44.7	43.7
Avg Slope Degrees	2.07	1.44	0.24	4.34	2.85	6.15	3.29
Avg Comp	5973.63	77.29	12.88	143.95	49.11	222.44	173.34
% HM Lower Swash	13.04	3.61	0.60	3.86	0.81	8.03	7.21
& HM Mid Swash	17.10	4.14	0.69	4.42	0.89	9.07	8.18
% HM Upper Swash	49.30	7.02	1.17	8.38	2.58	17.42	14.84
% HM Dune	126.30	11.24	1.87	13.74	4.60	28.74	24.14
Average %HM	0.47	0.69	0.11	1.85	1.09	2.52	1.43

Table 5 – The 2016 statistics analyzing the variance, standard deviation, standard error, mean, minimum, maximum, and ranges of the mineral and benthic data collected from each survey (winter, spring, summer, fall).

2017 Sand Survey Statistics

2017 Statistics							
	VAR	STD	STE	mean	Min	Max	Range
Avg. Grain Size	0.01	0.09	0.02	0.78	0.67	0.87	0.19
Mean sand grain size lower swash (mm)	0.05	0.22	0.04	1.10	0.83	1.32	0.49
Mean sand grain size mid swash (mm)	0.01	0.10	0.02	0.74	0.60	0.84	0.24
Mean sand grain size upper swash (mm)	0.00	0.07	0.01	0.51	0.45	0.61	0.16
Mean sand grain size toe of dune (mm)	0.00	0.03	0.00	0.35	0.33	0.39	0.05
Total Benthos	620117.6	787.5	131.2	727.3	45.0	1801.0	1756.0
Avg. Species	160.5	12.7	2.1	11.7	0.7	29.0	28.3
Avg Slope Degrees	0.21	0.46	0.08	3.83	3.32	4.32	1.00
Avg Comp	453.37	21.29	3.55	164.87	145.36	191.88	46.51
% HM Lower Swash	15.60	3.95	0.66	4.61	0.87	10.19	9.32
& HM Mid Swash	16.38	4.05	0.67	5.99	1.14	11.05	9.91
% HM Upper Swash	16.22	4.03	0.67	7.49	1.49	9.80	8.31
% HM Dune	34.09	5.84	0.97	17.52	11.28	22.61	11.33
Average %HM	12.20	3.49	0.58	8.92	3.69	10.98	7.29

Table 6 – The 2017 statistics analyzing the variance, standard deviation, standard error, mean, minimum, maximum, and ranges of the mineral and benthic data collected from each survey (winter, spring, summer, fall).

2018 Sand Survey Statistics

2018 Statistics							
	VAR	STD	STE	mean	Min	Max	Range
Avg. Grain Size	0.01	0.10	0.02	0.70	0.59	0.79	0.20
Mean sand grain size lower swash (mm)	0.21	0.46	0.08	1.29	0.79	1.76	0.97
Mean sand grain size mid swash (mm)	0.01	0.09	0.02	0.60	0.47	0.70	0.23
Mean sand grain size upper swash (mm)	0.00	0.06	0.01	0.50	0.46	0.59	0.13
Mean sand grain size toe of dune (mm)	0.00	0.02	0.00	0.43	0.41	0.45	0.04
Total Benthos	130528.9	361.3	60.2	329.3	10.0	825.0	815.0
Avg. Species	35.1	5.9	1.0	5.4	0.2	13.5	13.4
Avg Slope Degrees	1.78	1.33	0.22	4.60	3.47	6.53	3.06
Avg Comp	125.54	11.20	1.87	180.66	163.93	187.06	23.13
% HM Lower Swash	0.54	0.73	0.12	1.25	0.64	2.29	1.65
& HM Mid Swash	2.18	1.48	0.25	1.87	0.97	4.07	3.09
% HM Upper Swash	3.84	1.96	0.33	2.44	0.98	5.24	4.25
% HM Dune	53.66	7.33	1.22	13.75	6.14	22.11	15.97
Average %HM	6.97	2.64	0.44	4.83	2.31	8.43	6.12

Table 7 – The 2018 statistics analyzing the variance, standard deviation, standard error, mean, minimum, maximum, and ranges of the mineral and benthic data collected from each survey (winter, spring, summer, fall).

2019 Sand Survey Statistics

2019 Statistics							
	VAR	**STD**	**STE**	**mean**	**Min**	**Max**	**Range**
Avg. Grain Size	0.05	0.21	0.04	0.78	0.58	1.02	0.45
Mean sand grain size lower swash (mm)	0.35	0.59	0.10	1.31	0.63	1.96	1.33
Mean sand grain size mid swash (mm)	0.02	0.14	0.02	0.69	0.55	0.89	0.33
Mean sand grain size upper swash (mm)	0.04	0.19	0.03	0.64	0.46	0.83	0.38
Mean sand grain size toe of dune (mm)	0.00	0.06	0.01	0.49	0.44	0.58	0.14
Total Benthos	2667603.0	1633.3	272.2	1223.5	7.0	3590.0	3583.0
Avg. Species	716.9	26.8	4.5	20.1	0.1	58.9	58.7
Avg Slope Degrees	6.59	2.57	0.43	5.10	1.36	6.84	5.48
Avg Comp	37102.27	192.62	32.10	199.82	53.56	418.06	364.51
% HM Lower Swash	4.38	2.09	0.35	2.83	0.81	5.65	4.83
& HM Mid Swash	2.77	1.66	0.28	1.84	0.70	4.30	3.60
% HM Upper Swash	0.83	0.91	0.15	1.74	0.81	2.55	1.74
% HM Dune	1.19	1.09	0.18	1.88	0.75	3.29	2.54
Average %HM	1.94	1.39	0.23	2.07	0.77	3.95	3.18

Table 8 – The 2019 statistics analyzing the variance, standard deviation, standard error, mean, minimum, maximum, and ranges of the mineral and benthic data collected from each survey (winter, spring, summer, fall).

2020 Sand Survey Statistics

2020 Statistics							
	VAR	STD	STE	mean	Min	Max	Range
Avg. Grain Size	0.01	0.09	0.02	0.73	0.67	0.87	0.20
Mean sand grain size lower swash (mm)	0.15	0.39	0.07	1.07	0.64	1.55	0.91
Mean sand grain size mid swash (mm)	0.01	0.12	0.02	0.71	0.60	0.87	0.28
Mean sand grain size upper swash (mm)	0.01	0.08	0.01	0.54	0.46	0.62	0.16
Mean sand grain size toe of dune (mm)	0.05	0.22	0.04	0.62	0.41	0.84	0.43
Total Benthos	14789.1	121.6	20.3	111.0	15.4	288.9	273.4
Avg. Species	211.9	14.6	2.4	58.7	38.7	71.2	32.5
Avg Slope Degrees	1.08	1.04	0.17	5.30	4.07	6.59	2.53
Avg Comp	475.21	21.80	3.63	175.99	143.88	190.96	47.08
% HM Lower Swash	0.03	0.17	0.03	0.64	0.45	0.87	0.42
& HM Mid Swash	0.01	0.10	0.02	0.87	0.75	0.98	0.22
% HM Upper Swash	0.15	0.39	0.06	1.37	1.02	1.74	0.73
% HM Dune	4.06	2.01	0.34	6.21	3.95	8.23	4.28
Average %HM	0.26	0.51	0.09	2.27	1.62	2.73	1.11

Table 9 – The 2020 statistics analyzing the variance, standard deviation, standard error, mean, minimum, maximum, and ranges of the mineral and benthic data collected from each survey (winter, spring, summer, fall).

2021 Sand Survey Statistics

2021 Statistics							
	VAR	STD	STE	mean	Min	Max	Range
Avg. Grain Size	0.01	0.11	0.02	0.66	0.54	0.77	0.22
Mean sand grain size lower swash (mm)	0.10	0.32	0.05	1.09	0.77	1.49	0.72
Mean sand grain size mid swash (mm)	0.01	0.12	0.02	0.62	0.51	0.76	0.25
Mean sand grain size upper swash (mm)	0.00	0.04	0.01	0.45	0.43	0.50	0.07
Mean sand grain size toe of dune (mm)	0.00	0.01	0.00	0.47	0.46	0.48	0.02
Total Benthos	1910996.3	1382.4	230.4	945.3	33.0	2967.0	2934.0
Avg. Species	466.6	21.6	3.6	14.8	0.5	46.4	45.8
Avg Slope Degrees	1.48	1.21	0.20	5.28	4.26	6.80	2.54
Avg Comp	1123.24	33.51	5.59	187.43	137.60	210.21	72.61
% HM Lower Swash	6.30	2.51	0.42	2.26	1.16	6.01	4.86
& HM Mid Swash	13.73	3.70	0.62	3.14	1.70	8.67	6.96
% HM Upper Swash	19.28	4.39	0.73	4.04	3.16	10.44	7.28
% HM Dune	214.55	14.65	2.44	11.67	3.09	33.50	30.41
Average %HM	39.43	6.28	1.05	5.28	2.28	14.66	12.38

Table 10 – The 2021 statistics analyzing the variance, standard deviation, standard error, mean, minimum, maximum, and ranges of the mineral and benthic data collected from each survey (winter, spring, summer, fall).

Winter 2012-2021 Sand Survey Statistics

Winter 2012-2021 Statistics							
	VAR	STD	STE	mean	Min	Max	Range
Avg. Grain Size	0.03	0.18	0.03	0.72	0.54	1.02	0.48
Mean sand grain size lower swash (mm)	0.17	0.41	0.06	1.09	0.71	1.96	1.25
Mean sand grain size mid swash (mm)	0.02	0.13	0.02	0.66	0.51	0.89	0.38
Mean sand grain size upper swash (mm)	0.02	0.16	0.02	0.50	0.37	0.81	0.44
Mean sand grain size toe of dune (mm)	0.01	0.07	0.01	0.37	0.28	0.47	0.19
Total Benthos	6656.40	81.59	11.66	74.80	7.00	278.00	271.00
Avg. Species	1.63	1.27	0.18	1.17	0.11	4.34	4.23
Avg Slope Degrees	1.17	1.08	0.15	3.97	1.36	5.13	3.77
Avg Comp	2866.10	53.54	7.65	133.50	49.11	187.97	138.86
% HM Lower Swash	6.27	2.50	0.36	2.19	0.45	8.03	7.58
% HM Mid Swash	8.30	2.88	0.41	2.64	0.70	9.07	8.37
% HM Upper Swash	13.05	3.61	0.52	3.52	0.81	10.45	9.64
% HM Dune	57.06	7.55	1.08	12.55	0.75	22.40	21.65
Average %HM	8.61	2.93	0.42	3.47	0.77	10.50	9.73

Table 11 – The statistics analyzing the variance, standard deviation, standard error, mean, minimum, maximum, and ranges of the mineral and benthic data collected from each winter survey between 2012-2021.

Spring 2012-2021 Sand Survey Statistics

Spring 2012-2021 Statistics							
	VAR	STD	STE	mean	Min	Max	Range
Avg. Grain Size	0.01	0.10	0.02	0.78	0.65	0.89	0.24
Mean sand grain size lower swash (mm)	0.09	0.29	0.05	1.29	0.88	1.61	0.72
Mean sand grain size mid swash (mm)	0.02	0.15	0.02	0.81	0.65	1.09	0.44
Mean sand grain size upper swash (mm)	0.01	0.11	0.02	0.57	0.46	0.83	0.37
Mean sand grain size toe of dune (mm)	0.02	0.13	0.02	0.44	0.32	0.77	0.45
Total Benthos	25128.94	158.52	26.42	197.50	30.00	564.00	534.00
Avg. Species	6.13	2.48	0.41	3.09	0.47	8.81	8.34
Avg Slope Degrees	0.37	0.61	0.10	4.27	3.58	5.45	1.87
Avg Comp	1132.44	33.65	5.61	168.87	115.85	222.97	107.12
% HM Lower Swash	2.96	1.72	0.29	1.82	0.63	6.01	5.39
% HM Mid Swash	7.48	2.73	0.46	2.26	0.82	8.67	7.85
% HM Upper Swash	12.75	3.57	0.60	3.67	1.05	10.44	9.39
% HM Dune	96.36	9.82	1.64	11.38	1.37	33.50	32.13
Average %HM	18.56	4.31	0.72	4.78	1.32	14.66	13.33

Table 12 – The statistics analyzing the variance, standard deviation, standard error, mean, minimum, maximum, and ranges of the mineral and benthic data collected from each spring survey between 2012-2021.

Summer 2012-2021 Sand Survey Statistics

Summer 2012-2021 Statistics							
	VAR	STD	STE	mean	Min	Max	Range
Avg. Grain Size	0.01	0.09	0.01	0.73	0.63	0.87	0.24
Mean sand grain size lower swash (mm)	0.12	0.34	0.06	1.11	0.64	1.76	1.12
Mean sand grain size mid swash (mm)	0.01	0.09	0.02	0.64	0.47	0.78	0.31
Mean sand grain size upper swash (mm)	0.00	0.07	0.01	0.44	0.36	0.59	0.23
Mean sand grain size toe of dune (mm)	0.02	0.15	0.03	0.43	0.32	0.84	0.52
Total Benthos	679774.10	824.48	137.41	2222.10	825.00	3590.00	2765.00
Avg. Species	165.96	12.88	2.15	34.72	12.89	56.09	43.20
Avg Slope Degrees	1.92	1.39	0.23	5.68	2.73	7.19	4.46
Avg Comp	1254.82	35.42	5.90	176.52	114.81	239.62	124.81
% HM Lower Swash	9.26	3.04	0.51	2.90	0.59	10.19	9.59
% HM Mid Swash	11.23	3.35	0.56	3.24	0.82	11.05	10.23
% HM Upper Swash	25.17	5.02	0.84	4.94	0.62	17.42	16.79
% HM Dune	76.72	8.76	1.46	10.83	2.12	28.74	26.61
Average %HM	10.54	3.25	0.54	4.16	1.40	10.98	9.59

Table 13 – The statistics analyzing the variance, standard deviation, standard error, mean, minimum, maximum, and ranges of the mineral and benthic data collected from each summer survey between 2012-2021.

Fall 2012-2021 Sand Survey Statistics

Fall 2012-2021 Statistics							
	VAR	STD	STE	mean	Min	Max	Range
Avg. Grain Size	0.02	0.13	0.02	0.70	0.46	0.88	0.41
Mean sand grain size lower swash (mm)	0.12	0.34	0.06	1.15	0.63	1.55	0.93
Mean sand grain size mid swash (mm)	0.03	0.17	0.03	0.74	0.52	1.08	0.56
Mean sand grain size upper swash (mm)	0.02	0.13	0.02	0.53	0.30	0.78	0.48
Mean sand grain size toe of dune (mm)	0.01	0.08	0.01	0.39	0.32	0.58	0.26
Total Benthos	51192.90	226.26	37.71	605.30	324.00	1010.00	686.00
Avg. Species	12.50	3.54	0.59	9.46	5.06	15.78	10.72
Avg Slope Degrees	1.81	1.34	0.22	4.70	2.85	6.84	3.98
Avg Comp	2009.21	44.82	7.47	188.25	111.23	266.08	154.85
% HM Lower Swash	2.32	1.52	0.25	1.39	0.52	5.65	5.12
% HM Mid Swash	1.13	1.06	0.18	1.45	0.61	4.30	3.69
% HM Upper Swash	0.32	0.56	0.09	1.97	1.19	2.80	1.61
% HM Dune	5.97	2.44	0.41	6.85	3.29	11.28	7.99
Average %HM	0.57	0.75	0.13	2.91	2.12	4.21	2.09

Table 14 – The statistics analyzing the variance, standard deviation, standard error, mean, minimum, maximum, and ranges of the mineral and benthic data collected from each fall survey between 2012-2021.

Overall Sand Survey Statistics Between Seasons 2012-2021

Overall Stats Between Seasons 2012-2021							
	VAR	STD	STE	mean	Min	Max	Range
Avg. Grain Size	0.02	0.13	0.01	0.73	0.46	1.02	0.56
Mean sand grain size lower swash (mm)	0.12	0.34	0.01	1.16	0.63	1.96	1.34
Mean sand grain size mid swash (mm)	0.02	0.15	0.01	0.71	0.47	1.09	0.62
Mean sand grain size upper swash (mm)	0.02	0.12	0.01	0.51	0.30	0.83	0.53
Mean sand grain size toe of dune (mm)	0.01	0.12	0.00	0.41	0.28	0.84	0.57
Total Benthos	931579.46	965.18	40.22	774.93	7.00	3590.00	3583.00
Avg. Species	227.44	15.08	0.63	12.11	0.11	56.09	55.98
Avg Slope Degrees	1.64	1.28	0.05	4.65	1.36	7.19	5.83
Avg Comp	2053.66	45.32	1.89	167.64	49.11	266.08	216.98
% HM Lower Swash	5.12	2.26	0.09	2.08	0.45	10.19	9.73
% HM Mid Swash	6.93	2.63	0.11	2.40	0.61	11.05	10.44
% HM Upper Swash	12.98	3.60	0.15	3.52	0.62	17.42	16.79
% HM Dune	59.19	7.69	0.32	10.40	0.75	33.50	32.76
Average %HM	9.34	3.06	0.13	3.83	0.77	14.66	13.89

Table 15 – The overall statistics analyzing the variance, standard deviation, standard error, mean, minimum, maximum, and ranges of the mineral and benthic data collected from each survey between 2012-2021.

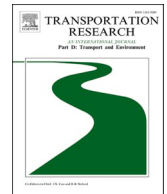**APPENDIX B: 2021 Burn Regions for PINWR**

811_812_1154ac_022521

813_339ac_022821

813_46ac_110420

APPENDIX C: Published Papers

Effectiveness of indicators for assessing the vulnerability of barrier island highways

Adam Behr, Emily Berglund, Elizabeth Sciaudone [*]

Dept. Civil, Construction and Environmental Engineering, N.C. State University, 915 Partners Way, Raleigh, NC 27606, USA

ABSTRACT

Highways along barrier islands are highly susceptible to storm impacts like overwash, erosion, and island breaching. The present research evaluates the effectiveness of 14 morphological indicators in predicting highway vulnerability to storm impacts from a data set of seven storms with documented roadway impacts. Multi-indicator functions were also developed and assessed. The research finds that distance from edge-of-pavement to dune toe, volume above mean high water between edge-of-pavement and ocean shoreline, distance from edge-of-pavement to ocean shoreline, and dune crest height above the road are the most skilled individual indicators of highway vulnerability. A multi-indicator function of dune toe elevation and distance from edge-of-pavement to dune toe is more skilled than any of the individual indicators that were evaluated. Some of these indicators can be projected to assess future vulnerability, as well. The results convey the value of geomorphology-based indicators and their potential in larger-scale coastal infrastructure vulnerability assessments.

1. Introduction

Coastal areas are attractive places to live and work, drawing in a large portion of the human population. Small and Nicholls (2003) estimated that 1.2 billion people live within 80.5 km of a coastline, which Neumann et al. (2015) predicted will grow. Due to their proximity to the ocean, coastal communities are susceptible to a unique combination of processes that impact infrastructure, such as tides, storm surge, and waves. The regularity and severity of impacts that occur are likely to worsen into the future due to sea level rise (SLR) (Mimura, 2013; Enríquez et al., 2019) and increasing occurrences of extreme weather events (USGCRP, 2018; EASAC, 2013). Barrier islands face these hazards, in addition to island breaching. Island breaching occurs when elevated soundside water levels and oceanside wave erosion cut new inlets through the island (Safak, Warner, and List, 2016). In the context of this paper, the vulnerability of infrastructure is defined as the susceptibility to damage or reduced functionality due to these coastal hazards. Engineers and stakeholders use coastal vulnerability assessments to identify the components of infrastructure that are most vulnerable to storm impacts, which helps them strategically plan projects. Methods to assess the vulnerability of infrastructure can include modeling of inundation processes that inundate infrastructure (Li, Lin, and Burks-Copes, 2013; Kafalenos et al., 2008); empirical parameterization of different erosion regimes (Stockdon, Plant, and Sallenger, 2009); computation of vulnerability indices using a combination of geomorphology and process-based variables (Francis et al., 2019); and computation of simple, geomorphology-based indicators (Velasquez-Montoya et al., 2021).

---

* Corresponding author at: Fitts-Woolard Hall, 915 Partners Way, Raleigh, NC 27695, USA.
E-mail addresses: abehr@ncsu.edu (A. Behr), emily_berglund@ncsu.edu (E. Berglund), ejsciaud@ncsu.edu (E. Sciaudone).

Geomorphology-based indicators used in previous studies are based on logical understanding of coastal processes and experience with previous events. However, little work has been done to evaluate the effectiveness of a wide range of coastal vulnerability indicators with multiple real-world storms. The aim of the present study is to compare the success of a wide range of vulnerability indicators in predicting coastal highway impacts from a series of seven storm events that were recorded along the North Carolina coast. Documented storm impacts to the highway were used to directly assess the performance of various vulnerability indicators, with the frequency of impacts being a proxy for observed vulnerability. This proxy was chosen, as opposed to another proxy like severity of impacts, because the observed storm impacts led to roadway closure for all of the storms in the dataset. Severe physical damage to the roadway occurred in only a few of the storms. Roadway closure leads to residents of the barrier island communities being unable to access hospitals and other emergency services available off-island. This research additionally tests the use of weighted sums of multiple indicators on improving the accuracy of predicting coastal highway vulnerability. Empirically driven optimization methods were used to objectively identify the relative contribution of each indicator to the total level of vulnerability.

This research focuses on assessing vulnerability at a small spatial scale for project planning and monitoring purposes. Therefore, larger-scale process variables like wave climate and tidal range did not vary over the study area, and the research's scope is limited solely to geomorphology-based indicators because their spatial variability is assumed to be the main factor in vulnerability. While on a larger spatial scale factors like the condition of the roadway and/or the criticality of the roadway may also contribute to vulnerability, for this study we are focused on a unique situation where one roadway connects multiple barrier island communities to the mainland. It is assumed that the baseline pavement condition is similar along the analyzed stretch of roadway.

2. Literature review

The purpose of coastal vulnerability assessments is to identify infrastructure that is vulnerable to long- and short-term storm impacts, which informs engineers and policy makers. Numerical hydrodynamic and sediment-transport models have been used to identify vulnerable infrastructure under different storm and SLR cases (Li, Lin, and Burks-Copes, 2013). It is computationally intensive to map vulnerability at a fine resolution with numerical morphodynamic models, however, so their usage at regional or larger scales or for periodic vulnerability analyses may be infeasible. "Bathtub" style mapping is an approach, which intersects water levels with highway infrastructure to determine the areas inundated for a given scenario (FHWA, 2012). Studies have used bathtub mapping to illustrate long-term projections of coastal highway vulnerability by modeling the still water-level, including storm surge and SLR, and mapping the consequently inundated roads (Kafalenos et al., 2008). This method allowed researchers to identify vulnerable stretches of road at a regional level, between Galveston, TX and Mobile, AL, USA (Kafalenos et al., 2008). The USGS National Assessment of Coastal Change Hazards program (Stockdon, Plant, and Sallenger, 2009) combined beach and dune topography, storm surge model outputs, and parameterized wave runup (Stockdon et al., 2006) to give a probabilistic representation of dune vulnerability across US coasts based on the predicted severity of erosion. The Coastal Vulnerability Index (CVI) (Gornitz et al., 1994) can be adapted to a given study region and purpose, such as to classify roads vulnerable to erosion across Hawaii, USA, by selecting the most relevant variables (Francis et al., 2019). The CVI is a composite of discretized classes of geological, morphological, and process-based variables, such as landform type, coastal slope, relative sea level change, rock type, tidal range, and wave climate (Gornitz et al., 1994). Performance of an index like the CVI can be sporadic depending on the definitions of risk classes for each variable (Koroglu et al., 2019). Inconsistencies in the definition of risk classes for each variable can lead to significant differences in the resultant calculated CVI and, thus, vulnerable areas (Koroglu et al., 2019). For a study area that is small relative to the scale that physical process variables vary, morphological indicators alone can be used to assess vulnerability (Velasquez-Montoya et al., 2021). The North Carolina Department of Transportation's (NCDOT) Coastal Monitoring Program (CMP) uses simple geomorphology-based indicators like island width, dune crest height above the road, and distance from edge-of-pavement (EOP) to ocean shore to assess the vulnerability of a barrier island highway off the coast of North Carolina, USA on a cross-shore transect basis (Velasquez-Montoya et al., 2021). The study additionally predicts future vulnerability at a decadal time scale by using a linear regression of shoreline positions, from which EOP to ocean shore can be calculated (Velasquez-Montoya et al., 2021).

Simple indicators of coastal highway vulnerability are valuable because they can be easily computed with updated topography, enabling researchers to monitor spatial and temporal changes in vulnerability. There is limited research on the effectiveness of geomorphology-based vulnerability indicators across a range of storms because robust datasets of pre-storm topography along with documentation of the precise locations of post-storm impacts are scarce. Without data for precise locations of storm impacts to infrastructure, past research has largely focused on effectiveness of indicators from the perspective of dune well-being under the assumption that dunes are the primary protection for infrastructure behind them. Island width, height and width of the dune fields, vegetation type, distance from the dunes to the ocean, and dune field continuity explained the most variation in dune survival versus failure after two hurricanes that affected a FL, USA barrier island (Claudino-Sales, Wang, and Horwitz, 2008). Controls of longshore variation in dune changes can depend on characteristics of the study area. Beuzen et al. (2019) sought to determine the major geomorphological controls of dune and beach berm erosion across a wide study area covering 400 km of southeast Australian coast. Erosion of beach berms and dunes increased as exposure to the incident waves increased; berm erosion was controlled by the pre-storm volume of the berm, such that berms with high pre-storm volumes led to high erosion; and dune erosion was equally linked to the width of the berm and the dune toe elevation, such that wide berms and elevated dune toes resulted in low erosion (Beuzen et al., 2019). In a wave flume, under experimental conditions, the geometry that most effectively limited overwash was a berm with dune configuration (Figlus et al., 2011). A berm with the dune led to less dune volume loss, compared to wide dune and sloping beach and dune configurations (Figlus et al., 2011), which agreed with results of Beuzen et al. (2019). Judge, Overton, and Fisher (2003) tested the effectiveness of using empirical models of expected dune erosion (Hallermeier and Rhodes, 1988; Kriebel et al., 1996) as dune
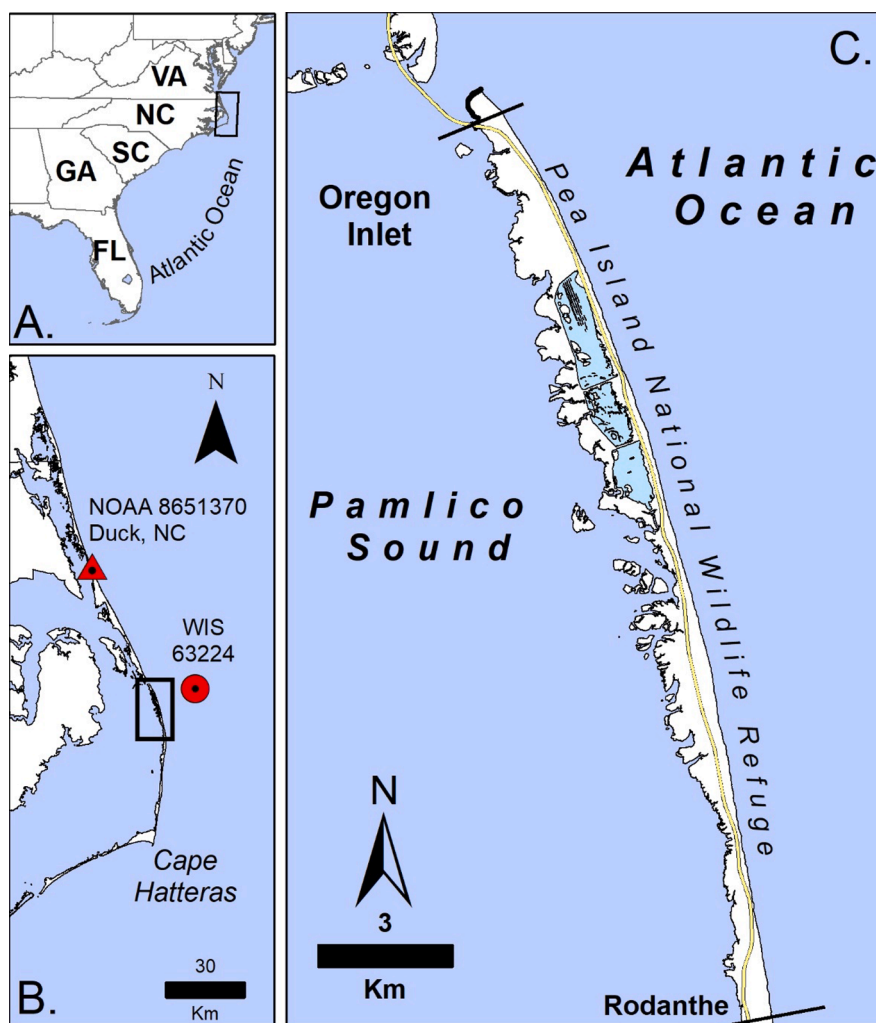
Fig. 1. Map showing (a) location along the southeastern coast of the U.S., (b) locations of water level (NOAA 8651370) and wave (Wave Information Study 63224) data employed in this research, and (c) extent of study area along Pea Island, NC. Note that at the scale of this figure the Oregon Inlet Waverider Buoy (NDBC 44095) is approximately co-located with the WIS station shown.

vulnerability indicators, assessed the Storm Impact Scale (Sallenger, 2000), and described two new dune vulnerability indicators, dune cross-sectional centroid and mass moment of inertia. They found the mass moment of inertia compared to water level with setup had the most success at predicting dune failure versus survival (Judge, Overton, and Fisher, 2003). While failure of a beach and dune system does imply that infrastructure behind the dunes are affected, there are other processes, like infiltration and frictional energy losses (Donnelly et al., 2009), that affect the level of infrastructure vulnerability. There is limited research that directly analyzes the relationship between geomorphology and infrastructure vulnerability. An analysis of the geomorphological controls of road impacts ascertained that offshore bathymetry, dune height, and island width were major factors (Houser, 2009). The analysis was only concerned with locations that were physically damaged during two hurricanes, therefore more common impacts that occur to coastal highways like overwash were excluded (Houser, 2009).

3. Study area

Barrier islands off the coast of North Carolina are crucial ecosystems, popular tourist destinations, and desirable places to live. The NC Division of Coastal Management (NCDCM) found that Dare County accounts for $957 million USD per year of the state's travel expenditures, which is approximately 5% of North Carolina's total travel income (NCDCM, 2016). The region attracts a significant amount of research attention due to its dynamic geography and plethora of biodiversity (Sciaudone et al., 2016; Velasquez-Montoya and Overton, 2017; Pfaller et al., 2020; Levine et al., 2017; Halls and Randall, 2018, and others).

Hatteras Island—the northern tip locally known as Pea Island—is a barrier island in Dare County that is host to the communities of Rodanthe, Waves, and Salvo, as well as the 5,834 acre Pea Island National Wildlife Refuge (USFWS, 2020). Oregon Inlet to the north
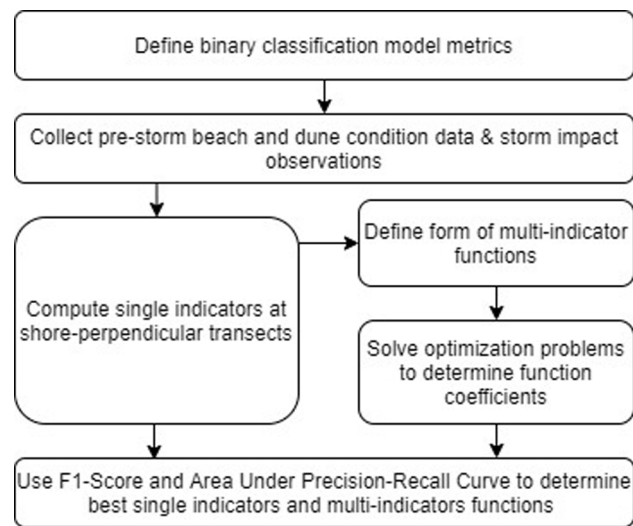
Fig. 2. Flowchart of steps in methodology.

separates the island from the northern Outer Banks and the Pamlico Sound lies between the mainland and the island (Fig. 1). NC-12 is the sole highway that connects Hatteras Island and its communities with the northern Outer Banks and serves as the only evacuation route. This makes reliability of the highway between Oregon Inlet and Rodanthe of critical importance. One of the most common impacts to NC-12 that causes closures is sand and ocean overwash, due to a combination of elevated water levels and runup of waves that can overtop dunes. The Final Environmental Impact Statement for the replacement of the bridge over Oregon Inlet noted the high frequency of highway maintenance activities required along Pea Island to move sand off the road (NCDOT, 2008). Another common impact to the road is flooding, which occurs from the bay (sound) side when winds drive up sound water levels. Flooding can make the road hazardous to traverse, sometimes requiring NCDOT to temporarily close the road. Island breaching is the impact which occurs most rarely but that is most severe. Most recently, breaches occurred in two locations on Hatteras Island during hurricane Irene in 2011 (Velasquez-Montoya et al., 2018). At each location where breaching occurred, the road was damaged. More frequent road impacts are expected along the study area because of increasing storm events (USGCRP, 2018) and predicted SLR between 10.9 and 18.5 cm by 2045 at the nearby Oregon Inlet (NC Coastal Resources Commission Science Panel, 2015). Because of North Carolina's strict laws prohibiting structures on the oceanfront, structural (hardening) measures to protect the roadway (i.e. revetments, seawalls, or similar) are not allowed (NC Coastal Area Management Act § 113A-115.1.).

Since 2010, NCDOT has sponsored a Coastal Monitoring Program in place to assess and predict the vulnerability of the 21.1 km stretch of highway to short- and longer-term hazards (Velasquez-Montoya et al., 2021). A significant part of the CMP involves long-term data collection in the form of bimonthly aerial photogrammetry and quarterly digital elevation models (DEMs). Because of this program, there is an extensive set of imagery and topographic data in this study area, which provides an opportunity to assess the performance of morphological indicators at predicting infrastructure vulnerability. In the present study, the focus is on impacts to highway NC-12, but the methods are applicable to coastal infrastructure in other areas with similar geomorphological settings (i.e. barrier islands with relatively straight and continuous coastlines).

4. Methods and data

Binary classification metrics were used to assess and compare indicators. Binary classification metrics use an accounting of correct and incorrect predictions, shown as a confusion matrix, as input. Observed storm impacts to the road were identified by comparing pre- and post-storm aerial imagery, and 14 geomorphological parameters were used as indicators in developing pre-storm vulnerability predictions. To develop functions of multiple indicators, optimization problems were formulated based on the same data that were used for the indicator evaluations. The performance of alternative solvers was explored, and one solver was selected that best fit the needs of this research. Fig. 2 illustrates the methodology workflow.

4.1. Binary classification

Binary classification involves predicting the classes of items with two possible outcomes or types. Predicting highway vulnerability is a binary classification problem: transects are classified as vulnerable, or not. In the present binary classification model, the indicators are used to separate transects along the highway into vulnerable and not-vulnerable classes, depending on the indicator values relative to a specified threshold.

Binary classification model metrics were used to measure each indicator's performance, allowing for comparison between the various morphological parameters. Binary classification metrics are calculated using a confusion matrix of the different outcomes and

Table 1
Confusion matrix of vulnerability classifications.

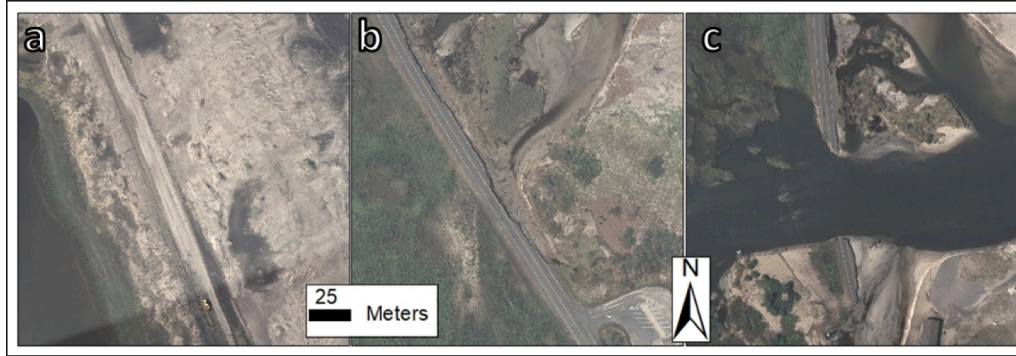|	**Predicted Vulnerable**	**Predicted Not Vulnerable**
Observed Vulnerable	True Positives	False Negatives
Observed Not Vulnerable	False Positives	True Negatives

Fig. 3. Storm impacts to the highway after Hurricane Irene in August 2011: (a) overwash sand covered road; (b) ocean-side erosion damaged pavement; (c) island breach damaged pavement.

the proportions of correct and incorrect predictions. For example, in this case of highway vulnerability classification, if a certain transect was predicted to be vulnerable, that prediction would be a "true positive" if the transect was observed to be vulnerable during a storm, and a "false positive" if the transect was not observed to be vulnerable. "Positive" refers to the class that is identified or predicted. The converse is true for transects predicted to not be vulnerable. These are "true negatives" and "false negatives". Many binary classification model metrics are calculated using different combinations of the total numbers of these "true positives", "true negatives", "false positives", and "false negatives". An example of the confusion matrix including all of the possible outcomes that result from an indicator evaluation is shown in Table 1.

Accuracy (Eq. (1)) represents the percentage of true predictions. Accuracy is a suitable metric for balanced class problems, where the two classes occur at approximately the same frequency. However, if the problem is imbalanced, such that one class occurs much more frequently than the other, accuracy can be skewed by a model that is biased towards the dominant class (Provost, Fawcett, and Kohavi, 1998).

Other metrics used to evaluate binary classification models include precision, recall, F-score, area under the receiver-operating-characteristic curve (ROC AUC), and area under the precision-recall curve. Precision (Eq. (2)) calculates the percentage of the positive class that were correctly predicted out of all items predicted to be in the positive class. Recall (Eq. (3)) computes the percentage of true positives out of all of the items in the positive class. Precision and recall are opposed measurements, with the maximum of one being the minimum of the other. If precision and recall are given an equal weight, the harmonic mean of a model's precision and recall is calculated as the F1-Score (Eq. (4)). The F1-Score, therefore, takes into account both metrics.

Accuracy, precision, recall, and F1-Score all are threshold-sensitive because they change depending on the threshold that is used in the classification model. Being threshold-sensitive is a drawback when the goal in assessing a binary classification model is to give an overall determination of skill. The area under precision-recall curve (PR AUC) and area under receiver-operating-characteristics curve (ROC AUC) are metrics that are both independent of threshold value and appropriate for imbalanced class problems (Davis and Goadrich, 2006). The ROC curve illustrates the inverse relationship between the rates of correctly predicting the positive class and incorrectly predicting the negative class, and the PR curve illustrates the tradeoff between precision and recall at different thresholds (Davis and Goadrich, 2006). Davis and Goadrich (2006) argued that, for imbalanced class problems, the PR AUC can be a more appropriate and robust metric than ROC AUC.

Binary classification model metrics are relative measurements, and there are no defined bounds for "good" or "bad" models. However, the metrics do allow for comparison among models or binary indicators applied to a mutual problem. For this study, F1-Score and PR AUC metrics were used to compare the effectiveness of vulnerability indicators because predicting highway vulnerability is an imbalanced class problem, where the more important class (impacted road transect) occurs infrequently. F1-Score and PR AUC are both compositions of precision and recall scores. Thus, they put the most weight on correctly predicting vulnerability (TP) while also including a cost for incorrect classifications (FP, FN).

$$Accuracy = \frac{TP + TN}{TP + TN + FP + FN} \tag{1}$$
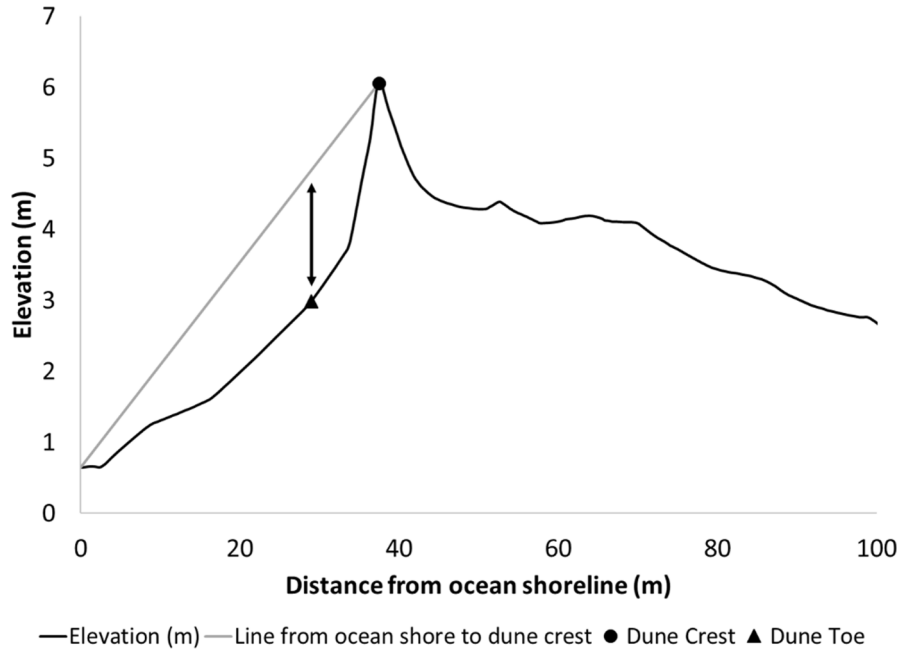
$$Precision = \frac{TP}{TP + FP} \tag{2}$$

Fig. 4. Example of dune crest and dune toe extraction from cross-shore profile with a semi-automated algorithm.

$$Recall = \frac{TP}{TP + FN} \tag{3}$$

$$F1 - Score = \frac{2*Precision*Recall}{Precision + Recall} \tag{4}$$

where

TP = Number of true positives, TN = Number of true negatives, FP = Number of false positives, and FN = Number of false negatives.

4.2. Roadway storm impacts

Observed highway vulnerability was quantified using the frequency of storm impacts that occurred over the course of seven storms. Storm impacts to the road were digitized by visually comparing pre- and post-storm georeferenced aerial imagery, using ArcGIS. The three types of impacts observed are shown in Fig. 3, including overwash, ocean-side erosion damaged pavement, and island breach damaged pavement. To avoid considering occurrences of windblown sand on the road as ocean overwash, it was required that the road should be at least 50% obscured by sand coverage at a specific transect for it to be considered impacted by ocean overwash. An example of the road being highly obscured by sand is shown in Fig. 3(a). Instances of damage to the pavement due to ocean-side erosion and island breaching, shown in Fig. 3(b) and Fig. 3(c), respectively, were also visually identified. Because shadows or water coverage could be misinterpreted as missing or damaged pavement, these types of impacts were verified with NC DOT maintenance engineers to confirm that documented damages did occur during the specific storms. In the available aerial photographs, observed impacts from the sound side were limited to roadway damage from breaching. The most frequent type of sound-side impact within the study area is flooding, however, this impact cannot be easily observed with post-storm aerial imagery because it has generally receded by the time of the photography.

To describe the storm climate of the study area and contextualize the storms used to locate impacts and evaluate indicators, return period analyses were performed on three different wave and water level parameters. Storm events were identified from the wave height time series by using a significant wave height of > 2 m for > 8 h criterion. Then, the maximum significant wave heights, non-tidal residuals (surge), and storm durations were collected for each of these storm events. The Traditional Gumbel plotting position formula was applied to this partial duration series, and a log-linear trend line was fit to the data to identify the relationship between each parameter and its respective return period, as described in the U.S. Army Corps of Engineers (USACE) Coastal Engineering Manual (USACE, 2008).

4.3. Vulnerability indicators

Using ArcGIS, geomorphological features were extracted from DEMs and aerial imagery for the closest available date prior to each storm with documented storm impacts. With extracted coastal landforms, various indicator values were determined on a transect basis
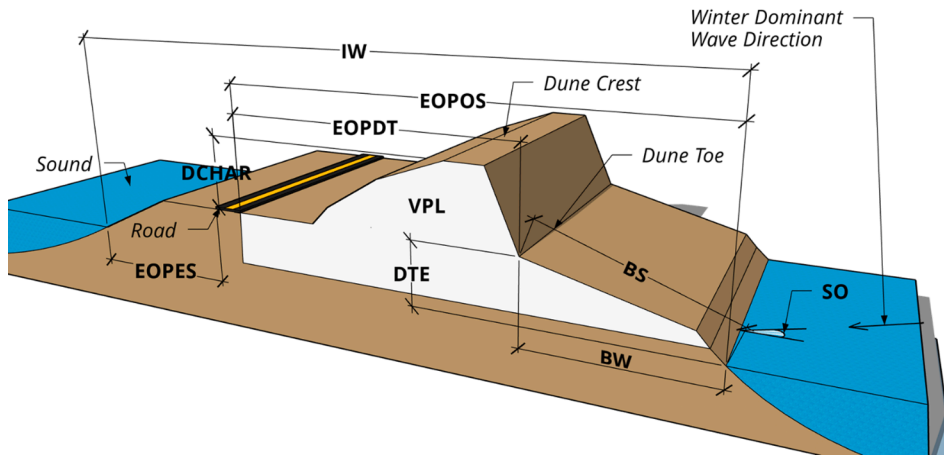
Fig. 5. Schematic of main parameters tested as indicators of highway vulnerability: Island Width (IW), Dune Crest Height Above Road (DCHAR), EOP to Ocean Shore (EOPOS), EOP to Estuary Shore (EOPES), EOP to Dune Toe (EOPDT), Volume Per Length (VPL), Dune Toe Elevation (DTE), Beach Slope (BS), Beach Width (BW), and Shore Orientation (SO).

across the study area. Ocean and inlet shorelines along the study area were digitized using the wet-dry line method (Dolan et al., 1980). Aerial imagery was examined at 1:1200 scale to maintain a consistent degree of precision while digitizing the shoreline. Estuarine shorelines were digitized by following the visible edge of the vegetation when possible, or the wet-dry line along sandy areas. Estuarine shorelines were digitized at 1:800 scale because the marsh edges are generally more intricate than the ocean shoreline's wet-dry line. Dune crests (maximum elevations) were extracted from cross-shore profiles at each transect by an algorithm that selects the highest elevation point between the road edge of pavement and shoreline, as illustrated in Fig. 4. Dune toes were extracted from the cross-shore profiles using an algorithm that picks the point on the profile with the greatest deviation between the terrain and a line from the dune crest to shoreline (Fig. 4). The highway's centerline elevations were interpolated at each transect from the DEM surface using GIS tools.

Using the extracted coastal features, the following geomorphological parameters were calculated on a transect basis so the parameters could then be tested as indicators of road vulnerability to storm impacts:

1. Island width from the estuary shoreline to the ocean shoreline (Island Width)
2. Dune crest elevation relative to NAVD 88 (Dune Crest Elevation)
3. Road elevation relative to NAVD 88 (Road Elevation)
4. Difference in elevation between the dune crest and the road (Dune Crest Height Above Road)
5. Three-transect moving averaged Dune Crest Height Above Road (Smoothed Dune Crest Height Above Road)
6. Distance from road edge-of-pavement (EOP) to ocean shoreline (EOP to Ocean Shore)
7. Distance from road EOP to estuarine shoreline (EOP to Estuary Shore)
8. Distance from road EOP to dune toe (EOP to Dune Toe)
9. Volume above MHW between EOP and ocean shoreline (Volume Per Length)
10. Dune toe elevation relative to NAVD 88 (Dune Toe Elevation)
11. Distance from the dune toe to the ocean shoreline (Beach Width)
12. Beach slope found according to the USGS 2 point method (Doran, Long, and Overbeck, 2015) (Beach Slope)
13. The reciprocal of beach slope (Inverse Beach Slope)
14. The angular difference between shore-normal orientation and the weighted mean wave direction. To calculate the weighted mean wave direction, similar to the weighted mean wind direction used by Ortiz, Roy, and Edmonds (2017), the data were filtered to only include significant wave heights>2 m, and wave direction was weighted by the square of significant wave height to better represent the directional distribution of wave energy. (Shore Orientation)

It was assumed that wave parameters for purposes of computing the Shore Orientation indicator could be extracted at the nearest hindcast station or buoy and approximated along the entire study area. This is because the bathymetry is relatively consistent alongshore and the study area is only 21 km in length.

Fig. 5 shows a schematic of the primary geomorphological parameters tested. Applying each indicator, each transect was predicted to be vulnerable or not vulnerable to storm impacts. These vulnerability predictions were compared with observed vulnerability to determine whether each prediction was correct or incorrect. F1-Score (Eq. (4)) and PR AUC were used to evaluate indicators because predicting vulnerability is an imbalanced class problem with the positive class (road impacts) occurring in 36% of transects during storms in this dataset. An optimal threshold was found iteratively for each indicator based on the F1-Score, with the optimal threshold
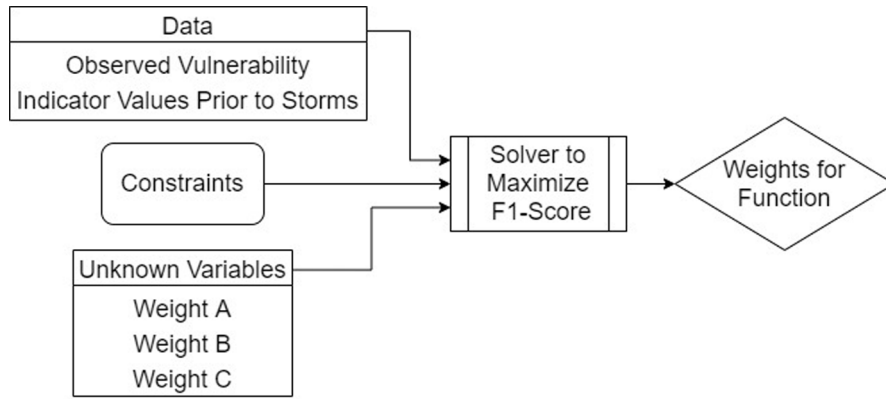
Fig. 6. Optimization process to solve for weights used in multi-indicator functions. Inputs going in to MILP solver include data, constraints, and unknown variables, and weighting coefficients are output.

for each indicator corresponding to the max F1-Score of the indicator. The optimal threshold found in this way was determined from the impacts caused by storms in this dataset. Thus, the F1-Score and optimal threshold could differ for an alternative set of storms of different severity. The PR AUC was considered the most important metric of indicator skill because it is composed of the skill at all thresholds, meaning it is independent of a single threshold value. Being threshold-independent makes the PR AUC a convenient way to compare different indicators. An indicator with a greater PR AUC is better at ranking transects from most vulnerable to least vulnerable, which would make it a more valuable indicator. Additionally, a high PR AUC implies that an indicator's performance is less sensitive to the chosen threshold value. This quality is important because indicator thresholds are set based on the available data. If an indicator's performance is less sensitive to the threshold, it should be better at predicting vulnerability for storms outside of the dataset, in a validation setting.

4.4. Functions of multiple indicators

It was hypothesized that a function of multiple indicators could more accurately predict vulnerability than any one indicator on its own. To incorporate indicators as continuous variables that could each provide unique information about the vulnerability at each transect, a weighted linear function (Eq. (5)) was explored. The indicator values are known geomorphological parameters that are collected at each transect, and the vulnerability function's threshold is set to an arbitrary value without physical meaning. Thus, the only unknown parameters in the vulnerability function are the weighting coefficients. The weighting coefficients are needed because the indicators can vary in units, scale, and relative importance. The weighting coefficients also may change depending on the combination of indicators featured in the function. Optimization problems were set up for assorted combinations of indicators to relate unknown coefficients of assumed vulnerability functions (Eq. (5)) to resultant confusion matrices, with the goal of maximizing the F1-Score. Fig. 6 is a flowchart that summarizes the optimization setup.

The optimization problems were solved using a Mixed Integer Linear Programming (MILP) solver because the problems included a combination of binary and continuous variables. The MILP solver requires that the objective function be linear, so F1-Score was linearized (Eq. (6)). When given enough constraints and time, the MILP solver can converge on a deterministic solution (Integer Programming). Genetic Algorithm (GA) is another solver for optimization problems featuring a mixture of continuous and binary variables. The GA solver takes an evolutionary approach to iteratively test variables and adjust parameters based on the value of the objective function at each generation. The solver is more flexible, allowing for a non-linear objective function, such as the full F1-Score (Eq. (4)) (Genetic Algorithm). In preliminary tests of the solvers, there were not significant differences in the weights determined with the GA solver when compared with results from the MILP solver, despite the MILP solver's linearized objective function (Eq. (6)). The MILP solver was chosen because it results in a more definitive solution than the GA solver, for which the solution is not guaranteed. Optimization problems were solved for many different combinations of indicators and each of these subsequent functions were then evaluated using the binary classification model metrics described above.

$$F(indicator1, indicator2, indicator3) = A*indicator1 + B*indicator2 + C*indicator3 \qquad (5)$$

where:

indicator1, indicator2, indicator3 are indicator values, and *A, B, C* are coefficients that scale the indicator values such that they contribute to the overall vulnerability function's value.

IF F(*indicator1, indicator2, indicator3*) < Threshold, THEN transect is vulnerable.

$$Linearized\ F1 - Score = 2*TP - FP - FN \qquad (6)$$

where:

TP = Number of true positives, *FP* = Number of false positives, and *FN* = Number of false negatives.

Table 2
Data sets used to evaluate storm impacts and vulnerability indicator performance.

Storm	Data Set	Dates	Data Source	Notes
Hurricane Irene, 27 August 2011	DEM	2 August 2011	NC DOT	Pre-Storm
Hurricane Irene, 27 August 2011	Aerial Imagery	2 August 2011	NC DOT	Pre-Storm
Hurricane Irene, 27 August 2011	Aerial Imagery	28 August 2011	NC DOT	Post-Storm
Hurricane Sandy, 26 October 2012	DEM	11 October 2012	NC DOT	Pre-Storm
Hurricane Sandy, 26 October 2012	Aerial Imagery	11 October 2012	NC DOT	Pre-Storm
Hurricane Sandy, 26 October 2012	Aerial Imagery	31 October 2012	NC DOT	Post-Storm
Hurricane Arthur, 4 July 2014	DEM	12 April 2014	NC DOT	Pre-Storm
Hurricane Arthur, 4 July 2014	Aerial Imagery	2 June 2014	NC DOT	Pre-Storm
Hurricane Arthur, 4 July 2014	Aerial Imagery	4 July 2014	NOAA	Post-Storm
Nor'easter, 7 February 2016	DEM	7 October 2015	NC DOT	Pre-Storm
Nor'easter, 7 February 2016	Aerial Imagery	8 December 2015	NC DOT	Pre-Storm
Nor'easter, 7 February 2016	Aerial Imagery	8 February 2016	NC DOT	Post-Storm
Hurricane Matthew, 5 October 2016	DEM	22 August 2016	NC DOT	Pre-Storm
Hurricane Matthew, 5 October 2016	Aerial Imagery	22 August 2016	NC DOT	Pre-Storm
Hurricane Matthew, 5 October 2016	Aerial Imagery	10 October 2016	NOAA	Post-Storm
Nor'easter, 2 March 2018	DEM	9 February 2018	NC DOT	Pre-Storm
Nor'easter, 2 March 2018	Aerial Imagery	9 February 2018	NC DOT	Pre-Storm
Nor'easter, 2 March 2018	Aerial Imagery	26 March 2018	NOAA	Post-Storm
Hurricane Dorian, 5 September 2019	DEM	29 August 2019	NC DOT	Pre-Storm
Hurricane Dorian, 5 September 2019	Aerial Imagery	29 August 2019	NC DOT	Pre-Storm
Hurricane Dorian, 5 September 2019	Aerial Imagery	7 September 2019	NOAA	Post-Storm

4.5. Data sets

Raster data consisting of 76.2 cm resolution digital elevation models and 15.2 cm resolution aerial imagery were sourced from NCDOT's Coastal Monitoring Program (Velasquez-Montoya, 2021). These DEMs were selected based on the time of collection relative to storms that affected the study area. The DEMs cover the entire Coastal Monitoring Program's study area, from north of Oregon Inlet, southward to the town of Rodanthe (Fig. 1). A subset of previously established transects developed for the Coastal Monitoring Program was used in this study. These transects are spaced at 45.7 m and are approximately shore-perpendicular. Fig. 1 shows the northern and southernmost transects comprising the study area.

Post-storm aerial images with 30.5 cm resolution were sourced from the National Oceanic and Atmospheric Administration's (NOAA) Emergency Response Imagery Index (NOAA, 2020). Table 2 details the data sets employed to identify impacts in the present study, as well as the dates of the storms.

The timing of imagery relative to the date of each storm could potentially influence the quality of data collection efforts, due to possible pre-storm morphological changes and because with each passing day after the storm, NCDOT would have had additional opportunities to clean sand from the road and make repairs. To alleviate this as much as possible, pre-storm and post-storm imagery, as well as DEMs, were compared with special attention to differences, like the appearance of overwash fans on the sound side of the road, that would suggest road impact.

The Duck, NC Field Research Facility and U.S. Army Corps of Engineers Wave Information Studies (WIS) station 63224 were the closest sources of long-term ocean-side water level and wave data, respectively. Wave and water level data from 1980 to 2018 were collected from WIS station 63224 and the NOAA water level gauge at Duck, NC (Station 8651370). The WIS data is a hindcast product produced by the Coastal and Hydraulics Laboratory Engineer Research and Development Center (Tracy and Cialone, 2006).

Additional significant wave height and dominant wave period data were sourced from the NOAA National Data Buoy Center's station 44095 near Oregon Inlet for the year 2019. This station provided an observational time series of wave conditions near the study area going back to 2012 (NOAA, 2018).

5. Results

This section details the results of the present study analysis. The return period analysis results provide context for the storms in the data set. The spatial distribution of the storm impacts from the entire storm data set is summarized to give the reader an idea of the degree of observed vulnerability across the study area. Single vulnerability indicators are evaluated, followed by functions of multiple indicators.

5.1. Return period analysis

The majority of the storms used in this study were hurricanes because of the availability of NOAA post-storm aerial imagery of these events; however, there were also two winter storms, or "nor'easters", that were included in the dataset. The nor'easters, which occurred in February 2016 and March 2018, were included because post-storm aerial imagery from NC DOT was available to identify impacts.

The suite of storms used to evaluate the vulnerability indicators fell within a range of return periods for surge, duration, and wave
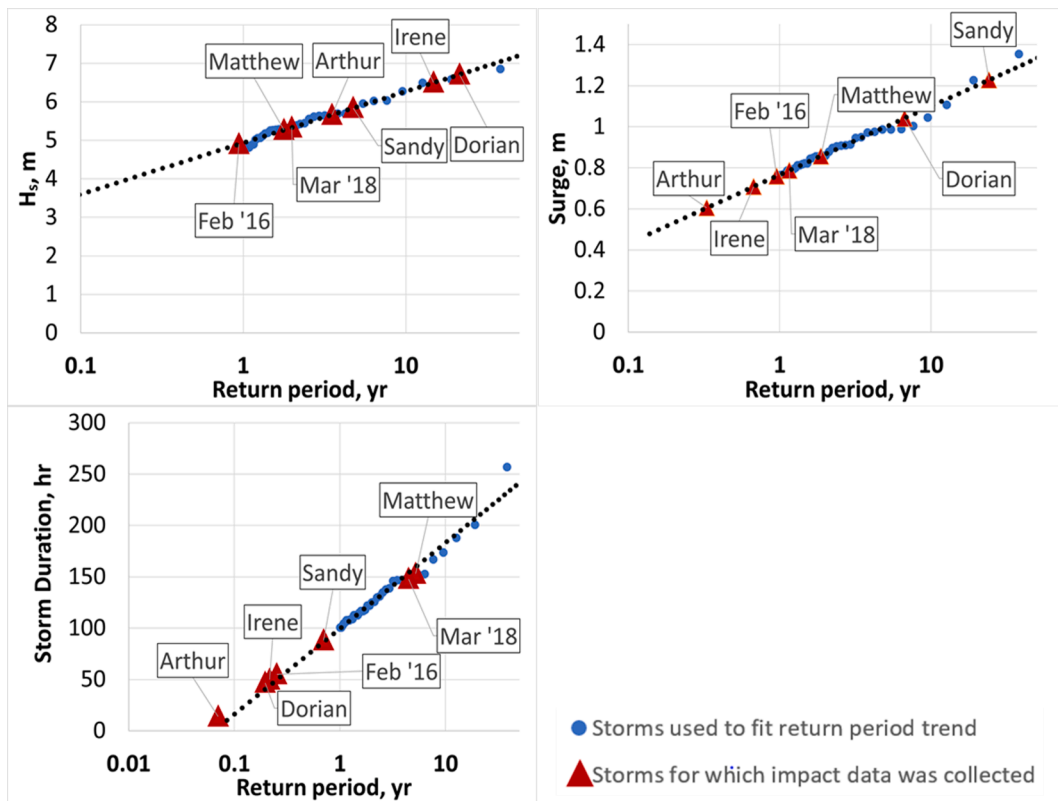
Fig. 7. Return period analyses shown by blue dots and black-dotted best-fit line for each parameter: (a) Significant Wave Height; (b) Surge; and (c) Total Water Level. The return periods of the seven storms in the data set are shown by red triangles. (For interpretation of the references to colour in this figure legend, the reader is referred to the web version of this article.)

height characteristics, as shown in Fig. 7. Significant wave height return periods ranged from 0.9 to 21 years, storm surge return periods ranged from 0.3 and 24 years, and storm duration return periods ranged from 0.1 and 5 years. Hurricane Dorian occurred in 2019, which was not encompassed by WIS hindcast data (1980–2018); therefore, the maximum significant wave height for this hurricane was taken from the Oregon Inlet Waverider Buoy (Station 44095). The significant wave height was shoaled from 18.4 m to 15.0 m depth using linear wave theory to make the buoy data compatible with the return period analysis that was performed using WIS data.

5.2. Distribution of observed vulnerability

As shown in Fig. 8, the number of storm impacts that occurred per transect ranged from zero (no storms caused impacts) to seven (all storms caused impacts). Impacts were most frequently observed in the northern third of the study area and in two smaller regions near the southern portion of the study area. Near the center of the study area, a temporary bridge was constructed shortly after hurricane Irene formed a breach in August of 2011 (Velasquez-Montoya et al., 2018). This temporary bridge was replaced by an interim structure (footprint indicated in Fig. 8) which opened in November 2017. Impacts to the road in this section were lessened after bridge construction, and afterwards, the few occurrences of impacts were mainly caused by sand washing onto the bridge from the adjacent areas.

5.3. Single indicators

Variability in PR AUC arises mainly due to differences in storms and the magnitude of impacts caused. Storms with more impacts result in greater PR AUC scores, in general, because there is a greater chance to correctly identify true positives. To account for this, a random indicator was simulated and its AU PRC confidence interval was calculated to give an idea of the uncertainty in the AU PRC which stems from variability in the storms' severities. Because a completely random indicator could predict the positive class—road impacts—at the rate that they occur (approximately 36%), and because there is some uncertainty around that mean, indicators were considered completely unskilled if their PR AUC was less than 0.47 (95% confidence interval for a random indicator).

Table 3 summarizes the evaluation results with each indicator ranked in order of most to least skill based on the PR AUC metric. Several indicators were found to be good predictors of vulnerability. The most skilled indicator was the EOP to Dune Toe based on its
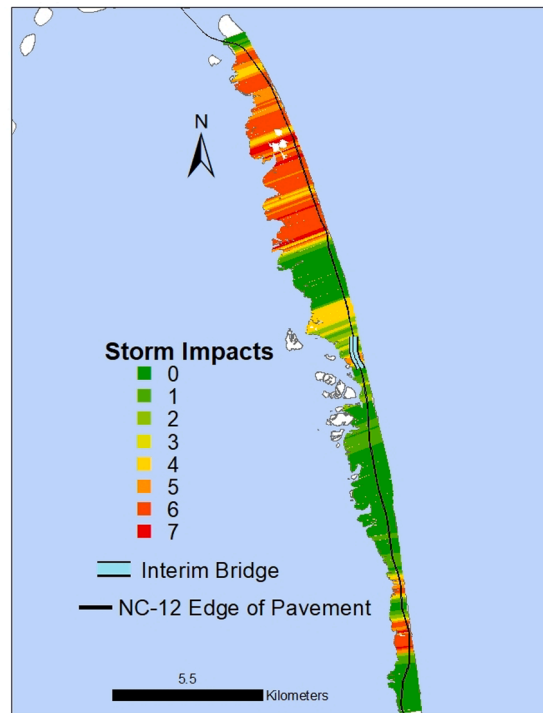
Fig. 8. Distribution of highway impacts along the study area.

Table 3
Indicators ranked by skill based on PR AUC.

Indicator	Threshold for max F1-score	Max F1-score	PR AUC
EOP to Dune Toe	92 m	0.79	0.77
Volume Per Length	11.1 m³/m	0.72	0.74
EOP to Ocean Shore	126.8 m	0.73	0.73
Smoothed Dune Crest Height Above Road	5.8 m	0.65	0.56
Dune Crest Height Above Road	5.5 m	0.63	0.55
Dune Crest Elevation	6.7 m	0.62	0.54
Shore Orientation	9°	0.63	0.52
Dune Toe Elevation	2.4 m	0.60	0.49
Beach Slope	0.09 m/m	0.58	0.49
Island Width	1.47 km	0.55	0.39
Beach Width	106.1 m	0.54	0.37
Inverse Beach Slope	96 m/m	0.53	0.30
Road Elevation	2.7 m	0.53	0.27
EOP to Estuary Shore	292.9 m	0.25	0.05

PR AUC metric of 0.77, as well as its max F1-Score of 0.79. The threshold optimization results suggested that EOP to Dune Toe most accurately predicted vulnerability with a threshold value of 302 m. Volume Per Length was the second most skilled with a PR AUC of 0.74. The third most skilled indicator, EOP to Ocean Shore, was close behind with a PR AUC of 0.73. Despite its lower PR AUC, the F1-Score of EOP to Ocean Shore was slightly better than that of Volume Per Length. This suggests that EOP to Ocean Shore is more sensitive to the threshold value, but with its optimal threshold, it was marginally better at predicting vulnerability than the Volume Per Length.

Several different representations of the maximum elevation between the road and the ocean shoreline (dune crest) were tested. Dune Crest Height Above the Road was slightly more skilled than Dune Crest Elevation, which suggests that the road elevation has some influence on the level of vulnerability. Specifically, this result suggests to a minor extent that the elevation of the road may be inversely related to the highway's level of vulnerability. Road Elevation had a very low PR AUC of 0.27, which is only 8% greater than the bottom of the 95% confidence interval for a random indicator. Predictors found to have less skill than a random predictor are called naïve because they are more indicative of the negative class, which further suggests that Road Elevation may be inversely related to road vulnerability. It was found that Smoothed Dune Crest Height Above the Road is a better predictor of vulnerability than Dune Crest Height Above the Road, which is likely because a 3-transect moving average allows for consideration of the state of nearby transects.

Table 4
Vulnerability functions ranked by skill.

Solution #	Island Width	Dune Crest Ht. Above Rd.	Smoothed Dune Crest Ht. Above Rd.	EOP to Ocean Shore	Volume Per Length	Beach Width	Beach Slope	Inverse Beach Slope	Dune Toe Elevation	EOP to Dune Toe	Shore Orientation	Max F1 score	PR AUC
1									49.8	2.1		0.79	0.82
2		4.3							48.9	2.0		0.79	0.82
3		0.7							45.6	2.0	13.0	0.82	0.79
4		10.3								2.3	22.8	0.77	0.78
5		20.7								2.4		0.78	0.78
6										2.7	23.1	0.77	0.78
7		6.0		1.3					47.3			0.75	0.77
8		13.6		1.0					47.3		8.5	0.74	0.76
9		7.5		1.6				2917.0				0.75	0.76
10			32.4	1.1								0.74	0.75
11		19.7		1.5								0.75	0.75

For example, from the first row (Solution # 1) the vulnerability function would be: $F = 49.8*(DuneToeElev.) + 2.1*(EOPtoDuneToe)$.

The vulnerability of the road at a given transect is affected by its cross-shore beach profile, as well as the adjacent transects' profiles. Shore Orientation was the seventh best indicator, with a PR AUC only slightly less than that of Dune Crest Elevation.

Beach slope and inverse beach slope were both tested as indicators, with the presumption that the reciprocal of beach slope would be a skilled indicator and beach slope would be an unskilled, random indicator. This presumption was based on the fact that beach slope is the primary morphological parameter in wave runup and total water level formulations like that of Stockdon et al. (2006). The parameterization of runup shows that for the same given deep water wave height, the runup on a steep beach should be greater than on a flat beach. The greater the runup in an area, the greater the likelihood for dune overwash. The performance evaluations of beach slope and the reciprocal of beach slope contradicted the presumption that steeper beaches should result in greater vulnerability. The results showed the reciprocal of beach slope to be an unskilled, random indicator of highway vulnerability and beach slope to be slightly skilled, with a PR AUC only 0.02 greater than the upper 95% confidence bound of a random indicator. Dune Toe Elevation was also found to be slightly more skilled than a random indicator.

Of the documented impacts, 97.6% were sand overwash. There were only two occurrences of breaches during the seven storms, which made it difficult to fairly assess the island width indicator. Island width was originally devised as an indicator of the island's vulnerability to breaching and, to a lesser extent, sound side flooding (Velasquez-Montoya et al., 2021), so it was not intended to be predictive of other impacts, like overwash. Because of the types of impacts caused by the storms in the dataset, the island width indicator performed poorly and appeared to be an unskilled, random indicator. EOP to Estuary Shore was the most unskilled of all and was found to be a naïve indicator with a PR AUC significantly worse than that of a random indicator.

5.4. Functions of multiple indicators

The goal in exploring vulnerability functions was to determine if any weighted combinations of indicators were more skilled than the best indicator, EOP to Dune Toe. Weighting coefficients for each combination of indicators were determined by maximizing the F1-Score. These coefficients for the top 11 vulnerability functions are shown in Table 4. Shown along each row of Table 4 is a different combination of indicators tested as a function following the form of Eq. (5). Along each row, blank spaces indicate that the corresponding indicators were not included in the development of the function. The functions that utilized unique combinations of multiple indicators resulted in the most favorable outcomes. For instance, the most skilled function, Solution #1 in Table 4, included an elevation variable representing the exposure of dunes to ocean processes like wave runup, Dune Toe Elevation, and a variable representing the distance ocean overwash would have to travel to reach the road, EOP to Dune Toe. The second best function included another elevation-based variable, Dune Crest Height, but the variable had a negligible effect on vulnerability predictions. The third best function featured these three aforementioned variables in addition to Shore Orientation, representing the shore's exposure to direct wave attack.

The results shown in Tables 3 and 4 present the indicators and functions of indicators identified as skilled and unskilled, ranked by PR AUC. This information can inform decisions on which indicators or functions of indicators are used in larger scale (regional or state) evaluations of coastal highway vulnerability in similar geomorphological settings. As other data sets of highway impacts are obtained by other researchers, this methodology could be employed to investigate whether these results hold in other locations or for other storm conditions.

6. Discussion

Binary classification model metrics were employed to assess the skill of 14 indicators in predicting coastal highway vulnerability. There are several simple morphological indicators that can predict highway vulnerability to coastal storm impacts; however, some indicators are significantly better at predicting vulnerability. EOP to Dune Toe, Volume Per Length, and EOP to Ocean Shore were significantly more skilled at predicting vulnerability than the other indicators tested.

Other indicators that were more skilled than a random indicator were Dune Crest Height Above the Road, Moving Averaged Dune Crest Height Above the Road, Beach Slope, Dune Toe Elevation, and Shore Orientation. Island Width, Distance from EOP to Estuary Shore, Beach Width, Inverse Beach Slope, and Road Elevation were found to be unskilled indicators of highway vulnerability to storm impacts. The predominance of overwash impacts in the dataset should be considered when considering the results. Using the present storm datasets, Island Width and Distance from EOP to Estuary Shore appear to be unskilled indicators; but a different framework should be devised to appropriately assess them in future work, since they may be more indicative of island breaching and estuarine-side events than ocean-side events.

EOP to Ocean Shore and Shore Orientation proved to be robust indicators, and they are especially powerful because they are easily computed and can be used to predict vulnerability on a decadal timescale. Shoreline positions with 95% prediction bounds can be projected at a decadal time scale by performing a regression on the time series of shoreline positions (Velasquez-Montoya et al. 2021). Then, the distance from EOP to ocean shoreline indicator can easily be computed at any desired spatial scale and resolution with the predicted ocean shorelines and known highway alignment. Using the same projected shorelines, shoreline orientation could be calculated and used to estimate future vulnerability, as well. These qualities of EOP to Ocean Shore and Shoreline Orientation indicators make regional-scale coastal highway vulnerability assessments feasible. Because Shoreline Orientation's influence on vulnerability is dependent on the wave angle (and therefore the approach angle of the storm), this indicator may be most useful in real-time assessments, or in consideration of a suite of potential storms with varying approach angles. To illustrate the potential, EOP to Ocean Shore was used to perform a present-day vulnerability assessment across the entire coastline of North Carolina, using publicly-available datasets of transects employed by the North Carolina Division of Coastal Management, NC DOT road shapefiles, and shoreline
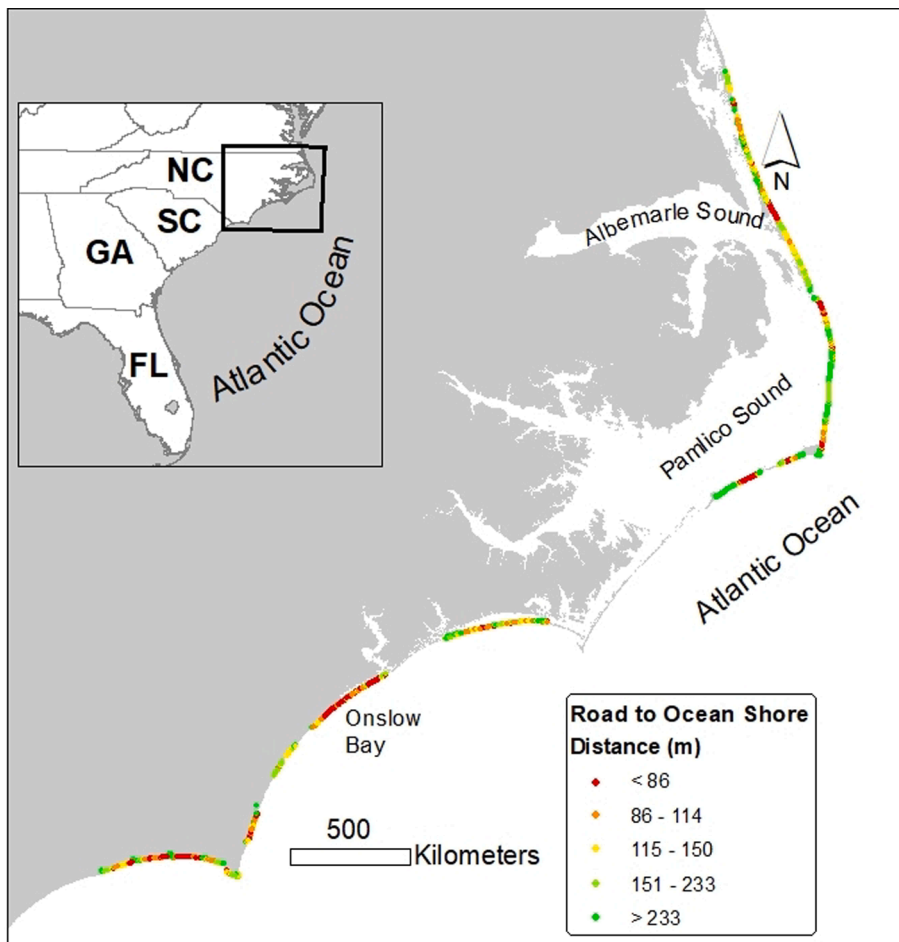
Fig. 9. Statewide vulnerability assessment of North Carolina's most coastal roads based on the EOP to Ocean Shore indicator.

shapefiles publicly available via the North Carolina Department of Environmental Quality. Fig. 9 displays the degree of vulnerability to storm impacts based on the value of the EOP to Ocean Shore at each transect. This assessment was done on the most recent shorelines to illustrate the potential application of the concepts presented here. However, as mentioned previously, with the incorporation of historical shoreline data, the future vulnerability could also be mapped at a decadal time scale.

Road Elevation on its own was found to be an unskilled indicator; however, consideration of Road Elevation as an indicator may have been limited by the fact that there was minimal spatio-temporal variation in the highway's elevation along the study area. Dune Crest Height Above the Road predicted vulnerability slightly better than Dune Crest Elevation alone for the present storm dataset.

The dataset of storm impacts to the road was limited by the availability of post-storm imagery. Storms with post-storm imagery were generally larger and more intense, like hurricanes; however, it is well known that much smaller events can also cause impacts to the most vulnerable portions of NC 12 in the study area, as evident in social media posts by NC DOT as well as closure alerts at the DriveNC.gov website. The optimal threshold and Max F1-Score are dependent on the storms in the dataset. As the overall severity of storms increases, the optimal threshold is likely to increase to classify more transects in the study area as vulnerable. Therefore, the optimal threshold determined from a given set of storms might not be the threshold that is best for a particular application. For example, if the goal is to capture impacts that are severe enough to make the road impassible, the threshold may be tuned to the minimum severity of storms that results in road closures. Future work can employ numerical modeling to create a more robust dataset of storms and corresponding roadway impacts, or could explore methods to accurately project more dynamic and stochastic indicators, such as Dune Crest Height and Dune Toe Elevation, to predict future vulnerability.

In addition, in this study, frequency of impacts is used as a proxy for roadway vulnerability. This was primarily because severe (pavement damage, breaching) impacts occurred infrequently in our dataset. Future work could investigate weighting impacts by severity to determine whether more severe impacts are linked to particular morphological indicators.

The optimization results supported the hypothesis that a function of multiple, continuous indicator variables would be more skilled than any single indicator. The appropriate weights needed to scale indicator variables were found by applying mixed integer linear programming to a dataset of observed highway impacts and pre-storm indicator values. Research has pointed out the difficulties and inconsistencies in applying existing multivariable coastal vulnerability indices (i.e., Koroglu et al., 2019), so this optimization
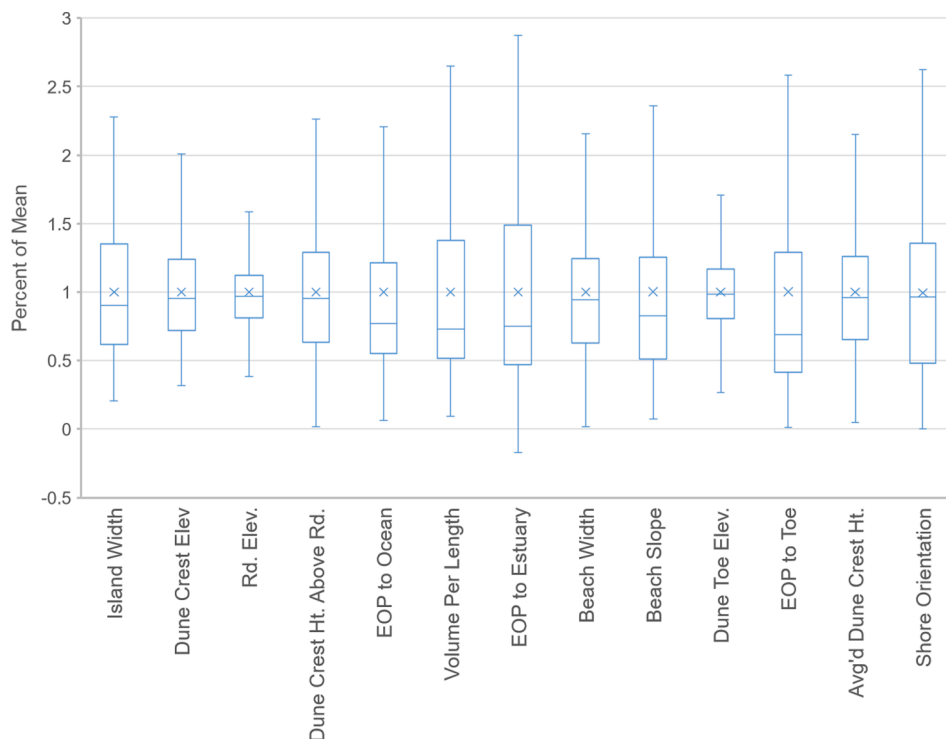
Fig. 10. Box-and-whisker plot of each indicator's values normalized by their average, which summarizes the spread of values around each indicator's mean. The top and bottom whiskers correspond to the maxima and minima. The tops and bottoms of the boxes correspond to the upper and lower quartiles of the data. The × represents the mean, 1 in all cases because the data have been normalized by the mean. The line within each box represents the median.

technique may be a valuable tool for objectively identifying variable weights. Additionally, usage of a weighted linear function, rather than an index, allows the individual variables to remain continuous, eliminating issues surrounding discretizing variables into suitable classes. A weighted linear function of Dune Toe Elevation and EOP to Dune Toe was found to be 6.5% more skilled than the best individual indicator (EOP to Dune Toe), based on PR AUC. There are six other functions [in Table 4] found to be slightly more skilled than EOP to Dune Toe, as well.

The underlying uncertainties and variabilities in indicators may have affected the results of this study. An indicator's distribution of values is a characteristic of the study area, the location's morphology, the size of the area, the resolution and precision of geospatial data used, and the precision associated with the method to compute the indicator. Narrowly distributed indicators do not allow for adequate differentiation between transects with at the low end of an indicator's spectrum versus the high end, which can make vulnerability predictions less distinct. Road Elevation was found to be an unskilled indicator; however, consideration of Road Elevation as an indicator may have been limited by the fact that there was minimal spatial or temporal variation in the highway's elevation along the study area. The limited spread of Road Elevation values can be seen in Fig. 10, which compares the box-and-whisker plots of 56 mean-normalized values for each indicator. The data for each indicator has been divided by its mean to allow for comparison of all the indicators. Road Elevation values are the least widely distributed of all the indicators, with the values ranging between 38 and 156% of the indicator's mean. The evaluated performance of other indicators was not restricted by statistical distributions. The next most narrowly distributed indicator was Dune Toe Elevation, but this indicator was found to be significantly skilled.

7. Conclusions

From a dataset of observed storm impacts that occurred to a barrier island highway over seven storms, it was found that EOP to Dune Toe, Volume per Length, EOP to Ocean Shore Distance, and Dune Crest Height Above the Road (in order of decreasing skill) were the best predictors of highway vulnerability to storm impacts. Additionally, it was found that incorporating multiple geomorphological parameters into a weighted linear function–such as of EOP to Dune Toe and Dune Toe Elevation–improved predictions of vulnerability. This study provides empirical evidence supporting that these simple, geomorphological variables are good indicators of coastal highway vulnerability, as they can predict a significant amount of the spatial variability of storm impacts. Thus, resilience planners can be confident that coastal infrastructure vulnerability studies employing these indicators can effectively identify the most at-risk areas. Future work could focus on expanding storm impact data sets, evaluating the most appropriate threshold values for particular storm impacts (by severity), and reducing the uncertainty of both storm impact data and computation of indicator values as topographic data sets become more frequently available.

Glossary

Hindcast – numerically modeled simulation of a past storm event.

Shoal – transformation where waves' heights increase as they move into shallower water.

Significant wave height – the average wave height of the tallest 1/3rd of waves.

Declaration of Competing Interest

The authors declare that they have no known competing financial interests or personal relationships that could have appeared to influence the work reported in this paper.

Data availability

Data will be made available on request.

Disclaimer

The contents of this manuscript reflect the views of the authors and not necessarily the views of the University. The authors are responsible for the facts and the accuracy of the data presented herein. The contents do not necessarily reflect the official views or policies of either the North Carolina Department of Transportation or the Federal Highway Administration at the time of publication. This report does not constitute a standard, specification, or regulation.

References

Beuzen, T., Harley, M.D., Splinter, K.D., Turner, I.L., 2019. Controls of Variability in Berm and Dune Storm Erosion. J. Geophys. Res. Earth Surf. 124, 2647–2665. https://doi.org/10.1029/2019JF005184.

Claudino-Sales, V., Wang, P., Horwitz, M.H., 2008. Factors controlling the survival of coastal dunes during multiple hurricane impacts in 2004 and 2005: Santa Rosa barrier island, Florida. Geomorphology 95 (3-4), 295–315. https://doi.org/10.1016/j.geomorph.2007.06.004.

Davis, J., Goadrich, M., 2006. The Relationship Between Precision-Recall and ROC Curves, in: Proceedings of the 23rd International Conference on Machine Learning. Pittsburgh, PA.

Dolan, R., Hayden, B.P., May, P., May, S., 1980. The reliability of shoreline change measurements froms aerial photographs. Shore and Beach 48, 22–29.

Donnelly, C., Larson, M., Hanson, H., 2009. A numerical model of coastal overwash. Proc. Inst. Civ. Eng. Marit. Eng. 162 (3), 105–114. https://doi.org/10.1680/maen.2009.162.3.105.

Doran, K.S., Long, J.W., Overbeck, J.R., 2015. A method for determining average beach slope and beach slope variability for U.S. sandy coastlines. Reston, VA, USA. https://doi.org/10.3133/ofr20151053.

Enríquez, A.R., Marcos, M., Falqués, A., Roelvink, D., 2019. Assessing beach and dune erosion and vulnerability under sea level rise: A Case study in the Mediterranean Sea. Front. Mar. Sci. 6, 1–12. https://doi.org/10.3389/fmars.2019.00004.

EASAC (European Academies Science Advisory Council), 2013. Trends in extreme weather events in Europe: implications for national and European Union adaptation strategies EASAC.

Federal Highway Administration (FHWA), 2012. Climate Change and Extreme Weather Vulnerability Assessment Framework.

Figlus, J., Kobayashi, N., Gralher, C., Iranzo, V., 2011. Wave overtopping and overwash of dunes. J. Waterw. Port. Coast. Ocean Eng. 137 (1), 26–33. https://doi.org/10.1061/(ASCE)WW.1943-5460.0000060.

Francis, O., Brandes, H., Zhang, G., Ma, D., Yang, L., Doygun, O., Togia, H., Rossi, C., Costanzo, G., 2019. Statewide Coastal Highway Program Report. Prepared for the State of Hawaii Department of Transportation, Project Number HWY-06-16.

Genetic Algorithm [WWW Document], n.d. . MATLAB & Simulink. URL https://www.mathworks.com/discovery/genetic-algorithm.html.

Gornitz, V.M., Daniels, R.C., White, T.W., Birdwell, K.R., 1994. The Development of a Coastal Risk Assessment Database: Vulnerability to Sea-Level Rise in the U.S. Southeast. J. Coast. Res. 327–338.

Hallermeier, R.J., Rhodes, P.E., 1988. Generic treatment of dune erosion for 100-year event. Coast. Eng. 1197–1211 https://doi.org/10.9753/icce.v21.89.

Halls, J., Randall, A., 2018. Nesting patterns of loggerhead sea turtles (Caretta caretta): Development of a multiple regression model tested in North Carolina, USA. ISPRS Int. J. Geo-Information 7 (9), 348. https://doi.org/10.3390/ijgi7090348.

Houser, C., 2009. Geomorphological controls on road damage during hurricanes Ivan and Dennis. J. Coast. Res. 25, 558–568. https://doi.org/10.2112/07-0923.1.

Integer Programming [WWW Document], n.d. . MATLAB & Simulink. URL https://www.mathworks.com/discovery/integer-programming.html.

Judge, E.K., Overton, M.F., Fisher, J.S., 2003. Vulnerability indicators for coastal dunes. J. Waterw. Port. Coast. Ocean Eng. 129 (6), 270–278. https://doi.org/10.1061/(ASCE)0733-950X(2003)129:6(270).

Kafalenos, R., Leonard, K., Beagan, D., Burkett, V., Keim, B., Meyers, A., Hunt, D., Hyman, R., 2008. What are the Implications of Climate Change and Variability for Gulf Coast Transportation?, Impacts of Climate Change and Variability on Transportation Systems and Infrastructure: Gulf Coast Study. Phase I, Washington, DC, USA.

Koroglu, A., Ranasinghe, R., Jiménez, J.A., Dastgheib, A., 2019. Comparison of Coastal Vulnerability Index applications for Barcelona Province. Ocean Coast. Manag. 178, 104799. https://doi.org/10.1016/j.ocecoaman.2019.05.001.

Kriebel, D., Dalrymple, R., Pratt, A., Sakovich, V., 1996. Shoreline risk index for northeasters, in: Proceedings of the 1996 Conference on Natural Disaster Reduction. Washington, DC, USA, pp. 251–252.

Levine, J.F., Apperson, C.S., Levin, M., Kelly, T.R., Kakumanu, M.L., Ponnusamy, L., Sutton, H., Salger, S.A., Caldwell, J.M., Szempruch, A.J., 2017. Stable Transmission of Borrelia burgdorferi Sensu Stricto on the Outer Banks of North Carolina. Zoonoses Public Health 64 (5), 337–354. https://doi.org/10.1111/zph.12302.

Li, H., Lin, L., Burks-Copes, K.A., 2013. Modeling of coastal inundation, storm surge, and relative sea-level rise at Naval Station Norfolk, Norfolk, Virginia, U.S.A. J. Coast. Res. 29, 18–30. https://doi.org/10.2112/JCOASTRES-D-12-00056.1.

Mimura, N., 2013. Sea-level rise caused by climate change and its implications for society. Proc. Japan Acad Ser. B Phys. Biol. Sci. 89 (7), 281–301. https://doi.org/ 10.2183/pjab.89.281.

NC Coastal Area Management Act. § 113A-115.1. Limitations on erosion control structures. https://dEq.nc.gov/about/divisions/coastal-management/coastal-management-rules/cama.

NC Coastal Resources Commission Science Panel, 2015. NC Sea Level Rise Assessment Report.

NCDCM (North Carolina Division of Coastal Management), 2016. Beach Nourishment - A Report to the North Carolina General Assembly Joint Legislative Oversight Committee on Agriculture, Natural and Economic Resources.

NCDOT (North Carolina Dept. of Transportation), 2008. Final Environmental Impact Statement and Section 4(f) Evaluation. Dare County, NC.

Neumann, B., Vafeidis, A.T., Zimmermann, J., Nicholls, R.J., Kumar, L., 2015. Future Coastal Population Growth and Exposure to Sea-Level Rise and Coastal Flooding - A Global Assessment. PLoS ONE 10 (3), e0118571. https://doi.org/10.1371/journal.pone.0118571.

NOAA, 2018. NDBC About Us [WWW Document]. URL ndbc.noaa.gov/ndbc.shtml.

NOAA, 2020. Emergency Response Imagery [WWW Document]. URL https://storms.ngs.noaa.gov.

Ortiz, A.C., Roy, S., Edmonds, D.A., 2017. Land loss by pond expansion on the Mississippi River Delta Plain. Geophys. Res. Lett. 44 (8), 3635–3642. https://doi.org/ 10.1002/2017GL073079.

Pfaller, J.B., Pajuelo, M., Vander Zanden, H.B., Andrews, K.M., Dodd, M.G., Godfrey, M.H., Griffin, D.B., Ondich, B.L., Pate, S.M., Williams, K.L., Shamblin, B.M., Nairn, C.J., Bolten, A.B., Bjorndal, K.A., Fuentes, M.M.P.B., 2020. Identifying patterns in foraging-area origins in breeding aggregations of migratory species: Loggerhead turtles in the Northwest Atlantic. PLoS ONE 15 (4), e0231325. https://doi.org/10.1371/journal.pone.0231325.

Provost, F., Fawcett, T., Kohavi, R., 1998. The Case Against Accuracy Estimation for Comparing Induction Algorithms. Proc. Fifteenth Int. Conf. Mach. Learn.

Safak, I., Warner, J., List, J., 2016. Barrier island breach evolution: Alongshore transport and bay-ocean pressure gradient interactions. J. Geophys. Res. Ocean. 121, 1–14. https://doi.org/10.1002/2016J.

Sallenger, A.H., 2000. Storm impact scale for barrier islands. J. Coast. Res. 16, 890–895.

Sciaudone, E.J., Velasquez-Montoya, L., Smyre, E.A., Overton, M.F., 2016. Spatial and Temporal Variability in Dune Field: Pea Island, North Carolina. Shore & Beach 84, 49–58.

Small, C., Nicholls, R.J., 2003. A global analysis of human settlement in coastal zones. J. Coast. Res. 19, 584–599.

Stockdon, H.F., Holman, R.A., Howd, P.A., Sallenger, A.H., 2006. Empirical parameterization of setup, swash, and runup. Coast. Eng. 53 (7), 573–588. https://doi. org/10.1016/j.coastaleng.2005.12.005.

Stockdon, H.F., Plant, N.G., Sallenger, A.H., 2009. National assessment of hurricane-induced coastal change vulnerability. Shore & Beach 77, 15–20.

Tracy, B.A., Cialone, A., 2006. Comparison of Gulf of Mexico Wave Information Studies (WIS) 2-G Hindcast with 3-G Hindcasting. Vicksburg, Mississippi, USA.

USACE (US Army Corps of Engineers), 2008. Coastal Engineering Manual, 1110-2-1100, Part II. Washington, DC, USA.

USFWS (United States Fish and Wildlife Service), 2020. About pea island national wildlife refuge [WWW Document]. accessed 10.8.20. https://www.fws.gov/refuge/ Pea_Island/about.html.

USGCRP (United States Global Change Research Program), 2018. Impacts, Risks, and Adaptation in the United States. Washington, DC, USA. https://doi.org/ 10.7930/NCA4.2018.CH21.

Velasquez-Montoya, L., Overton, M.F., 2017. Impacts of seasonal forcings on the hydrodynamics of Oregon Inlet. NC, in: Coastal Dynamics. 1240–1250.

Velasquez-Montoya, L., Sciaudone, E.J., Mitasova, H., Overton, M.F., 2018. Observation and modeling of the evolution of an ephemeral storm-induced inlet: Pea Island Breach, North Carolina, USA. Cont. Shelf Res. 156, 55–69. https://doi.org/10.1016/j.csr.2018.02.002.

Velasquez-Montoya, L., Sciaudone, E.J., Smyre, E., Overton, M.F., 2021. Vulnerability indicators for coastal roadways based on barrier island morphology and shoreline change predictions. Nat. Hazards Rev. 22, 1–16. https://doi.org/10.1061/(ASCE)NH.1527-6996.0000441.

Article

Importance of Pre-Storm Morphological Factors in Determination of Coastal Highway Vulnerability

Jorge E. Pesantez [1] , Adam Behr [2] and Elizabeth Sciaudone [2,*]

1. Department of Civil and Environmental Engineering, University of Illinois Urbana-Champaign, 2521 Hydrosystems Lab, 205 N. Mathews Ave., Urbana, IL 61801, USA
2. Civil, Construction, and Environmental Engineering Dept., North Carolina State University, Raleigh, NC 27695, USA
* Correspondence: ejsciaud@ncsu.edu

Abstract: This work considers a database of pre-storm morphological factors and documented impacts along a coastal roadway. Impacts from seven storms, including sand overwash and pavement damage, were documented via aerial photography. Pre-storm topography was examined to parameterize the pre-storm morphological factors likely to control whether stormwater levels and waves impact the road. Two machine learning techniques, *K*-nearest neighbors (*K*NN) and ensemble of decision trees (EDT), were employed to identify the most critical pre-storm morphological factors in determining the road vulnerability, expressed as a binary variable to impact storms. Pre-processing analysis was conducted with a correlation analysis of the predictors' data set and feature selection subroutine for the *K*NN classifier. The EDTs were built directly from the data set, and feature importance estimates were reported for all storm events. Both classifiers report the distances from roadway edge-of-pavement to the dune toe and ocean as the most important predictors of most storms. For storms approaching from the bayside, the width of the barrier island was the second most important factor. Other factors of importance included elevation of the dune toe, distance from the edge of pavement to the ocean shoreline, shoreline orientation (relative to predominant wave angle), and beach slope. Compared to previously reported optimization techniques, both machine learning methods improved using pre-storm morphological data to classify highway vulnerability based on storm impacts.

Keywords: coastal roadways; vulnerability; morphological indicators; machine learning; management; water resources

1. Introduction

Coastal road infrastructure represents one of the main components of cities located at or near the ocean. This infrastructure suffers inevitable damage due to natural hazards that pose not only life-threatening events to population, but also a burden to the satisfactory operation of infrastructure [1]. In the United States, there is an average general cost of 20.5 billion USD per hurricane each year at places exclusively located close to shorelines [2]. Particularly, the state of North Carolina, which has the second largest shoreline (484 km) of the US Atlantic coast, reported a value of 181 million USD, on average, over the years of 2016 and 2020, due to the presence of inclement weather events, such as hurricanes [3]. In recent years, local authorities have conducted prevention programs, including the regular measurement of the physical characteristics of coastal areas. These data-collecting efforts have guided researchers and transportation agencies to perform prevention-related activities, such as the development of vulnerability indicators for coastal roadways. The analysis of these indicators may provide a better understanding of the drivers of coastal roadway vulnerability and assist transportation departments with preventive actions in response to natural hazards.

Pre-storm coastal morphology, in partnership with storm properties (waves and storm surge), has long been assumed to control impacts on beaches, dunes, barrier islands, and the infrastructure present on those islands. Coastal morphology features, including island width, dune crest elevation, and distance from the road edge to the ocean shoreline, are indicators to assess whether road infrastructure is vulnerable to damage or not [4]. Vulnerability analysis reflects the susceptibility of the infrastructure to reduce its functionality, ranging from debris removal without interruption to temporary road closures [5]. Processes such as storm surges and sea-level rise are the main drivers of the overall damage to coastal infrastructure. Previous research works and agency reports agree that the increment in the number of storms and rising sea levels will likely affect coastal communities at different severity levels [6,7]. Furthermore, as mentioned by [8], there is a need for local coastal road systems to handle dynamic conditions. This work aims to contribute to the literature by developing a classifier model coupling past storm information with current and historical local morphology factors to inform stakeholders of the vulnerability of coastal roadways to hurricanes and tropical storms.

The monitoring of areas close to coastal roadways provides critical information about the past and current conditions of the existing road infrastructure. Especially in barrier islands, where bridges and roadways are likely the first infrastructure systems facing the ocean, monitoring indicators have provided managers valuable insights for beach restoration projects and natural habitat conservation programs [9,10]. Moreover, state agencies use field-measured data coupled with visualization from aerial photographs to monitor the morphological conditions of coastal zones, such as barrier islands, over time, especially after natural hazards events. Therefore, modeling and analyzing these dynamic data sets are the backbone of the current and future action plans to protect coastal infrastructure, such as roadways.

Recently, machine learning techniques have been explored to inform land cover classifications and storm responses [10]. A review of machine learning techniques to classify land cover is provided by [11], with the random forest algorithm having the highest accuracy level for this application. An examination of machine learning in land use and cover change detection and modeling was provided by [12]. These authors stated that machine learning has the strong potential to advance the modeling of land use and cover changes by identifying and incorporating new exploratory variables.

An application of machine learning to storm response and recovery, considering power utility, was detailed by [13]. The authors developed a data-driven predictive model to aid the utility in its emergency planning efforts. Another power utility application was presented in [14], with a focus on quantification of uncertainty in machine-learning-based prediction modeling. Other works have focused on predicting physical and social storm impacts; ref. [15] developed a convolutional-neural-network-based model to rapidly predict storm surge across an extensive coastal region using a storm track. Other studies have examined storm impacts and responses via social media data [16–18].

In parallel to the machine learning work, much work regarding the control of variable storm impacts has focused on damage to protective dunes [19,20]. These studies linked controls on hydrodynamic forcing to erosion of the dune. Recently, ref. [5] developed a data set of seven storms and the corresponding impacts on a coastal highway, along with a robust collection of varying morphological factors that could be used to predict impact. They used deterministic optimization techniques (i.e., mixed integer linear programming) and found that the distance from edge-of-pavement to dune toe, volume above mean high water between edge-of-pavement and ocean shoreline, distance from edge-of-pavement to ocean shoreline, and dune crest height above the road were the most skilled individual predictors of highway vulnerability. A multi-indicator function of dune toe elevation and distance from edge-of-pavement to dune toe was found to be more skilled than any of the individual indicators.

This paper aims to apply two machine learning techniques to the storm impact data set presented in previous studies [5], in order to classify roadway vulnerability and iden-

tify the indicators that best infer storm impacts. We applied two classifiers, *K*-nearest neighbor (*KNN*) and ensemble of decision trees (EDT), to classify whether different longitudinal segments or transects of a coastal roadway are considered vulnerable (class of interest) or not. Our models were applied to a 13-mile (21-km) expanse of state highway North Carolina 12 (NC 12), along Hatteras Island, NC (Figure 1). NC 12 is an essential, 148.0-mile-long (238.2 km) coastal highway that connects Corolla to Cedar Island on the northern side of the Outer Banks in the state of North Carolina, USA [4].
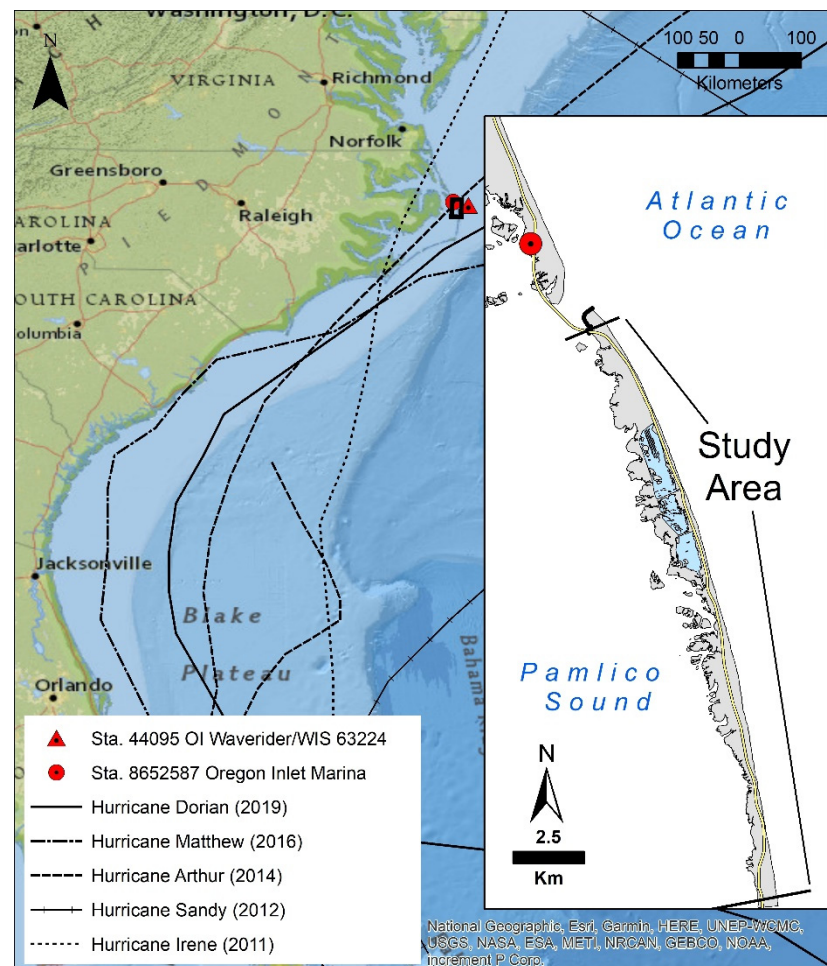

Figure 1. Map of hurricane tracks in the study dataset with year of landfall in parentheses, location of wave and water level data stations, and study area extents.

2. Materials and Methods

2.1. Dataset

This section describes the data set and methods used in the analysis. The data sets comprise seven groups, corresponding to seven storm events registered by the North Carolina Department of Transportation (NCDOT) between 2011 and 2019 [4]. The storms featured in this paper are summarized in Table 1. Of the seven storms in the data set, five were hurricanes, and their tracks, in relation to the study area, are shown in Figure 1. Two of the storms in the data set were winter extra-tropical storms, or "nor'easters", which are not tracked in the same way as hurricanes. Locations of storm impacts to the study area's highway, NC 12, were identified for each of the seven storms. Aerial imagery from the National Oceanic and Atmospheric Administration (NOAA) national geodetic survey and imagery, collected under the NCDOT Coastal Monitoring Program [4], were manually examined at the 1:1250 scale to locate road impacts along NC 12 (Table 1). These data collection efforts were described in detail in [5] and summarized in this section. A section

of roadway was determined to be impacted if more than 50 percent of the roadway was covered with sand or visibly damaged. In general, post-storm imagery was available on the order of days post-storm, which precluded the inclusion of visible flooding as a storm impact, as it had already receded.

Table 1. Summary of storms and their impacts on the study area. Peak wave heights and water levels were obtained from the stations shown in Figure 1.

Storm #	Storm	Date and Duration	Storm Approach	Peak Wave Height (ft)	Max Water Level (ft NAVD88)	Storm Impacts to Study Area
1	Hurricane Irene	August 2011 50 h	Sound-side	21.4	3.0	Island breaches, erosive damage to the road, and overwash on road
2	Hurricane Sandy	October 2012 88 h	Ocean-side	18.8	4.5	Wide-spread overwash on road
3	Hurricane Arthur	July 2014 14 h	Sound-side	18.5	1.3	Erosive damage to pavement, overwash on road
4	Nor'easter	February 2016 55 h	N/A	15.7	3.5	Overwash on road
5	Hurricane Matthew	October 2016 153 h	Ocean-side	17.2	3.3	Overwash on road
6	Nor'easter	March 2018 148 h	N/A	17.5	3.7	Overwash on road
7	Hurricane Dorian	September 2019 47 h	Ocean-side	21.9	4.6	Overwash on road

The indicators used to determine an impacted road transect are numerical values of the geomorphologic characteristics extracted from the coastal features of the area; they are listed in Table 2 and illustrated in the schematic in Figure 2 [5]. Most of the geomorphological measurements provided in Table 2 are straightforward and visible in Figure 2. It is noted that the shoreline was identified as the visible wet-dry line on aerial photographs and is approximately the mean high-water line [21]. In this area, the mean high-water elevation is approximately 1.1 ft (0.34 m) above the North American Vertical Datum of 1988 (NAVD88) [22]. The "angular difference between shore-normal orientation and weighted mean wave direction", however, is a bit complicated to illustrate. The hypothesis was that the shore's orientation can be used as a proxy for exposure to average storm waves. Transects along the study area that are more exposed to direct storm waves are more likely to see significant erosion and overwash, which can affect the highway. To calculate the weighted mean wave direction (similar to the weighted mean wind direction used by [23]), wave data from the Oregon Inlet waverider buoy (NDBC station 8652587, Figure 1), between 2012–2020, were filtered to only include significant wave heights greater than 2 m, and wave direction was weighted by the square of significant wave height to better represent the directional distribution of wave energy. Circle statistics functions were used to ensure that angular directions were preserved. The mean wave direction was assumed to be constant across the relatively small (13-mile, 21-km) study area. The orientation of a line normal to the shore at each transect was computed at each transect along the study area. The angular difference between the wave height weighted mean wave direction and shore-normal orientation was computed on a transect basis. The measurement could vary from 0 to 90 degrees, where 0 degrees would suggest that the shoreline is most exposed to the average storm wave direction, and 90 degrees would be most sheltered from the mean storm wave impact.

Table 2. Geomorphological characteristics and units used as indicators for vulnerability classification.

Geomorphological Characteristic

(1) Island width (ft) from the estuary shoreline to the ocean shoreline (island width)

(2) Dune crest elevation (ft) relative to NAVD 88 (dune crest elevation)

(3) Road elevation (ft) relative to NAVD 88 (road elevation)

(4) Difference in elevation (ft) between the dune crest and the road (dune crest height above road)

(5) Distance from road edge-of-pavement (EOP) to ocean shoreline (ft) (EOP to ocean shore)

(6) Volume above MHW between EOP and ocean shoreline (ft³/ft) (volume per length)

(7) Distance from road EOP to estuarine shoreline (ft) (EOP to estuary shore)

(8) Distance from the dune toe to the ocean shoreline (ft) (beach width)

(9) Beach slope found according to the USGS 2-point method [24] (beach slope)

(10) Dune toe elevation (ft) relative to NAVD 88 (dune toe elevation)

(11) Distance from road EOP to dune toe (ft) (EOP to dune toe)

(12) The angular difference between shore-normal orientation and the weighted mean wave direction (degrees)
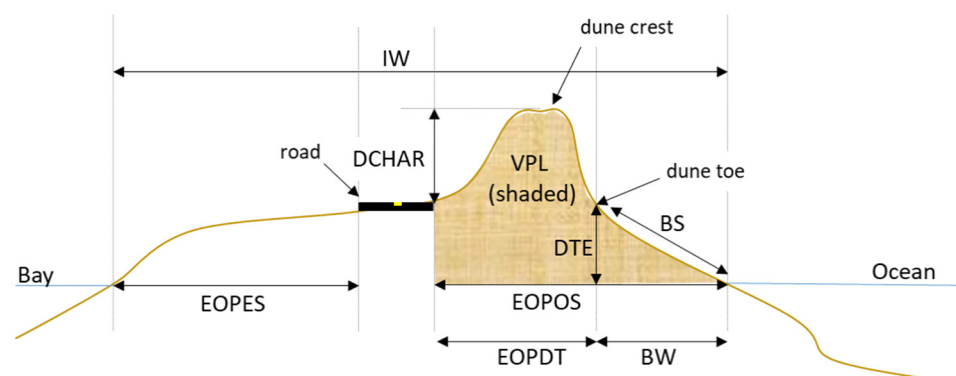
Figure 2. Morphological indicators used in the present study to classify the vulnerability of a coastal road. Island width (IW), edge of pavement to ocean shore (EOPOS), edge of pavement to dune toe (EOPDT), dune crest height above road (DCHAR), edge of pavement to estuary shore (EOPES), volume per length (VPL), dune toe elevation (DTE), beach slope (BS), and beach width (BW). Adapted from [5].

The binary outputs of each data set assign 0 if the road transect was not impacted by a storm and 1 otherwise. These data sets have an imbalance problem, as the class of interest (impacted road transect or 1) happens less frequently than the not impacted road class (0). Therefore, the evaluation of the proposed methodology includes metrics of performance that reduce this implicit bias from the results, as explained below.

2.2. Correlation Analysis

A correlation analysis was performed to identify linear dependence among predictors prior to building one classification model, as explained below. The correlation matrix, where rows represent observations and columns the variables, shows the Pearson correlation coefficient calculated as shown in Equation (1):

$$\rho(A, B) = \frac{1}{N-1} \sum_{i=1}^{N} \left(\frac{A_i - \mu_A}{\sigma_A} \right) \left(\frac{B_i - \mu_B}{\sigma_B} \right) \tag{1}$$

where *A* and *B* are two random variables with *N* observations; μ and σ are the mean and standard deviations of *A* and *B*, respectively.

The preprocessing step filters predictors based on the correlation (ρ) and implements a feature selection subroutine. The Chi-square test reports low *p*-values when the corresponding predictor is dependent on the response variable and considered an important feature. If ρ between two variables is equal to or higher than 0.95 (e.g., considered perfectly correlated), the most important feature reported by the Chi-square test remains in the data set.

2.3. Binary Classifiers

We apply two widely known classifiers methods for binary classification as the *K*-nearest neighbors (*K*NN) [25] and the ensemble of decision trees (EDT) [26]. These two classifiers were selected because *K*NN and EDT have been proven as classifiers that effectively handle imbalanced data sets [27–29]. For the *K*NN classifier, we filter perfectly correlated variables based on their rank correlation and select the most important predictors based on a feature selection subroutine that uses the Chi-square test [30]. This step avoids inflating the distance from correlated predictors. Decision trees do not assume relationships between features, but split data into subsamples that boost their classification performance. To overcome overfitting issues, related to creating a single decision tree, we use the EDT model that improves its performance, albeit decreasing interpretability. Additionally, these classifiers are not considered black boxes with random initial parameters, which makes them feasible to reproduce for similar potential problems.

2.3.1. *K*-Nearest Neighbor (*K*NN)

*K*NN is a simple supervised-learning classifier that assigns a new variable to the class with the most values from the closest *k* neighbors located on a search space, determined by the number of predictors [25]. The two inputs required to train and predict a *K*NN model are the number of neighbors (*k*) and type of distance used to determine the closest neighbors in a *j*th dimension, where *j* corresponds to the number of predictors (Figure 3). In this work, we performed an optimization subroutine to find the best hyperparameters of the *K*NN model for each storm. A Bayesian optimization algorithm [31] was applied to improve the performance of the *K*NN classifier model for each storm. The Bayesian optimization subroutine decision variables include the number of neighbors, distance metric, distance weight, and whether the data are standardized. Table 3 shows the search range used for the hyperparameter optimization of the *K*NN model [32].
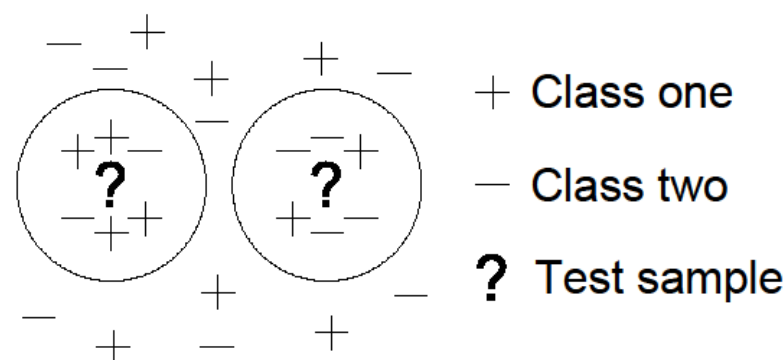

Figure 3. *K*NN for binary classification scheme with *k* = 6. Adapted from [25].

Table 3. *K*NN optimizable hyperparameters and search range.

Hyperparameter	Search Range
Number of neighbors	max(1, *Num Observations*/2)
Distance metric	City block, Chebychev, Correlation, Cosine, Euclidean, Hamming, Jaccard, Mahalanobis, Minkowski (cubic), Spearman
Distance weight	Equal Inverse Squared inverse
Standardize data	True False

*K*NN takes, as response, a binary variable called impact, where 1 represents the road is vulnerable to storms impacts and 0, otherwise. The model includes the most important features retrieved from the correlation analysis and feature selection subroutine as predictors. These features, as shown in Table 2, include (1) island width (ft), (2) dune crest elevation (ft), (3) road elevation (ft), (4) dune crest height above road (ft), (5) EOP to ocean shore (ft), (6) volume per length (ft^3/ft), (7) EOP to estuary shore (ft), (8) beach width (ft), (9) beach slope, (10) dune toe elevation (ft), (11) EOP to dune toe (ft), and (12) shore orientation (degrees).

2.3.2. Ensemble of Decision Trees (EDT)

Decision trees are part of machine learning methods widely applied in the water quality, risk assessment, and forecasting domains to classify the risk of events, including pipe failure and water quality problems [27–29,33]. Decision trees graphically represent a classification or regression problem. The components of a single decision tree include a root node, internal nodes, and terminal nodes (see Figure 4). For classification models, a decision tree starts by assigning a class label to each leaf node. The non-terminal nodes, which include the root and other internal nodes, contain feature test conditions to separate records that have distinct characteristics. The root node has no incoming edges and can have multiple outgoing edges. Each internal node has exactly one incoming edge and two or more outgoing edges, and each leaf node has exactly one incoming edge and no outgoing edges [27,28,33,34]. In terms of bias and variability, a decision tree has low bias and high variance; therefore, averaging the result of many decision trees reduces the variance, while maintaining low bias. The application of ensembles enhances the performance of a single tree. Ensemble of decision trees (EDTs) group individual trees as one model to predict or fit numerical and categorical data (Figure 4). EDTs are built by comparing the "out-of-bag" (OOB) error value from all the individual decision trees and a voting combination of their results. EDTs have proved to be more robust when dealing with bias and variance, thus leading to generally a better prediction performance. However, EDTs are complex models to analyze, compared to individual decision trees [35].
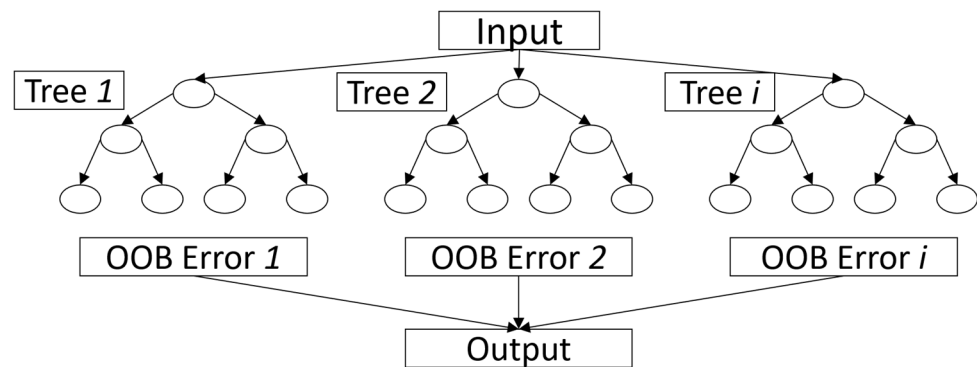
Figure 4. An Ensemble of decision trees for classification.

EDTs start by identifying the root node. We used the well-known Gini index (G_{idx}) (Equation (2)) of a node as the split criterion to identify the root node of each tree in the ensemble. The G_{idx} with the lowest value is selected as the root node, and each tree grows until no more features remain for splitting [36]. EDTs are built using mainly two types of methods: bootstrap aggregation (bagging) and boosting. Bagging creates data set replicas using bootstrapping to incorporate single decision trees. A random selection of the observations with replacement is applied to create the bootstrap replicas. The most common application of bagging is the random forest method [36], where every tree of the ensemble randomly selects predictor variables for each split along the decision tree. Boosting methods, on the other hand, build the ensemble sequentially by using the output of the previous decision tree as input for the next one. The adaptive logistic regression (LogiBoost) algorithm, which is a variation of the adaptive boosting methods, can improve model performance when dealing with binary classification problems [37]. LogiBoost is a type of the widely applied adaptive boosting algorithm, where the objective function is to minimize the binomial deviance rather than the exponential loss, as shown in Equation (3):

$$G_{idx} = 1 - \sum_i pr(i)^2 \tag{2}$$

where *pr* is the probability of an observation *i* classified into a particular class.

$$\sum_{n=1}^{N} w_n log(1 + exp(-2y_n f(x_n))), \tag{3}$$

where:

$y_n \in \{-1, +1\}$ is the true class label;
w_n are normalized weights;
$f(x_n) \in (-\infty, +\infty)$ is the predicted classification score calculated, as shown in Equation (4):

$$f(x) = \sum_{t=1}^{T} a_t h_t(x), \tag{4}$$

where:

$a_t = \frac{1}{2} log \frac{1-\varepsilon_t}{\varepsilon_t}$ are weights of the weak hypotheses (*h*) in the ensemble that are used to determine weighted error (ε), as shown in Equation (5):

$$\varepsilon_t = \sum_{n=1}^{N} d_n^{(t)} \blacksquare (y_n \neq h_t(x)), \tag{5}$$

where:

x_n is a vector of predictor values for observation *n*;
y_n is the true class label;

h_t is the prediction of learner with index *t*;

■ is the indicator function;

$d_n^{(t)}$ is the weight of observation *n* at time step *t*.

In this study, we implemented a binary classification based on the analysis of the impacted roads with data collected from a set of storms that struck the North Carolina coast between 2011 and 2018.

2.3.3. EDT Settings

The number of trees or learners, their depth, and the overall learning rate are needed to set up an EDT model. Accuracy improves with the number of trees but also increases EDT's complexity and computation time. Based on previous applications in water-related problems [27–29,33] and a series of preliminary analyses to determine the number of trees, a range between 10 and 100 trees was evaluated. A suitable option was found at 27 trees for the ensemble, as the performance did not improve with more trees. The maximum number of splits determines how deep a tree can be expanded. We analyzed a range between 10 and 100 observations, where 34 splits per tree produced the best results. Similarly, the learning rate that defined the step size of the error minimization was analyzed between 0.01 and 1.0, and a value of 0.65 was defined as suitable for the application of this model.

2.3.4. Model Training and Testing

The data sets for each storm were randomly partitioned into training (70%), validation (10%), and testing (20%) sets. Based on previous applications [33], each model was trained ten times to account for the stochasticity of the sampling method, and the average metrics of performance associated with each storm are reported as the results of the analysis. For the application of each classifier method, we optimize its hyperparameters, using the validation subset of each storm. Additionally, we compare the performance of these two classifiers using metrics that include the F1 score and precision-recall area under the curve (PR AUC) values, which are suitable for dealing with imbalanced data sets [38]. Finally, feature selection is presented to give a comprehensive analysis of the predictors with different effects on the model performance.

2.4. Metrics of Performance

The performance of classification models uses a set of commonly known metrics that are calculated using the confusion matrix, which shows the performance of a model in predicting samples within four classes (Table 4). True positives (*TP*) and true negatives (*TN*) denote the number of positive and negative events that are correctly identified, respectively. In this research, positive events correspond to events with a value of 1, which means that the predicted and observed outputs are vulnerable, and negative events correspond to events with a value of 0, which means that predicted and observed outputs are not vulnerable. False positives (*FP*) denote the number of not vulnerable events incorrectly identified as vulnerable, and false negatives (*FN*) indicate the number of vulnerable events incorrectly identified as not vulnerable. Performance metrics, including accuracy (Equation (6)), precision (Equation (7)), recall (Equation (8)), and the F-1 score (Equation (9)), were calculated using the confusion matrix, as follows.

Table 4. Confusion matrix of vulnerability. Adapted from [5].

	Classified Vulnerable	**Classified Not Vulnerable**
Observed vulnerable	True positives	False negatives
Observed not vulnerable	False positives	True negatives

$$Accuracy = \frac{TP + TN}{TP + TN + FP + FN} \tag{6}$$

$$Precision = \frac{TP}{TP + FP} \tag{7}$$

$$Recall = \frac{TP}{TP + FN} \tag{8}$$

$$F - 1\ Score = \frac{2 * Precision * Recall}{Precision + Recall} \tag{9}$$

3. Results

3.1. Correlation Analysis and Feature Selection

This section reports on the correlation analysis and feature selection subroutine applied prior to the *KNN* implementation. Then, the performance metrics of the two machine learning methods used for the binary classification problem are discussed. The correlation analysis (Equation (1)) of the predictors shows that, for all storm events, Pearson's correlation coefficient indicates perfect correlation among several variables. As expected, "(1) Island Width" is perfectly correlated to "(7) EOP to Estuary Shore"; "(2) Dune Crest Elevation" correlated to "(4) Dune Crest Height above Road"; and "(5) EOP correlated to Ocean Shore" to "(11) EOP to Dune Toe" (Figure 5).
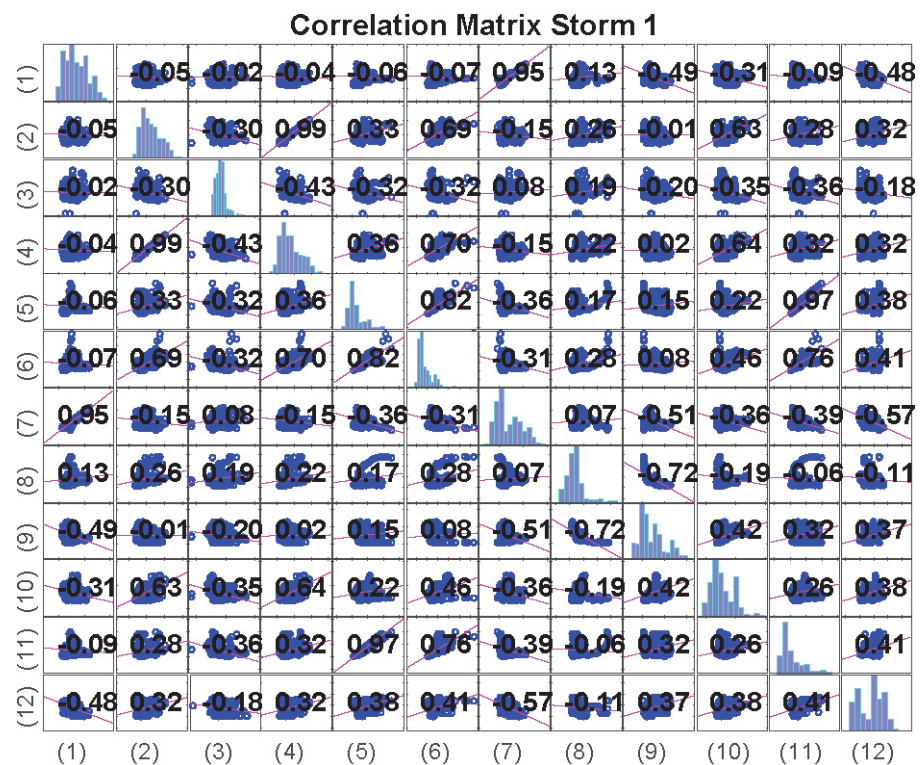

Figure 5. Correlation matrix for storm 1. Numbers in parentheses refer to morphological indicators described in Table 2. The rest of the correlation matrices are presented in the Supplemental Information.

Feature selection is used to determine which perfectly correlated variable remains in the predictors' data set. Using the Chi-square test, the method reports that "Island Width" is a slightly better estimate than "EOP to Estuary Shore" for storm events 1 to 5 (Figure 6a–e), and the opposite occurs for storms 6 and 7 (Figure 6f–g). Similarly, "Dune Crest Height above Road" is more important than "Dune Crest Elevation" for all storms, except for storm 5. Finally, "EOP to dune toe" is a better predictor than "EOP to Ocean" for all storms, except for storm 4 (Figure 6).
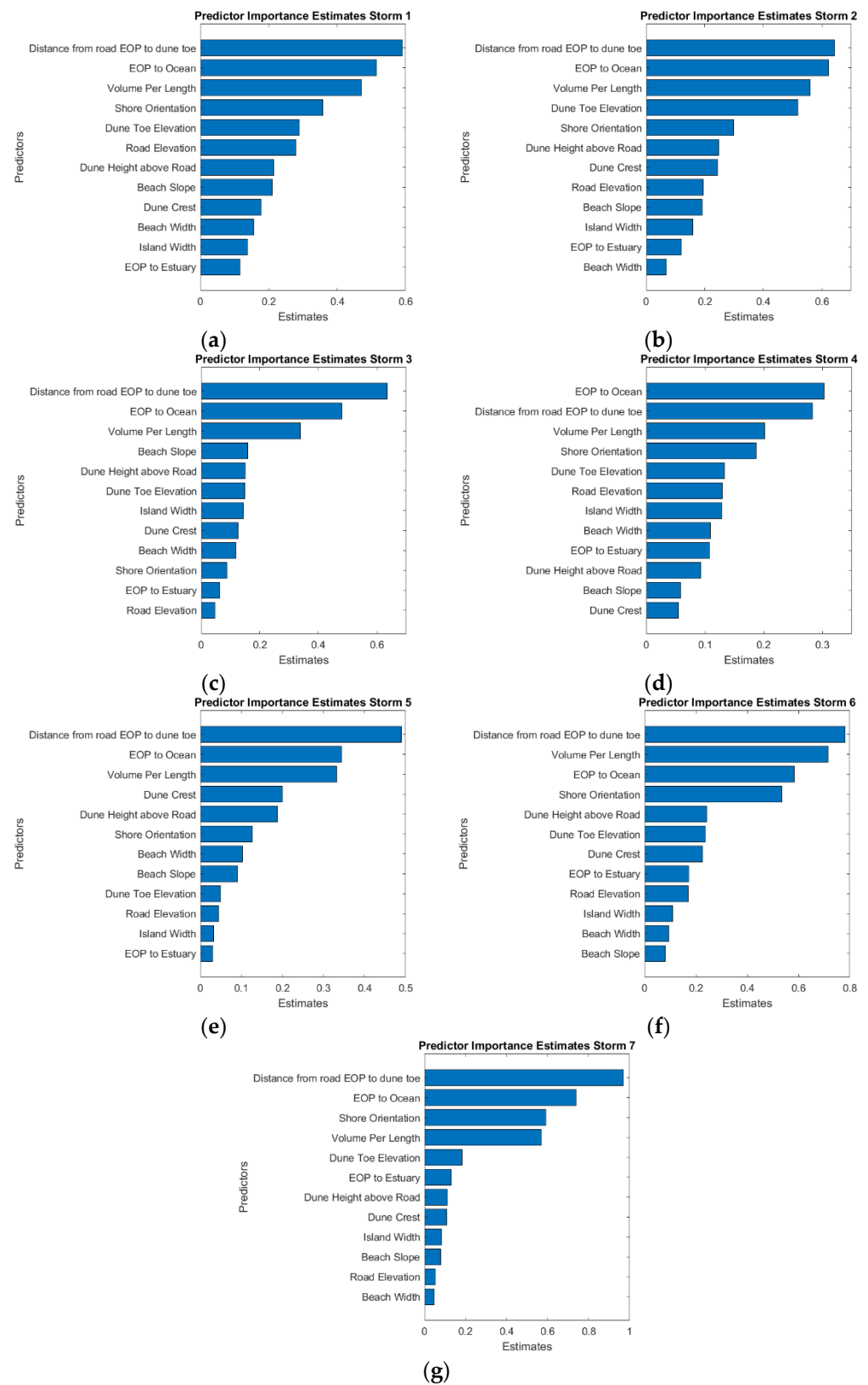
Figure 6. Feature selection analysis reported by the chi-square test for the seven storm events. "Distance from road EOP to dune toe" is the most important predictor for all storms (**a**–**c**,**e**–**g**), except storm 4 (**d**).

3.2. KNN and EDT Performances

The classifier performances (Figure 7) show that the F-1 score reported by the *KNN* classifier looks similar to the EDT classifier's F-1 score across the seven storm events. However, the *KNN* F-1 score had a slightly higher value than EDT in all storms, except storm number 4. We performed a *t*-test to examine the statistical relevance of the difference between the reported F-1 scores. The following hypothesis was evaluated:

H_0 = The pairwise difference between F-1 scores from KNN and EDT has a mean equal to zero at the 5% significance level. $\mu_{F-1\ KNN} - \mu_{F-1\ EDT} = 0$

H_A = The pairwise difference between F-1 scores from KNN and EDT has a mean not equal to zero at the 5% significance level. $\mu_{F-1\ KNN} - \mu_{F-1\ EDT} \neq 0$
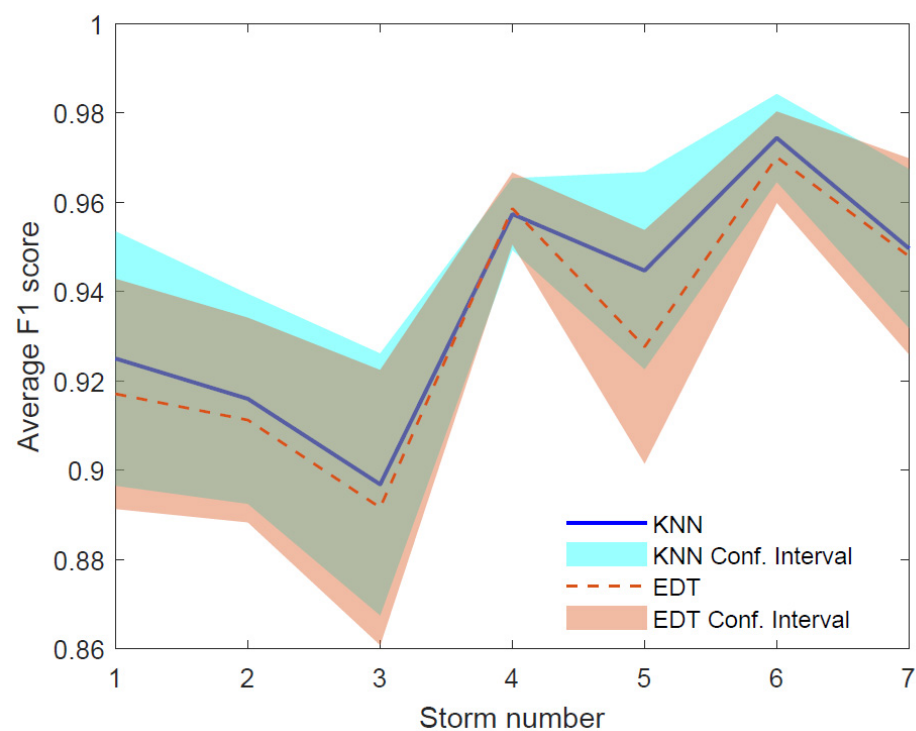

Figure 7. Average F-1 scores reported by the KNN and EDT classifiers, with their respective confidence intervals calculated by adding and subtracting one standard deviation for high and low boundaries, respectively.

The two-tailed *t*-rest resulted in a *p*-value of 0.04, indicating that the test rejects the null hypothesis (H_0) of having identical mean values, in favor of the alternate hypothesis (H_A) that the mean *KNN* F-1 score is significantly different than that of the EDT F-1 score at the 5% significance level.

The *KNN* and EDTs models' performance, in terms of the F-1 score, shows that the models correctly classified a coastal road as vulnerable, based on the morphological indicators, at least 90% of the time. In the remaining 10%, the methods cannot classify an observation into the correct class. These high F-1 score values demonstrate the robustness of the classifiers to handle an imbalanced data set, where the class of interest (i.e., the road is vulnerable) is less frequent than the majority class (i.e., the road is not vulnerable to impact).

In terms of the area under the curve (AUC) reported by the classifiers, the EDT outperformed *KNN* classifier across the seven storms events (Figure 8). Both classifiers reported their maximum value during the storm event number 6, where *KNN* AUC represented 97% of EDT AUC. This difference increased for the lowest performance of both

classifiers that occurs during storm event number 4, where *KNN* AUC only represented 86% of EDT AUC. Similar to the F-1 score analysis, the following hypothesis of the AUC values was evaluated:

H_0 = The pairwise difference between AUC values from KNN and EDT has a mean equal to zero at the 5% significance level. $\mu_{AUC\ KNN} - \mu_{AUC\ EDT} = 0$

H_A = The pairwise difference between AUC values from KNN and EDT has a mean not equal to zero at the 5% significance level. $\mu_{AUC\ KNN} - \mu_{AUC\ EDT} \neq 0$
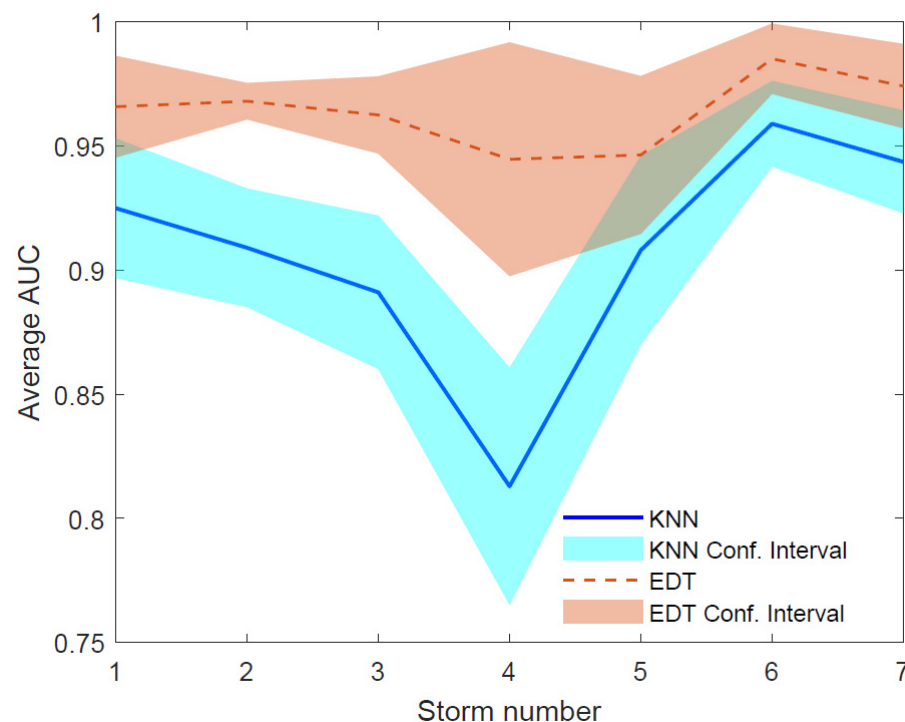

Figure 8. Average AUC values reported by the KNN and EDT classifiers, with their respective confidence intervals calculated by adding and subtracting one standard deviation for high and low boundaries, respectively.

The two-tailed *t*-test resulted in a *p*-value of 0.0063, indicating that the test rejects the null hypothesis (H_0) of having identical mean values, in favor of the alternate hypothesis (H_A) that the mean *KNN* AUC value is significantly different than that of the EDT AUC value at the 5% significance level.

For further interpretation of the performance metrics' values, each storm's receiver operating characteristic (ROC) curve is presented (Figure 9). The predictability of the classifiers reports a recall or sensitivity higher than 90% at a very low FPR. Furthermore, the EDT model reports high F-1 scores and AUC values for all storms and samples selected, as explained in the "Model Training and Testing" subsection (Figure 10).
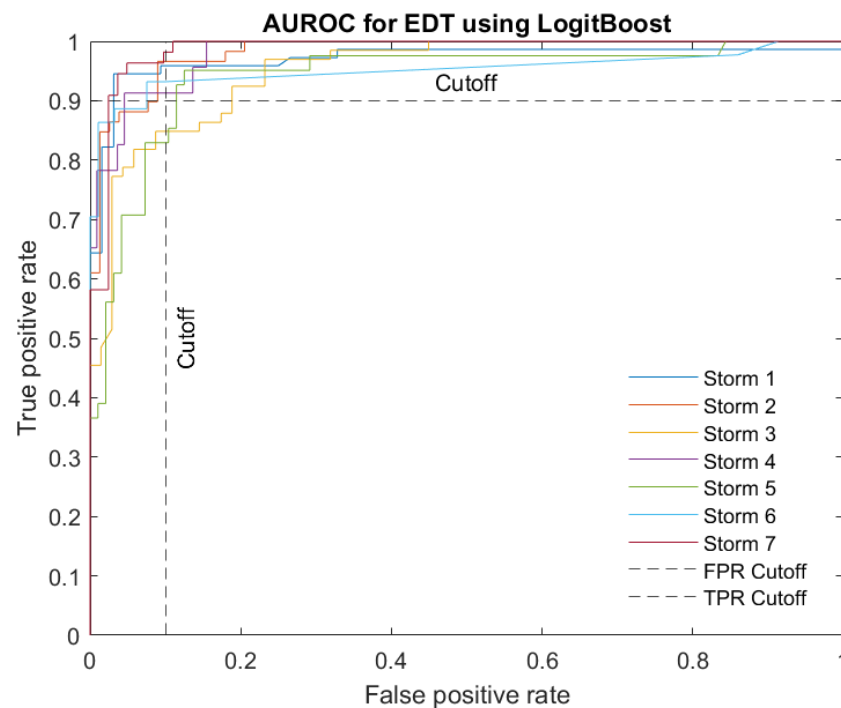
Figure 9. Area under the receiver operating characteristics (AUROC) for each storm event. Cutoff points showed that, with 10% of false positive rate (FPR), storm events 1, 2, 4, 6, and 7 reported true positive rates (TPR) higher than 90% of the time.
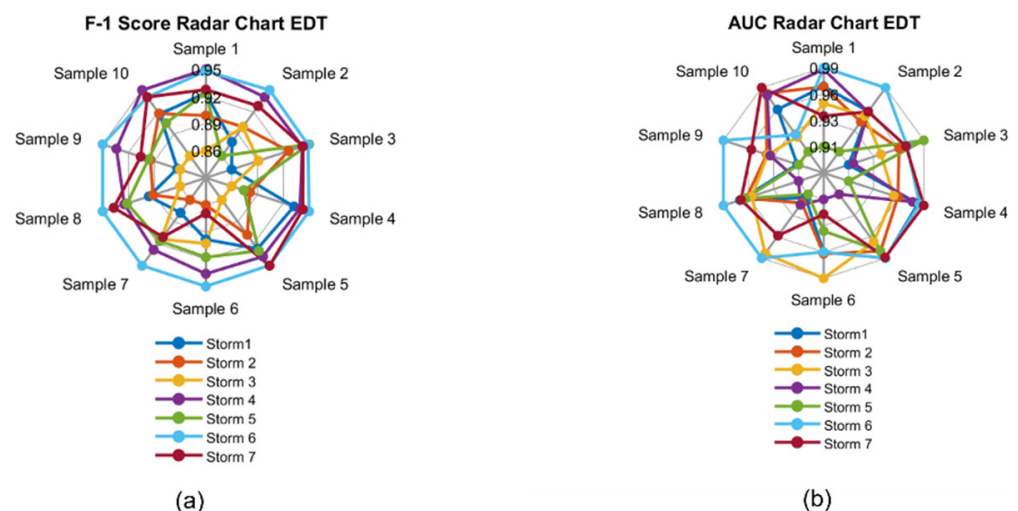

Figure 10. (**a**) F-1 score and (**b**) AUC values reported by the EDT model for each storm event and random sample.

A comparison with a recent related application to the analysis of vulnerability assessment [5] was conducted to highlight the performance of the proposed two classifiers (Table 5). *KNN* and EDT classifiers show an improvement in the classification of highway vulnerability, with respect to the previous application across all the storm events. For the F-1 score, *KNN* that reported the best performance, when compared to EDT, had an average F-1 score of 0.94, with a minimum of 0.90, corresponding to storm event 3. The average F-1 score reported by [5] was 0.82, with a minimum of 0.57, corresponding to storm event 4. Similarly, the proposed classifiers showed an improvement in the AUC values (Table 6). For the AUC value, EDT that reported the best performance, when compared to EDT, had an average AUC value of 0.96, with a minimum of 0.94, corresponding to storm event 4. The average AUC value reported by [5] was 0.83, with a minimum value of 0.53,

corresponding to storm event 4. The classifying capabilities of both the *K*NN and EDT methods outperformed the previous implementation [5] by an average of 10% across the storm events.

Table 5. Comparison of the F-1 score values of classifying highway vulnerability.

Storm	Parameter	[5]	*K*NN	EDT
1		0.85	0.93	0.92
2		0.88	0.92	0.91
3		0.83	0.90	0.89
4	F-1 Score	0.57	0.96	0.96
5		0.76	0.94	0.93
6		0.89	0.97	0.97
7		0.93	0.95	0.95

Table 6. Comparison of the AUC values of classifying highway vulnerability.

Storm	Parameter	[5]	*K*NN	EDT
1		0.91	0.92	0.97
2		0.85	0.91	0.97
3		0.89	0.89	0.96
4	AUC values	0.53	0.81	0.94
5		0.74	0.91	0.95
6		0.94	0.96	0.99
7		0.94	0.94	0.97

3.3. EDT Feature Importance Analysis

Different attributes contribute to the model with different magnitudes. For the EDT classifier, a feature importance analysis was conducted to determine how attributes affected the model performance for each of the seven storm events (Figure 11). The most important predictor across all the events is the "(11) Distance from road EOP to dune toe (ft)" (see Table 2). The second-best predictor depends on the evaluated storm. While "(5) Distance from road edge-of-pavement (EOP) to ocean shoreline (ft)" ranks second in storms 2 and 7, and the "(10) Dune toe elevation (ft) relative to NAVD 88" ranks second in storms 1 and 5. The rest of predictors that are part of the top three vary across the storm events and include "The angular difference between shore-normal orientation and the weighted mean wave direction (degrees)", "(6) Volume above MHW between EOP and ocean shoreline (ft^3/ft)", "(1) Island Width (ft)", "(8) Beach Width (ft)", and " (9) Beach Slope".
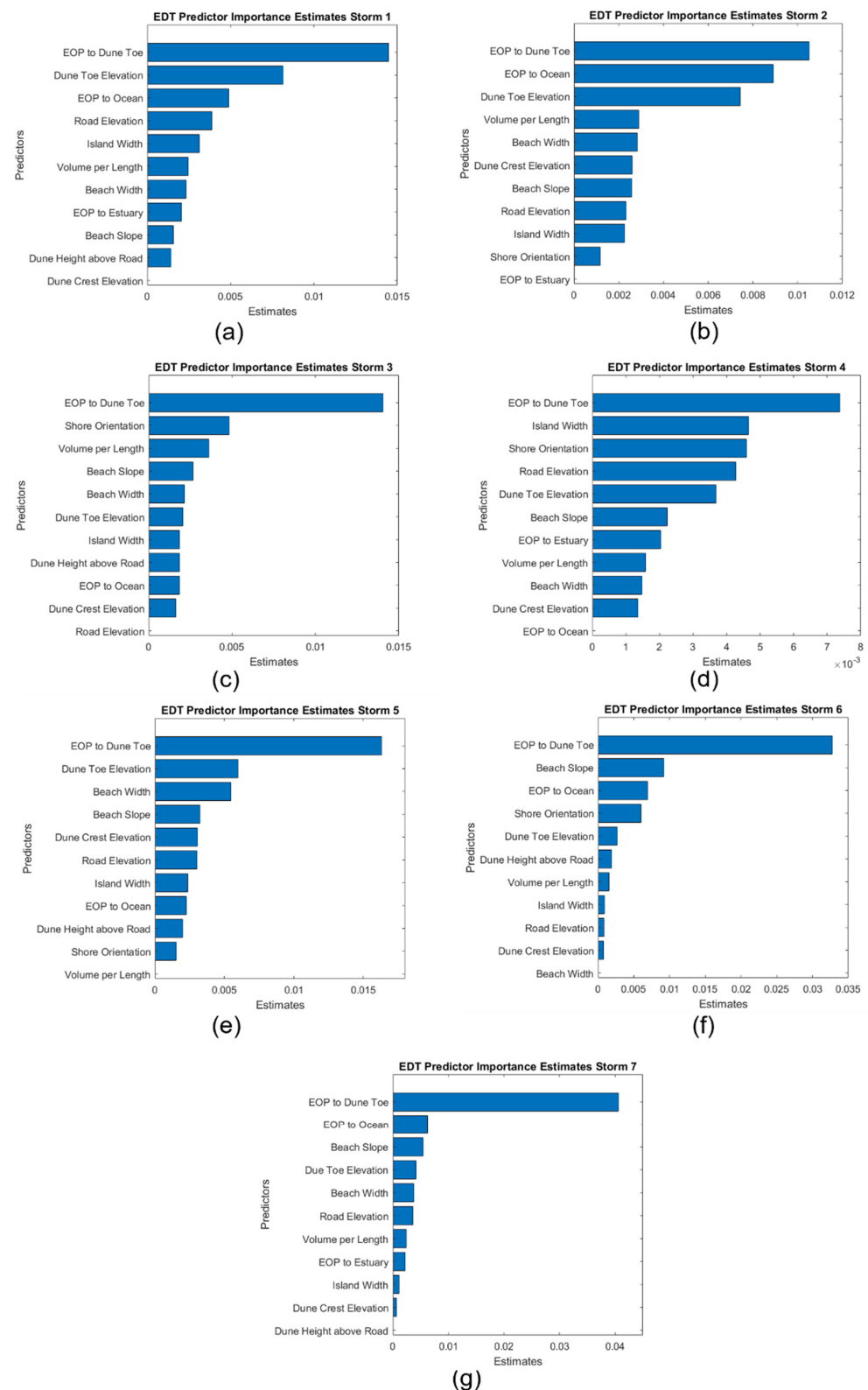
Figure 11. Feature importance results reported by the EDT models for all the storm events. Storms 1 to 7 correspond to the panels (**a**–**g**), respectively. The "(11) Distance from road EOP to dune toe (ft)" was the best predictor across all the storm events. (10) Dune Toe Elevation is the second-best predictor for (**a**) storm 1 and (**e**) storm 5. (5) EOP to Ocean Shore is also the second-best predictor for (**b**) storm 2 and (**g**) storm 7. Finally, (12) Shore orientation (degrees) is part of the top five predictors in storm 3 (**c**), 4 (**d**), and 6 (**f**).

4. Discussion

The results of coastal highway vulnerability studies inform decisions regarding when and where to implement projects. Examples of projects that could be informed by highway vulnerability studies include highway realignment, artificial dune construction, shoreline hardening, bridge construction, and regular maintenance. Maximizing the accuracy of vulnerability assessment is crucial for assuring the effectiveness of these projects and making the most out of limited transportation budgets.

A previous study [5] sought to evaluate geomorphological indicators and determine whether a weighted linear function of multiple indicators could improve the prediction of highway vulnerability, beyond that of individual indicators. Ref. [5] (2022) found that combining multiple indicators, namely the distance from road EOP to dune toe and dune toe elevation, did improve performance. However, it was not clear whether the attained accuracy (F1 score and PR AUC) was limited by the assumed function form, and there were open questions regarding whether more complex function form or machine learning methods could improve the performance.

This present study supported the hypothesis that machine learning methods would improve the classification of highway vulnerability as impacted or not. This study also affirmed the finding of [5], i.e., that distance from EOP to dune toe is a powerful and reliable predictor of highway vulnerability. Distance from EOP to dune toe was found, in this study, to be the most important predictor among most of seven storms of varying intensity and approach, relative to the study area. Some of the results seemed counterintuitive, such as the finding that dune crest elevation is not important for certain storms (Figures 6 and 10). However, this area is highly managed, as discussed in [4], with frequent dune rebuilding. This may lead to dunes with relatively high crest elevations being quite close to the shoreline, where the dune is essentially a high, narrow barrier between storm waves and the roadway. In this situation, a high dune crest does not substantially lessen vulnerability.

Other factors, such as the angular difference between the shore-normal orientation and weighted mean wave direction, are shown to be important for some storms but not others. With regard to this angular difference, the relative angle between waves and structures has been shown to lead to complex effects by [39–43]. The research performed by [39] examined low-crested structures under an oblique wave attack. It was found that, for smooth (asphalt) structures, there was a strong dependency between the transmission coefficient and angle of wave attack, with the transmission decreasing with increasing incident wave angles. The stability of placed block revetments under oblique wave attack was investigated by [40], with the results showing that waves induce a pressure difference across the cover layer that is more complicated than that of perpendicular wave attack. Ref. [41] examined an oblique wave attack on open granular (sand) filters underneath armored slopes via physical model tests, showing that, for larger wave angles (where 0 degrees is perpendicular), the amount of filter erosion decreases. The effect of wave structure angles for tsunami loads on bridges was examined by [42,43], with the findings including the result that complex three-dimensional effects are generated by the interaction of the waves and structure. Ref. [44] examined the wave-structure interactions on bridge decks with varying geometries, also finding that loading is complex. Although these studies were not focused on ground-based roadways, similar complexity could be contributing to the results, showing the angular difference to be important for specific storms, while not as influential for others, and presenting an opportunity for further study.

While this research investigated 12 geomorphological factors that were applicable to the study area, there are other parameters cited in the literature that may be useful indicators for vulnerability assessments of roadways in other locations. A previous work [14] found that the width of elevated coastal decks affects the hydrodynamic loads imparted by waves on the structure, as well as that the ratio of "wavelength-to-deck width" is a critical factor. In the region of the present study, the roadway width did not significantly vary along the study area; therefore, this factor could not be examined. Similarly, dune vegetation was not included in this study. Past work [45–48] has shown that vegetation impacts

wave-induced pressures, loads, and erosion on dunes and other structures. The fact that vegetation on dunes enhances their resiliency and dunes generally serve as protection for roadways on their landward side suggests that vegetation could have a significant effect on the vulnerability of coastal roadways. This factor was not included in the vulnerability classification models of this current study because it was difficult to adequately quantify vegetation density along a transect cross-section. In is noted that, for this specific study area, the sections that had more dense vegetation between the road and shoreline, which also had a large distance from roadway EOP to dune toe and/or roadway EOP to shoreline—this would lead to a high correlation of these variables. These two factors (roadway width and dune vegetation) could be crucial indicators in classifying roadway vulnerability for other study areas, where there may be substantial spatial variation not captured by other indicators. The study area extent was a limitation for the current research, which hindered our ability to more comprehensively assess additional vulnerability indicators. Future research could add data sets from other barrier islands, where additional variables, such as vegetation and roadway properties, could be included in the model to potentially improve the vulnerability assessment.

It is noted that the most important feature for both classifiers used in this study, distance from EOP to dune toe, can also be measured without digital computation, using aerial photographs. The development of the presented study allows researchers and practitioners to classify road vulnerability as impacted or not, based on local geomorphological observations. The models' performance outperforms previous works significantly and can be applied to different locations where these features are available. Distance from EOP to ocean shoreline has been previously employed to evaluate highway vulnerability in this study area [4], as have long-term erosion rates and deterministic numerical modeling [49]. However, the results of this study indicate that coastal managers may be able to employ data-driven models to evaluate variability in coastal highway vulnerability on barrier islands. As remote sensing technology improves, and frequently updated topography becomes available [50,51], having a data-driven model that will classify portions of the roadway as vulnerable, without the high computational cost of deterministic numerical modeling, will be beneficial. The success of EDT in this study implies that this machine-learning model may be a useful tool for highway vulnerability studies. The model could be run with the most up-to-date geomorphology data available, in order to provide predictions regarding barrier island highway locations that are most susceptible to storm impacts. The application of the models used in this study are limited to the vulnerability classification of land-lying roadways located on wave-dominated barrier islands with sandy coastlines. Additionally, the models may not perform well for study regions where vegetated dunes are not well-correlated to distance from EOP to dune toe because vegetation was not included as a distinct variable within the model. The long-term effects of sea-level rise may bias the performance of the models, unless elevation datums are adjusted over time.

Author Contributions: Conceptualization, E.S., A.B. and J.E.P.; methodology, J.E.P.; validation, J.E.P.; formal analysis, J.E.P.; investigation, J.E.P.; resources, E.S. and A.B.; data curation, J.E.P.; writing—original draft preparation, J.E.P. and A.B.; writing—review and editing, E.S., A.B. and J.E.P.; visualization, J.E.P. and A.B.; supervision, E.S.; project administration, E.S. All authors have read and agreed to the published version of the manuscript.

References

1. Daniel, J.S.; Jacobs, J.M.; Douglas, E.; Mallick, R.B.; Hayhoe, K. Impact of climate change on pavement performance: Preliminary lessons learned through the infrastructure and climate network (ICNet). In *Climatic Effects on Pavement and Geotechnical Infrastructure*; ASCE: Reston, VA, USA, 2014; pp. 1–9.
2. Office for Coastal Management, NOAA. Hurricane Costs. 25 May 2022. Available online: https://coast.noaa.gov/states/fast-facts/hurricane-costs.html (accessed on 26 May 2022).
3. NCDOT. Maintenance Operations and Performance Analysis Report (MOPAR) (31 December 2020). Asset Management NCDOT. Connect NCDOT. Available online: https://connect.ncdot.gov/resources/Asset-Management/Pages/default.aspx (accessed on 26 May 2022).
4. Velásquez-Montoya, L.; Sciaudone, E.J.; Smyre, E.; Overton, M.F. Vulnerability indicators for coastal roadways based on barrier island morphology and shoreline change predictions. *Nat. Hazards Rev.* **2021**, *22*, 04021003. [CrossRef]
5. Behr, A.; Berglund, E.; Sciaudone, E. Effectiveness of indicators for assessing the vulnerability of barrier island highways. *Transp. Res. Part D Transp. Environ.* **2022**, *105*, 103234. [CrossRef]
6. Helderop, E.; Grubesic, T.H. Hurricane storm surge in Volusia County, Florida: Evidence of a tipping point for infrastructure damage. *Disasters* **2019**, *43*, 157–180. [CrossRef] [PubMed]
7. Neumann, J.E.; Emanuel, K.; Ravela, S.; Ludwig, L.; Kirshen, P.; Bosma, K.; Martinich, J. Joint effects of storm surge and sea-level rise on US Coasts: New economic estimates of impacts, adaptation, and benefits of mitigation policy. *Clim. Chang.* **2015**, *129*, 337–349. [CrossRef]
8. Pennison, G.P.; Cloutier, R.J.; Webb, B.M. Local Coastal Roads–Next Generation. In Proceedings of the IIE Annual Conference Proceedings, Norcross, GA, USA, 19–22 May 2018; pp. 943–948. Available online: https://www.proquest.com/scholarly-journals/local-coastal-roads-next-generation/docview/2553578393/se-2?accountid=1455 (accessed on 11 March 2022).
9. Gutierrez, B.T.; Plant, N.G.; Thieler, E.R.; Turecek, A. Using a Bayesian network to predict barrier island geomorphologic characteristics. *J. Geophys. Res. Earth Surface* **2015**, *120*, 2452–2475. [CrossRef]
10. Enwright, N.M.; Wang, L.; Wang, H.; Osland, M.J.; Feher, L.C.; Borchert, S.M.; Day, R.H. Modeling barrier island habitats using landscape position information. *Remote Sens.* **2019**, *11*, 976. [CrossRef]
11. Talukdar, S.; Singha, P.; Mahato, S.; Shahfahad; Pal, S.; Liou, Y.-A.; Rahman, A. Land-Use Land-Cover Classification by Machine Learning Classifiers for Satellite Observations—A Review. *Remote Sens.* **2020**, *12*, 1135. [CrossRef]
12. Wang, J.; Bretz, M.; Dewan, M.A.A.; Delvar, M.A. Machine learning in modelling land-use and land cover-change (LULCC): Current status, challenges and prospects. *Sci. Total Environ.* **2022**, *822*, 153559. [CrossRef]
13. Angalakudati, M.; Calzada, J.; Farias, V.; Gonynor, J.; Monsch, M.; Papush, A.; Williams, J. Improving emergency storm planning using machine learning. In Proceedings of the 2014 IEEE PES T&D Conference and Exposition, Chicago, IL, USA, 14–17 April 2014; pp. 1–6.
14. Yang, F.; Wanik, D.W.; Cerrai, D.; Bhuiyan, M.A.E.; Anagnostou, E.N. Quantifying Uncertainty in Machine Learning-Based Power Outage Prediction Model Training: A Tool for Sustainable Storm Restoration. *Sustainability* **2020**, *12*, 1525. [CrossRef]
15. Lee, J.-W.; Irish, J.L.; Bensi, M.T.; Marcy, D.C. Rapid prediction of peak storm surge from tropical cyclone track time series using machine learning. *Coast. Eng.* **2021**, *170*, 104024. [CrossRef]
16. Harvey, J.; Kumar, S.; Bao, S. Machine Learning-Based Models for Assessing Impacts Before, During and After Hurricane Florence. In Proceedings of the 2019 IEEE Symposium Series on Computational Intelligence (SSCI), Xiamen, China, 6–9 December 2019; pp. 714–721. [CrossRef]
17. Fan, C.; Wu, F.; Mostafavi, A. A Hybrid Machine Learning Pipeline for Automated Mapping of Events and Locations From Social Media in Disasters. *IEEE Access* **2020**, *8*, 10478–10490. [CrossRef]
18. Devaraj, A.; Murthy, D.; Dontula, A. Machine-learning methods for identifying social media-based requests for urgent help during hurricanes. *Int. J. Disaster Risk Reduct.* **2020**, *51*, 101757. [CrossRef]
19. Claudino-Sales, V.; Wang, P.; Horwitz, M.H. Factors controlling the survival of coastal dunes during multiple hurricane impacts in 2004 and 2005: Santa Rosa barrier island, Florida. *Geomorphology* **2008**, *95*, 295–315. [CrossRef]
20. Beuzen, T.; Harley, M.D.; Splinter, K.D.; Turner, I.L. Controls of Variability in Berm and Dune Storm Erosion. *JGR Earth Surf.* **2019**, *124*, 2647–2665. [CrossRef]
21. Dolan RO BE, R.T.; Hayden, B.P.; May, P.; May, S. The reliability of shoreline change measurements from aerial photographs. *Shore Beach* **1980**, *48*, 22–29.

22. National Oceanic and Atmospheric Administration (NOAA). Online Vertical Datum Transformation (VDatum). 2022. Available online: https://vdatum.noaa.gov/vdatumweb/ (accessed on 16 July 2022).
23. Ortiz, A.C.; Roy, S.; Edmonds, D.A. Land loss by pond expansion on the Mississippi River Delta Plain. *Geophys. Res. Lett.* **2017**, *44*, 3635–3642. [CrossRef]
24. Doran, K.S.; Long, J.W.; Overbeck, J.R. *A Method for Determining Average Beach Slope and Beach Slope Variability for US Sandy Coastlines*; US Department of the Interior, US Geological Survey: Reston, VA, USA, 2015.
25. Zhang, Z. Introduction to machine learning: K-nearest neighbors. *Ann. Transl. Med.* **2016**, *4*, 218. [CrossRef]
26. Freund, Y.; Schapire, R.E. Experiments with a new boosting algorithm. *ICML* **1996**, *96*, 148–156.
27. Mounce, S.R.; Ellis, K.; Edwards, J.M.; Speight, V.L.; Jakomis, N.; Boxall, J.B. Ensemble decision tree models using RUSBoost for estimating risk of iron failure in drinking water distribution systems. *Water Resour. Manag.* **2017**, *31*, 1575–1589. [CrossRef]
28. Winkler, D.; Haltmeier, M.; Kleidorfer, M.; Rauch, W.; Tscheikner-Gratl, F. Pipe failure modelling for water distribution networks using boosted decision trees. *Struct. Infrastruct. Eng.* **2018**, *14*, 1402–1411. [CrossRef]
29. Fasaee MA, K.; Pesantez, J.; Pieper, K.J.; Ling, E.; Benham, B.; Edwards, M.; Berglund, E. Developing Early Warning Systems to Predict Water Lead Levels in Tap Water for Private Systems. *Water Res.* **2022**, *221*, 118787. [CrossRef] [PubMed]
30. Guyon, I.; Elisseeff, A. An introduction to variable and feature selection. *J. Mach. Learn. Res.* **2003**, *3*, 1157–1182.
31. Gelbart, M.A.; Snoek, J.; Adams, R.P. Bayesian optimization with unknown constraints. *arXiv* **2014**, arXiv:1403.5607.
32. Yang, L.; Shami, A. On hyperparameter optimization of machine learning algorithms: Theory and practice. *Neurocomputing* **2020**, *415*, 295–316. [CrossRef]
33. Pesantez, J.E.; Berglund, E.Z.; Kaza, N. Smart meters data for modeling and forecasting water demand at the user-level. *Environ. Model. Softw.* **2020**, *125*, 104633. [CrossRef]
34. Zhou, X.; Lu, P.; Zheng, Z.; Tolliver, D.; Keramati, A. Accident prediction accuracy assessment for highway-rail grade crossings using random forest algorithm compared with decision tree. *Reliab. Eng. Syst. Saf.* **2020**, *200*, 106931. [CrossRef]
35. Rokach, L. Ensemble-based classifiers. *Artif. Intell. Rev.* **2010**, *33*, 1–39. [CrossRef]
36. Breiman, L. Random forests. *Mach. Learn.* **2001**, *45*, 5–32. [CrossRef]
37. Friedman, J.; Hastie, T.; Tibshirani, R. Additive logistic regression: A statistical view of boosting (with discussion and a rejoinder by the authors). *Ann. Stat.* **2000**, *28*, 337–407. [CrossRef]
38. Gaudreault, J.G.; Branco, P.; Gama, J. An Analysis of Performance Metrics for Imbalanced Classification. In *Discovery Science, Proceedings of the International Conference on Discovery Science, Halifax, NS, Canada, 11–13 October 2021*; Springer: Cham, Switzerland, 2021; pp. 67–77.
39. Van der Meer, J.W.; Briganti, R.; Zanuttigh, B.; Wang, B. Wave transmission and reflection at low-crested structures: Design formulae, oblique wave attack and spectral change. *Coast. Eng.* **2005**, *52*, 915–929. [CrossRef]
40. Breteler, M.K.; Bezuijen, A.; Provoost, Y. Influence of oblique wave attack on stability of placed block revetments. In *Coastal Engineering 2008*; McKee Smith, J., Ed.; World Scientific: Hackensack, NJ, USA, 2009; Volume 4, pp. 3032–3057.
41. Van Gent, M.R.A.; Wolters, G. Effects of storm duration and oblique wave attack on open filters underneath rock armoured slopes. *Coast. Eng.* **2018**, *135*, 55–65. [CrossRef]
42. Istrati, D.; Buckle, I.G. *Tsunami Loads on Straight and Skewed Bridges-Part 1: Experimental Investigation and Design Recommendations*; Report Prepared for Oregon Dept. of Transportation & Federal Highway Administration; Oregon Dept. of Transportation: Salem, OR, USA, 2021; 193p + appx.
43. Istrati, D.; Buckle, I.G. *Tsunami Loads on Straight and Skewed Bridges-Part 2: Numerical Investigation and Design Recommendations*; Report Prepared for Oregon Dept. of Transportation & Federal Highway Administration; Oregon Dept. of Transportation: Salem, OR, USA, 2021; 88p.
44. Xiang, T.; Istrati, D. Assessment of extreme wave impact on coastal decks with different geometries via the arbitrary Lagrangian-Eulerian method. *J. Mar. Sci. Eng.* **2021**, *9*, 1342. [CrossRef]
45. Coops, H.; Geilen, N.; Verheij, H.J.; Boeters, R.; van der Velde, G. Interactions between waves, bank erosion and emergent vegetation: An experimental study in a wave tank. *Aquat. Bot.* **1996**, *53*, 187–198. [CrossRef]
46. Vuik, V.; Jonkman, S.N.; Borsje, B.W.; Suzuki, T. Nature-based flood protection: The efficiency of vegetated foreshores for reducing wave loads on coastal dikes. *Coast. Eng.* **2016**, *116*, 42–56. [CrossRef]
47. Lo, V.B.; Bouma, T.J.; van Belzen, J.; Van Colen, C.; Airoldi, L. Interactive effects of vegetation and sediment properties on erosion of salt marshes in the Northern Adriatic Sea. *Mar. Environ. Res.* **2017**, *131*, 32–42. [CrossRef]
48. Sundar, V.; Murali, K.; Noarayanan, L. Effect of vegetation on run-up and wall pressures due to cnoidal waves. *J. Hydraul. Res.* **2011**, *49*, 562–567. [CrossRef]
49. Overton, M.F.; Fisher, J.S. *NC Coastal Highway Vulnerability*; Report No. FHWA/NC/2004-04; Prepared for U.S. Department of Transportation; US Dept. of Transportation: Washington, DC, USA, 2005; 88p. Available online: https://connect.ncdot.gov/projects/research/RNAProjDocs/2002-05FinalReport.pdf (accessed on 11 March 2022).
50. Brodie, K.L.; Bruder, B.L.; Slocum, R.J.; Spore, N.J. Simultaneous Mapping of Coastal Topography and Bathymetry From a Lightweight Multicamera UAS. *IEEE Trans. Geosci. Remote Sens.* **2019**, *57*, 6844–6864. [CrossRef]
51. Salameh, E.; Frappart, F.; Almar, R.; Baptista, P.; Heygster, G.; Lubac, B.; Raucoules, D.; Almeida, L.P.; Bergsma, E.W.J.; Capo, S.; et al. Monitoring Beach Topography and Nearshore Bathymetry Using Spaceborne Remote Sensing: A Review. *Remote Sens.* **2019**, *11*, 2212. [CrossRef]

APPENDIX D: Revisions to Physical and Biological Monitoring Protocols

Timeline and Description of Contents

Only July 27, 2022, NCDOT requested a reduction in scope of the physical and biological monitoring protocols after discussions with the Coastal Monitoring Team. This letter is attached in this Appendix. On October 11, 2022, USFWS replied to the request for revisions; this letter is also attached. This letter specifies that:

"The number and location of the targeted samples for each survey year (i.e., calendar year) should be discussed at the prior Coastal Monitoring Team meeting(s), collectively agreed upon by the Coastal Monitoring Team, and summarized either in the annual Coastal Monitoring Report (as currently in Appendix A with the complete Physical and Biological Monitoring Report) or as a separate annual addendum to the report with similar existing reporting deadline and requirements (e.g., proposed sampling plan for the 2024 sampling year would be provided with the 2022 Coastal Monitoring Report in October 2023 as currently scheduled)."

A meeting was held on Thursday, November 3, 2022, to discuss the proposed sampling protocols for 2023. The team agreed that the heavy minerals sampling would take place at mid-beach. Additionally, the team agreed to designate approximately 21 transects as "Sentinel Transects" to maintain continuity with the long-term sampling dataset, with additional transects designated each year by the team to add information where the most critical information would be provided. The decision on the sampling transects was as follows:

Sentinel Transects: TG2, T5, T11, 17, 23, 29, 32, 35, 38, 41, 44, 47, 50, 53, 56, 59, 62, 65, 68, 71, 74 (21 TOTAL transects).

For 2023, add:

Canal Zone: 13, 15, 19, 21

Visitor Center: 36

Pea Island Breach (Split Pea): 49, 51

S-Curves: 69, 70, 72, 73

Maps showing these transects are also included in this appendix.

STATE OF NORTH CAROLINA
DEPARTMENT OF TRANSPORTATION

ROY COOPER
GOVERNOR

J. ERIC BOYETTE
SECRETARY

July 27, 2022

Rebecca Harrison, PhD
USFWS Pea Island National Wildlife Refuge
P.O. Box 1969
Manteo, NC 27954

Dear Dr. Harrison,

This letter outlines the NCDOT's requested revisions to future Pea Island National Wildlife
Refuge (PINWR) sand surveys

Purpose of Current Sand Survey
The Pea Island sand study was designed to continue the work of Dolan and others on PINWR to
determine the effects of the US Army Corps of Engineers sand bypassing program on Pea Island-
how alteration to the physical environment impacts biological processes on the beach face of the
Refuge. This sand bypassing is a direct effect of the dredging of Oregon Inlet resulting from the
Terminal Groin installation.

On August 9, 2012, the USFWS signed the Right of Way easement agreement between the
USFWS and the NCDOT to authorize the retention of the existing terminal groin and connected
revetments on the northern terminus of PINWR. This was a renewal of the permit dated June 20,
1989, for the NCDOT to use PINWR lands for the retention of the existing terminal groin and
connected revetments on the northern terminus of Pea Island.

The easement document was authorized by the Secretary of the Interior, through his authorized
representative, the Regional Director, USFWS, in Atlanta, Georgia in accordance with applicable
authorities and regulations published in 50 CFR 29.21.

Documents Requiring the Sand Surveys
This easement agreement and other documents specify the physical and biological monitoring of the sand on PINWR and the Coastal Monitoring Program (CMP) work as project commitments. Excerpts from these documents are listed below.

From the 2012 Terminal Groin easement agreement:
	"Consideration for this grant shall be the conservation, management, and where designated the enhancement of wildlife habitat affected by stabilization of dynamic inlet over-wash, dominated habitats along the north end of the Refuge, and partially restoring habitat lost to both allusive and erosive action or degradation due to interference with the natural movement of sand and sediments through structural stabilization of the inlet shoreline."

Section II of the easement specifies the terms and conditions of the monitoring programs that NCDOT will be responsible for. NCSU scientists are and have been conducting the Coastal Monitoring Program (CMP). The CMP involves aerial photography, tracking of shoreline changes and geo-spatial habitat analysis and modelling for detecting habitat change over time. The area to be covered (monitored area) is on the Refuge and is to include the terminal groin to the new inlet approximately 6 miles south and from ocean to sound in the first mile south of the terminal groin and from the ocean to the west side of NC 12 ROW for miles 2-6. This monitoring area applies to the NCSU work.

This section also describes the conditions of the sand surveys: "*NCDOT shall monitor physical and biological parameters along transects across the beach at approximately 0.2-mile intervals within the monitored area. Monitoring transects shall include, but are not limited to, dune width and height, beach width, beach slope, sand grain size as determined through one sample from the upper beach, and one sample each from the upper, mid and lower swash zone, and mineral content of swash zone sand. Biological data collection shall include but is not limited to beach invertebrates such as the ghost crab, swash zone invertebrates such as the mole crab, coquina, amphipods, and polychaete worms*." In a letter from the Refuge to NCDOT dated January 24, 2012, the Refuge manager requested the physical/biological sand survey be extended the entire length of the Refuge to replace previous SUP #2006-014.

Section II of the easement also includes an *Adaptive Management statement* that requires *"an analysis that evaluates the effectiveness of the established monitoring protocols with recommendations identifying protocols to continue and protocols to change or add. The purpose of this analysis is to evaluate the effectiveness of monitoring as it relates to transportation maintenance needs and the status of migratory bird and T&E species resources and their habitats on the monitored area. If recommendations are made to continue, modify, add, or change protocols and are mutually agreed to, then revisions to those requirements may be made."*

From the USFWS Compatibility Determination for Retention of the Terminal Groin Page 8

"After reviewing the available information and according to my best professional judgement, I find that issuing a permit to allow the Terminal Groin to remain in place cannot be found compatible without stipulations to offset impacts on refuge land accruing from the structure. Strict adherence to the stipulations listed in this determination and full compliance with all conditions of the permit are mechanisms for making a favorable Compatibility Determination." (USFWS, Refuge Manager).

Section II: Monitoring Conditions:
        ii. (PAGE 14) "*NCDOT shall be responsible for monitoring physical and biological parameters along transects across the beach at approximately 0.2 mile intervals within the zone described herein. Monitoring transects shall include, but are not limited to, dunes to lowest point of the swash zone.*
1) *Physical data collection shall include, but is not limited to, dune width and height, beach width, beach slope, sand grain size as determined through one sample from the upper beach, and one sample each from upper, mid- and lower swash zone, and mineral content of each swash zone sand."*
2) *Biological data collection shall include but is not limited to beach invertebrates such as ghost crab, swash zone invertebrates such as the mole crab, coquina, amphipods, and polychaete worms. Observations on other wildlife should be recorded and reported to the refuge especially where nesting birds or turtles are observed."*

NCDOT's Requested Revisions to the PINWR Sand Surveys
Based on efforts to reduce the cost of the Pea Island Sand surveys to the Division 1, B-2500 budget, the NCDOT put together a plan for reducing the scope of the project to be discussed with the coastal monitoring team to determine how to do this while still maintaining the quality and integrity of data to satisfy the needs of the Refuge.
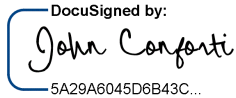
After meetings with the Refuge staff and members of the Coastal Monitoring Team, the NCDOT makes the following requested changes to the sand survey protocols:

- Reduce the number of transects to around 36. The number and location of transects to include in the surveys each year will remain flexible and will be re-evaluated at the two annual meetings or as needed based on several factors such as storm events
- Reduce heavy minerals analysis by eliminating the swash zone samples and eliminate minerals speciation
- Beginning with the 2021 report, include each year an analysis of the relationship to grain size and heavy minerals to see if adequate information can be obtained through analysis of grain size alone.
- Maintain status quo until the Refuge develops a protocol for making these changes to the project commitments as per the Terminal Groin easement document.

- Maintain the January survey as this data will become increasingly important with the changing climate.

We appreciate the understanding and collaboration of the Refuge on this request. If you have any questions, please call me at (919) 707-6015 or email at jgconforti@ncdot.gov.

Sincerely,

DocuSigned by:

John Conforti

5A29A6045D6B43C...

John Conforti, REM
Senior Project Manager
NCDOT Project Management Unit

United States Department of the Interior

FISH AND WILDLIFE SERVICE

ALLIGATOR RIVER NATIONAL WILDLIFE REFUGE
Pea Island National Wildlife Refuge
P. O. Box 1969
Manteo, North Carolina 27954
(252) 473-1131

John Conforti, REM
North Carolina Department of Transportation
Project Management Unit – Divisions 1-4 & 6
1582 Mail Service Center
Raleigh, NC 27699-1582

October 11, 2022

Dear Mr. Conforti,

Thank you for the proposed revisions to the future Pea Island National Wildlife Refuge (Refuge) sand surveys summarized in the letter dated July 27, 2022. On September 10, 2012, the Right of Way easement agreement between the U.S. Fish and Wildlife Services (Service) and the North Carolina Department of Transportation (NCDOT) was recorded to authorize the retention of the existing terminal groin and connected revetments on the northern terminus of the Refuge. This was a renewal of the permit dated June 20, 1989, for the NCDOT to use PINWR lands for the retention of the existing terminal groin and connected revetments on the northern terminus of the Refuge.

The general stipulations as outlined in the 2012 easement in Section I(4) require the Service and NCDOT to develop monitoring programs to measure changes in the Refuge habitat and shoreline. Section II of the 2012 easement describes the monitoring conditions: "*NCDOT shall monitor physical and biological parameters along transects across the beach at approximately 0.2 mile intervals within the monitored area. Monitoring transects shall include, but are not limited to, dunes to lowest point of the swash zone. Physical data collection shall include, but is not limited to, dune width and height, beach width, beach slope, sand grain size as determined through one sample from the upper beach, and one sample each from the upper, mid-and lower swash zone, and mineral content of swash zone sand. Biological data collection shall include, but is not limited to beach invertebrates such as the ghost crab, swash zone invertebrates such as the mole crab, coquina, amphipods, and polychaete worms.*" As noted in a letter from the Refuge to NCDOT dated January 24, 2012, the Refuge manager requested the physical and biological sand surveys be extended the entire length of the Refuge to replace previous Refuge Special Use Permit #2006-014. These changes resulted in 64 transects being surveyed quarterly along the entire oceanside shoreline of the Refuge.

We acknowledge the specific changes requested for the current sand surveys as listed in the letter from July 27, 2022. We recommend maintaining the quarterly surveys in January, April, July, and October. During early discussions, it was suggested NCDOT eliminate the January surveys due to low abundance levels of the invertebrates, but we believe with increasing winter temperatures this dataset will be important for tracking changes in the invertebrate communities. We acknowledge the heavy mineral analyses are a costly component of these efforts and recommend continuing evaluation of the contributions of these analyses within the annual Coastal Monitoring Report. As a first step, we also approve the requested reduction of collection of heavy mineral samples in the swash zone and to eliminate minerals speciation. Lastly, we also support the reduction sampled transects from 64 to 32 during each quarterly sampling effort. The number and location of the targeted samples for each survey year (i.e., calendar year) should be discussed at the prior Coastal Monitoring Team meeting(s), collectively agreed upon by the Coastal Monitoring Team, and summarized either in the annual Coastal Monitoring Report (as currently in Appendix A with the complete Physical and Biological Monitoring Report) or as a separate annual addendum to the report with similar existing reporting deadline and requirements (e.g., proposed sampling plan for the 2024 sampling year would be provided with the 2022 Coastal Monitoring Report in October 2023 as currently scheduled). We support allowing the flexibility to annually determine which transects would provide the most critical information depending on multiple factors including storm events, ongoing transportation corridor projects, and changing resource management needs. We also acknowledge that it is possible the highest priority transects may be located where the transportation corridor no longer will exist (i.e., transects 600-630 in the most southern portion of the Refuge).

The 2012 easement also created an opportunity for adaptative management and required the regular review of the monitoring protocols as described in Section II: "*Once every five years the Monitoring Report will include a section with an analysis that evaluates the effectiveness of the established monitoring protocols with recommendations identifying protocols to continue and protocols to change or add. The purpose of this analysis is to evaluate the effectiveness of monitoring as it relates to transportation maintenance needs and the status of migratory bird and threatened and endangered species resources and their habitats on the monitored area. If recommendations are made to continue, modify, add, or change protocols and are mutually agreed to, then revisions to those requirements may be made.*" We recommend any proposed changes to the biological monitoring surveys be collectively discussed at the biannual Coastal Monitoring Team meetings (usually held in March and November) and recorded in the annual Coastal Monitoring Report within Appendix A with the complete Physical and Biological Monitoring Report.

We appreciate the communications and continued collaboration of the NCDOT and its contractors engaged in the coastal monitoring efforts on the Refuge. If you have any questions, please contact Refuge Biologist Dr. Becky Harrison at 252-423-1839 or rebecca_harrison@fws.gov.

Sincerely,

Pea Island National Wildlife Refuge Manager

T-11 - T-29 "Canal Zone"

PREPARED BY:
RK&K

NORTH CAROLINA
DEPARTMENT OF TRANSPORTATION

STATE OF NORTH CAROLINA
DEPARTMENT OF TRANSPORTATION

Monitoring NC-12
Dare County

Monitoring Locations Map TG2 - T-38   **Figure 1**

Source: NOAA, Esri

T-38

T-41

T-44

T-47

T-49

T-50

T-51

T-53

T-47 - T-53 Narrow area
South of PI Inlet Area

T-56

T-59

T-62

T-65

T-68

T-69

T-70

T-71

T-72

T-73

T-74

T-65 - T-74 Beach
nourishment area and
"S Curves"

N
W   E
S

0   0.25   0.5 Miles

PREPARED BY:

RK&K

NORTH CAROLINA
DEPARTMENT OF TRANSPORTATION

STATE OF NORTH CAROLINA
DEPARTMENT OF TRANSPORTATION

Monitoring NC-12
Dare County

Monitoring Locations Map T38-T74   **Figure 2**

Source: NOAA, Esri